A UNIFIED SWCC-CLAY MINERALOGY BASED FRAMEWORK FOR PREDICTING SWELL BEHAVIOR OF EXPANSIVE SOILS

by

ALEJANDRO HERNAN PINO BRAVO

Presented to the Faculty of the Graduate School of

The University of Texas at Arlington in Partial Fulfillment

of the Requirements

for the Degree of

DOCTOR OF PHILOSOPHY

THE UNIVERSITY OF TEXAS AT ARLINGTON

December 2015

Acknowledgements

I would like to start extending my deepest thankfulness to Dr. Anand Puppala for the support he has given to me in different ways, not only the academic guidance on the theoretical and experimental research study, but the material and personal support during my PhD time at UTA as well. It has been an honor to work under Dr. Puppala's direction, I have learnt countless significant lessons for future, but the most important is that he taught me how to become an open-minded and intellectually relevant researcher, maintain high standards and good reputation as person, professor and professional but still keeping the kindness and greatness in heart for sharing to others the knowledge at all fields. I will retain all of these lessons with me for the rest of my life.

Words of gratitude are also given to other members of my dissertation committee: Dr. Laureano Hoyos; Dr. Xinbao Yu, Dr. Shih-Ho Chao, for revising this document and providing valuable remarks and feedback. I extend my appreciation to the civil engineering staff for their support during my time at UTA. I would like to thank as well to all the former and present undergraduate, graduate and postdoctoral fellows, who gave me a helping hand. Rewards will be returned to their lives due to this support.

Also, I express my gratitude to my beloved mate of every day, Paola. My wife's support has been unique, exceptional; she is a helper suitable for me that God made to complete the doctoral program successfully. As well, infinite thanks must be extended to my parents. My father living always encouraged me to continue, despite of the weakness of his health. To my mother's memory is dedicated any achievement I reach. She was my first master in life; her advice endures shining in my mind like burning flame.

Finally, thanks to the eternal Lord in heaven, the reason why I breathe, the energy to be alive and the strength to wake up every morning, amen.

October 21, 2015

Abstract

PREDICTION AND SIMULATION OF SOIL SWELLING BEHAVIOR THROUGH A UNIFIED SWCC-CLAY MINERALOGY BASED METHODOLOGY AND MODEL

Alejandro Hernan Pino Bravo, PhD

The University of Texas at Arlington, 2015

Supervising Professor: Anand Puppala

Expansive soils are spread over different climatic zones around the world with varying mineralogical content and microstructure, making the soil to absorb moisture between their mineral layers and therefore undergo volume changes. This behavior generates swell and shrinkage surface movements which affect the integrity of infrastructure built on them. A practice currently employed correlates swell-shrink behavior to soil index parameters, however, variable soil mineralogy limits this approach, which generates poor soil swell characterization. Thus, characterizing efforts must be emphasized on identification of real parameters governing the swell/shrink behavior, such as mineralogy, variation of suction with moisture content and pore distribution. The present work intends to validate previously formulated swell behavior models for clays based on these parameters and to utilize the data obtained from the validation process to generate a unified formulation that assesses the effect of the mentioned key parameters in the prediction and characterization of soil swell behavior. The unified model was defined using multiple linear regression (MLR) and artificial neural network (ANN) techniques. Both approaches exhibited acceptable prediction capacity, however, ANN models showed higher prediction capability than MRL models. ANN proved its usefulness for complementing or replacing MLR in soil swell behavior characterization.

Table of Contents

List of Illustrations

List of Tables

Chapter 1

Introduction

1.1 Expansive soils

Soils with expansive or shrink-swell characteristics are usually those types of soils that heave when subjected to an increase in moisture content, the change starts at partially saturated condition and then may reach saturated condition. These soils have another feature as well, which is termed as shrink behavior, which is the reverse process to swelling. Shrinkage is exhibited with presence of fissures on soil surface and occurs when an expansive soil loses moisture content due to natural or artificial processes. In general, swelling soils also have moderate to high plastic index and high variability on bearing capacity and strength depending on the moisture condition (Kalantari, 2012).

Swelling soils are identified in many places around the world, however, they are mainly found in areas with climatic conditions ranging from arid to semiarid. Clayey type minerals predominate in swelling soils microstructure, generating these soils to absorb water in between their layers and then undergo volume changes (Bowels, 1988; Kalantari, 1991; Murphy, 2010).

Mother Nature induced hazards in the United States of America can be categorized into six types according to their capacity to affect or even destroy the built infrastructure, as follows: earthquakes, landslides, swelling soils, hurricanes, tornados and floods. Expansive soils as well as hurricanes might be allocated the second place among the most destructive natural hazards in terms of economic losses (Chen, 1988; Murphy, 2010). The expansive soil distresses induced are primarily linked to differential movements occurring in the foundation soil that supports the infrastructure. Residential building foundations, retaining walls, slopes and pavements are put under threat due to this anomalous behavior of soil. Also, damage is generated to structures due to the fact

that swelling pressure induces internal stresses greater than the design stresses ((Kalantari, 2012).

Laboratory procedures for identifying and classifying swelling soils are many, but mostly, these methods applied around the world and in the USA include the use of Atterberg limits, clay size, clay content and activity properties to characterize expansive nature of the soils. These methods allow for obtaining an approximate qualitative swelling potential description of a particular soil which might be designated low, medium, high or very high (Kalantari, 1991; U.S. Department of Transportation, 2006). Recently, other approaches for soil swelling classification have been attempted; they apply variables such as matric suction, cation exchange capacity (CEC), specific surface area (SSA), and others. However, at the present there is no unified procedure to obtain a classification which may be considered as a more reliable approach.

The wide spectrum of particulate materials composing expansive as well as other types of soils affects the swelling potential prediction accuracy when it is based only on the previously mentioned parameters, making the use of index properties not completely successful and reliable. Therefore, the development of a comprehensive methodology to better understand the swelling behavior of soils and the factors playing an important role in it is crucial. Hereafter, a methodology is instituted for identifying the parameters that in reality rule the swell/shrink behavior of soils and for establishing a reliable framework which allows evaluating the qualitative and quantitative soil swelling potential.

Mineralogy plays a relevant role in the swelling and shrinkage behavior of soil. Large cation exchange capacity as well as broaden specific surface area of clayey mineral particles like Montmorillonite permit it to absorb more water than other minerals like Kaolinite.

Soil suction has been proven to be a crucial factor affecting clays volume change behavior. Generally, natural soils in arid and semiarid areas remain most part of the year under partially saturated conditions with their moisture contents varying only seasonally. A relationship between these two variables is represented by the soil water characteristic curve (SWCC). Recent studies suggest that expansive behavior of soils is better understood if the matric suction is considered in the analysis (Alonso et al. 1999). Latest studies suggest that suction is independent of soil mineralogy but highly dependent on the chemistry of the pore water saturating the soil (Pulat et al. 2014).

Soil hydraulic conductivity and the soil characteristics to absorb water depend on the pore distribution, thus, pore size and distribution influence the soil swell behavior (Mitchell and Soga, 2005). Recently, new techniques have been used to determine soil porous condition. One is Mercury intrusion porosimetry (MIP) in which the mercury intrinsic non wetting condition is used to intrude this liquid like metal into a soil sample by applying incremental pressure and then extrude it by applying the reverse process (Washburn, 1921). The test reveals the pores sizes according to the pressures applied to fill them, the pores volume and therefore the total voids volume. Another technique is designated X-ray computed tomography (XCT) used to identify the solid internal structure present in a soil specimen. Both techniques yield information on the soil specimen's internal structure and were performed during the development of the present study.

Thus, it is clear that most problems at the field where expansive soils have been found arise from inappropriate soil characterization and inadequate soil swell potential evaluation. A reason for this undesirable phenomenon not to be unforeseen is the limited current state of knowledge and practice, since as previously outlined; soil mineralogy variations and unsaturated features of soil are not often considered (Nelson and Miller, 1992, Al Rawas et al., 2005, Puppala et al, 2012). Henceforth, fundamentals factors

affecting swelling of soils need to be understood, thus it is necessary to perform an innovating research under the sight of mineralogy quantification and unsaturated soil mechanics practices, which would define a realistic framework that includes detailed soil characterization procedures and methodologies for soil swelling potential evaluation.

1.2 Research Objectives

The present research work will be concentrated on these specific objectives:

1. To perform experimental tests on six natural expansive clays from different geographical origin in Texas and suspected variable mineralogy and degree of swell potential.
2. Evaluation of swell related to clay volume change behavior based on variables as mineralogy, initial moisture content, variation of suction with moisture content increment, overburden stress, density and pore distribution.
3. To validate previously formulated swell behavior models for clays by comparing their prediction results to the measured swell data of the present study.
4. To generate a unified formulation that assesses the effect of the observed variables in the prediction and characterization of swelling soil behavior established using multiple linear regression and artificial neural network techniques to analyze the data obtained from the validation process performed on the previously formulated swell behavior models for clays.
5. To demonstrate the inadequacy of clay swelling behavior characterization by use of soil index correlations, and establish the usefulness in this topic of prediction formulations considering modern unsaturated soil principles and composition features of clay.

The outcome of the proposed studies is a better understanding of the swelling soil behavior and the development of a general and unified approach that includes both analytical and numerical formulation for the prediction of the volume change properties and responses of expansive soils by considering clay mineralogy, pore distribution and unsaturated soil mechanics principles.

The methodology to be presented is intended to be a more useful characterization tool for assessing expansive soil swelling behavior and its potential and thereby to be a help for civil infrastructure designers, when dealing with these types of soils.

A flowchart presenting the experimental design for the present research is shown in Figure 1-1. Parameters representing advanced soil features are used to establish the soil swelling behavior prediction framework. All the predictions will be validated by using conventional swell properties obtained from the six soils studied in this research.

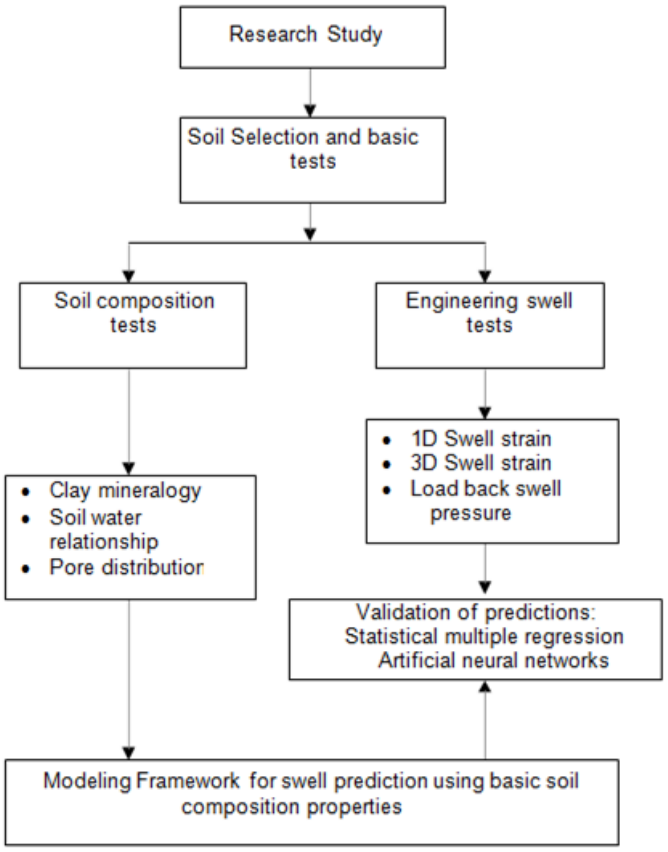

Figure 1-1 Flowchart

1.3 Dissertation organization

Chapter 1 encloses an introduction to the research as well as the contextual history supporting the connotation of the project. The chapter also presents the research objectives and the dissertation organization to provide the appropriate structure to the current study.

Chapter 2 includes a literature review in relation to swelling soils that covers behavior, commonly measured properties, devices used to determine swell properties and models to predict swell potential. The factors affecting the swell/shrink response of clayey soils are detailed in this chapter as well as the studies conducted up to the date on these factors.

Chapter 3 presents the factors considered in the selection of the soils used to perform the research and the basic classification for the latter. The laboratory work was focused on the determination of basic soil properties, performance of chemical test for mineralogy quantification and the engineering tests needed to characterize the swell potential of the soils. The laboratory devices, procedures and methods used for obtaining relevant data to be applied during the present study are explained in this chapter as well.

Chapter 4 condenses the results for the 1-D swell strain; 3-D swell strain and load back swell pressure performed on each of the clays included in the research work. Additionally, an evaluation of the influence on swelling behavior of the changes in dry density and overburden confining pressure conditions is presented.

Chapter 5 presents the relationships between suction and moisture content for all the clays. The soil water characteristic curve was determined by using filter paper method and axis translation technique. Moreover, the results from Mercury Intrusion Porosimetry (MIP) and Xray Computed Tomography (XCT) techniques to study and evaluate the pore size distribution are described in this chapter. Evaluation of the pores structure in the soil specimen, as well as the structure variation from dried to saturated condition for simulating the swelling process, were generated by XCT studies and are presented in depth in this chapter.

Chapter 6 describes the formulation of a novel single variable model that predicts the swell behavior of clays based on the diffuse double layer (DDL) theory. Also, in this chapter it is included a validation of three previously formulated swell behavior models for clays (Pedarla 2013), which consider composition parameters like clay mineralogy, soil suction behavior and total surface area. These models are assumed to be independently validated since their prediction results are compared to the measured swell data of the present soils.

Chapter 7 presents a general and unified approach that includes analytical and numerical formulation for the prediction of the volume change properties and responses of expansive soils by considering clay mineralogy, pore distribution and unsaturated soil mechanics principles. Neural networks and statistical multiple linear regression procedures were applied to find the most suitable correlations.

Chapter 8 includes a summary on the findings of the present research as well as the relevant conclusions derived from the engineering analysis. Recommendations for future research work are also presented in this chapter.

Chapter 2

Literature review

2.1 Expansive soils

Expansive soils might be defined as soils that experience slight or even dramatic changes in volume when the environmental conditions induce fluctuations to its moisture content. Locations where these types of soils are found coincide mostly with semi-arid to arid regions, at tropical or temperate climatic zones around the world. Usually in these areas the evapo-transpiration is greater than the precipitation (Jones and Holtz, 1973). The continuous variations in volume make them to be instable for supporting infrastructure and therefore are often avoided for construction.

Expansive soils are fine grained, therefore, their mineralogy and pore size distribution will play a fundamental role in their swelling behavior. There other factors affecting the swell and shrink volume changes on these soils like stress history and current stress state. Soil foundation might be influenced by three different categories of factors: soil intrinsic characteristics (clay mineral, plasticity and pore connectivity), environmental factors (climate, groundwater, vegetation, soil suction, dry density and drainage) and the state of stresses (Nelson and Miller 1992).

Typical problems experienced by structures built on swelling soils are described in the beginning of this chapter, under the sight of the present design standards. Nowadays, the common design practices rely on soil index properties for evaluation and prediction of the soil swell potential. Consequently, a concise review of the correlations and techniques considering index properties is presented in this chapter.

In literature it was found the important role the mineralogy plays in swell behavior of clays and hence a summarized review of the studies was conducted.

In recent decades, several researchers have highlighted the relevance that in the soil swelling behavior has the soil water characteristic curve which represents the suction-moisture content relationship. SWCC definition for the six soils is presented in this chapter according to the procedures presented in the methodology chapter. These curves have been determined using filter paper method and axis translation technique using Tempe cell method. Soil volume changes and related correlations based on soil suction conditions are presented.

An overview on literature related to Mercury Intrusion Porosimetry (MIP) and X-ray Computed Tomography techniques is presented in this chapter as well. These technologies were applied to expose internal structure of pores in a soil specimen. Further applications and analysis performed are discussed later in this chapter.

2.1.1 Problems associated to expansive soils

Modifications to the environmental conditions will cause the expansive soils to experience volume changes that might be problematic to infrastructure. The differential movements in the soil mass as well as the pressure exerted by the soil to the structures generally generate distresses that may induce damages of various degrees to the structures built on swelling soils. Also, the continuous population growth and the consequent urbanization have led to build in areas encompassing with expansive soils escalating the damages to infrastructure (Williams 2003). Problems coupled typically to the presence of expansive soils beneath the foundation system of structures include the following (Kalantari 1991):

2.1.1.1 Pavement distresses

Buckling as well as distortion and cracking in all directions generate bumps which increase the roughness of pavements resulting in poor riding comfort. These problems usually occur due to the swelling potential of the subsoil system (subgrade, subbase, and

base). Figure 2-1 and Figure 2-2 depict rigid and flexible pavement distresses due to expansive soils, respectively.

Figure 2-1 Rigid pavement slab cracking (Caltrans, 2008)

Figure 2-2 Flexible pavement failure (Al Rawas et al., 2005)

2.1.1.2 Floor slab cracking and retaining and building walls cracking

These types of damages are sequential and generally result in a hogging like deformation due to differential movements occurred in the structure in both lateral and vertical directions. Figure 2-3 and Figure 2-4 show a schematic of this type of failure suffered by light structures.

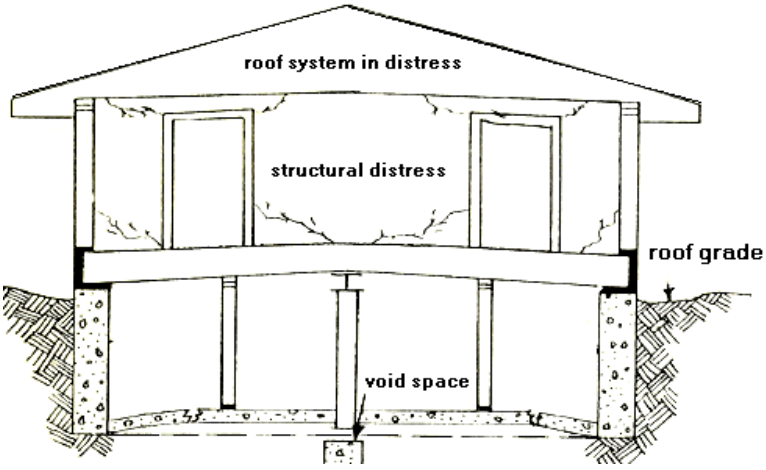

Figure 2-3 Light structures damages caused by subgrade swelling (Kalantari, 2012)

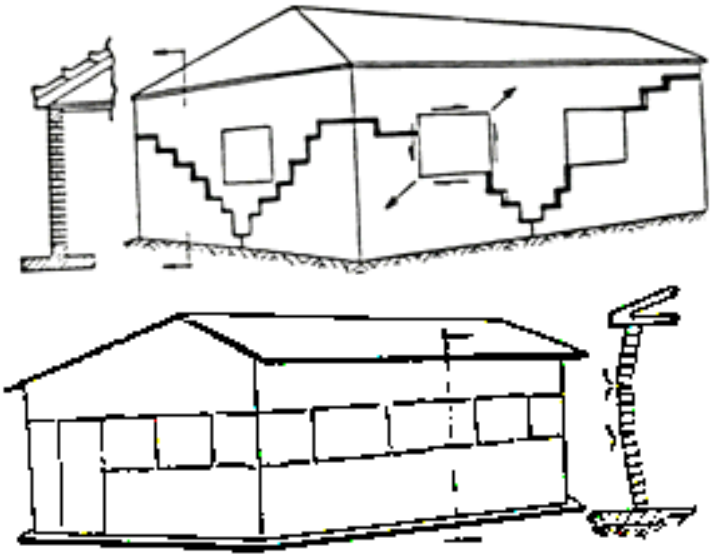

Figure 2-4 Damages in building due to subsoil movement (Kalantari, 2012)

2.1.1.3 Buried pipes - differential movement and cracking

Buried pipes may disjoint or even broke when buried in swelling soils especially when water may be encountered in the surrounding area to the expansive soil. Good practice does not allow pipes to be embedded directly in swelling soils since seasonal rise and shrink differential shifting of the soil mass due to changes in moisture may affect the pipe. Usually, the movements are relatively small however the moisture fluctuation may generate considerable differential displacements between two adjacent points in the soil mass which adversely affect the pipe performance. Mitigation of such adverse effects is accomplished using short lengths with flexible joints for rigid pipes. Flexible pipes are considered to have sufficient longitudinal and diametrical flexibility to allow the pipe to conform to these differential movements without structural distress. Soil mass stabilization is another option (Moser 2001).

2.1.1.4 Slope failures

Slopes stability is affected when the seasonal drying-wetting process generate desiccation cracks during dry season which are filled with water during the rainfall time. It leads to the reduction of the soil shear strength, thus triggering the failure (Rahardjo et al., 2001; Cho and Lee, 2002).

2.2 Identification of swell behavior

Several methods and test have been established to estimate the volumetric change potential of swelling soils. They can be classified as direct and indirect methods. Direct methods comprise a real physical assessment of soil swelling characteristics (i.e. swell percent, swell strain and swell pressure), by means of tests performed in consolidometer apparatus, triaxial test, and free index tests. Indirect methods are supported by developing relations of swell properties with related soil physical, chemical or mineralogical properties (Uzundurukan et al., 2013). Indirect methods yield

correlations which are usually obtained from the application of statistical analysis or more refined techniques including artificial neural network models.

The remaining part of this chapter section presents the most typical apparatus and procedures used to generate a direct physical assessment of swell properties as well as the usually measured swelling characteristics of soil. Indirect methods for estimation of the swelling soils volumetric change potential based on correlations derived from the measured properties are also reviewed.

2.2.1 Laboratory devices used for swell properties determination

In this study, natural soils were used to conduct studies on remolded statically compacted specimens in order to determine the swelling potential of the soils. One dimensional (1D) swell test and swell pressure tests procedures normalized by the ASTM D4546 – 08 standards were followed. Also, a novel three dimensional (3D) swell strain measurement apparatus was used for the measurement of swell strains in all directions (Pedarla, 2013). A brief review on the tests conducted for soil swell potential determination is given in the following.

2.2.1.1 One dimensional (1D) swell strains and pressures

The conventional engineering practice for measuring 1D swell strains has established the use of consolidometer units as a routine procedure. Holtz and Gibbs (1956) and Lambe and Whitman (1959) studied the performance of swell test in consolidometers for assessing expansive soil potential. Since then, numerous efforts have been made to evaluate soil swell behavior with direct measurements of one dimensional strain and swell pressure using consolidometer type apparatus.

Swell pressure becomes important when a soil mass is restrained to swell freely. The swell pressure that a soil may exhibit depends on several intrinsic factors contributing to swell. Generally, lateral and vertical movements are undergone by

structures due to the soil heaving effect exerted by the soil to the structures during the swelling. As a result, variable degrees of damage might be experienced in the structures at locations where expansive soils are found.

To establish the swell pressure in expansive soils, a load back procedure is usually followed. The procedure aims to bring a soil specimen back to its initial height state under fully saturated conditions. The summation of the loads put on top of the soil specimen for making the sample to reach its initial height is computed, and the swell pressure value is calculated as the ratio between the total surcharge load and the specimen area.

In the last decade, the ASTM standardized the engineering procedure for swell strain and pressure determination using consolidometer units by the standard D4546 – 08. This standard presents three alternative methods, designated as Method A, B and C. In the current study, the Method C (loading-after-wetting test) has been followed. Method C requires the specimen to swell under a vertical stress of 1 kPa (20 lbf/ft^2) and to be returned to its initial height as previously explained.

Figure 2-5 taken from the mentioned standard depicts the normal variation of clay swell deformation with logarithmic of time.

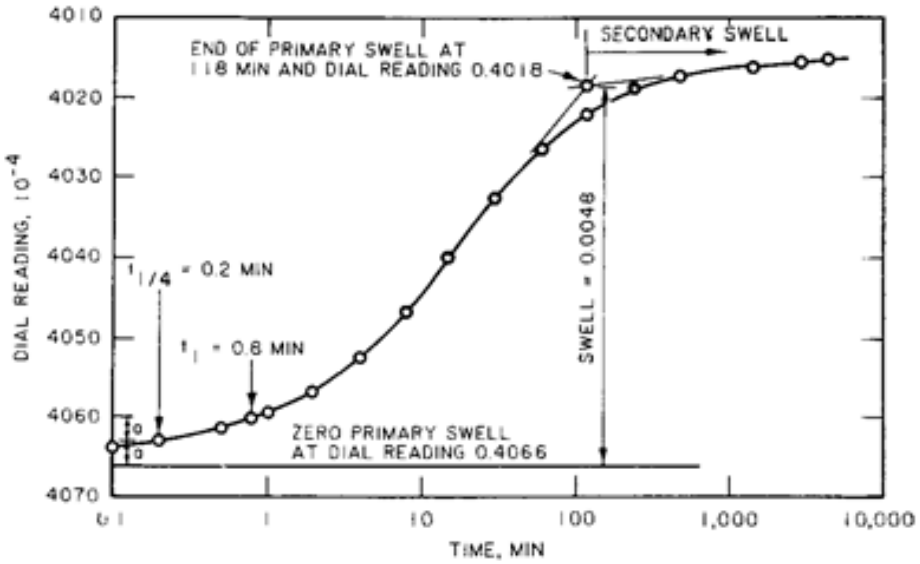

Figure 2-5 Time-swell curve for clay (ASTM D4546 – 08)

Pedarla (2013) developed an extensive literature review on soil swell potential determination using consolidometer like devices. This researcher also performed a comprehensive testing work for determining one dimensional (1D) swell strain and pressure values using a conventional consolidometer setup as shown in Figure 2-6.

Figure 2-6 1-D swell and load back swell pressure test setup (Pedarla, 2013)

Pedarla (2013) collected 8 soils from different places in the USA and tested them following ASTM D4546 – 08 Method C for obtaining 1-D swell strains and pressures of each soil at two different compaction dry densities: maximum dry density (MDD) and 95% of maximum dry density (95% MDD). The results were presented in figures and summarized in tables. Below shown Figure 2-7 presents typical graphs found by Pedarla (2013), which for the case corresponds to the soil from Anthem location.

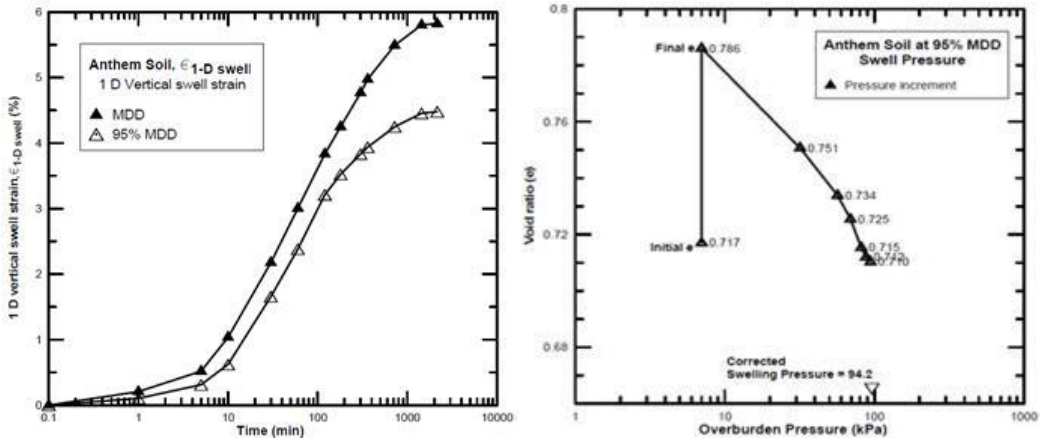

Figure 2-7 Swell strains and pressure for Anthem soil (Pedarla, 2013)

Later, Pedarla (2013) used the data for establishing 3 novel methodologies for indirect determination of swell behavior potential.

In swelling strain and pressure determination, Pedarla (2013) was aware of the procedural factors that affect the swell results obtained from a standard Oedometer as reported by Fredlund (1969). Hence, compressibility of different elements like filter paper and porous disks as well as appliance arm deformation was considered, and in consequence, correction factors for all these types of procedural elements responsible for the inaccurate swell prediction were applied during the research development.

Kayabali et al. (2009) performed test for determining 1D swell strains and pressures on reconstructed identical soil samples produced from 12 natural soils.

Different procedures for testing were employed which they designated as direct method and 4 indirect methods listed next: restricted swell, swell-consolidation, double oedometer, and zero swell tests.

The direct method comprised an apparatus with a main frame, a load cell of 5 kN capacity, a floating ring–type conventional oedometer cell, and a digital read-out unit as shown in Figure 2-8. The technique was designated direct method since it provides the swelling force directly.

Figure 2-8 Apparatus for direct method (Kayabali et al., 2009)

When running this test, the soil sample in the consolidation ring was first placed into the oedometer cell or the consolidometer. Then, it was placed in the loading device and a seating load of 10 N was applied, so that there was no gap between the metal bar connected to the load cell and the upper cap on the soil sample. Finally, the soil sample was inundated and left to swell. The swell force was recorded at the end of 24 hours and the initial seating force was deducted. The remaining net force was divided by the cross-

sectional area of the soil sample and recorded as the swelling pressure for the direct method.

In the restricted swell tests, 4 identical specimens of each soil were placed in consolidometer cells and vertical stresses were applied to it in a range in which the expected swelling pressure may remain. After loading, the specimens were inundated and swelling was expected to take place. However, the specimens loaded at less than the swelling pressure expanded, while those loaded at more than the swelling pressure compressed. The results were plotted as the percent change in specimen height versus vertical stress. The point on the vertical stress axis where the zero deformation line crosses the experimental curve was selected as the swelling pressure.

In the swell-consolidation test, three specimens for each soil sample were placed in the consolidometer and immediately inundated and allowed to swell freely. A record of the free swell was taken at the end of 24 hours when an incremental vertical stress usually starting at 25 kPa was applied to the sample. An increment ratio of 1 was assumed. The stress increment was kept until the amount of free swell was totally eliminated. A graph containing the percent change in sample height and the vertical stress was plotted. The point at which the curve crosses the horizontal zero percent change line was assumed to be the swelling pressure.

Three couples of specimens of just one soil chosen among the 12 soils used in the research were used in the double oedometer test (Jennings et al, 1957). Each pair of samples was subjected to consolidometer tests. Simple swell test was conducted on one of the samples, in which the soil specimen was first inundated and the percent change in the sample height (i.e., free swell) was recorded at the end of 24 h. The second sample was tested at its natural water content and was subjected to a vertical stress generally in the range of 25 to 100 kPa. Loading continued until the amount of expansion experienced

with the free swell test was surpassed. A plot with the percent change (i.e., compression) in the sample height versus vertical stress was drawn. The vertical stress corresponding to the decimal value of the percent of expansion change (from the free swell test) in the vertical axis was determined to be the swelling pressure.

In the zero swell tests, three specimens of each soil were used. All the samples were placed in a consolidometer, and an initial seating load of 7 kPa (1 psi) was applied, and the extensometer deformation device was adjusted to read zero. The specimen was then inundated and increments of vertical stress were applied to prevent swelling. Variations from the deformation reading at the time the specimen was inundated were preferably kept between 0.005 and 0.010 mm. The specimen was kept under pressure until there was no tendency to swell. The vertical stress at this point was recorded as the swelling pressure.

After running the testing previously outlined, the researchers concluded, for instance, that while the restricted swell test slightly underestimated swell pressure, swell-consolidation and zero swell tests overestimated it. Also, that no correlation was found among the results of swell pressures yielded by the double oedometer test and the direct method. Lastly, that the free swell and swell pressure data from the direct method correlated reasonably well. After performing this comprehensive testing work, by trying the different methods previously summarized, Kayabali et al. (2009) came up with an empirical correlation established from the free swell and direct methods data. The relationship allows the swell pressure to be estimated.

However, a very important observation made by the same authors after developing swell tests involving different physical mechanisms was related to their concern on the reliability of the results reported by researchers and intended to be used to predict swelling behavior.

Researchers had used several types of devices for determining the soil swelling characteristics. Thus, at this point it is important to remark that due to the intrinsic differences in the devices reported by the literature and also to procedural issues, the characterization of expansive soils might generate scattered or inaccurate results and characterizations from one research to other, even when testing the same type of soils. It represents a limitation on swelling behavior characterization and might be revised in future with further detail.

2.2.1.2 Three dimensional (3D) swell strains

Punthutaecha et al. (2006) conducted a study based on three-dimensional free swell tests aiming to determine the soil maximum volumetric swell potential with an acceptable level of reliability and repeatability. The test investigated the maximum vertical, radial and volumetric swell potentials. Specimens of 4 in diameter and 6 in height were tested. The samples were placed with porous stones at top and bottom and protected by a rubber membrane. Then, water was allowed to inundate the samples at their ends and the increments on vertical and radial dimensions due to swell were recorded until the expansion stopped. The radial swell movement measuring procedure was kept simple by using only Pi tape at the predefined intervals of recording. The results were reported as the percentage of swell strain versus time.

Pedarla (2013) performed tests using the 3-D swell strain apparatus designed at the University of Texas at Arlington and targeting to determine the lateral swell strains exhibited by a soil specimen when confined in all the perpendicular three dimensions.

The test main objective was to simulate the swell strains of a soil mass present at a desired overburden depth. The 3-D swell strain apparatus is depicted in Figure 2-9.

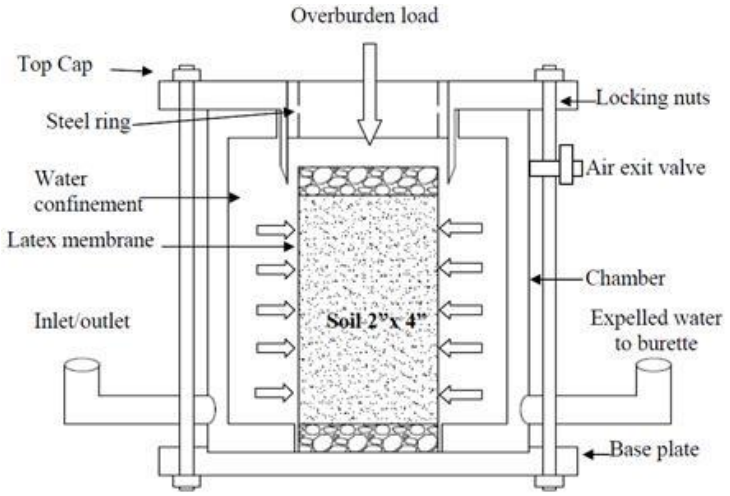

Figure 2-9 3-D Swell strain test setup designed at UTA (Pedarla, 2013)

The soil specimen dimensions were 10.16 cm (4 in) in height and 5.08 cm (2 in) in diameter. The soil sample was placed inside the pressure acrylic chamber coated with a latex membrane to avoid the water in chamber to moist the sample. Then, the chamber had to be filled with de-aired water as a confinement medium. Porous disks were located at top and bottom of the soil specimen, and a steel ring was attached to the top porous disk to prevent the horizontal or lateral confinement to interfere with the vertical surcharge. Hence both the confinements were achieved independently. A general view of the test setup is shown in Figure 2-10.

Figure 2-10 3-D Swell strain test setup (Pedarla, 2013)

After following the procedure outlined above, the soil specimen was allowed to saturate for a period of 24 hours at confinement levels of 7 kPa (1 psi), 50 kPa (7.25 psi), and 100 kPa (14.5 psi) acting on the sample at all times. A dial gauge recorded the vertical strains and a correlation between the water volume change and the areal change for the soil specimen was made to obtain the horizontal strains. The apparatus design principle allowed to assume the height of the chamber to remain constant during the volume change, thus, the latter is only related to the specimen areal change.

To account for the water absorption in the acrylic material a calibration procedure using a steel bar of similar dimensions as soil specimen was performed and the correction factors for the volume change measurements were presented in a graphical form and considered during the results analysis.

Pedarla (2013) tested 8 soils collected from different places in the USA in the 3-D Swell strain apparatus following the previously explained procedure. The soil samples were compacted and tested only at 95% of their maximum dry densities (95% MDD). The results were presented in figures and summarized in tables. Later the researcher performed statistical simple linear analyses with the data for obtaining relations for indirect determination of the three dimensional swell behavior potential of soil at three different confinements.

2.2.2 Indirect methods for assessing swelling behavior

Since assessing swelling potential based on indirect methods is relatively simple, quick and inexpensive, several methods of this type have been established and may be found in the literature. In general, the majority of indirect methods correlations is determined from statistical procedures bearing on simple or multiple regression analysis or may be found from more sophisticated techniques (i.e. neural networks). The relations usually rely on plasticity based soil properties or on activity and compaction properties. Further refined indirect methods include more advanced soil index properties as cation exchange capacity, specific surface area, and suction, among others.

2.2.2.1 Correlations based on basic soil indexes

Time constrains or simply lack of funds make often contractors to consider impractical the development of a comprehensive study for assessing soils swelling behavior according to the procedures required by direct methods. When it occurs,

correlations are available which are generally semi-empirical since are derived from some mechanics or purely empirical based on statistical analysis.

The correlations may evaluate the swelling potential of clays from parameters like liquid and plastic limit, activity and clay content. However these correlations have been obtained from solely these basic soil parameters without considering other important factors influencing swelling (suction, soil texture or pore structure). Hence, the relationships might not represent the real expansive soil potential. Some of the indirect methods used for swell potential prediction and based on basic soil indexes are given below.

Holtz (1959) presented the currently known as the Bureau of Reclamation method. It involves the direct correlation of observed volume change with colloidal content, plastic index, and shrinkage limit. The measured volume change is taken from odometer swell tests using 1 psi surcharge pressures and represents the change from a dry to a saturated condition. Therefore, much less expansion is expected to occur in the field since such extreme moisture variation may not take place and the subgrade will have been compacted to the appropriate density. Also, all the three index tests should be considered in estimating expansive properties.

The degree of expansion and limits of correlated properties are shown in the following tabulation:

Table 2-1 Classification of expansive soils (Holtz, 1959)

Degree of expansion	Probable expansion (%)	Colloid content %-1 μm	Plasticity Index	Shrinkage Limit (%)
Low	<10	<15	<18	>15
Medium	10-20	13-23	15-28	10-16
High	20-30	20-31	24-41	7-12
Very high	>30	>28	>35	<11

Seed et al. (1962) developed a classification chart based exclusively on the amount and type (activity) of clay size particles. When using this chart, the percent clay size refers to the clay fraction of the whole sample. Activity is defined as the ration between plastic index and clay fraction, which is that part of the soil specimen that is finer than 0.002 mm, based on dry weight. Figure 2-11 depicts the Seed's chart.

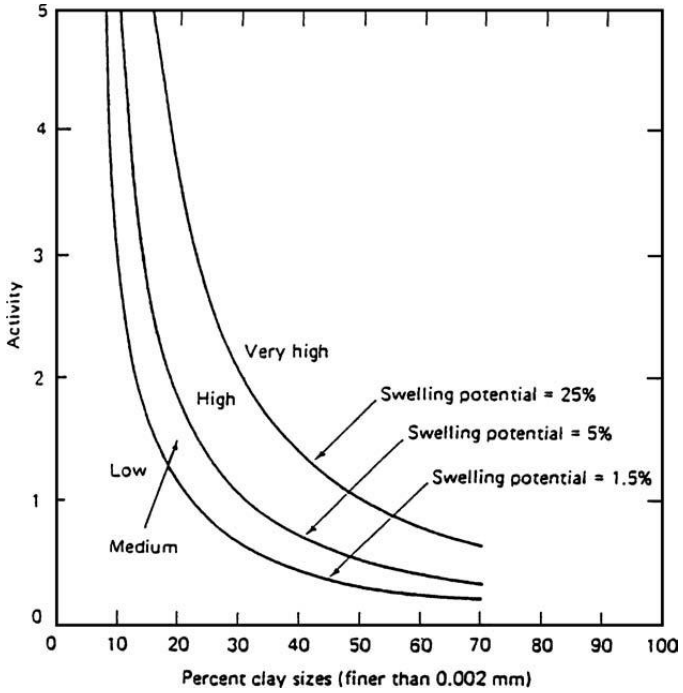

Figure 2-11 Swelling potential classification chart (Seed et al., 1962)

Van der Merwe (1964) also proposed a chart that requires three items: plasticity index and clay percent of the whole sample, and activity of the clay size particles. This chart shown below in Figure 2-12 was frequently used by many practitioners to assess the expansiveness of clays.

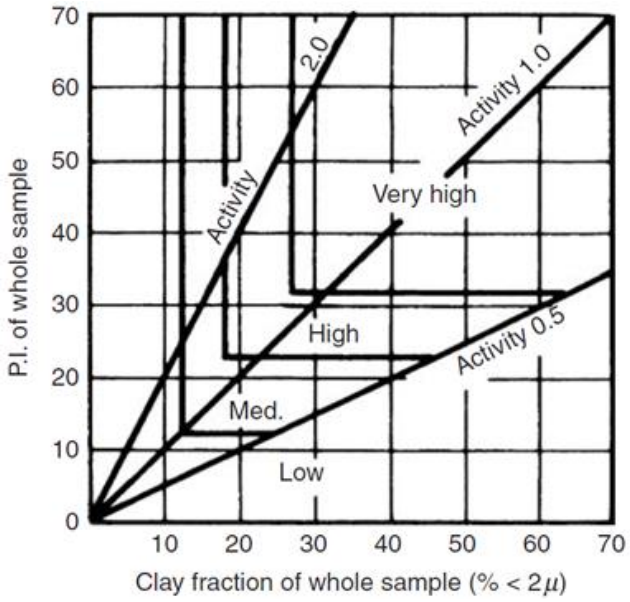

Figure 2-12 Swelling potential classification chart (Van der Merwe, 1964)

Dakshanamurthy et al. (1973) proposed another frequently used graphical chart to estimate the soil swelling potential. In this case, only the liquid limit and the plasticity index are necessary for assessing the swelling behavior of clays. Figure 2-13 presented below shows the chart proposed by these authors.

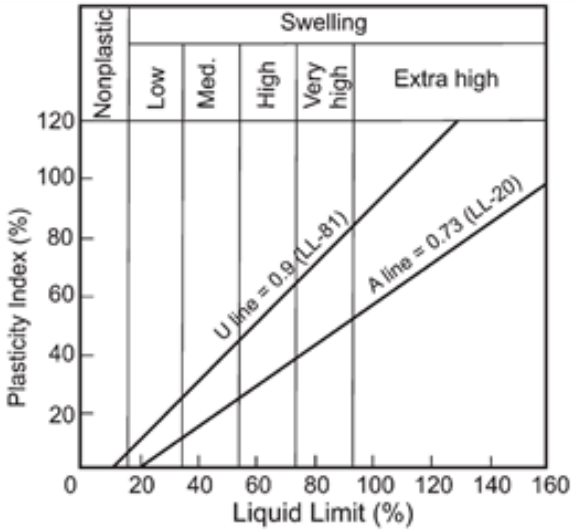

Figure 2-13 Swelling potential classification chart (Dakshanamurthy et al., 1973)

Sridharan et al. (2000) suggested a classification of expansive soils following different criteria given by the literature. It was established in accordance with the USA Bureau of Reclamation (USBR) basic guidelines as given by Holtz (1959).

USBR method followed considers the total volume change of a soil from air dry to a saturated condition under a surcharge of 7 kPa, in an oedometer apparatus as the main criterion to be considered when evaluating the expansiveness of a soil.

Thus, the results obtained from oedometer swell tests conducted on air dry soils must be taken as a reference point.

The classification provided by Sridharan et al. is shown in Table 2-2.

Table 2-2 Classification of expansive soils (Sridharan et al., 2000)

Degree of expansion	Colloid content: %-0.001 mm	Shrinkage Limit (%)	Shrinkage Index (%)	Free swell Index (%)	Percent expansion in oedometer (Holtz et al.)	Percent expansion in oedometer (Seed et al.)
Low	<17	>13	<15	<50	<10	0-1.5
Medium	12-27	8-18	15-30	50-100	10-20	1.5-5.0
High	18-37	6-12	30-60	100-200	20-30	5-25
Very high	>27	<10	>60	>200	>30	>25

As with swelling potential, numerous researchers developed correlations and models for the prediction of swell pressure having basic soil parameters as input variables (moisture content, density, clay content, etc.).

Table 2-3 presents selected correlations and models for swell pressure prediction established by several researchers.

Table 2-3 Correlations for swell pressure prediction (Hanumantha Rao et al., 2011)

Relationship	Reference
$Log(Sp) = 2.132 + 0.0208LL + 0.000665\gamma_d - 0.0269w$	Komornik et al. (1969)
$Sp = 0.035817PI^{1.12}(C^2/w_i^2) + 3.7912$ $Sp = 0.0229PI^{1.45}(C/w_i) + 6.38$	Nayak et al. (1971)
$Log(Sp) = 0.9(PI/w_0) - 1.19$	Schneider et al. (1974)
$Log(Sp) = -2.89 - 7w + 6.65CL$	McCormack et al. (1975)
For $PI \geq 40$, $Sp = 23.82 + 0.7346PI - 0.1458H - 1.7w0 + 0.0025PI*w0 - 0.00884PI*H$ For $PI < 40$, $Sp = -9.18 + 1.5546PI + 0.08424H + 0.1w0 - 0.0432PI*w0 - 0.01215PI*H$	Johnson (1978)
$Sp = 0.0446LL - 1.572$ or $Sp = 0.057PI - 0.566$	Nayak (1979)
$Log(Sp) = -4.812 + 0.01405PI + 2.394\gamma_d - 0.0163w_i$ $Log(Sp) = -5.197 + 0.01405PI + 2.408\gamma_d - 0.819IL$ $Log(Sp) = -5.020 + 0.01383PI + 2.356\gamma_d$	Erzin et al. (2004)
$Sp = 63.78e^{0.1528S}$	Sridharan et al. (2004)

Where Sp: swelling pressure (kg/cm^2, psf)

LL: liquid limit

γd: dry density (g/cm^3)

w: moisture content (%)

PI: plasticity index

wi, w0: initial moisture content (%)

CL: clay content (%)

H: depth of sample (ft)

IL: liquidity index

e: void ratio

S: percentage swelling (%)

As previously outlined, correlations supported on basic index parameters like plasticity index or liquid limit or combinations of two or more of these like PI, activity, compaction density or void ratio have been developed by several researchers.

However, it is important to mention that soil plasticity is typically identified by a process that demands remolding the soil, therefore, the above presented methods are unreliable since the influence of soil texture, moisture content, soil suction or pore structure is not considered for swelling potential evaluation. As previously explained, the latter factors are important to assess the volume change potential of expansive soils.

2.2.2.2 Correlations considering advanced soil parameters

In the last two decades, researchers have made efforts to improve the correlations for assessing the soil swelling behavior by considering more advanced index parameters of soil like cation exchange capacity, specific surface area and suction. Some of these approaches are presented in the following paragraphs. Also, a detailed description for mentioned advanced index parameters is presented in later sections of this chapter.

Yilmaz (2006) described the dependence of the swell percent on index soil properties named liquid limit (LL) and cation exchange capacity (CEC). The correlation was found after the development of a statistical analysis supported on the results given by testing 141 soil samples taken from various places in Turkey for swell strain and pressure. The analysis allowed the author to propose a model based on a multiple regression with high prediction performance. The author provided a graphical classification having four respective zones indicating the low, moderate, high, very high swelling potential. In this study, the swelling percent and pressure of the 141 undisturbed soil samples taken from various locations were carried out in accordance with ASTM D-4546 (1994). A 0.07 kgf/cm^2 pre-loading pressure and samples with a radius of 5.0 cm

were used. The LL was determined according to the procedure defined by the British Standard (BS) 1377 (1975). The CEC of soils were determined by using the ammonium acetate (NH4OAc) method (Bache, 1976). The classification graph is shown below in Figure 2-14.

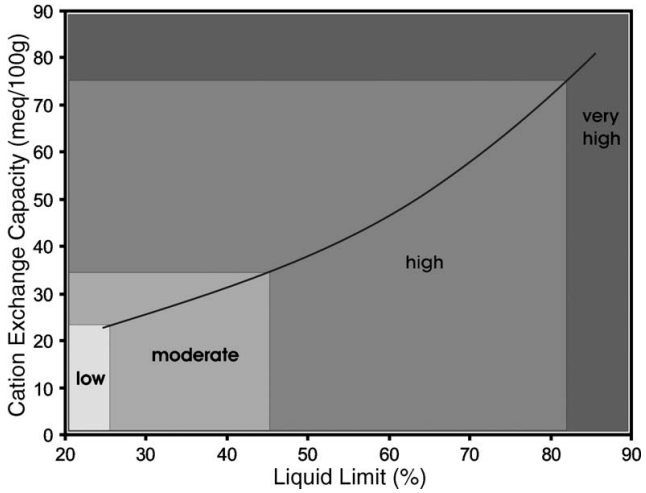

Figure 2-14 Swelling potential of soils based on CEC and LL (Yilmaz, 2006)

Erzin et al. (2013) were aware about the time consuming and special and expensive equipment required to measure swelling soil properties and therefore in the study the authors attempted to investigate the relationship among the swelling properties and easily obtained soil properties using two pure Turkish commercially traded clay minerals (Kaolinite and Bentonite) and four mixtures at various percentages of them (Kaolinite: 5, 10, 15, 20%; Bentonite: 95, 90, 85, 80%) to obtain soils in a wide range of plasticity indices. As a result, free swell percent was correlated to clay percent, water content, dry unit weight, plasticity index, liquidity index and cation exchange capacity by applying multiple regression analyses. A reasonable high coefficient of correlation was found for the relationship between the percent swell and swell pressure values for samples having a swell pressure less than 300 kPa.

The authors assumed the proposed equations to offer a rapid and inexpensive substitute for laboratory testing of swell percent/swell pressure in the preliminary stages of site investigations. Finally the authors conclude that an increase in the bentonite content in the clay mixtures yielded an increase in the CEC, SSA, LL and plasticity index (Ip) values while the plastic limit (PL) was virtually unaffected by increases in the bentonite content. They highlighted according to the previously outlined, that the CEC, SSA, LL and Ip values of the clay mixtures are more sensitive to changes in clay mineralogy than the case for PL, and observed that the LL values are controlled by the CEC and SSA values.

In this research, the swelling characteristics of the clay mixtures were performed in general accordance with ASTM D-4546-96 using a 76 mm id oedometer cell. Also, the liquid and plastic limits (LL, PL) were assessed according to ASTM D-4318-05 (1994); the cation exchange capacity (CEC) was found using the Na method (Chapman, 1965); the specific surface area (SSA) using the BET-N2 adsorption method with a Quantachrome NovaWin2 device (Branauer et al., 1938).

The correlations they found for prediction of percent swell (S) and swell pressure (Sp) values are given below by Equations 2-1 to Equation 2-3.

$$S = -31.321 + 0.592\,C + 0.717\,Ip - 0.807\,CEC - 0.891\,w + 2.2668\,\gamma d \qquad 2-1$$

$$S = -9.567 + 0.606\,C + 0.636\,Ip - 0.792\,w - 0.487\,\gamma d + 6.289\,LI \qquad 2-2$$

$$Sp = 1.9319 * S^{1.2897} \qquad 2-3$$

Where,

C: clay percent (C)

Ip: plasticity index

CEC: cation exchange capacity

w: initial water content

γd: initial dry unit weight

LI: liquidity index (LI).

De Bruyn et al. (1956) published maybe the first academic reference in highlighting the importance of the specific surface area (SSA) as a tool for determining the swelling potential of soils with engineering purposes. The researchers outlined that the water affinity of soils is a necessary condition for potential expansiveness, and that it is determined by (i) the pore dimensions, (ii) the amount of the specific surface, and (iii) the chemical composition of that surface (De Bruyn, 1955). Since expansive soils generally contain appreciable amounts of montmorillonite and illite types of clay minerals having high specific surface area, the determination of this soil feature by means of, for example, the glycol method (Dyal and Hendricks, 1950) is affordable and yield a reliable index for water affinity and hence also for the possibility of potential expansiveness. Moreover, the researchers underlined the advantage this method has of being much simpler than a clay mineralogical analysis.

In this study, twenty five (25) soil samples from the literature were investigated to conclude that soils with total specific surface areas of less than 70 m^2/g and equilibrium moisture contents (at 85 per cent. humidity) of less than 3 per cent. may be classified as non-expansive (good samples) and those with total specific surface areas of more than 300 m^2/g and equilibrium moisture contents (at 85 per cent. humidity) of more than 10 per cent. as expansive (bad samples).

The samples with results within the intermediate ranges were classified as medium expansive soils. Finally, the researchers remarked the tentativeness of the mentioned classification since the ranges were arbitrarily established.

Yukselen-Aksoy et al. (2010) intended to predict the swelling potential of soils by a direct correlation to specific surface area. SSA was determined by three different

methodologies: BET-N2 adsorption ((Brunauer et al., 1938)); ethylene glycol monoethyl ether (EGME, Cerato et. al, 2002) and methylene blue (MB, Santamarina et al., 2002) and then correlated with the swell index and modified free swell index of soils according to the results obtained from 16 remolded and 15 undisturbed soil samples consisting of a wide range of mineralogy.

The swell indices of the samples were investigated with a one-dimensional consolidation test apparatus according to ASTM D-2435 (1992). The samples were tested in a standard fixed-ring consolidometer using stainless steel rings.

The investigators noticed significant correlation between the SSA and the swelling behavior of the tested clayey soils, as well as a linear increasing relationship between the swell index and the specific surface area found using methylene blue method (SSA-MB). According to these finding a swelling potential classification was proposed as presented in Table 2-4.

Table 2-4 Classification of expansive soils (Yukselen-Aksoy et al., 2010)

SSA-MB (m^2/g)	Degree of expansion
<70	Low
70-150	Medium
150-300	High
300-400	Very high
>400	Extra high

Correlations for soil swell behavior determination based on suction have been also developed by several researchers (McKeen, 1992; Cocka, 2000, 2002, Pedarla, 2013; Uzundurukan et al., 2013). However, since suction is highly related to the objectives pursued by the present research, and it substantially influences the soil

behavior, it will be discussed with further detail in a subsequent section of this literature review dedicated solely to soil suction.

2.2.3 Final remarks on swell prediction practice

Researchers have developed several indirect methods supported by correlations to identify the swell behavior of soil. These correlations has been widely used in common engineering practice due to their simplicity and also due to the time constrains in the construction projects or simply lack of funds for direct evaluation of soil swelling characteristics.

The correlations are usually based on basic index parameters of soil named: plasticity index, liquid limit, activity, compaction density, void ratio, cation exchange capacity, specific surface area, among others.

At this point it is important to underline that since the index parameters are found from remolded samples, the correlations they support do not consider key parameters of soil at intact or compacted condition as texture, moisture content, suction and pore structure which highly influence the volumetric changes undergone by a sample of soil. Hence, the generation of a more robust framework which includes fundamental variables to evaluate the swelling behavior of soils under natural or laboratory made condition is a need.

The present research tries to perform a comprehensive study on the parameters responsible for the soil volume change behavior based on direct determination of swelling features of soil like mineralogy, variation of suction with moisture content (SWCC) and pore distribution. Also, this study will intend to establish a comprehensive methodology and to propose a model based on SWCC-Clay mineralogy for obtaining a more accurate prediction and simulation of swelling soil behavior.

2.3 Mineral components of clayey soil

Geologic history, sedimentation, and present local climatic conditions have a crucial role in the origin and distribution of expansive materials around the world. The individual action of one of these factors or their combined action contribute to the expansive soils formation. The expansive material term refers to any earth material which exhibits significant volume changes in the presence of water (Snethen et al., 1975).

Expansive soils may have a sedimentary or residual origin. The latter are altered materials which have formed upon existing rocks or sediments and may owe their expansive character to the parent material and/or to the weathering processes under which the soils were formed.

Although each category of material possesses different intrinsic properties, each may exhibit varying degrees of expansion due to the presence of active clay minerals in the material.

The active clay minerals include montmorillonite, mixed-layer combinations of montmorillonite and other clay minerals, and under some conditions chlorites and vermiculites. Kaolinites and illites are usually not considered active although they may contribute to expansive properties if sufficient amounts are present in the material (Snethen et al., 1975).

In general, the distribution of expansive materials is controlled by those conditions which facilitate the formation, accumulation, and preservation of montmorillonite.

The formation or origin of montmorillonite is facilitated by the individual or conjunct action of the following conditions: weathering, diagenetic alteration of preexisting minerals and hydrothermal alteration. From them, weathering and diagenesis are maybe the more important (Millot 1970)

The sedimentary accumulation of montmorillonite originates in those areas which receive land-derived montmorillonite and/or volcanic ash sediments. The areas must either lie near or be stream connected to land areas where montmorillonite was formed by weathering and/or lie sufficiently near volcanic areas such that volcanic ash sediments can be carried either in the air or by streams to the areas of accumulation (Carrol 1970).

The preservation of sedimentary deposits of montmorillonite involves all those factors which may affect the material from the time that it was deposited until it is exposed at the earth's surface; basically, this falls within the limits of diagenesis. The diagenetic factors that may affect a sedimentary deposit consist of the following: (a) deep burial resulting in high lithostatic (overburden) pressure, (b) temperature increases resulting from the burial, (c) chemical effects produced by pore solutions, and (d) time exposed to high pressures (Snethen et al., 1975).

A brief review on the main features of the dominant clay minerals: montmorillonite, illite and kaolinite is given in the next paragraphs. Also a summary of a novel procedure for quantification of these dominant minerals in a particular soil is presented (Chittoori et al., 2011). The method relies on parameters such as cation exchange capacity (CEC), specific surface area (SSA) and total potassium content (TP).

2.3.1 Montmorillonite

Montmorillonite is a three-layer clay mineral, which has one octahedral layer bonded between two tetrahedral layers. The term montmorillonite normally indicates the dioctahedral magnesium bearing member of the smectite group. Montmorillonite occurs dioctahedral and usually contains some magnesium substituted for aluminum in the octahedral layer. This substitution results in a lattice charge deficiency which is neutralized by the presence of cations such on interlayer positions (Grim 1968).

Although these ions possess ionic radii that would permit occupancy of the space within the hexagonal opening at the surface of the tetrahedral layers, the ions are hydrated and as a result of increased ionic radii must occupy space on and above the tetrahedral layers. Such a position props adjacent layers apart and permits access of more water to interlayer positions. Since the interlayer ions balance charge deficiencies in the octahedral layer, the ions are weakly held and thus may be removed by ion exchange. Ordinarily, montmorillonite exists as extremely small particles with dimension on the order of a few tens of Angstrom units.

2.3.2 Illite

This three-layer clay mineral exhibits minor interlayer swelling. This results from the presence of nonhydrated K+ ions in interlayer positions within the hexagonal openings of the tetrahedral layer. The K+ satisfies charge deficiencies residing mainly on the tetrahedral layer and is thus tightly bonded. These characteristics effectively preclude the admission of significant amounts of water between the unit layers (Snethen et al., 1975).

2.3.3 Kaolinite

The clay mineral kaolinite is a two-layer clay mineral, consisting of one silica tetrahedral layer bonded to one aluminum octahedral layer. This mineral exhibits very minor interlayer swelling. This is explained by the virtual absence of ionic substitution in either the tetra- or octahedral layers which results in more or less complete electrical neutrality and the absence of compensating cations. Also, the individual two layer structures are more tightly bonded together by the opposing electrical charges on the adjacent octahedral and tetrahedral layers. Therefore, the volume change exhibited by this mineral is mainly due to water sorbed on the periphery of individual grains (Grim 1968).

2.3.4 Clay minerals quantification procedure

Chittoori et al. (2011) presented a rational and practical methodology to determine both clay mineralogy distribution and dominant clay mineral in any clays soil by using three measured chemical soil properties named cation exchange capacity (CEC), specific surface area (SSA) and total potassium (TP).

The basic assumption made was that the mentioned soil properties are dependent on clay mineral constituents, thus, literature supported procedures to determine these properties were studied and applied to determine and evaluate clay minerals present in artificial and natural clayey soils of known and unknown clay mineralogy.

A total of twenty natural and six artificial soils were considered and used in the chemical analyses (Chittoori et al. 2011). Test results were analyzed using artificial neural network (ANN) based models for final determination of clay mineralogy distribution and dominant clay mineral.

2.3.4.1 Cation Exchange Capacity (CEC)

The cation exchange capacity can be defined as the soil capacity or the ability to exchange free cations available in the exchange locations. It is simply a measure of the quantity of readily exchangeable cations neutralizing negative charged ions in the clay mineral (Chapman 1965; Camberato 2001). Soil mineral composition is related to CEC because a high CEC value indicates the presence of a clay mineral such as montmorillonite, whereas a low CEC indicates the presence of inexpansive clay mineral such as kaolinite.

Several methods have been utilized to determine the CEC of a soil. These methods may be classified into four categories: summation method; direct displacement method; displacement after washing method; and radioactive tracer method (Rhoades,

1982). Significant differences in the results may be encountered when performing the methods in the same soil since there are many complicating interactions at the saturating, washing, and extracting solutions within the soil sample. Also CEC depends on soil pH and organic content (Rhoades 1982).

Chittoori et al. (2011) selected the method proposed by Chapman (1965) since it provides repeatable and reliable CEC results, requires simple apparatus for laboratory testing, and can be easily implemented or conducted in commercial and research laboratories.

Further details of the procedure proposed by Chapman (1965) may be seen in the present document references (Chittoori; 2009). Also a summary of this procedure will be presented in the methodology chapter of this document.

2.3.4.2 Specific Surface Area (SSA)

The specific surface area of a soil is the total surface area of the soil particles contained in a unit mass of soil. This property primarily depends on the particle size distribution of the soil mass; thus, soils having a large number of smaller particle sizes typically have higher specific surface areas. High SSA in a clayey soil implies that the soil has high capacity to hold inter particular water and in consequence might exhibit greater swell potential.

The hydrophilic behavior of clayey soils possessing large surface area is explained on the fact that the surface area is negatively charged and consequently attracts dipole positively charged-natured water.

Numerous approaches may be used to measure specific surface area, including adsorption of nitrogen and other gases on the soil (Yukselen and Kaya 2006). However, agronomic and soil sciences commonly use the adsorption of ethylene glycol monoethyl ether method (EGME; Carter et al. 1986).

Cerato and Lutenegger (2002) evaluated the method potential for application in the geotechnical field and concluded that it is applicable to a wide range of soils with diverse clay mineralogies and is suitable to be used on soils with SSA ranging from 15 m^2/g to 800 m^2/g. The authors found the procedure ensures obtaining repeatable and reliable results. Based on the previous mentioned advantages, in the research, Chittoori et al. (2011) selected the EGME method as proposed by Carter et al. (1986).

Further details of this procedure (Carter et al. 1986) may be seen in the present document references (Chittoori; 2009). Also a summary of the latter will be presented in the methodology chapter of this document.

2.3.4.3 Total Potassium (TP)

Potassium is the cation present at illite interlayers spaces. Also, it is only the illite mineral in clayey soils which possessing potassium in its structure. Therefore, a measurement of the potassium ions in a particular soil will provide a direct indication of the presence of illite.

Chittoori et al. (2011) followed the test procedure formulated by Knudsen et al. (1982) to obtain the amount of total potassium present in the tested soils.

Procedural steps followed for the determination of total potassium are outlined in this document references (Chittoori; 2009) and the methodology chapter.

2.4 Soil suction relationship and swelling prediction methodologies

2.4.1 Basic concepts and relationships

The measurement of soil suction (matric suction or total suction) and its relation to the amount of water present in the soil (either gravimetric, w, or volumetric water content, θ), is known as the soil–water characteristic curve (SWCC). The SWCC is an indispensable input data for modeling and understanding the behavior of unsaturated soil since it influences all the unsaturated soil properties i.e. strength, permeability, volume

change, solute and thermal diffusivity, among others (Fredlund and Rahardjo 1993; Fredlund and Xing 1994; Vanapalli et al. 1996; Burckhard et al. 2000; Yang et al. 2004; Thakur et al. 2005; Erzin and Erol 2007; Sreedeep and Singh 2011).

The term “characteristic” may be understood as intrinsic, implying that for a given soil there is only one SWCC profile (Nuth and Laloui 2008). However, it has been noticed that there are different parameters that would influence the SWCC, and hence, its uniqueness.

The full comprehension of the SWCC depends on the influence of parameters such as compaction state, measurement procedures, stress history, range of suction measurement on the SWCC, compaction water content, density, etc. (Barbour 1998; Jotisankasa 2005).

Total soil suction (ψ) is a measure of the energy required to expel a unit volume of water from an unsaturated soil (Fredlund and Rahardjo 1993). Matric suction and osmotic suction are the major components of total suction. Matric suction (ψm) may be attributed to the adsorptive and capillary force existing in the soil matrix. Osmotic suction (ψo) results from the presence of salts or contaminants in the soil pore water (Krahn and Fredlund 1972; Lu and Likos 2004). When there is no contamination total suction equals matric sution.

A typical SWCC under drying and wetting paths is depicted in Figure 2-15 (Malaya et al., 2011). As seen in the figure, hysteretic continuous S-shaped relationships are evident. The hysteretic behavior implies that at any specific water content, a drying SWCC has higher suction than a wetting curve (Birle et al. 2008).

Some of the fundamental features in the SWCC as shown in Figure 2-15 are the following (Malaya et al., 2011):

1. The volumetric water content at saturation, θs, describes the water content at which the soil is completely saturated. This depicts the initial state of the drying path.

2. The air-entry value (AEV), ψa, is the suction at which air first enters the largest pore present in the soil sample during a drying process (Brooks and Corey 1964).

3. Residual water content, θr, is the minimum water content below which there is no appreciable change in θ with ψ. Suction corresponding to θr is called residual soil suction, ψr (Yang et al. 2004).

4. The water-entry value, ψw, on the wetting SWCC is defined as the suction at which the water content increases significantly during the wetting process (Birle et al. 2008).

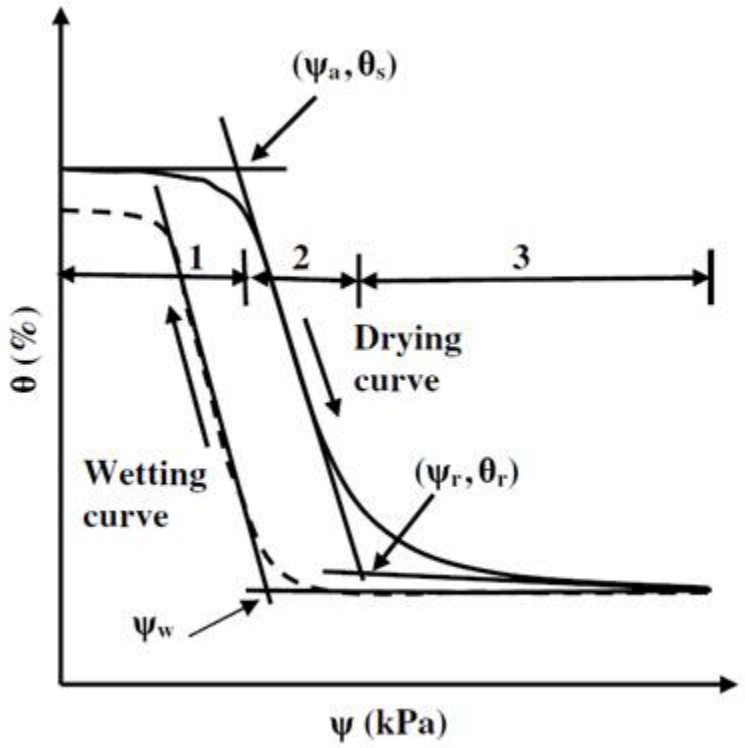

Figure 2-15 Idealized drying-wetting SWCC (Malaya et al., 2011)

A fully saturated soil specimen having a volumetric water content of θs desaturates in three stages, as displayed in Fig. 2.15 (Sillers et al. 2001).

Stage 1 (known as the capillary saturation zone) extends up to AEV. In this stage, the soil remains saturated with the pore-water held under tension as a result of capillary forces. In the desaturation zone (stage 2), ranging from AEV to ψr, there is a sharp decrease in water content, and the pores are increasingly occupied by air. The slope of the SWCC in this portion describes the rate of water lost from the soil (Agus et al. 2001). In the third stage also known as zone of residual saturation (>ψr), there is little hydraulic flow. However, there may be some water movement in the form of film flow (Huang et al. 1994). Beyond this point, an increase in soil suction does not result in significant changes in water content. The zone of residual saturation is terminated at oven dry conditions (i.e., water content equal to zero), corresponding to a theoretical soil suction of approximately 106 kPa (Croney and Coleman 1961).

Malaya et al., (2011) performed a comprehensive review of different parameters that influence the SWCC deducing the conclusion presented in the following. The compaction water content has a more significant influence on the SWCC than density. However the compaction density influences the SWCC when the suction measurement is mostly based on axis translation methods.

They noticed the lack of clarity on the influence that the imposed stress condition (e.g., air pressure from the axis translation method) has on the SWCC, which makes it to differ from the curve found using zero stress condition prevalent in the relative humidity methods and tensiometer. Thus, reviewers concluded that the suction measurement methodology and procedures influence the uniqueness of the SWCC.

It was found as well a smaller grade of hysteresis the coarse-grained soils exhibit when compared to nonuniform, fine-grained soils and collapsible soils. A special remark

was done on the very few studies that deal with the experimental quantification of hysteresis for different types of soils and its influence on unsaturated behavior modeling. They attributed this situation mainly to the complexity in obtaining a wetting SWCC.

Also, no conclusive evidence was found by the researchers that might relate variations in SWCC to volume changes undergone for different types of swelling soils (Malaya et al., 2011).

Malaya et al., (2011) observed that the extent of parametric (i.e. compaction state, measurement procedures, stress history, range of suction measurement on the SWCC, compaction water content, density, etc.) influence on the SWCC is soil specific, and recommended further experimental investigations to quantify this influence for different soil types.

Finally, Malaya et al. (2011) highlighted the relevance of investigating and quantifying the variations in unsaturated behavior modeling caused by the disparity in the SWCC (due to parametric influence), which may help to clearly evaluate the criticality of such influences on the SWCC for different types of soils.

2.4.2 Measurement of SWCC

A brief review on the apparatus used during the current research is presented in this document. However, further detail on other types of devices for determining the SWCC might be found in the literature references like the work done by Pedarla (2013) who reviewed and summarized some of the SWCC measurement techniques commonly used by researchers and engineers.

2.4.2.1 Pressure Cell Apparatus

Pressure cell tests make use of the axis translation technique. In this test a chamber is divided by a high air entry pressure ceramic disk. A saturated soil sample is placed on top of the high air entry pressure ceramic disk and a target value of air

pressure is applied in the chamber. Since no other pressure increment is put on the pore water the soil suction equals the applied air pressure at equilibrium. Measurements of the water volume extruded from the sample at each air pressure increment are recorded when equilibrium is reached (i.e. no more water is extruded from the sample at the target air pressure). Measurements of sample weight at saturation dry states allow determining the water retention curve (Nelson et al. 1992).

2.4.2.2 Filter paper method

The principle on which the filter paper technique is based is that the relative humidity inside the container will be controlled by the soil water content and suction. The filter paper will absorb water until it comes into equilibrium with the relative humidity inside the container. After equilibrium has been reached between the soil water, the filter paper, and the relative humidity in the container, the suction in the filter paper will be at the same value as that in the soil. The humidity, in this case, is influenced by both the osmotic and matric components of the soil suction. The equilibrium water content of the filter paper corresponds to the matric suction of the soil when the paper is placed in contact with the water in the soil (Fredlund and Rahardjo, 1993). Therefore, the same calibration curve is used for both the matric and total suction measurements.

In this method (standardized by ASTM D5928-94 - Standard Test Method for Measurement of Soil Suction), a sample of the soil along with a calibrated filter paper is placed in a closed container constructed of noncorrosive material. The filter paper should not be in contact with the soil. The soil sample and filter paper are allowed to equilibrate for a period of at least 7 days at a constant temperature. After the 7-day equilibration period, the filter paper is removed and its water content is determined by precise weighing (±0.0001 g) before and after oven drying. The filter paper method can be used over a wide range of suction up to approximately 150,000 psi (106 kPa).

2.4.3 Interpretation of SWCC

Several soil suction measurement devices have been used for establishing the SWCC. The determination of SWCC is often time consuming and strenuous depending on the type of soil. Many researchers have also attempted to model and interpret the SWCCs measured. Two of the best established SWCC models are those proposed by Van Genuchten (1980) and Fredlund and Xing (1994). These two methods were chosen in the present research to be applied for representation of the SWCC.

2.4.4 Swelling behavior assessment based on suction measurements

Several researchers have proposed prediction models for expansive soils behavior based on soil suction measurements. The present review revisits some of the more relevant efforts made to relate swelling behavior and soil suction.

McKeen (1992) proposed a model to classify expansive soils according to water content, suction and volume change measurements taken during drying process. The model was developed from observation of a big dataset related to swelling soils projects developed by the researcher. Each soil in the dataset was individually analyzed on its graphical relation between: i) soil water content and suction, and ii) soil suction and volume change for establishing three bench mark points in clay behavior, as follows:

First: the intercept at zero water content in the soil water content vs. suction graph is usually near to 6.25 pF (logarithm to the base 10 of the pressure in centimeters of water, Schofield, 1935). Second: The suction level at which the volume change ceases is close to 5.5 pF, according to the soil suction vs. volume change graph. Third: The volume change ceases at field capacity in the range 2 to 2.5 pF (9.8 to 31 kPa) as seen in the soil suction vs. volume change graph.

Typical soil water content vs. suction and soil suction vs. volume change graphs are shown below in Figure 2-16 and Figure 2-17, respectively.

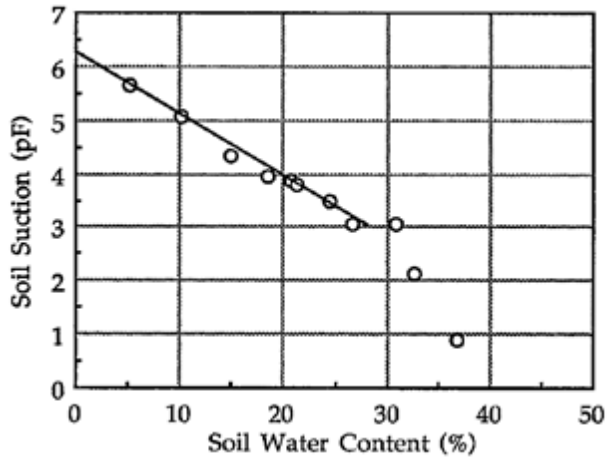

Figure 2-16 Soil water content vs. suction graph (McKeen, 1992)

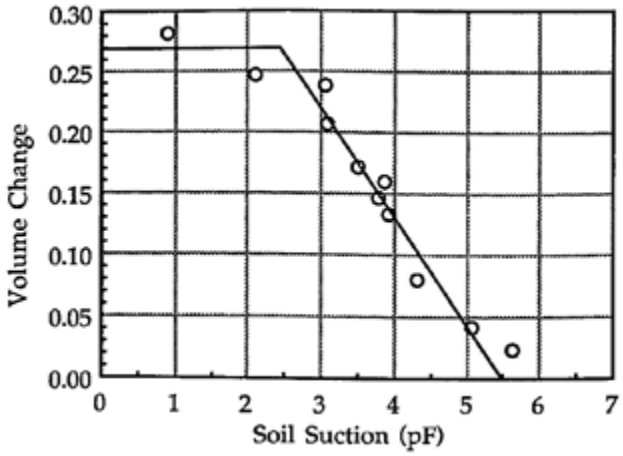

Figure 2-17 Soil suction vs. volume change graph (McKeen, 1992)

In order to make the method expedite and applicable, McKeen (1992) established 5 variables required to estimate the expansive soil behavior at any location: 1) the magnitude of suction change for design, Δh, 2) the active zone depth to which the suction change penetrates, Za, 3) the soil response to the suction change, Ch, (suction compression index), 4) the lateral restrain factor, f, and 5) the coefficient for load effect on heave, s. Thus, a general formula was provided as presented in Equation 2-4:

$$\Delta H = Ch\ \Delta h\ \Delta t\ f\ s \qquad 2-4$$

Where,

ΔH: vertical movement of the layer being considered

Ch: suction compression index, from the soil suction vs. volume change graph

Δh: suction change in the layer in pF

Δt: thickness of the layer

f: lateral restrain factor, f = 0.33*(1+2Ko), f = 1 if Ko = 1, f = 0.33 if Ko = 0

Ko: Coefficient of earth pressure at rest

s: coefficient for load effect on heave, s = 1.0 to 0.01 (%SP, for %SP < 50)

SP: percent of swell pressure applied.

Finally, according to the analysis made by the author, a new classification chart relying on the variables previously mentioned was proposed (Figure 2-18). 5 different categories of expansiveness were identified (I, II, III, IV and V). In the classification, the amount of the estimated heave decreases with each category, thus, category I represents extremely highly expansive soils which present a very serious threat to structural performance. On the other hand, Category V includes non-expansive soils.

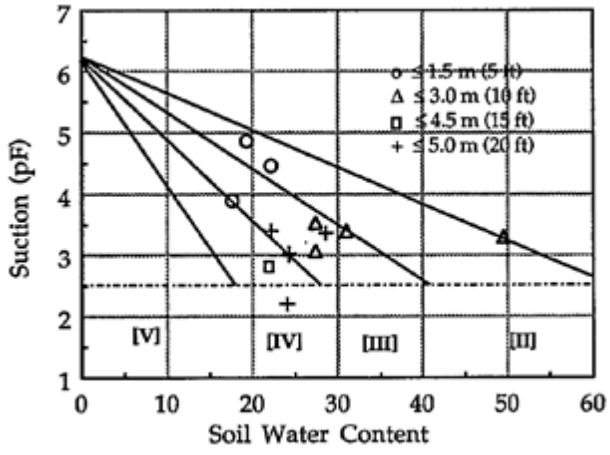

Figure 2-18 Expansive soil classification system (McKeen, 1992)

Likos et al. (2003) performed studies to validate McKeen's "benchmark intercept simplification'' for the slope of the soil water characteristic curve on a semilog plot (soil water content vs. suction in pF graph). The suction indices estimated using the benchmark intercept simplification were compared with indices measured directly using the noncontact filter paper technique for 80 undisturbed expansive shale specimens from the Colorado Front Range Corridor. The results showed that the suction-water content index is consistently overestimated using the benchmark simplification by amounts ranging from negligible to 50%, and averaging 23%. These discrepancies reflect potential errors that may arise from the use of the benchmark intercept simplification in classifying expansive soils.

Cocka (2000) developed a relationship between the logarithm of initial soil suction and swell pressure measured in the oedometer. In the study, the thermocouple psychrometric technique was used to measure the soil suction and asses the swell pressure. 11 kaolinite-bentonite clay mixtures were prepared to obtain expansive soils with wide range of plasticity. Constant volume swell tests following the ASTM D-4546-90 standard were performed on statically compacted specimens. The samples were 36 mm in diameter and 15 mm in height and were prepares at a dry density of 1.64 kg/m^3 and water content of 10%. The graphical representation of the relationship is shown in Figure 2-19. Also, the relation found by the researcher is presented next (Equation 2-5).

$$\mathrm{Ps} = -4610 + 2975 * \log_{10} \psi \qquad 2-5$$

Where,

Ps: swelling pressure (kPa)

ψ: initial total suction

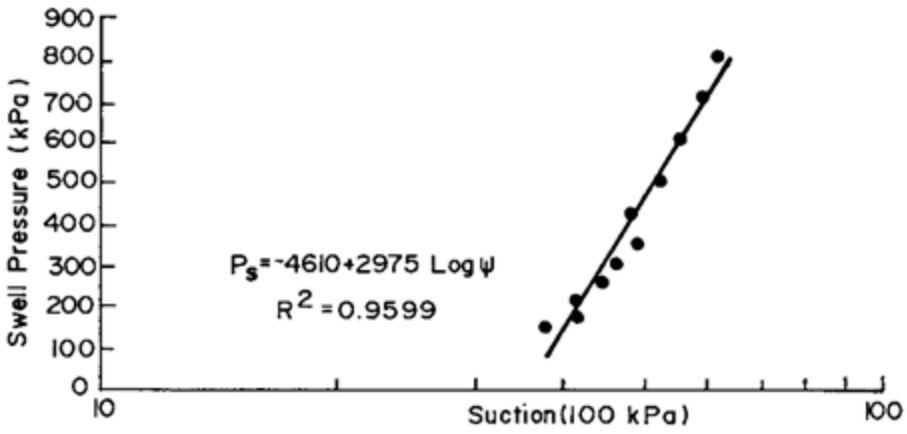

Figure 2-19 Initial soil suction and swell pressure (Cocka, 2000)

Cocka (2002) presented an extension of the previously outlined work. The 11 kaolinite-bentonite clay mixtures at different materials proportions were tested to determine their adsorption of methylene blue and free swell according to the ASTM D-4546-90 standard, under same compaction water content and dry density as presented before. The regression analysis made on the methylene blue value (MBV), soil suction and soil swell percent (S) data revealed the following correlation (Equation 2-6).

$$S = -121.807 + 12.1696 * \mathrm{MBV} + 27.6579 * \log_{10}\psi \qquad 2-6$$

Where,

MBV: methylene blue value

ψ: initial total suction

Pedarla (2013) proposed an indirect approach designated as the Mechanical Hydro Chemical (MHC) Model. The model was derived from a statistical analysis which correlated a so called Mechanical Hydro Chemical Parameter (MHCP) to the results of free swell tests and swell pressures (Method C ASTM D4546 – 08) performed on 8 different soils.

The MHCP weighs the influence of two different factors (chemical and hydro mechanical) on the soil swelling behavior and is found by the multiplication of these factors.

The first factor known as the chemical factor (C) represents the chemical activity of the soil. This factor is weighted by three components: 1) the clay fraction of soil (from hydrometer test); 2) a swell factor value subjectively assigned to the three main minerals in clay (90 for Montmorillonite, 9 for Illite and 1 for Kaolinite; and 3) the fraction of the three minerals in the clay (determined as per Chittoori, 2009).

A second factor known as hydro-mechanical factor considers the physic-mechanical attributes on the swelling behavior of soil: cumulative variation of void ratio (e), matric suction (ψ) and moisture content (w). The swell testing process generates the matric suction in the soil specimen to decrease as the void ratio increases. Thus, the matric suction-void ratio variation is assumed to follow a linear trend. Hence, the slope of the soil matric suction (X-axis) and void ratio (Y-axis) plot was considered as the second factor and was labeled with the symbol α (Figure 2-20).

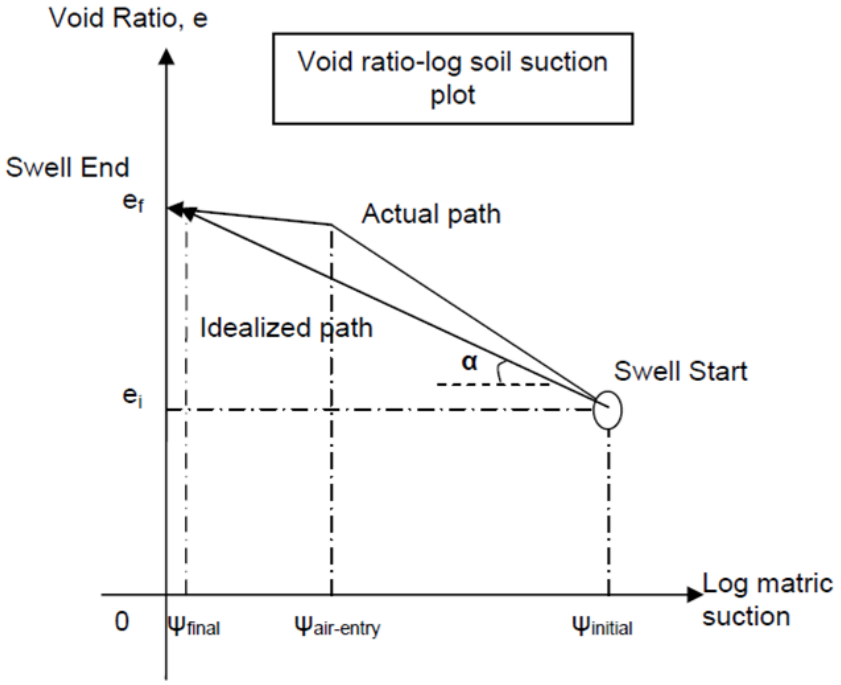

Figure 2-20 Slope of void ratio and logarithmic of matric suction (Pedarla, 2013)

In Pedarla's work, the SWCC's for all the 8 soils were performed on drying paths developed with information provided by pressure plate apparatus and filter paper technique, also, only soil samples compacted at 95% MDD were tested.

The typical swell behavior exhibited by a soil specimen on an e-w-log ψ plot, in this case corresponding to Anthem location soil, is shown in Figure 2-21.

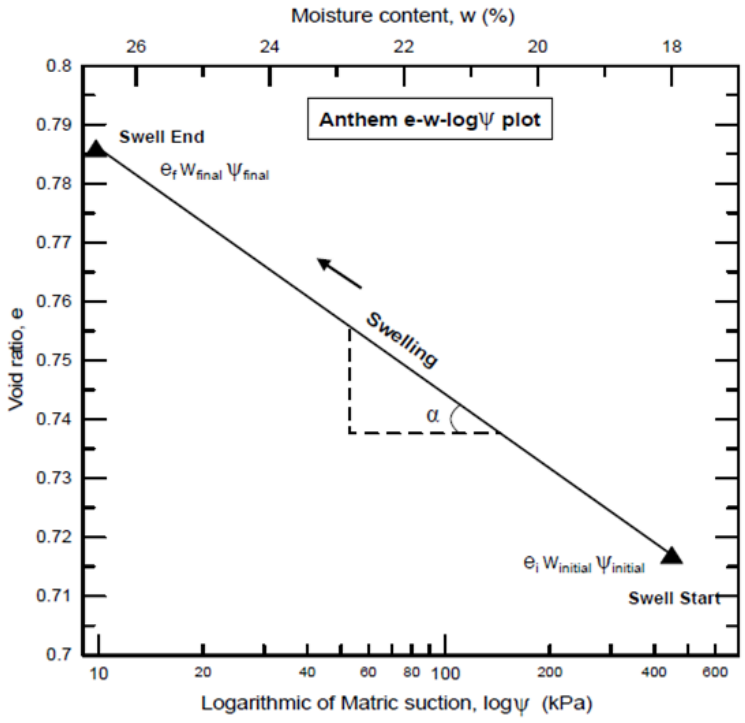

Figure 2-21 e-w-log ψ plot for Anthem soil specimen at 95% MDD (Pedarla, 2013)

Finally, an exponential variation between the measured swell strain and pressure and MHCP data was noticed and reported. These variations representing the MHC model as presented in Equation 2-7 and Equation 2-8.

$$\epsilon_{1-\mathrm{D\ swell}}\ (\%) = 6.12 * \mathrm{MHCP}^{0.263} \qquad 2-7$$

$$\mathrm{SP}\ (\%) = 107.83 * \mathrm{MHCP}^{0.29} \qquad 2-8$$

Where,

ϵ1-D swell: one dimensional swell strain (%); MHCP: Mechanical-hydro-chemical parameter;

SP: Swell pressure (kPa)

Uzundurukan et al. (2013) investigated the relationships between suction and swelling characteristics of clayey soils by testing swelling behavior of three soils named

A, B and C taken from different locations in the middle and west parts of Turkey. Swell tests were carried out according to ASTM D-4546 procedures by using oedometer equipment. Four 75 mm diameter and 20 mm height samples of each soil were compacted at same dry density (14.7 kN/m^3) but having different initial water content (15, 20, 25 and 30%). Suction on all the samples at their compaction water content was determined by thermocouple psychrometer technique. The results of experimental studies were evaluated and relationships between suction and swell characteristics were established showing a linear trend between percent swell and swelling pressure and suction, as shown below in Figure 2-22 and Figure 2-23, respectively.

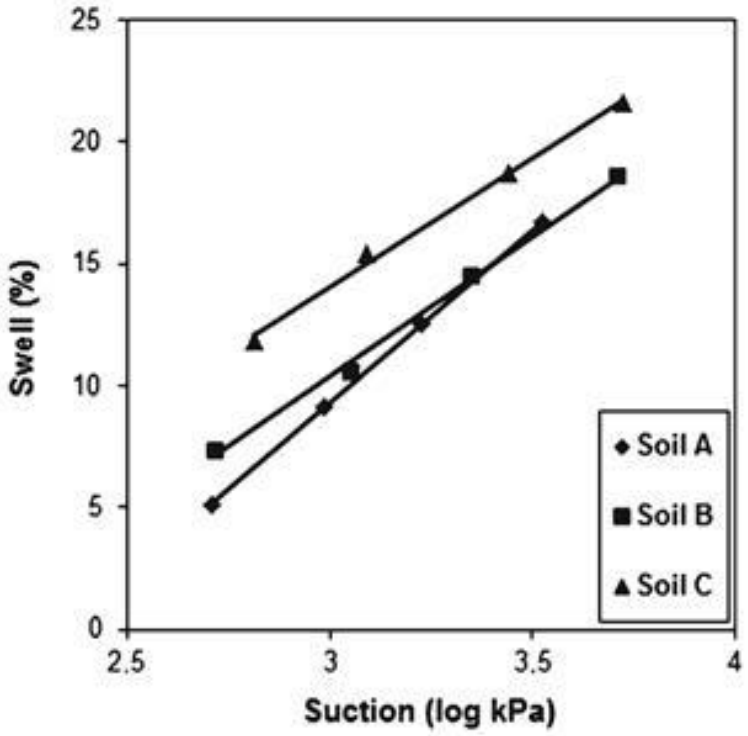

Figure 2-22 Swell strains vs. soil suction (Uzundurukan et al., 2013)

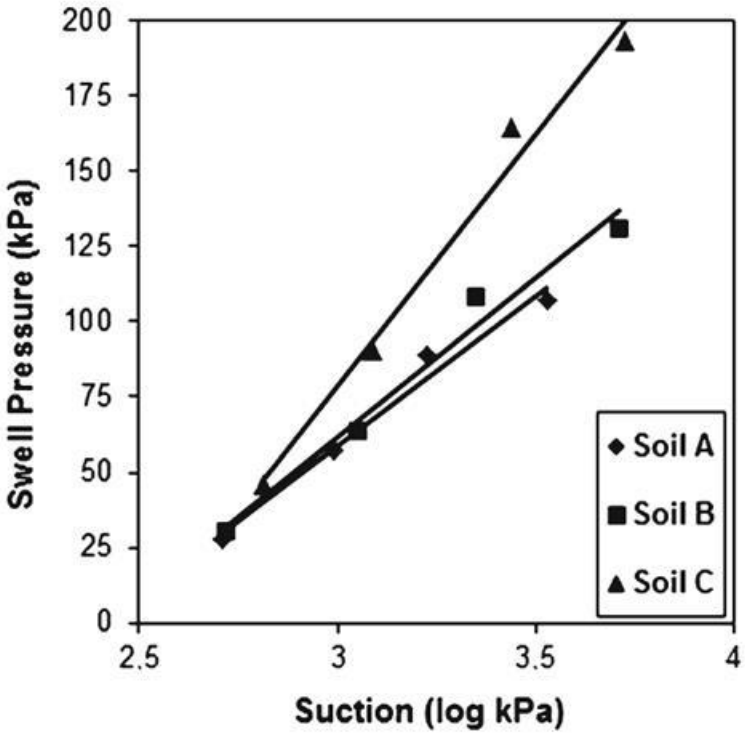

Figure 2-23 Swelling pressures vs. soil suction (Uzundurukan et al., 2013)

Pulat et al. (2013) performed a study intended to be applied to landfill liners. The study objective was to compare the swelling behavior of soils with different mineralogy and plasticity characteristics (bentonitic, kaolinitic and zeolitic soil) tested for determining matric and total suction values and for obtaining free swelling characteristics in the presence of salt solutions (NaCl, CaCl2, natural seawater) and distilled water as saturating fluids. The soil swelling behavior was determined by the modified free swell index (MFSI) following the method recommended by Sivapullaiah et al. (1987).

The authors observed that the bentonitic soil sample had the highest total suction value in the presence of seawater. Kaolinitic and zeolitic soil samples had the highest total suction values in the presence of NaCl solution. The highest modified free swell index value of the samples was obtained in the presence of NaCl solution for all the soil

samples. Also, they found no relationship between the total suction, matric suction and the modified free swell index value of the tested soils.

Finally, they remarked based on the results that the total or matric suction values cannot be used for the estimation of swelling behavior in soils. However, they mentioned, that since the permeability of unsaturated soils is related to the matric suction, it is important to know matric suction values in the presence of different pore fluids.

2.5 Pore Size distribution

The measurement of internal pore structure of a solid mass is the main challenge for the researchers in the last years. These measurements are possible with the help of techniques like Mercury Intrusion Porosimetry (MIP) and X-ray Computed Tomography (XCT). Details of these techniques are presented in the following.

2.5.1 Mercury Intrusion Porosimetry (MIP) Technique

In the MIP technique an absolute pressure p is applied to a non-wetting liquid (mercury) in order to enter the empty pores. The following Washburn equation (Equation 2-9) applies (Diamond 1970; Juang and Holtz 1986b; Webb and Orr 1997) for pores of cylindrical shape and parallel infinite plates (fissure-like microstructure).

$$\mathrm{P} = -\frac{n\sigma_{Hg}\cos\theta_{nw}}{x} \qquad 2-9$$

Where

σHg: surface tension of mercury (σHg = 0.484 N/m at 25°C)

θnw: contact angle between mercury and the pore wall

x: entrance or throat pore diameter (n = 4) or the entrance width between parallel plates (n = 2).

The value n = 4 is often used in MIP. The contact angle, which is very sensitive to surface roughness, is usually taken between 139 and 147 for clay minerals (Diamond

1970), although Penumadu and Dean (2000) have reported higher values with kaolin clay using the sessile drop technique (advancing angle of 162and receding angle 158).

MIP implicitly assumes a constant contact angle at equilibrium, whatever the penetration flow conditions are, and does not check the applicability of Equation 2-7, which is an equation for equilibrium state with null penetration velocity of mercury. In fact, the contact angle varies as a function of the flow dynamic conditions—penetration velocity—of the advancing interface, as shown experimentally by Hoffman (1975). At-Mokhtar et al. (2004) have studied the validity range of the constancy hypothesis of the contact angle of a non-wetting liquid during its penetration in a capillary. They showed, based on theoretical considerations using Poiseuille flow velocity that for a given value of pressure, the contact angle between the mercury and the capillary wall starts to change significantly only from a 'critical' value of capillary radius. For this reason, sufficient time must be let in the pressure rising to allow for the quasi-static state condition to be reached.

The main limitations of MIP are: (a) isolated pores enclosed by surrounding solids are not measured, this enclosed porosity is not significant in soils; (b) pores that are accessible only through smaller ones (constricted porosity) are not detected until the smaller pores are penetrated; (c) the apparatus may not have the capacity to enter the smallest pores of the sample (non-intruded porosity); and (d) the minimum practical pressure of the apparatus limits the maximum pore size to be detected (non-detected porosity). In this way, when the clay sample is intruded by mercury, the intruded void ratio estimated under the maximum applied pressure does not coincide with the estimated void ratio of the sample.

Differences mainly arise due to the non-intruded porosity with entrance pore sizes lower than 10 nm and the non-detectable porosity for pore sizes larger than 400 lm.

In addition, an intrusion (pressure increase) and extrusion (pressure decrease) cycle does not close when the initial pressure is restored, indicating that some mercury has been permanently entrapped in the constricted porosity.

Mercury intrusion is used to find the pore-size distribution, relating the volume of intruded pores to the pressure required for intrusion. A typical graph of the MIP technique includes the log differential intrusion curve vs. entrance or throat pore size (pore size density function or frequency distribution, PSD), which aids the visual detection of the dominant pore modes. As previously discussed, such a PSD is not necessarily the true distribution of pores, due to various issues including pore accessibility and sample treatment, yet it gives a useful quantitative characterization of microstructure.

Sample treatment for MIP requires the removal of water that occupies small pores and prevents the entry of mercury. Samples can be dehydrated using air-drying, oven-drying, freeze-drying or critical point-drying techniques (Delage et al. 1984). However, if the sample is heat and dry sensitive, then freeze drying is preferred, especially at high water contents (Ahmed et al. 1974). Freeze drying processes manipulate temperature and pressure conditions to eliminate the surface tension forces caused by air-water interfaces, and thus it is assumed that no shrinkage occurs on drying which could alter soil structure. Prior to freeze drying, soil samples must be cut into cubes less than 1 cm^3 in size to maximize heat transfer. (Ahmed et al., 1974; Delage et al., 1982, 1984, 1996; Penumadu et al., 2000; Mitchell and Soga, 2005).

When using MIP for evaluating the volume changes in soils, it is necessary to consider that different types of them occur at different scales. For example, estimations of volume at the largest scale may be affected by the presence of cracks and other large scale features. Therefore, volume change measured on the microscopic scale is often

only indirectly related to volume change at the macroscopic scale. However, there has been a strong correlation for some soils for a given range of suctions.

Simms and Yanful (2004) found that for compacted clayey soils of low or moderate plasticity, the volume change on drying measured by calipers on 5 mm diameter and 5 mm thick samples, strongly correlated with the volume change in the pores in the range measurable by MIP (0.01–100 lm). For these soils, little or no cracking was observed at the macroscopic scale.

It has been suggested that the volume change measured by MIP may overestimate large scale volume change, if lacunar porosity develops. This type of porosity is formed by the shrinkage of finer grained particles away from a coarser-grained skeleton of particles (Fies et al., 1998; Viola et al. 2005). The volume contributing to lacunar porosity must come from inter-aggregate, inter-particle, or inter-layer void space, of which the first two are measured by MIP. Variations in inter-layer spacing only occur with significant variation in the relative humidity of soil pores, which occur for suctions greater than 3 MPa.

Despite these limitations, MIP measurements at the microstructural level are a helpful tool to understand material behavior at macroscopic scale and to build up double-structure constitutive models with coupling functions relating micro and macrostructural behavioral features. In this way, MIP has been used to characterize the multiple-porosity network of different soils and to study their evolution along different mechanical and hydraulic stress paths.

Changes in the void ratio result only in changes in the inter-aggregate porosity or macropores (also been observed in compacted clayey soils as noticed by Delage et al. 1996).

Pedarla (2013) performed a study on 8 clayey soils to measure their internal pore structure and distribution. Since the variation of dry density of a soil specimen influences the internal pore structure and pore size distribution the researcher tested soil specimens of each soil at two different compaction conditions, i.e. at maximum dry density (MDD) condition and at 95% maximum dry density (95% MDD) condition. Figure 2-24 presents the standard MIP test equipment utilized for Pedarla's research.

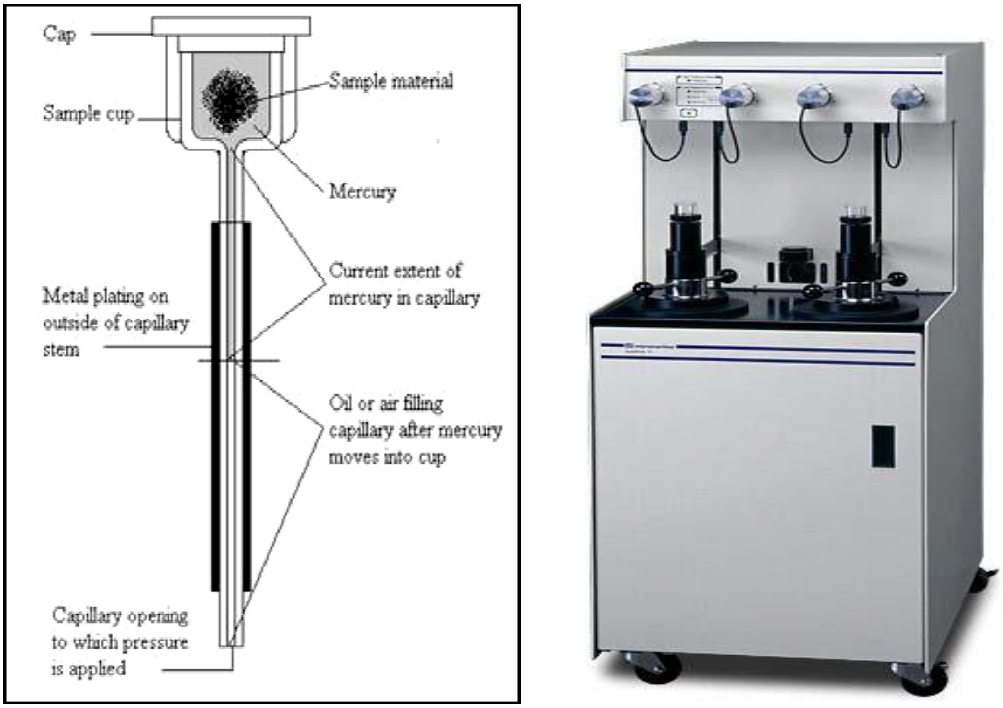

Figure 2-24 Penetrometer and equipment used for MIP technique (Pedarla, 2013)

Pedarla categorized the pores in the following way, according to their dimensions, for proper pore identification: pores ranging below 0.02 micro meters (μm) were classified as micro pores. Pores ranging from 0.02 μm to 12 μm came under medium pores and pores larger than 12 μm were classified as macro pores. As mentioned, during this study two soil specimens from the same clay at different density condition were tested for pore distribution. According to the author, the test results

showed variable volume of micro pores in the two specimens of any particular clay. Also, Perdarla observed a hysteresis on the results between the soil specimens at 95% MDD condition and at MDD condition which he related to the retention of mercury in the soil pores. He concluded the MIP test yielded good repeatability of test results. The mercury intrusion/extrusion curves of Anthem clay obtained at two compaction densities are shown in Figure 2-25. Also, the pore size distribution for the same soil at different dry density conditions is shown in Figure 2-26.

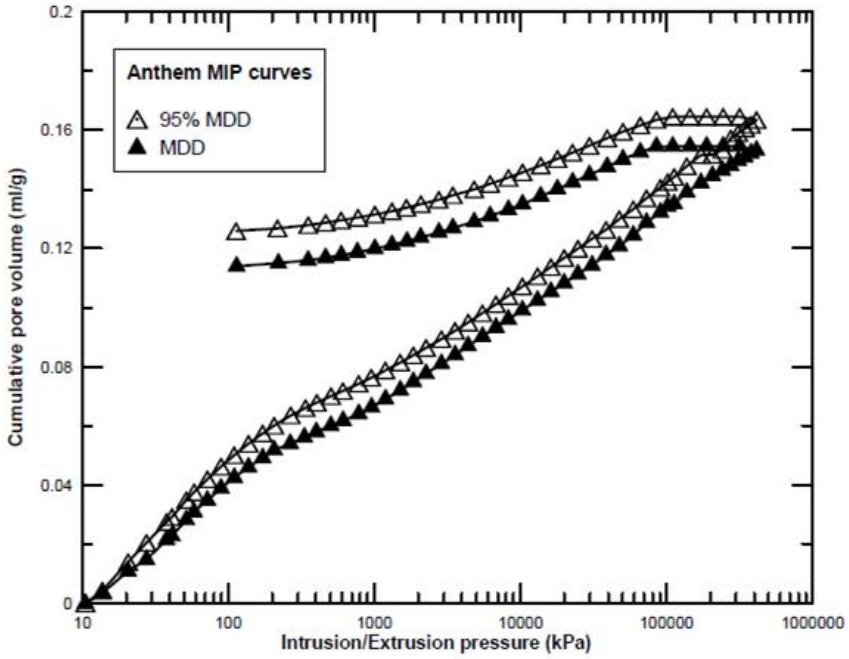

Figure 2-25 Anthem soil Intrusion/Extrusion curves (Pedarla, 2013)

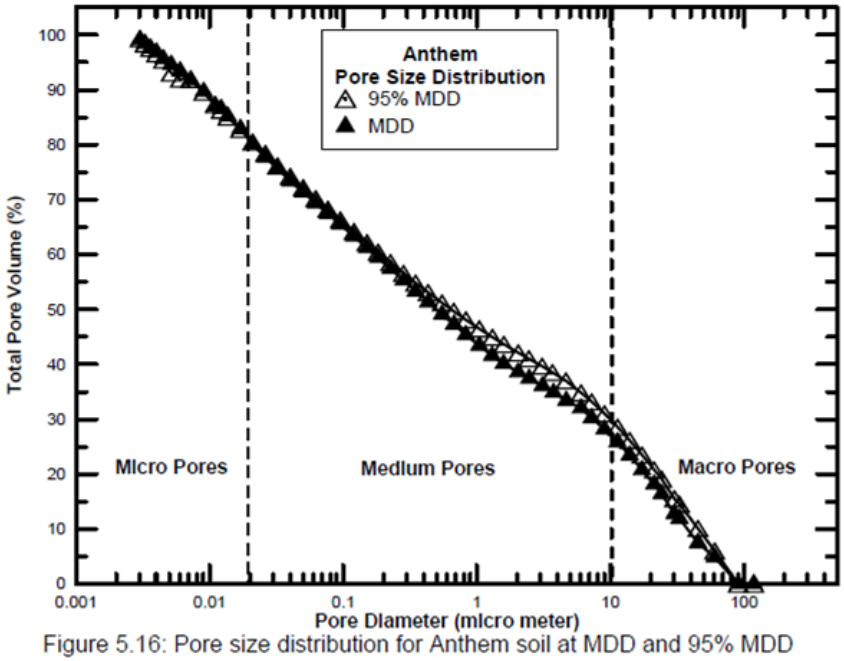

Figure 5.16: Pore size distribution for Anthem soil at MDD and 95% MDD

Figure 2-26 Anthem soil pore size distribution (Pedarla, 2013)

Pedarla (2013) defined the percentage of each category of pores in the sample and based on it proposed a procedure to calculate the total surface area of the clay minerals from MIP data. His aim was to determine the total pore area contributing to soil swell. These values were included in a model for prediction of the swelling behavior of clays designated as Total surface area ratio (TSAR) model. Procedure details can be seen in Pedarla's work.

Sasanian et al. (2013) perform a study on the effects of variations in moisture content on the pore size distribution of two clays, for specimens over a large range of liquidity indices from 0 to 3 (gravimetric moisture content range of 23 to 98%) prepared by freeze-drying. The analysis was also performed on air-dried specimens, to analyze the fabric changes and particle rearrangements due to air-drying. The MIP results they obtained confirmed the existence of two major groups of pores within the material, i.e.

intra- and inter-cluster pores. It was found that the addition of water to air-dried clay increased the volume of inter-cluster pores, leaving intra-cluster pores almost constant. Any further increase in the moisture content of the wet material was also attributed to changes in the inter-cluster pore volume. Amongst the inter-cluster pores, smaller diameter pores were more sensitive to changes in moisture content. They found an inability to detect all of the large pores, and that MIP underestimates the void ratio of specimens with moisture content higher than 50%, regardless of the liquidity index.

Zong et al., 2015 noticed that in the presence of swelling clays, the SWCC cannot provide unique estimates of the pore size distribution because water loss results from a combination of pore drainage and shrinkage. Therefore, in some studies, the pore size distribution (PSD) obtained from the MIP method was used as a reference for the PSD from the water retention curve (Hajnos et al. 2006; Lipiec et al. 2007).

2.5.2 X-ray Computed Tomography (XCT)

XCT is a non-invasive technique that can be used to visualize the interior of objects in 2D and 3D based on the principle of attenuation of an electromagnetic wave. A typical scan involves the collection of a series of radiograph images of a sample acquired at incremental angular positions, normally over 360°.

Generally, XCT scanners consist of three common parts: an X-ray source (either synchrotron light or a conventional X-ray tube), a sample manipulation stage and a detector. X-rays emitted from the source pass through the sample and are progressively attenuated by absorption and scattering as the object itself becomes a secondary source of X-rays and electrons through atomic interactions (Mooney et al., 2012).

The characteristic of a material to either absorb or scatter a photon is called the attenuation coefficient. Attenuation coefficients are related to the density of the absorbing material, electron density of the voxel of interest and incident X-ray energy, but are

predominantly controlled by four dominant processes: (i) photoelectric absorption, (ii) Rayleigh scattering, (iii) Compton scattering and (iv) pair production.

XCT systems can generally be grouped into three categories, namely industrial, medical and synchrotron. In industrial scanners the objects typically rotate in a cone beam of polychromatic X-rays (Figure 2-27).

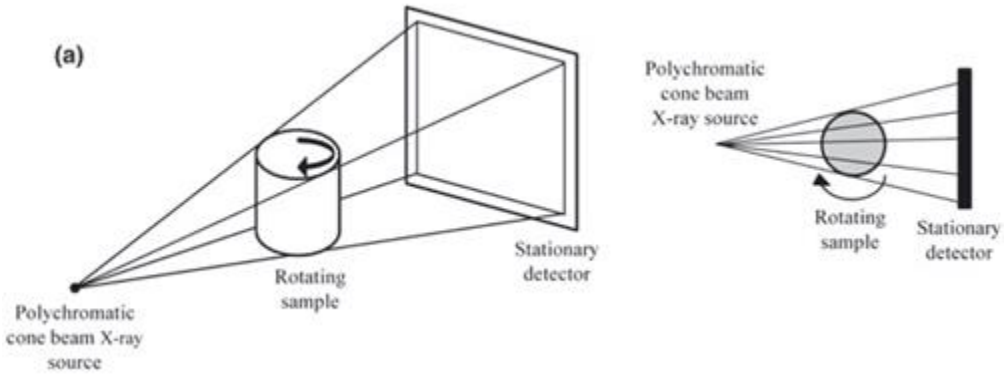

Figure 2-27 XCT system arrangement for industrial scanners (Helliwell et al., 2013)

In this case, as the entirety of the object passes through the beam with each angular rotation, a reduced focal spot size allows smaller objects to be moved nearer to the X-ray source and into a narrower section of the X-ray beam. This permits increased resolution through improved detector utilization, to image smaller sub-sections of the object in a single view (Ketcham & Carlson, 2001). Hence industrial scanners can span a range of scales from meter-wide scales of observation for large objects such as geological rock forms to large (≤1 μm) resolutions when resolving soil pores in a single micro-aggregate, for example.

As with all analytical equipment XCT has limitations, which at present limit its capacity to characterize certain soil properties. The identification of single objects through image thresholding may be limited by individual voxels containing multiple materials. The attenuation of materials within single voxels is proportionally averaged, potentially leading

to ‘partial volume effects’ as voxels are misclassified (Clausnitzer & Hopmans, 2000; Ketcham & Carlson, 2001). The magnitude of this effect is intensified as the resolution is increased below the pore size of the soil used (Heeraman et al., 1997; Kaestner et al., 2006; Flavel et al., 2012). Therefore the minimum object size detectable accurately is often viewed as twice (Rogasik et al., 2003) or three times (Wildenschild et al., 2002) the scanning resolution.

The strong contrast in X-ray attenuation between soil pores and related solid material has seen the development of various methods for the quantification of temporal changes in soil pore networks under different environmental stresses (Pires et al., 2007; Peth et al., 2010). Information on the 3D arrangement of the soil pore system can be derived from measurements of the actual morphology of soil pores, rather than inferring the soil pore system from flow dynamics and idealized pore diameter measurements (Grevers et al., 1989). To quantify properties such as pore connectivity and continuous pore networks within the soil matrix and to use them adequately to model pore networks, the visualization must be in 3D (Mooney, 2002). However, because of issues of scale still associated with XCT imaging, the understanding of how soils operate at the microscale has been limited, with most research focused on soil macroporosity (Nunan et al., 2006). For example, Perret et al. (1999) characterized pore tortuosity (the ratio of total pore length to that of the shortest possible path), numerical density and hydraulic radius in undisturbed cores at a coarse resolution of 0.195×0.195×2 mm, whilst Rogasik et al. (2003) assessed macropore size, length and connectivity of pores under different agricultural management practices at the spatial scale of 0.25×0.25×1 mm.

Many studies have used XCT to quantify various properties of macropore network morphology, including pore network structure (Baveye et al., 2002; Aravena et al., 2011), pore diameter (Anderson et al ., 1992; Zeng et al ., 1996), pore circularity

(Gantzer & Anderson, 2002) and crack formation (Peth et al., 2010). Used in this way, XCT provides data not obtainable by other means. Baveye et al. (2002) helped inform future research by revealing the dependence of macroscopic soil properties such as bulk density, volumetric water content and air content on sampling volume, shape and positioning. By comparing soil characteristics from different types and size of sampling volume, they were able to show how properties in small volumes can exhibit erratic fluctuations in measurements, which can be stabilized as sampling volume increases. Likewise, a recent important study by Peth et al. (2010) at a resolution of 25.3 μm revealed a very heterogeneous microscale soil environment when examining soil structure, localized soil deformation and local strain analysis over very small spatial scales (<1 mm). The present understanding of these mechanisms at the microscale level is crucial to further understanding of the processes behind soil stabilization and structural development and support improvements in conceptual model development of geometric pore networks. Delerue et al. (2003) successfully developed a pore network directly from soil images by integrating pore size and connectivity parameters, which enabled calculation of the equivalent hydraulic conductivity from a 3D image of any porous soil. Likewise, Al-Raoush & Willson (2005) used skeletonization algorithms (thinning operations, which systematically remove voxels from an object until a minimal but topologically identical structure is produced) to extract pore-bodies, pore-throats and size distributions in physically realistic pore network structures, which enabled the discrimination of active and inactive pores and the characterization of redundant pore throats, demonstrating a clear advantage of XCT over other, invasive techniques.

Pedarla (2013) performed a study using 8 soils to obtain 1 cm^3 specimens cut from the statically compacted soil at two different dry densities (at 95% MDD and at

MDD). Tomography scanning was performed on the soil specimens at different initial conditions (i.e. dry and saturated).

The three dimensional images yielded by the tomography scanning were sliced and studied for pore network and void ratio with the help of image processing code written for MATLAB software. To determine the void ratio of a soil specimen, Pedarla (2013) counted the numbers of black and white pixels in the images yielded by the slicing process of the Tomography digitally reconstructed specimens. The 3-D soil mass was sliced at different levels and the average of the computed void ratio was determined using the code at each analysis. The scanned images of the soil specimens were then used as input files for the software.

Figure 2-28 presents the X-ray computed tomography equipment used for Pedarla's research. Also, the 1 cm in height, width and depth specimen sliced from compacted soil specimens is shown in Figure 2-29.

Figure 2-28 X-ray tomography equipment used by Pedarla (2013)

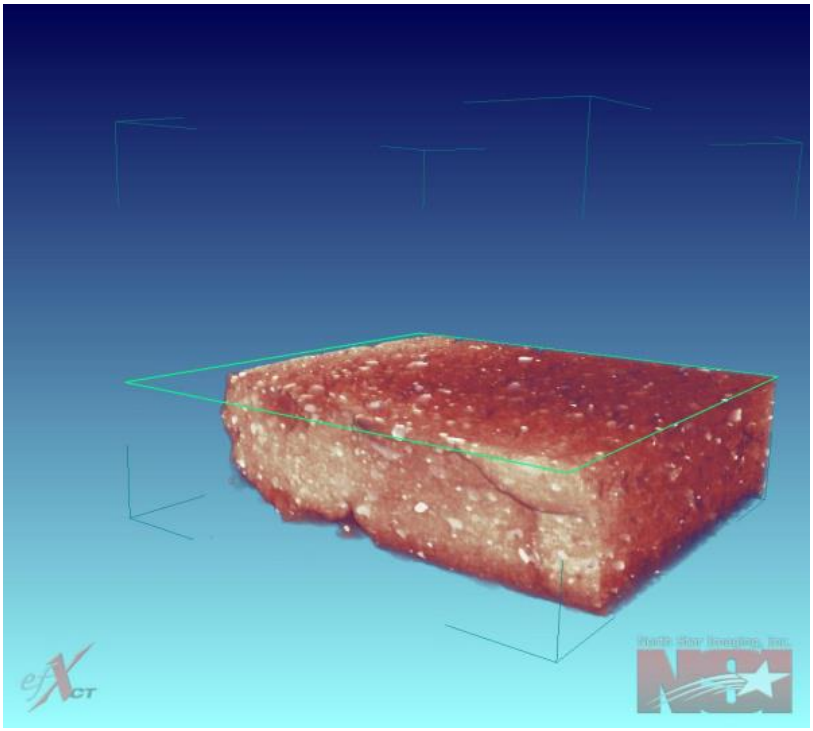

Figure 2-29 Sliced 3D soil specimen from CT scan (Pedarla, 2013)

Finally, Pedarla presented in a graphical form, the void ratio correlation found from XCT and the volume relationships for both conditions, i.e. dry and saturated, at 95% MDD and at MDD.

The Mercury Intrusion Porosimetry (MIP) and X-ray Computed Tomography (XCT) are utilized in the current study for the determination of pore size distribution and network connectivity in the soil mass.

2.6 Artificial Neural Networks

An artificial Neural Network (ANN) in general, simulates the biological structure of the human brain by means of their architecture. ANN technique has been increasingly applied in geotechnical engineering applications in which complexities and understanding of soil behaviors are difficult to simulate with theoretical models (Shahin et al. 2001; Lee

and Lee 1996; Teh et al. 1997). ANN models are appropriate to predict the relationships between the model input parameters and the corresponding output parameters. This has been achieved by repeatedly feeding the known examples of input/output relationships to the model and then minimizing the error function used to measure the variations between measured and predicted output results. Because of these reasons, ANN modeling was selected for analyzing the present test results.

The development of the neural network model consists of selecting model input/out parameters, data preprocessing, designing appropriate model architecture, model training, and model validation.

The modeling capability of the ANN, as well as the ability to learn from experience, have given this technique superiority over most traditional modeling methods since there is no need for making assumptions about what the underlying rules that govern the problem in hand could be.

Since the early 1990s, ANN method has been applied successfully to almost every problem in geotechnical engineering. The literature reveals that ANN have been used extensively for predicting the axial and lateral load capacities in compression and uplift of pile foundations (Abu-Kiefa 1998; Ahmad et al. 2007; Chan et al. 1995; Das and Basudhar 2006; Goh 1994a; Goh 1995a; Goh 1996b; Hanna et al. 2004; Lee and Lee 1996; Nawari et al. 1999; Rahman et al. 2001; Shahin 2008; Teh et al. 1997), drilled shafts (Goh et al. 2005; Shahin and Jaksa 2008) and ground anchors (Rahman et al. 2001; Shahin and Jaksa 2004; Shahin and Jaksa 2005a; Shahin and Jaksa 2005b; Shahin and Jaksa 2006).

Classical constitutive modeling based on the elasticity and plasticity theories is unable to properly simulate the behavior of geomaterials for reasons pertaining to formulation complexity, idealization of material behavior and excessive empirical

parameters (Adeli 2001). In this regard, many researchers (Basheer 1998; Basheer 2000; Basheer 2002; Basheer and Najjar 1998; Ellis et al. 1992; Ellis et al. 1995; Fu et al. 2007; Ghaboussi and Sidarta 1998; Habibagahi and Bamdad 2003; Haj-Ali et al. 2001; Hashash et al. 2004; Lefik and Schrefler 2003; Najjar and Ali 1999; Najjar et al. 1999; Najjar and Huang 2007; Penumadu and Chameau 1997; Penumadu and Zhao 1999; Romo et al. 2001; Shahin and Indraratna 2006; Sidarta and Ghaboussi 1998; Tutumluer and Seyhan 1998; Zhu et al. 1998a; Zhu et al. 1998b; Zhu et al. 1996) proposed neural networks as a reliable and practical alternative to modeling the constitutive monotonic and hysteretic behavior of geomaterials.

Liquefaction during earthquakes is one of the very dangerous ground failure phenomena that cause a large amount of damage to most civil engineering structures. Although the liquefaction mechanism is well known, the prediction of the value of liquefaction induced displacements is very complex and not entirely understood (Baziar and Ghorbani 2005). This has attracted many researchers (Agrawal et al. 1997; Ali and Najjar 1998; Baziar and Ghorbani 2005; Goh 2002; Goh 1994b; Goh 1996a; Goh et al. 1995; Hanna et al. 2007; Javadi et al. 2006; Juang and Chen 1999; Kim and Kim 2006; Najjar and Ali 1998; Ural and Saka 1998; Young-Su and Byung-Tak 2006) to investigate the applicability of ANN for predicting liquefaction.

The problem of predicting the settlement of shallow foundations, especially on cohesionless soils, is very complex, uncertain and not yet entirely understood. This fact has encouraged some researchers (Chen et al. 2006; Shahin et al. 2002a; Shahin et al. 2003a; Shahin et al. 2004a; Shahin et al. 2005a; Shahin et al. 2005b; Shahin et al. 2002b; Shahin et al. 2003b; Shahin et al. 2003c; Shahin et al. 2003d; Sivakugan et al. 1998) to apply the ANN technique to settlement prediction. The problem of estimating the

bearing capacity of shallow foundations by ANN has also been investigated by Padminin et al. (2008) and Provenzano et al. (2004).

Other applications of ANN in geotechnical engineering include retaining walls (Goh et al.

1995; Kung et al. 2007), dams (Kim and Kim 2008), blasting (Lu 2005), mining (Rankine and Sivakugan 2005; Singh and Singh 2005), geoenvironmental engineering (Shang et al. 2004), rock mechanics (Gokceoglu et al. 2004), site characterisation (Basheer et al. 1996; Najjar and Basheer 1996; Rizzo and Dougherty 1994; Rizzo et al. 1996; Zhou and Wu 1994), tunnels and underground openings (Benardos and Kaliampakos 2004; Lee and Sterling 1992; Moon et al. 1995; Neaupane and Achet 2004; Shi et al. 1998; Shi 2000; Yoo and Kim 2007) and slope stability (Ferentinou and Sakellariou 2007; Goh and Kulhawy 2003; Mayoraz and Vulliet 2002; Neaupane and Achet 2004; Ni et al. 1996; Zhao 2008).

It is important to recall as previously reviewed in this document, that geotechnical properties of soils are controlled by factors such as mineralogy; fabric; and pore water, among others. The interactions of these factors are difficult to establish solely by traditional statistical methods due to their interdependence (Yang and Rosenbaum 2002). Based on the application of ANN, methodologies have been developed for estimating several soil properties including the pre-consolidation pressure (Celik and Tan 2005), shear strength and stress history (Kurup and Dudani 2002; Lee et al. 2003; Penumadu et al. 1994; Yang and Rosenbaum 2002), compaction and permeability (Agrawal et al. 1994; Goh 1995b; Gribb and Gribb 1994; Najjar et al. 1996b; Sinha and Wang 2008), soil classification (Cal 1995), soil density (Goh 1995b), and), and swell pressure.

Swelling behavior of expansive soil is a complicated phenomenon. In an attempt to cope with the complications in describing the swelling behavior of expansive soil, researchers developed ANN particular applications.

These applications include prediction models of free-swell percent and swelling pressure of soil based on compaction state (dry density) and index properties as natural moisture content, liquid limit, plasticity index, and clay fraction, as well as determination of the transmitted lateral swelling pressure, and vertical swelling pressures on a retaining structure different thicknesses using expanded polystyrene (EPS) geofoam (Ashayeri et al., 2009; Erzin, 2009, Das et al., 2010, Banu Ikizler et al., 2010, Bekhor et al., 2014).

The performance of the ANN prediction for swell strain and pressure depending on index properties and compaction state has been revised by direct comparison with adaptive neuro-fuzzy inference system (ANFIS) and the traditional statistical model of multiple regression (Yilmaz et al., 2011) finding good agreement and superior performance of the ANN methodology.

Even though the evident ANN usefulness, investigators like Bekhor et al. (2013) had made warnings on the use of the ANN, recommending that the ANN outputs should be accompanied by an additional check to ensure that they follow the expected physical swelling behavior when characterized by soil index properties. In this particular case an alternative artificial neural network methodology did not predict swelling values as well as the ANN Excel-solver command (ESC) based model did.

Artificial neural networks (ANN) capability for prediction of soil swelling behavior will be compared with the statistical multiple regression results in the present research.

2.7 Summary

In this chapter, an effort of reviewing previous research performed on expansive soils has been made. Damages caused by the heaving of soils and the factors related to the soil swelling behavior were reviewed.

Direct and indirect methods for characterization of soil swelling based on soil index parameters and more advanced soil parameters were studied. Mineralogical investigations and the role of main clayey minerals in shaping the swell behavior of soil are written in the document. Also, moisture content soil suction effects in swelling behavior of clays are studied. Correlations given by literature to identify swelling of soils were presented in this chapter.

The use of mercury intrusion porosimetry and X-ray computed tomography for identifying the internal pore structure and its distribution are also presented.

In the next chapter, soil selection and basic soil classification results are provided.

Methodology of all the engineering tests along with their principles is provided in the coming chapter.

Chapter 3

Methodology

3.1 Introduction

The factors responsible for the swell shrink behavior of expansive clays are discussed in Chapter 2. To assess one of the objectives i.e. to better characterize expansive soils, six different clays of different forming conditions (i.e. weathering, minerals diagenesis and hydrothermal alteration) have been selected for this experimental study. Expansive soils from six different places in Texas: Cleburne, Denton, Grapevine 2, Mansfield, Plano and Waco were sampled and used.

Laboratory determination of the basic soil properties as well as the chemical and mineralogy features of the chosen soils were first performed. The results for the basic soil characterization and their classification are presented in the present chapter. Testing for minerals quantification on these soils is explained in this chapter. Engineering tests procedures conducted on the soils for swelling and soil composition properties determination are also presented.

Test procedures for the determination of 1-D free swell strain and swell pressures are detailed. A 3-D swell strain apparatus designed at The University of Texas at Arlington was used for measuring the swell potential of a soil specimen under different confinement conditions. Further details of this 3-D swell strain device are presented in this chapter.

The soil water characteristic curves relating moisture content and suction of each soil at different compaction conditions were obtained by means of the Pressure Cell apparatus and also with the help of the filter paper test method. Details of the laboratory procedures are also given in this chapter.

This chapter also deals with the study of the internal pore distribution and pore structure in the soils which are highly related to the expansive soil behavior. Mercury Intrusion Porosimetry (MIP) and X-ray Computed Tomography (XCT) techniques were used for this goal.

Figure 3-1 represents the flow chart for the research methodology followed in the current research. The final objective of this research is to reach a better understanding of the swelling soil behavior and the development of a general and unified approach that includes both analytical and numerical formulation for the prediction of the volume change properties and responses of expansive soils by considering clay mineralogy, pore distribution and unsaturated soil mechanics principles.

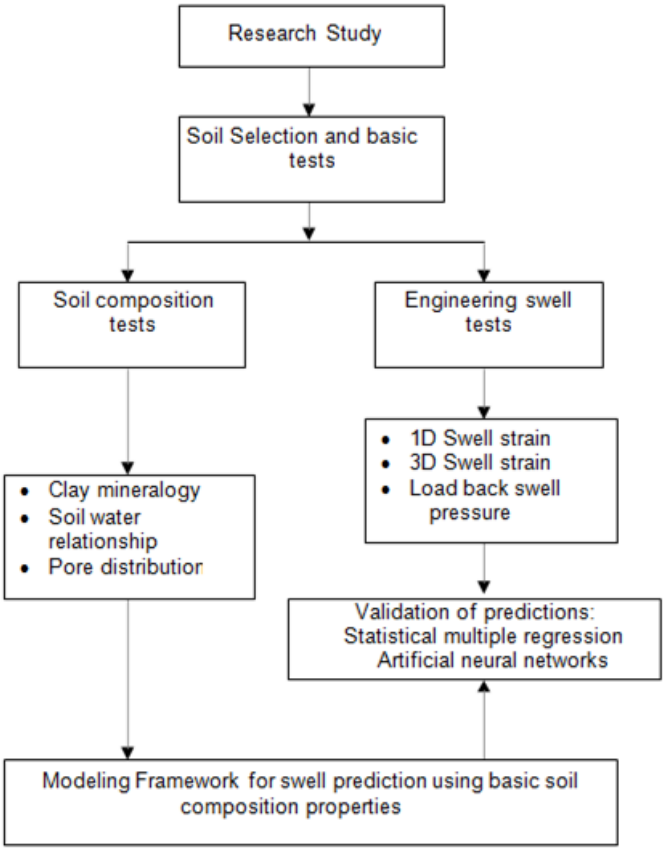

Figure 3-1 Research methodology

A synopsis of the laboratory procedures, equipment used and results obtained are presented in the present chapter.

3.2 Laboratory testing for soil characterization and classification

Basic soil properties for proper characterization and classification were found intending to comply with the general guidelines of geotechnical investigations for engineering purposes. The tests performed consist of specific gravity test, sieve analysis, hydrometer test, Atterberg limits, and Standard Proctor tests. Basic testing descriptions and procedures are presented in the following.

3.2.1 Specific Gravity, Sieve Analysis and Hydrometer tests

Specific gravity (G_s) is defined as the ratio of the mass of a given volume of solid or liquid to the mass of an equal volume of water, of testing materials was determined as per TxDOT procedure Tex-108-E. The distribution of the grain sizes in test materials was determined using TxDOT procedure Tex-110-E. This method was followed to determine the amount of soils finer than the No. 200 sieve opening. Finer particle size analysis was performed using hydrometer tests.

3.2.2 Atterberg Limits

Atterberg limit tests reveal properties related to consistency of the soil. These include liquid limit (LL), plastic limit (PL) and shrinkage limit (SL) and these are essential to correlate the shrink-swell potential of the soils with their respective plasticity indices. Upon addition of water the state of soil proceeds from dry, semisolid, plastic and finally to liquid states. The water content at the boundaries of these states are known as shrinkage (SL), plastic (PL) and liquid (LL) limits, respectively (Lambe and Whitman 2000). Therefore, the LL is measured as the water content at which the soil flows and the PL is determined as the water content at which the soil starts crumbling when rolled into a 1/8-inch diameter thread.

The numerical difference between LL and PL values is known as plasticity index (PI) and this index characterizes the plasticity nature of the soil. Representative soil samples from each location are tested following the procedure from Tex-104-E and Tex-105-E. The water content of the samples during tests is measured using oven drying method.

3.2.3 Standard Proctor Compaction Tests

In order to determine the compaction moisture content and dry unit weight relationships of the soils in the present research program, it is necessary to conduct standard Proctor compaction tests on soils to establish compaction relationships. The optimum moisture content of the soil is the water content at which the soils are compacted to a maximum dry unit weight condition. Standard Proctor test method using Tex-114-E procedure was followed. In this research the soil specimens are prepared and tested at two density conditions maximum dry density (MDD) and 95% MDD condition. It should be noted here that dry density is used in the notation system that is representative of dry unit weight condition.

The soil samples collected from different sites and locations were oven dried for a period of 24 hours. Once dried the soil samples were crushed and pulverized. Pulverized soil samples were then tested for Proctor compaction and other basic soil tests.

3.2.4 Basic laboratory test results

The six soils collected were tested for basic soil classification, specific gravity (Gs) and Atterberg limits and the results are shown in Table 3-1. The plasticity index (PI) value for the Mansfield soil is the highest whereas least plasticity properties are exhibited by Plano soil.

The soils were tested for wet sieve analysis passing through No.200 and the passing finer soil was used for Hydrometer analysis. Figure 3-2 to Figure 3-7 present the gradation curves for all the soils obtained from sieve analysis and hydrometer tests.

Table 3-1 Atterberg limits, Specific Gravity and USCS Classification

Soil	Liquid Limit (LL)	Plasticity Index (PI)	Specific Gravity (G_s)	USCS Classification
Cleburne	38	21	2.791	CL
Denton	55	30	2.803	CH
Grapevine 2	46	26	2.711	CL
Mansfield	67	38	2.782	CH
Plano	24	12	2.790	CL
Waco	58	34	2.701	CH

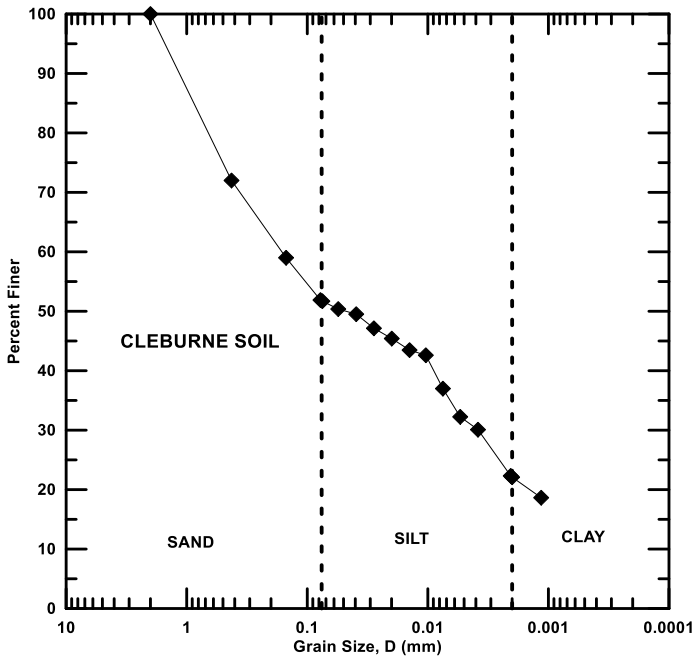

Figure 3-2 Gradation curve for Cleburne Soil

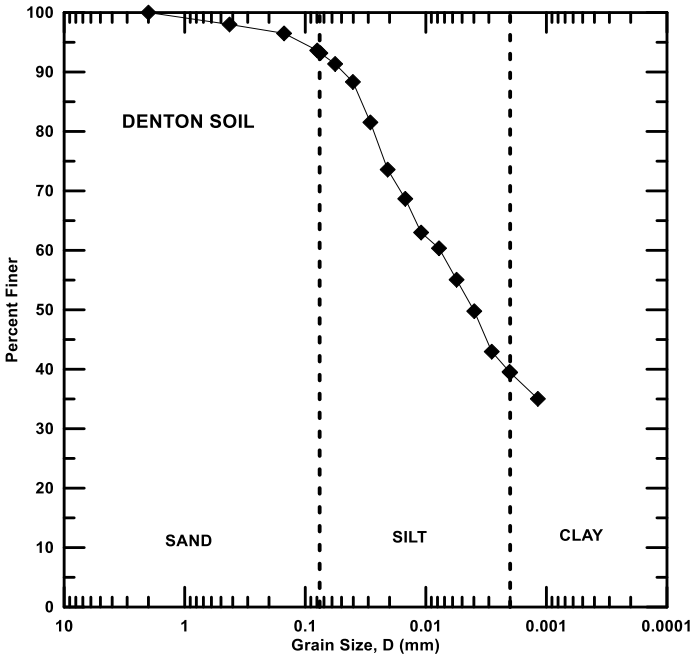

Figure 3-3 Gradation curve for Denton Soil

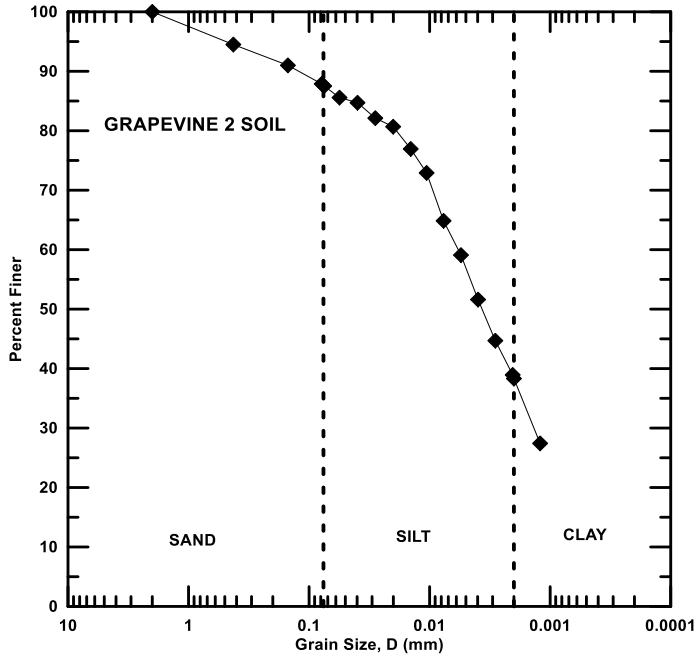

Figure 3-4 Gradation curve for Grapevine 2 Soil

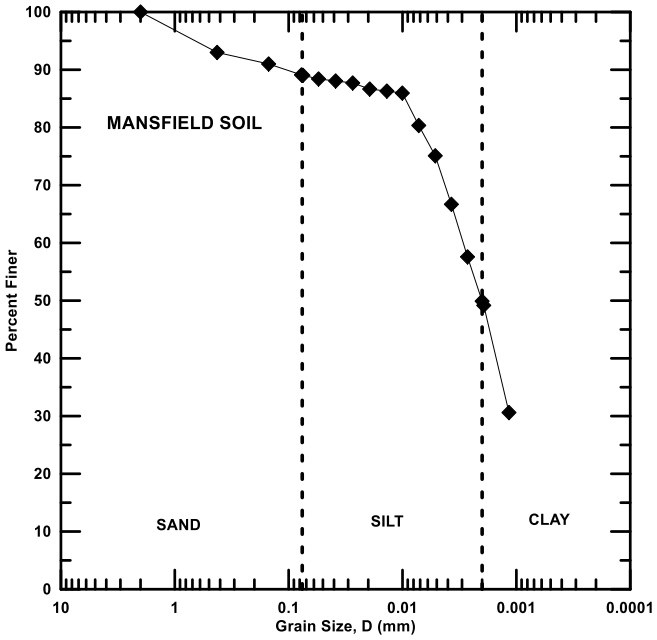

Figure 3-5 Gradation curve for Mansfield Soil

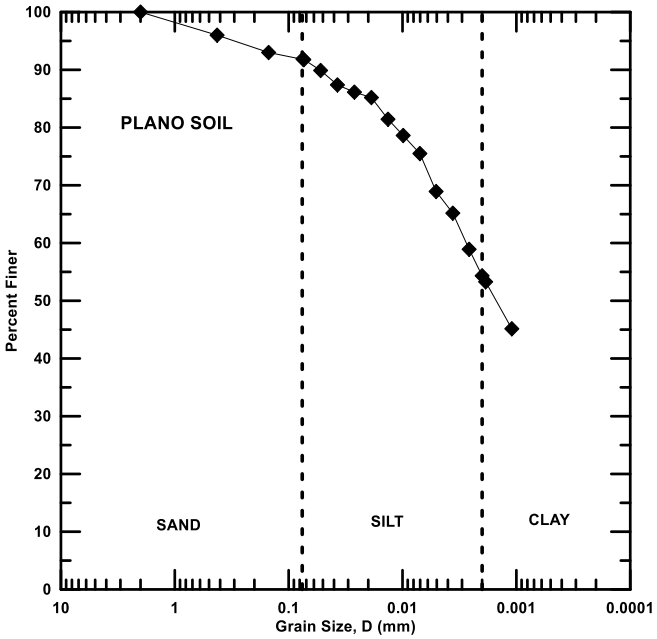

Figure 3-6 Gradation curve for Plano Soil

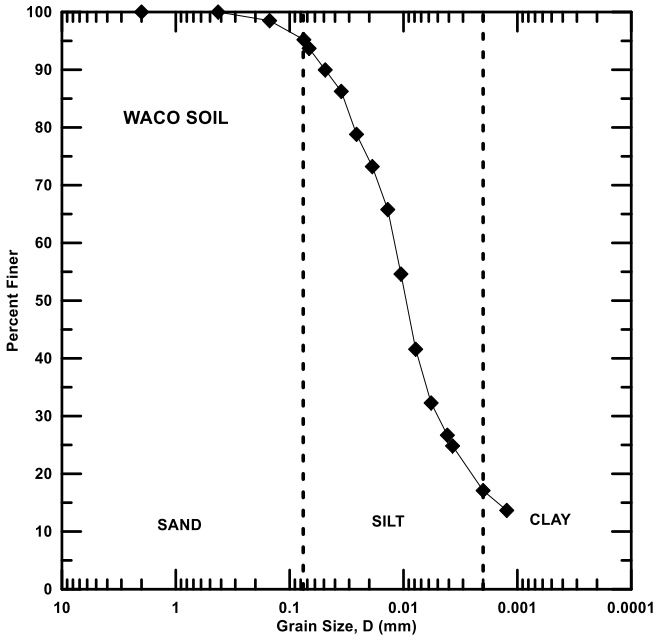

Figure 3-7 Gradation curve for Waco Soil

The summary of the gradation analysis are given in Table 3-2 below.

Table 3-2 Gradation test summary of the soils (dry and wet sieving and hydrometer tests)

Soil	Gradation			
	% Gravel	% Sand	% Silt	% Clay
Cleburne	0	48	30	22
Denton	0	7	54	39
Grapevine 2	0	13	49	38
Mansfield	0	11	39	50
Plano	0	8	38	54
Waco	0	5	78	17

Standard Proctor compaction tests were performed on the six chosen soils. Table 3-3 below shows the maximum dry density (MDD) and optimum moisture content (OMC) for all the six soils.

Table 3-3 Standard Proctor compaction test results

Soil	MDD (kg/m^3)	OMC (%)	95% MDD (kg/m^3)
Cleburne	1826	15	1735
Denton	1661	19	1578
Grapevine 2	1693	19	1608
Mansfield	1489	26	1415
Plano	1462	27	1389
Waco	1445	28	1373

3.3 Chemical and Mineralogical Tests

The procedure to determine clay mineralogy distribution and dominant clay mineral present in clays was presented in section 2.3.4 Clay minerals quantification procedure. It was applied in this research following the steps mentioned in the outlined section which are enclosed in the practical methodology given by Chittoori et al. (2011).

3.3.1 Determination of soluble sulfates content

The soluble sulfate in the soil is known for the cause of soil heaving when stabilized with calcium based stabilizers. In the present research, The Modified University of Texas Method (2002) formulated by Puppala et al. (2002) which is based on gravimetric procedure was used for measuring the amount of soluble sulfates in this research. Further details on the sulfate gravimetric method can be found in Wattanasanticharoen (2004).

3.3.2 Cation Exchange Capacity (CEC)

The CEC concept fundamentals are explained in section 2.3.4.1 Cation Exchange Capacity (CEC). The method involves addition of a saturating solution to the soil sample and then removal of the adsorbed cations by using an extracting solution. In the method used for this work, ammonium acetate (NH4OAc) is the saturating solution,

which has the ability to replace all the exchangeable cation locations with the ammonium (NH4+) cation. Hence, cation exchange process involving this saturating solution makes it appropriate for the reliable estimation of CEC of a soil. Detailed procedural steps are presented in Chittoori (2008). Also, a short review of the procedural steps of this method is presented graphically in Figure 3-8.

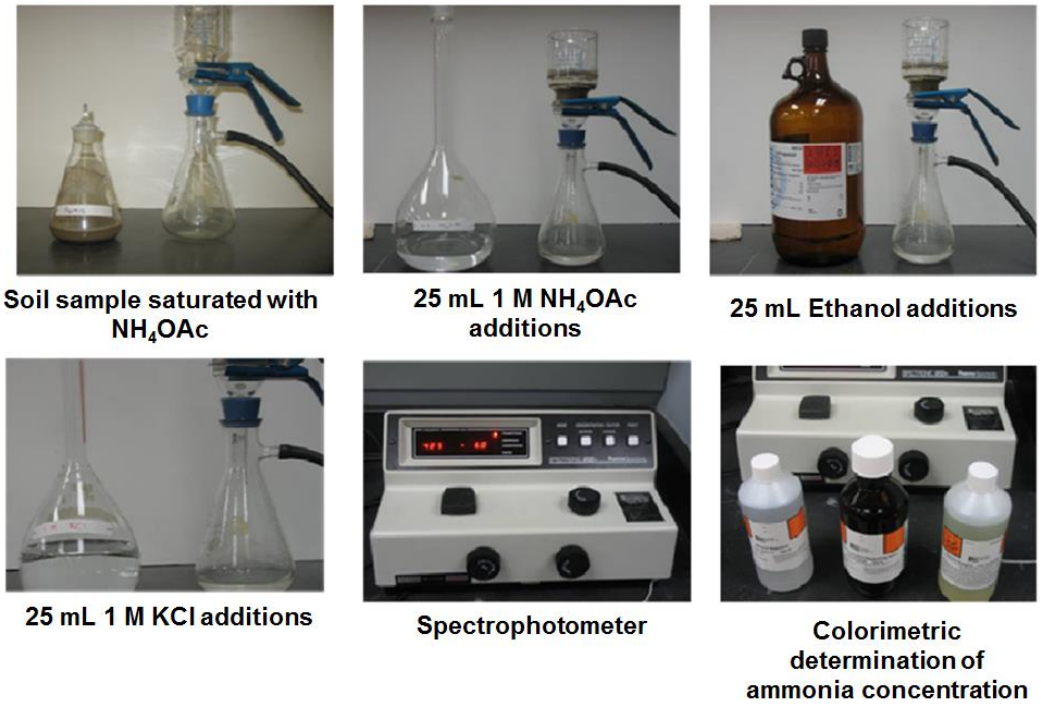

Figure 3-8 Showing the testing of Cation Exchange Capacity (CEC)

3.3.3 Specific Surface Area (SSA)

Definitions and importance of SSA in the swelling behavior of expansive soils are presented in section 2.3.4.2 Specific Surface Area (SSA).

This method comprises saturation of the prepared soil specimen, equilibration of the specimen in a vacuum over a calcium chloride-EGME (CaCl2-EGME) solvate and then determining the weight when the equilibrium of constant weight is achieved. Specific surface is then determined from the mass of retained EGME in comparison with the

amount retained by pure montmorillonite clay, which has a surface area of 810 m^2/g (Carter et al. 1986). This test procedure typically takes two days to complete.

The method consists of drying 1.1 g of soil sample in the oven at 100°C for 12 h and then recording the initial dry weight of the soil sample. Then, 3 ml of EGME is added and stirred. This mixture is kept in a desiccator containing EGME-CaCl2 solvate. The weight of the sample is monitored for every 2 h until there is no further decrease in weight. It normally takes 24 h to complete the test.

Detailed SSA procedure followed in this study by using the EGME method can be found in Chittoori (2008). Also, a short review of the procedural steps of this method is presented in a graphical manner in Figure 3-9.

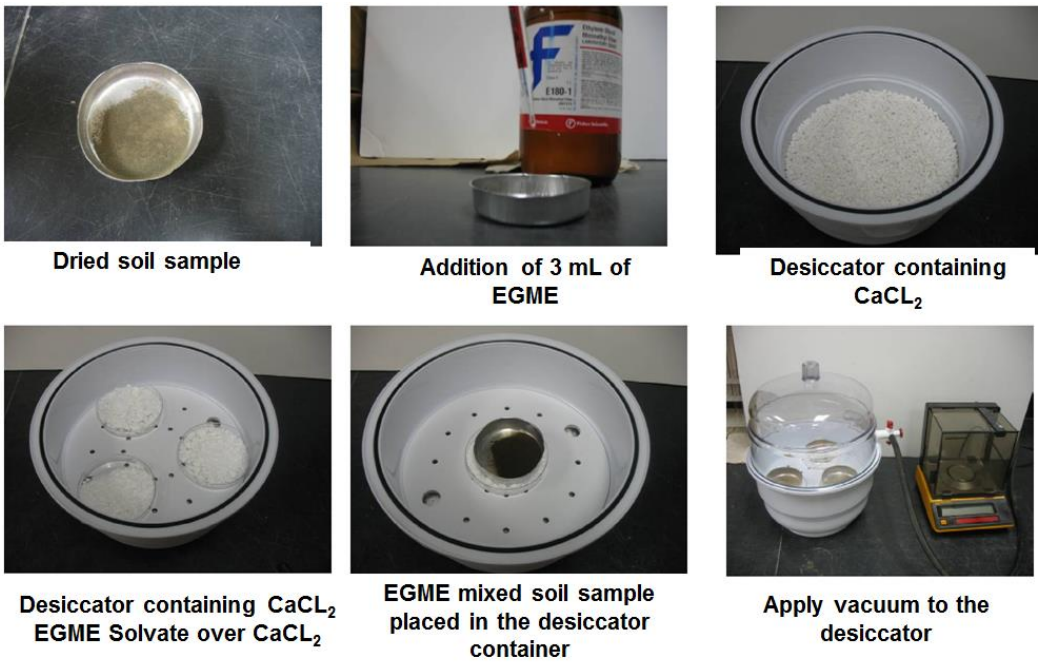

Figure 3-9 Testing procedure for Specific Surface Area (SSA)

3.3.4 Total Potassium (TP)

Important facts about the TP method and its relevance in the soil swelling behavior are presented in section 2.3.4.3 Total Potassium (TP).

The method involves a double acid digestion technique developed originally by Jackson (1958), which uses two acids, hydrofluoric and perchloric, to break the mineral structure of the soil and then extract the potassium ions from the structure.

Once the potassium is extracted, its concentration in the solution can be obtained with the help of a spectrophotometer or any other appropriate device.

Further details on the TP procedure followed in this research can be found in Chittoori (2008). Also, a brief step by step of this method is presented in a graphical fashion in Figure 3-10.

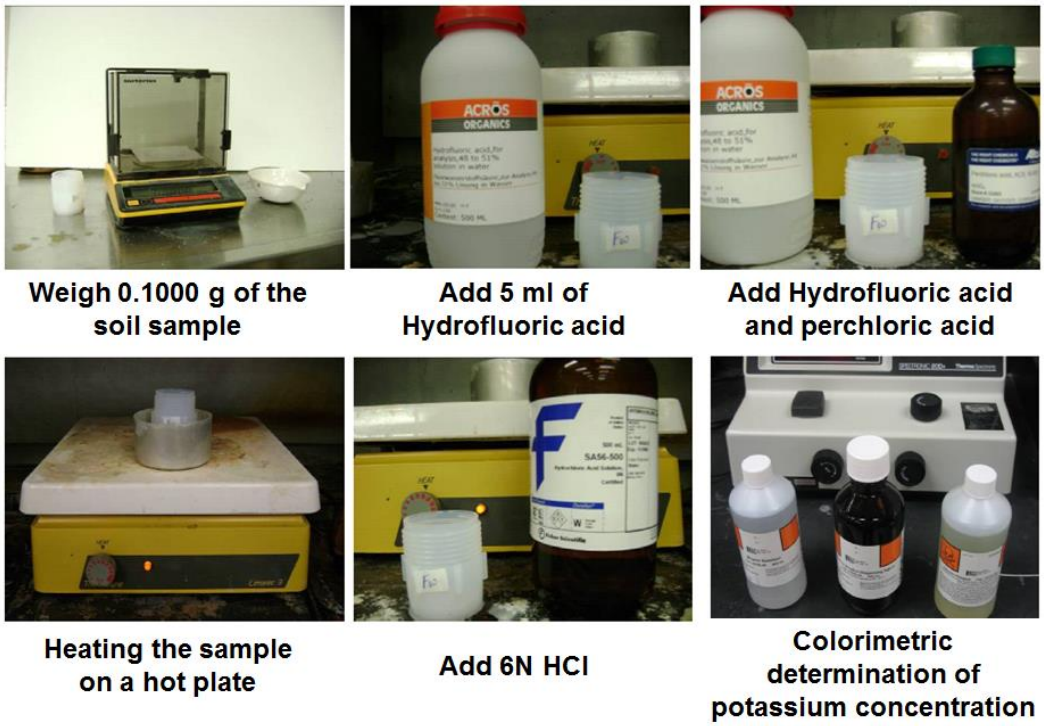

Figure 3-10 Testing procedure for Total potassium (TP)

As previously outlined, minerals present in all the tested soils were quantified according to the methodology proposed by Chittoori et al. (2011), and these results used

for quantification along with the mineral percentages are presented in Table 3-4 and Table 3-5.

The soluble sulfates determined for all the 6 soils are also presented in Table 3-5.

Table 3-4 Mineralogical tests results

Soil	CEC (meq/100g)	TP	SSA (m^2/g)
Cleburne	57.1	0.38	105.8
Denton	41.2	0.52	156.5
Grapevine 2	34.3	0.69	156.5
Mansfield	121.4	1.33	176.4
Plano	54.4	2.26	229.3
Waco	126.7	1.13	250.1

Table 3-5 Mineralogical properties of the tested clays

Soil	Soluble Sulfates (ppm)	% Montmorillonite	% Illite	% Kaolinite
Cleburne	1857	20.5	6.3	73.2
Denton	41280	20.4	8.6	71.0
Grapevine 2	1067	18.6	11.5	69.9
Mansfield	12431	42.8	22.1	35.1
Plano	5896	29.6	37.7	32.7
Waco	49	50.0	18.8	31.2

3.4 Engineering tests

Engineering tests in this research were used to study the swell behavior and pore void composition of the six selected soils. Tests like one dimensional swell strain, swell pressure and 3 dimensional swell strains under confinements were studied to understand

the swell behavior of the test soils. Determination of soil water characteristic curve (SWCC) which is the fundamental soil inherent composition property was also studied.

Determination of soil porosity and the pore networks are characterized using techniques like Mercury Intrusion Porosimetry (MIP) and X-ray computed Tomography (XCT).

3.4.1 Soil sample preparation

A static compactor, as suggested in the AASHTO T-307 method for preparing fine-grained soil specimens, was used in the present research. With this method, specimens with targeted moisture and density levels can be prepared in a short time frame. A comprehensive study was carried out by Wanyan et al. (2008) to develop a process for static compaction of clays in one layer with small variation in density. Pedarla (2013) presents a detailed summary of that sample preparation process which was followed in the present research for soil specimen preparation to maintain a low strain rate and thus preserve uniform density throughout specimen height.

Specimens of 2.54 cm (1 inch) height and 6.35 cm (2.5 inches) in diameter were prepared and used for the one dimensional swell and swell pressure testing. Samples having sizes of 10.16 cm (4 inches) in height and 5.08 cm (2 inches) in diameter were used for the 3-D Swell strain testing.

3.4.2 One Dimensional Swell and Swell Pressure Tests

In the present research, the six natural soils collected from different places of Texas were used to obtain remolded statically compacted specimens and to perform on them one dimensional (1D) swell tests and swell pressure tests procedures as determined by the Method C (loading-after-wetting test) normalized in the ASTM D4546 – 08 standard. Method C requires the specimen to swell freely under a vertical stress of 1

kPa (20 lbf/ft^2) at fully saturated conditions and then, when free swell expansion has taken place, to load increasingly the specimen to bring it back to its initial state.

Method C details were reviewed in section 2.2.1.1 One dimensional (1D) swell strains and pressures. Also additional ASTM D4546 – 08 Method C procedure details as applied during this research work may be seen in Pedarla (2013).

3.4.3 3-D swell strain apparatus

A three dimensional (3D) swell strain measurement apparatus as introduced by Pedarla (2013) was used for the measurement of swell strains in all directions. A brief review on the tests conducted with this device for soil swell potential determination by measuring the lateral swell strains exhibited by a soil specimen when confined in all the perpendicular three directions was given in section 2.2.1.2 Three dimensional (3D) swell strains. A depiction of the 3-D swell strain apparatus components is shown in Figure 3-11. Also, further information on the device and procedures followed during the present research may be seen in Pedarla's work (2013).

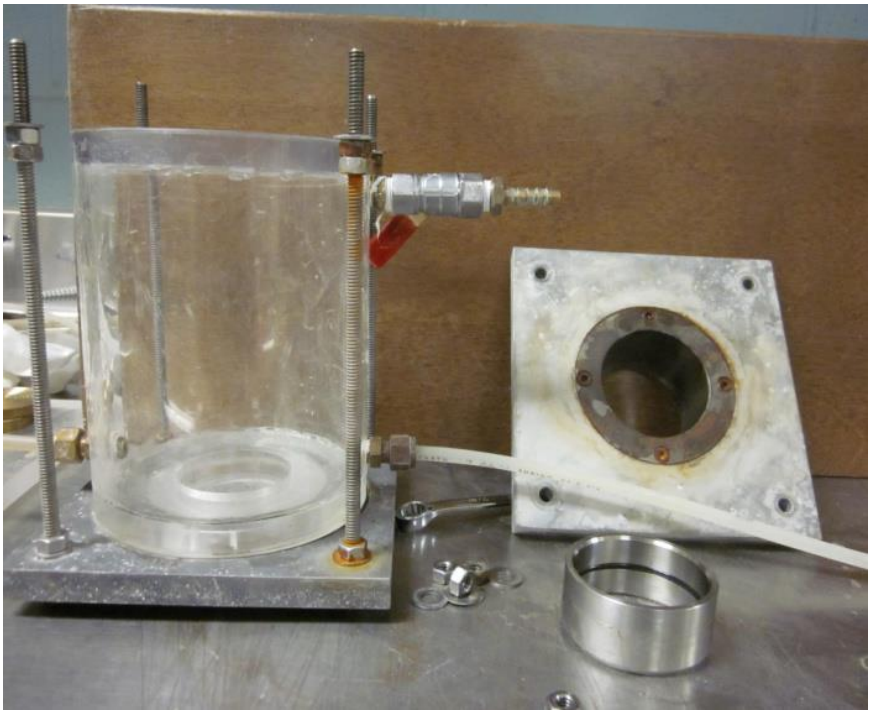

Figure 3-11 3-D swell strain apparatus components

3.5 Soil suction studies

Soil water characteristic curve (SWCC) is fundamental to correlate soil matric suction to different soil moisture content conditions. Several methods may be applied to determine the SWCC of a given soil. In the present study two methods were mainly used to determine the SWCC of the 6 tested soils.

3.5.1 Pressure Cell Apparatus

The pressure cell apparatus uses axis translation technique to measure the matric suction of a soil specimen. This is achieved with the help of a High Air Entry value disk (HAE).

This disk acts as an interface between the unsaturated soil and pore water and allows only water to pass through. Hence, the volume of water expelled from the soil sample was collected through the disk in to the burette columns. The flow of water

through the HAE disk was monitored for a period of time enough to allow equilibrium in height of water in the burettes.

Air pressure of a known value was applied until the sample reached an equilibrium stage and then the next pressure application was performed. The equilibrium can be identified by lack of change in height of water in the burettes. Figure 3-12 presents the pressure cell apparatus utilized in the current research.

The maximum matric suction that can be maintained across the HAE disk is called its air entry value. In the current research the HAE disks have an entry value of 5 bars. Functioning principles of the device is presented in section 2.4.2.1 Pressure Cell Apparatus.

Figure 3-12 Pressure cell apparatus

3.5.2 Filter paper method

The ASTM Filter Paper Method (ASTM D5928-94 - Standard Test Method for Measurement of Soil Suction) determines the matrix suction of the undisturbed and remolded specimens in the unsaturated state. Filter paper method is based on the assumption that the filter paper will come to equilibrium with a soil having a specific suction. This equilibrium state can be obtained with vapor moisture exchange or liquid exchange. When a dry filter paper is placed in direct contact with the soil specimen then liquid exchange occurs between the filter paper and soil specimen. The recorded moisture of the filter paper is the matric or solute suction for a soil specimen. Similarly when a dry filter paper is suspended above a soil specimen without contact, the moisture transfer between the soil and filter paper occur thorough vapor exchange. This measured moisture content in the filter paper corresponds to “total suction” of the soil.

The water content of the filter paper corresponds to a suction value given in the filter paper calibration curve designed by researchers. The same calibration curve is used to obtain total and matric suction for any soil. The filter paper method is used to measure a wide range of suctions. This method has been utilized in the current research to get the suction over higher ranges.

The filter papers used in the current research are as specified by ASTM E832. Figure 3-13 presents the Whatman No.42 filter papers used in the present study.

Figure 3-13 Filter paper technique

3.6 Pore studies

Porosity of a soil specimen is important in understanding the formation, structure, and voids. The porosity of a material influences its physical properties and, subsequently, soil behavior in its surrounding environment. The adsorption, permeability, strength, density, and many other factors are also influenced by the porosity of the material or a soil. Two methods are presented here to identify and measure the pore network present in a given soil specimen.

3.6.1 Mercury Intrusion Porosimetry (MIP)

Mercury intrusion porosimetry or MIP is based on the premise that a non-wetting liquid (contact angle greater than 90°) will intrude capillaries (pores of a solid) under external pressure.

Since mercury does not wet most substances and will not spontaneously penetrate pores by capillary action, it must be forced into the pores by the application of

external pressure. The required equilibrated pressure is inversely proportional to the size of the pores, only slight pressure being required to intrude mercury into large macro-pores, whereas much greater pressures are required to force mercury into small pores.

MIP procedure details were reviewed in section 2.5.1 Mercury Intrusion Porosimetry (MIP) Technique. Also additional MIP technique details as applied during this research work is presented by Pedarla (2013).

3.6.2 X-ray Computed Tomography (XCT)

XCT is a non-destructive, non-invasive technique used to investigate the pores and internal structure of a solid mass, and is based on the principle of the attenuation of an electromagnetic wave beam that is focused on the object. The characteristic of an absorbing material to scatter or absorb a photon is called the attenuation coefficient. A material with high density will attenuate more x-rays than a low-density material; therefore, two materials of different densities will appear differently in an X-ray image.

XCT is an imaging technique in which an object is placed between an X-ray source and a detector, and the object is rotated while the X-ray passes through it, collecting information about its internal structure. As the X-ray beam passes through an object, some photons are either scattered with some loss of energy, or completely absorbed in a photoelectric interaction. The digital image created during the CT process provides an internal cross-section of the specimen in which different materials can be distinguished.

During the XCT performing, a representative soil specimen of 1 cm in height, width and depth was sliced from compacted soil specimens as shown in Figure 3-14. Once sliced, the cubical 1 cm side specimens were oven dried or saturated depending on the requirement for computed tomography scan. The soil specimen has to be seated steady in the CT chamber, if any changes in the initial position occur, the CT scan will be

blurred. Hence, proper care needs to be taken when placing the specimen in the chamber.

Figure 3-14 Soil specimens prepared for Tomography testing

A review on the XCT technique features has been presented in section 2.5.2 X-ray Computed Tomography (XCT). Procedures applied during the present study on XCT also may be seen in the work performed by Pedarla (2013).

3.7 Summary

Basic soil classification and other geotechnical testing performed on the six expansive soils have been presented in this chapter. Chemical analysis to determine the mineral content of expansive clays is presented along with their procedures. Details of the test results for direct swelling behavior determination are presented in Chapter 4. The SWCC of the six soils as well as the variation of pore network with moisture content in these clays are studied in Chapter 5.

The present chapter summarizes the different techniques that are used to determine the soil swell and composition properties. Swell behavior of compacted soil

specimens was determined using different swell measurement procedures like 1-D vertical swell strain, swell pressures and novel 3-D swell strain tests. The details and working of each test procedure are discussed in this chapter. Determination of soil moisture relationships were developed using suction measurement techniques. Advanced techniques like mercury intrusion porosimetry and X-ray computed tomography which are used to study the pore space and distribution are discussed in detail along with their working principles. The next chapter deals with the test results obtained from different swell measurement test procedures.

Chapter 4

Swell behavior of soils

4.1 Introduction

The tendency to swell in soils is normally measured in the laboratory according to the amount of swell the soil undergoes when tested using direct methods as explained in Chapter 2. Thus, many laboratory devices and test procedures have been used to characterize the expansive behavior of soils. The differences between test procedures mainly rely on the type of confinement applied on the soil specimen, the swelling process and the monitoring of strains in vertical and radial directions.

The one dimensional consolidometer has been widely accepted method for testing swelling potential of soils (Holtz and Gibbs, 1956). In the present research, one dimensional vertical swell strains as well as load back swell pressures were measured in a conventional consolidometer setup. A novel 3-dimensional swell strain measurement apparatus was used for the measurement of swell strains in all directions. Details of the working principles and techniques are given in Chapter 2 and Chapter 3.

Expansive behavior exhibited by all the six soils in this research is presented in this Chapter, by describing swell strain conditions (one and three dimensions), and swell pressure variations in the soils.

4.2 Measured Swell Behavior

4.2.1 Cleburne Soil

Cleburne soil was collected from Cleburne city in Texas. Based on the USCS soil classification system the soil was classified as low plasticity clay (CL). The swelling behavior of Cleburne soil is presented in the following section.

4.2.1.1 1-D Swell strain and Load-back swell pressures

Figure 1-1 presents the 1-D swell strains exhibited by Cleburne soil specimen at two different compaction dry densities, i.e. maximum dry density (MDD) and 95% of maximum dry density (95% MDD).

The specimens exhibited a maximum swell strain of 5.8% at maximum dry density (MDD) condition and 3.2% swell strain at 95% MDD condition.

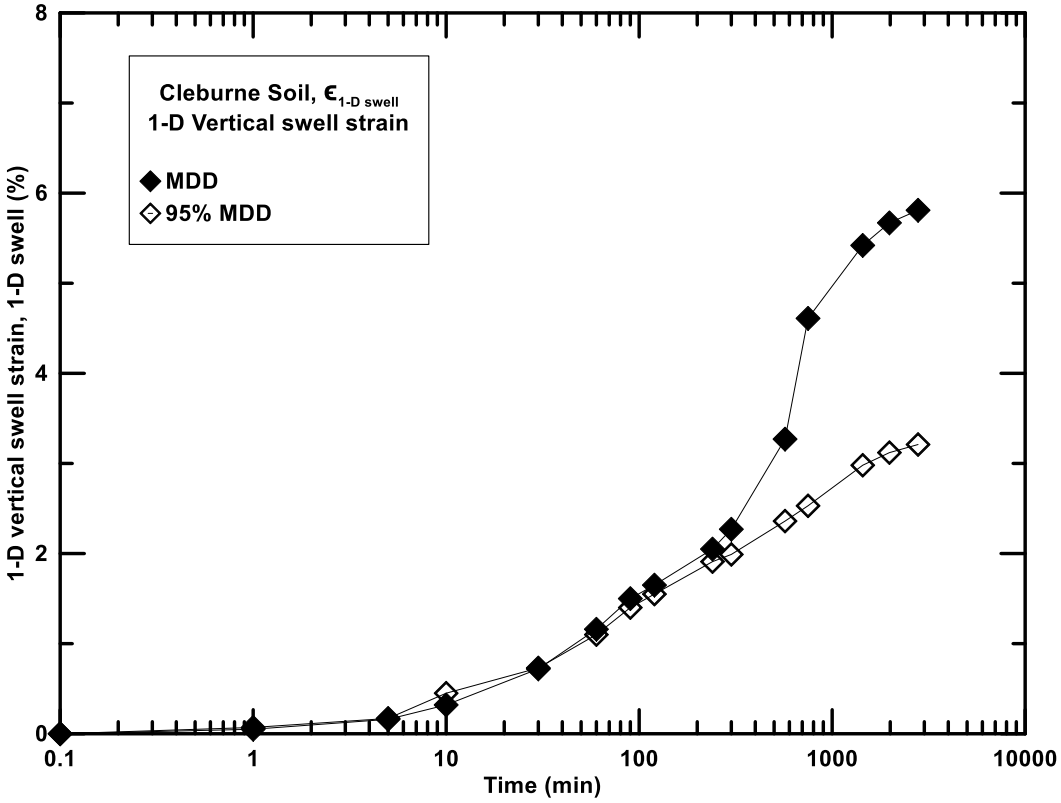

Figure 4-1 One dimensional swell strains for Cleburne soil

Figure 4-2 and Figure 4-3 present the load-back swell pressures exhibited by Cleburne soil at two different densities. Soil specimens compacted at 95% MDD and MDD condition exhibited swell pressures of 96.2 kPa (13.7 psi) and 141.7 kPa (20.2 psi), respectively.

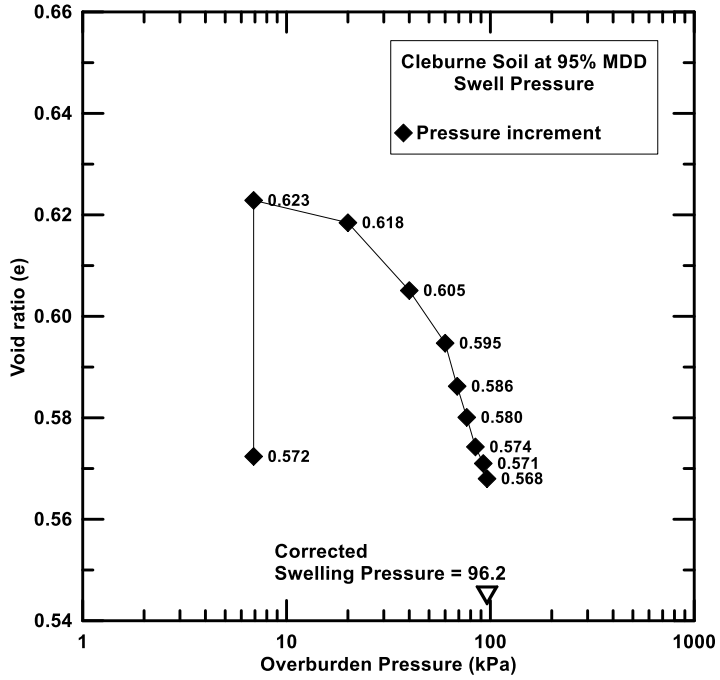

Figure 4-2 Load-back swell pressure test on Cleburne soil at 95% MDD

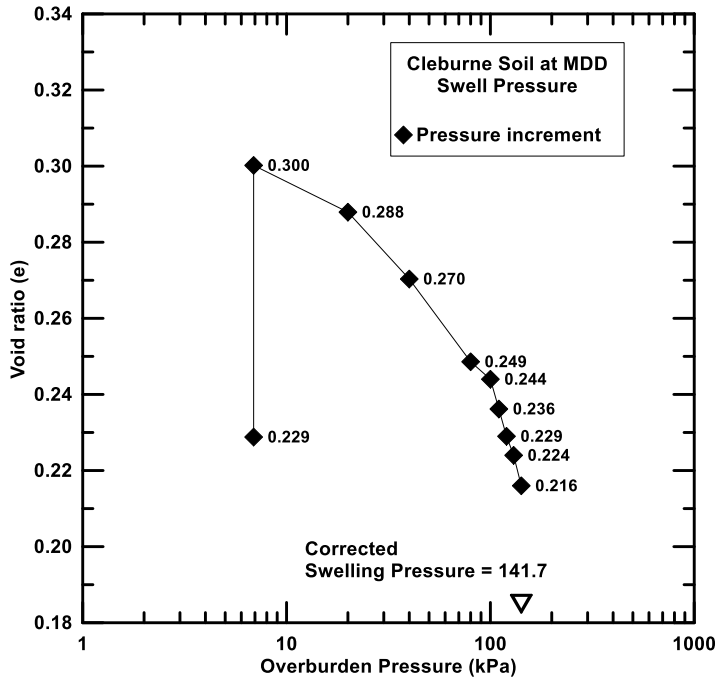

Figure 4-3 Load-back swell pressure test on Cleburne soil at MDD

4.2.1.2 3-D swell strains

Soil specimens of 50.8 mm (2 in.) diameter and 101.6 mm (4 in.) height were compacted at 95% MDD and were tested for 3-D volumetric swell strains. Figure 4-4 presents the 3-D vertical swell strains exhibited by Cleburne soil specimen at three different confinement levels. The specimen showed a maximum vertical swell strain of 0.73% at 7 kPa (1 psi) confinement whereas; it showed 0.05% strain at 100 kPa (14.5 psi) confinement. Similarly, Figure 4-5 shows the radial swell strain exhibited by the same soil specimen at different confinements. The specimen exhibited a maximum radial swell strain of 1.2% at 7 kPa (1 psi) confinement and least radial strain of 0.71% at 100 kPa (14.5 psi) confinement.

The total volumetric strain is calculated from the summation of vertical swell strain and twice of radial swell strain and is presented in Figure 4-6. The specimen showed maximum volumetric swell strains of 3.2% at 7 kPa (1 psi), 1.7% at 50 kPa (7.25 psi) and 1.5% at 100 kPa (14.5 psi) confinement levels.

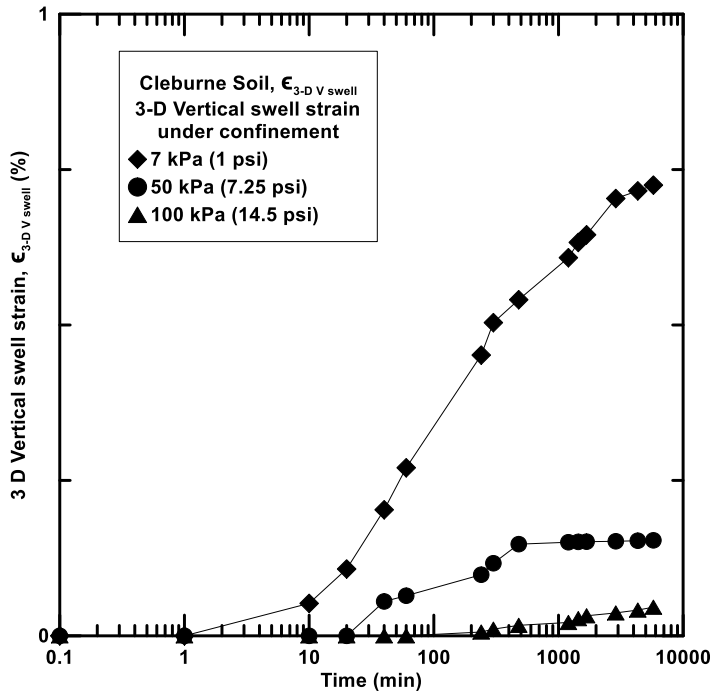

Figure 4-4 Vertical swell strain exhibited by Cleburne soil at different confinements

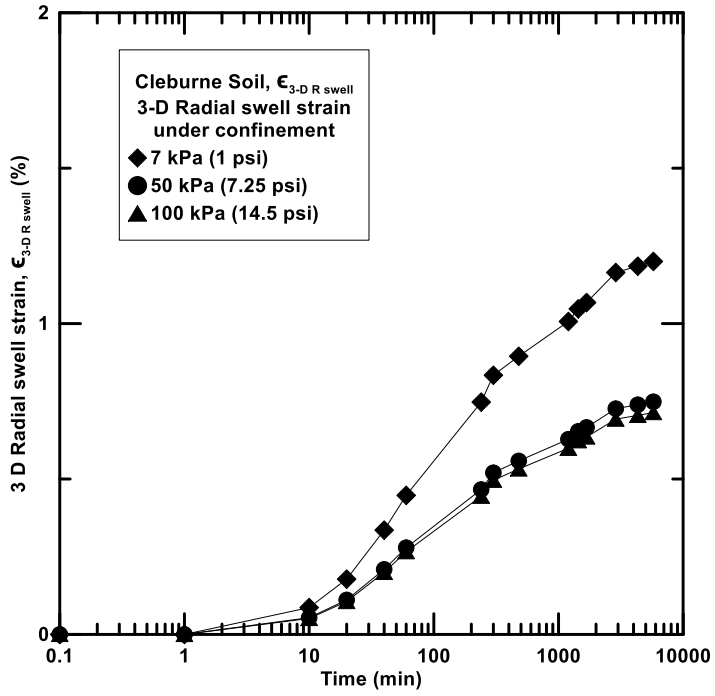

Figure 4-5 Radial swell strain exhibited by Cleburne soil at different confinements

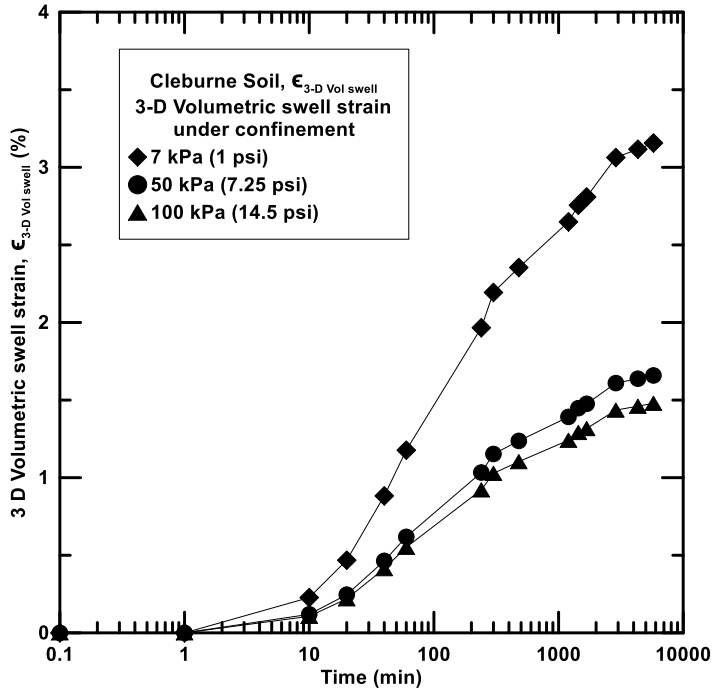

Figure 4-6 Volumetric swell strain exhibited by Cleburne soil at different confinements

4.2.2 Denton Soil

Denton soil was collected from Denton city in Texas. Based on the USCS soil classification system the soil was classified as high plasticity clay (CH). The swelling behavior of Denton soil is presented in the following section.

4.2.2.1 1-D Swell strain and Load-back swell pressures

Figure 4-7 presents the 1-D swell strains exhibited by Denton soil specimen at two different compaction dry densities, i.e. maximum dry density (MDD) and 95% of maximum dry density (95% MDD). The specimens exhibited a maximum swell strain of 6.5% at maximum dry density (MDD) condition and 3.5% swell strain at 95% MDD condition.

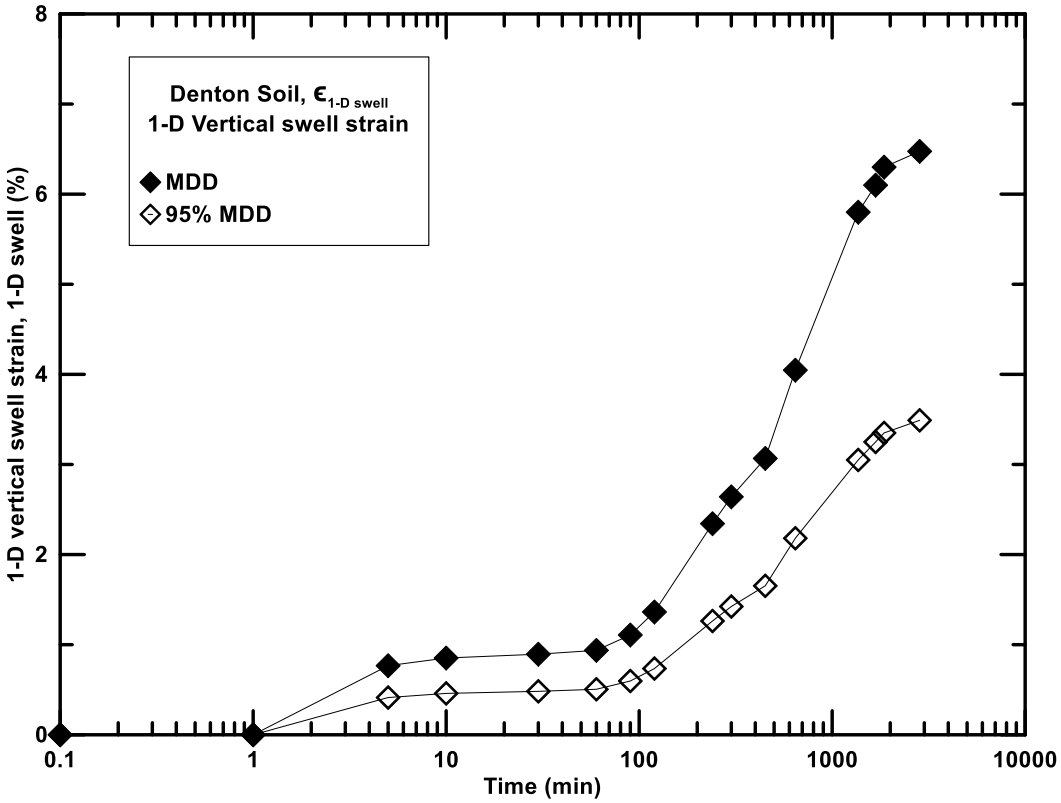

Figure 4-7 One dimensional swell strains for Denton soil

Figure 4-8 and Figure 4-9 present the load-back swell pressures exhibited by Denton soil at two different densities. Soil specimens compacted at 95% MDD and MDD condition exhibited swell pressures of 65.3 kPa (9.3 psi) and 67.4 kPa (9.6 psi), respectively.

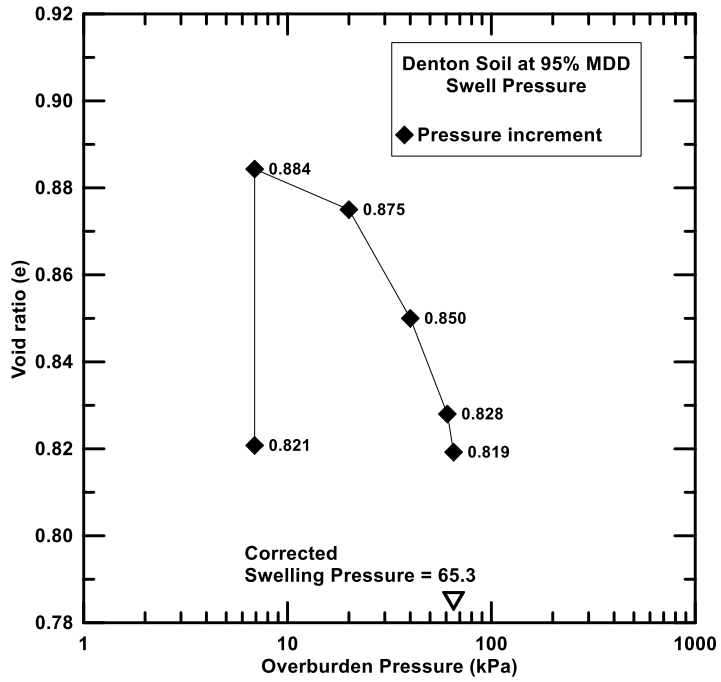

Figure 4-8 Load-back swell pressure test on Denton soil at 95% MDD

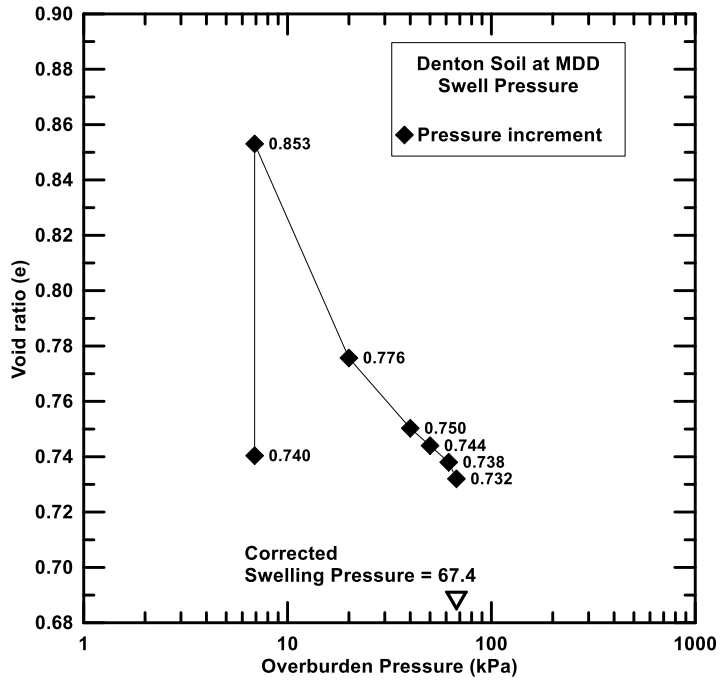

Figure 4-9 Load-back swell pressure test on Denton soil at MDD

4.2.2.2 3-D swell strains

Soil specimens of 50.8 mm (2 in.) diameter and 101.6 mm (4 in.) height were compacted at 95% MDD and were tested for 3-D volumetric swell strains. Figure 4-10 presents the 3-D vertical swell strains exhibited by Denton soil specimen at three different confinement levels. The specimen showed a maximum vertical swell strain of 0.9% at 7 kPa (1 psi) confinement whereas; it showed 0.07% strain at 100 kPa (14.5 psi) confinement. Similarly, Figure 4-11 shows the radial swell strain exhibited by the same soil specimen at different confinements. The specimen exhibited a maximum radial swell strain of 1.3% at 7 kPa (1 psi) confinement and least radial strain of 1.0% at 100 kPa (14.5 psi) confinement.

The total volumetric strain is calculated from the summation of vertical swell strain and twice of radial swell strain and is presented in Figure 4-12. The specimen showed maximum volumetric swell strains of 3.5% at 7 kPa (1 psi), 2.9% at 50 kPa (7.25 psi) and 2.5% at 100 kPa (14.5 psi) confinement levels.

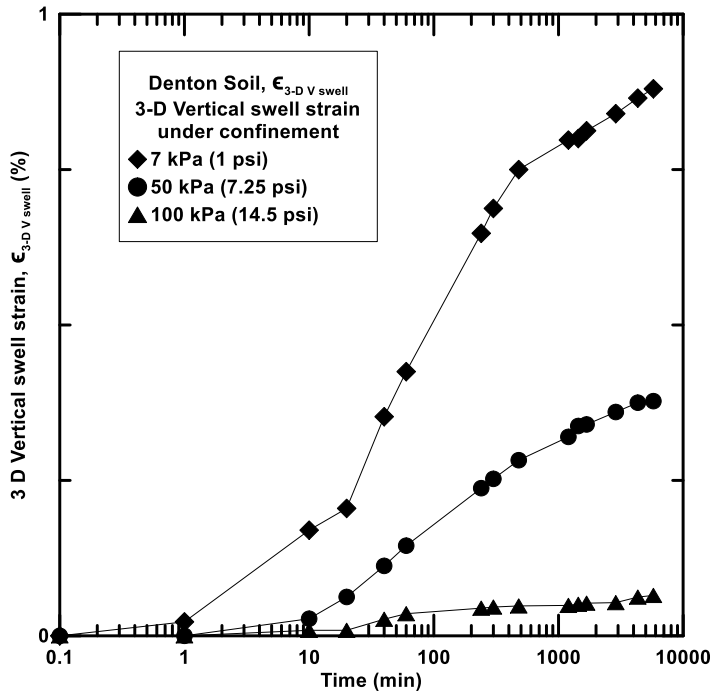

Figure 4-10 Vertical swell strain exhibited by Denton soil at different confinements

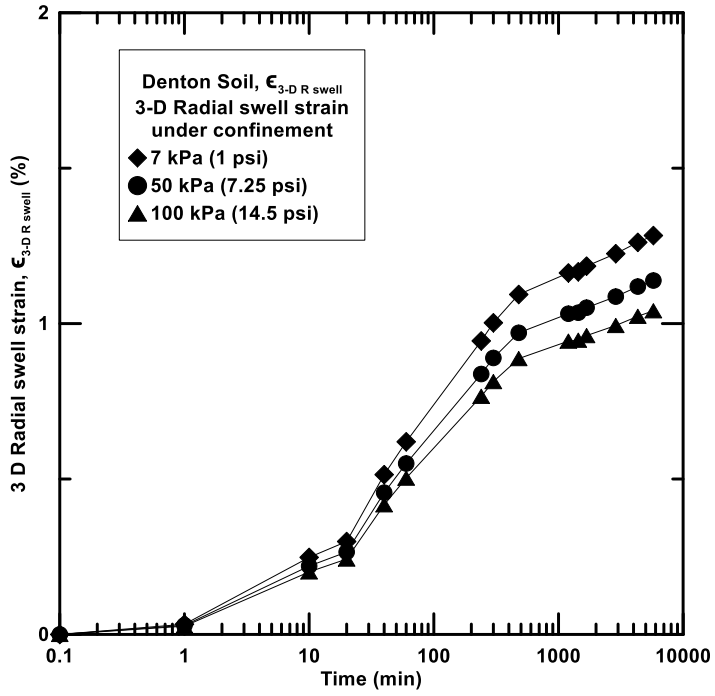

Figure 4-11 Radial swell strain exhibited by Denton soil at different confinements

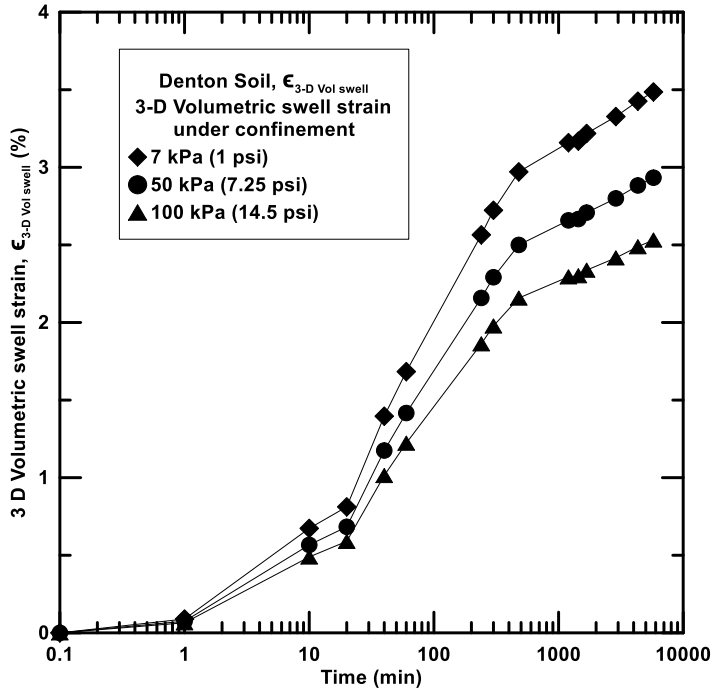

Figure 4-12 Volumetric swell strain exhibited by Denton soil at different confinements

4.2.3 Grapevine 2 Soil

Grapevine 2 soil was collected from Grapevine 2 city in Texas. Based on the USCS soil classification system the soil was classified as low plasticity clay (CL). The swelling behavior of Grapevine 2 soil is presented in the following section.

4.2.3.1 1-D Swell strain and Load-back swell pressures

Figure 4-13 presents the 1-D swell strains exhibited by Grapevine 2 soil specimen at two different compaction dry densities, i.e. maximum dry density (MDD) and 95% of maximum dry density (95% MDD).

The specimens exhibited a maximum swell strain of 6.2% at maximum dry density (MDD) condition and 4.3% swell strain at 95% MDD condition.

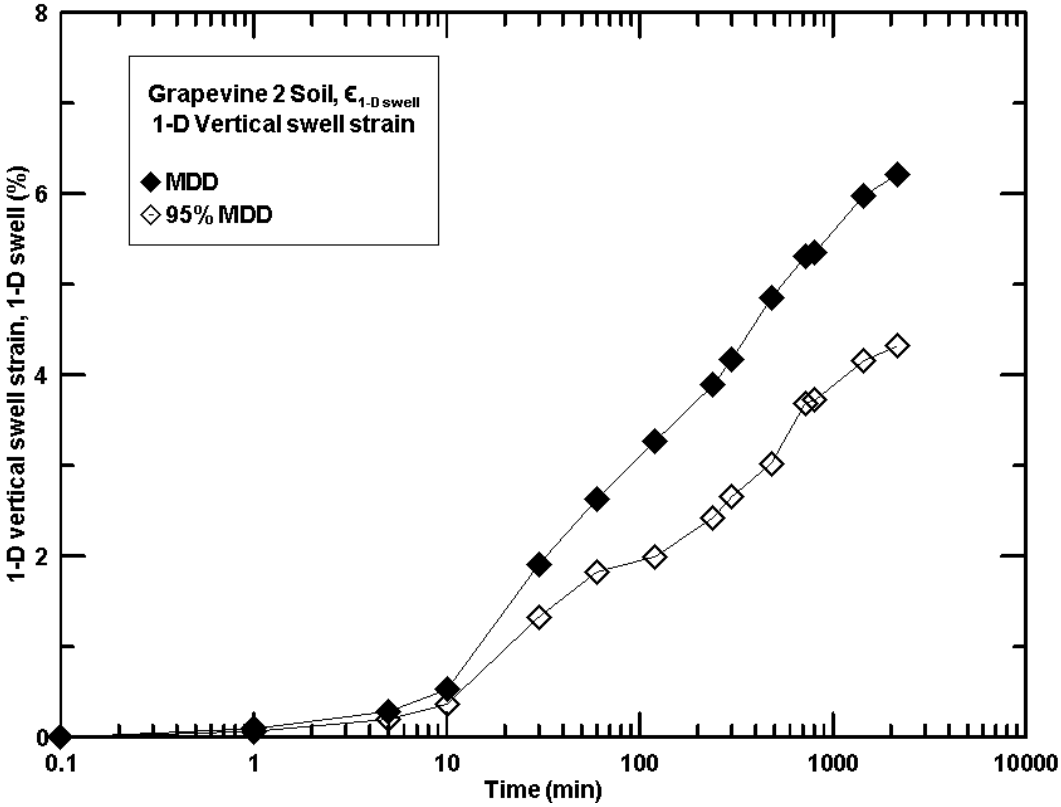

Figure 4-13 One dimensional swell strains for Grapevine 2 soil

Figure 4-14 and Figure 4-15 present the load-back swell pressures exhibited by Grapevine 2 soil at two different densities. Soil specimens compacted at 95% MDD and MDD condition exhibited swell pressures of 82.7 kPa (11.8 psi) and 88.4 kPa (12.6 psi), respectively.

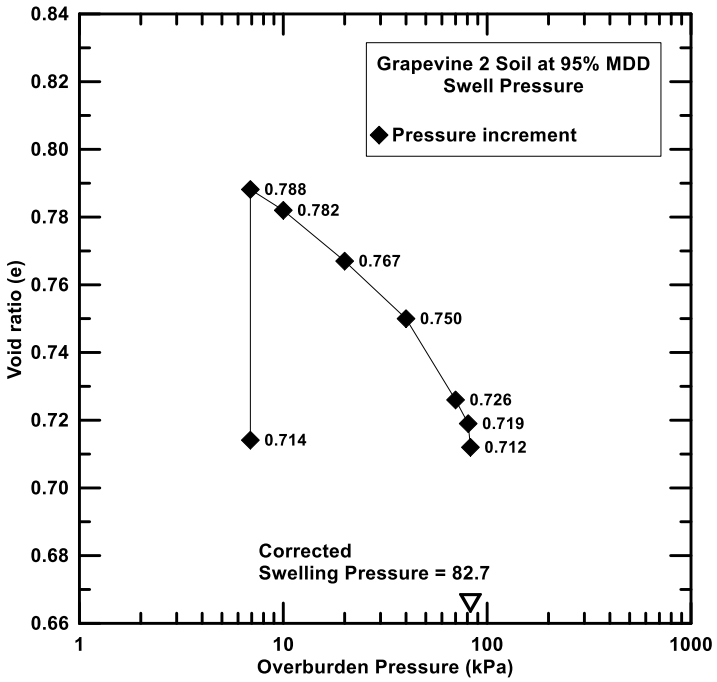

Figure 4-14 Load-back swell pressure test on Grapevine 2 soil at 95% MDD

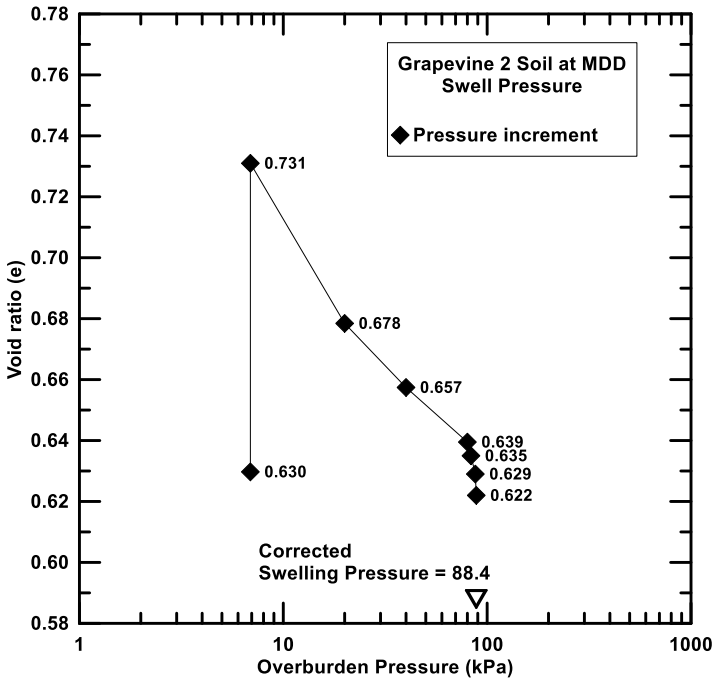

Figure 4-15 Load-back swell pressure test on Grapevine 2 soil at MDD

4.2.3.2 3-D swell strains

Soil specimens of 50.8 mm (2 in.) diameter and 101.6 mm (4 in.) height were compacted at 95% MDD and were tested for 3-D volumetric swell strains. Figure 4-16 presents the 3-D vertical swell strains exhibited by Grapevine 2 soil specimen at three different confinement levels. The specimen showed a maximum vertical swell strain of 1.7% at 7 kPa (1 psi) confinement whereas; it showed 0.29% strain at 100 kPa (14.5 psi) confinement. Similarly, Figure 4-17 shows the radial swell strain exhibited by the same soil specimen at different confinements. The specimen exhibited a maximum radial swell strain of 1.5% at 7 kPa (1 psi) confinement and least radial strain of 0.56% at 100 kPa (14.5 psi) confinement.

The total volumetric strain is calculated from the summation of vertical swell strain and twice of radial swell strain and is presented in Figure 4-18. The specimen showed maximum volumetric swell strains of 4.7% at 7 kPa (1 psi), 2.3% at 50 kPa (7.25 psi) and 1.4% at 100 kPa (14.5 psi) confinement levels.

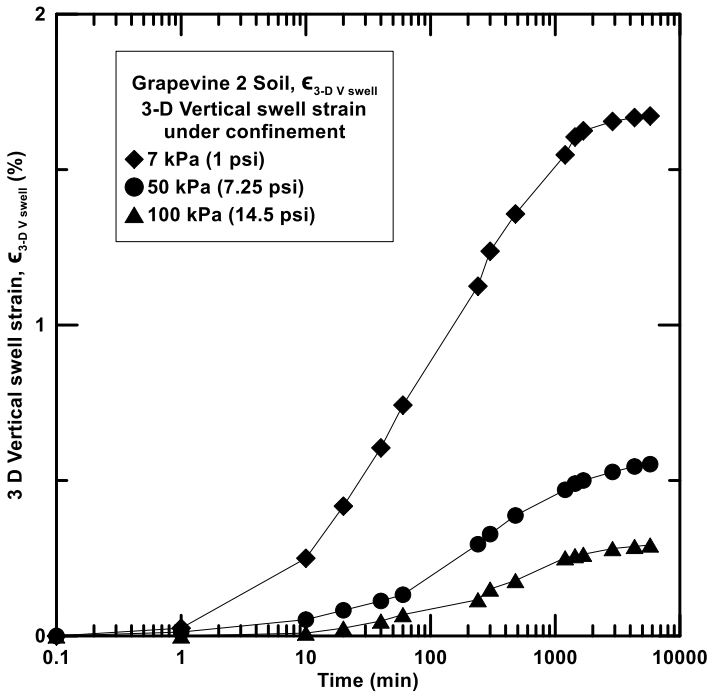

Figure 4-16 Vertical swell strain exhibited by Grapevine 2 soil at different confinements

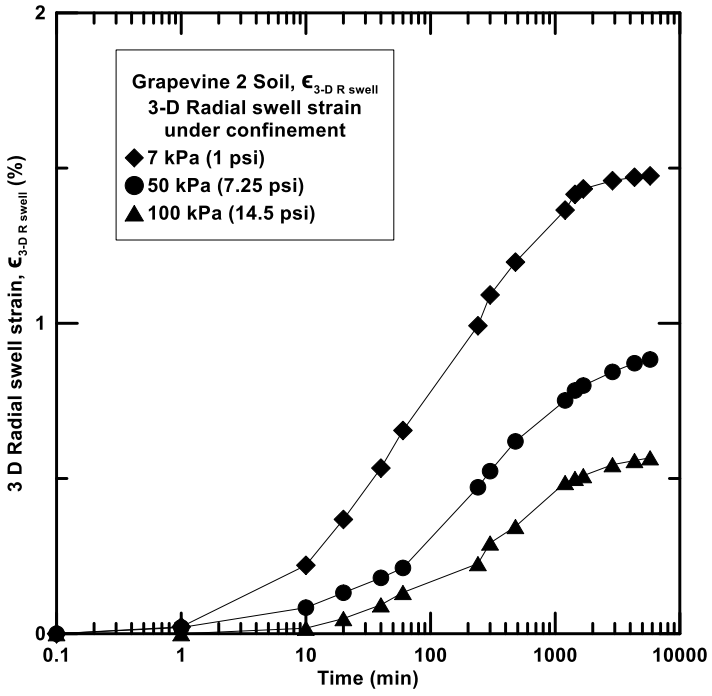

Figure 4-17 Radial swell strain exhibited by Grapevine 2 soil at different confinements

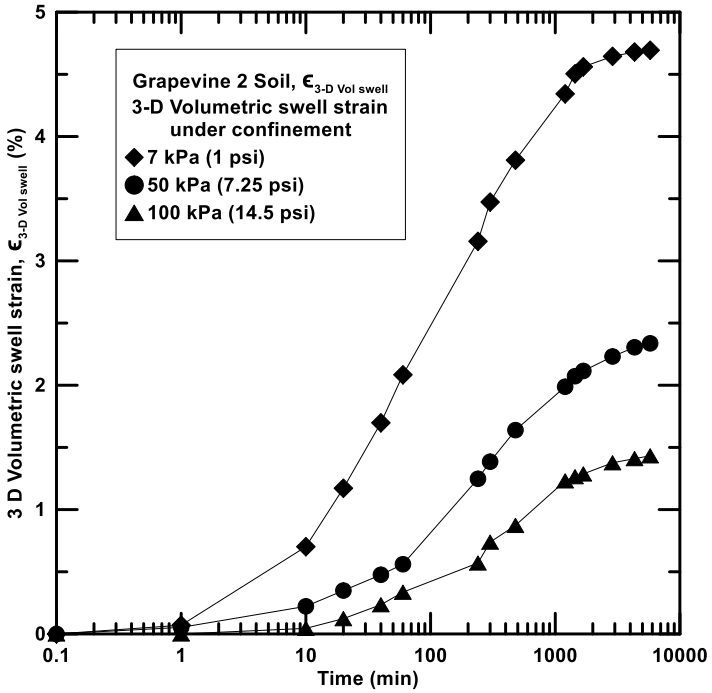

Figure 4-18 Volumetric swell strain exhibited by Grapevine 2 soil at different confinements

4.2.4 Mansfield Soil

Mansfield soil was collected from Mansfield city in Texas. Based on the USCS soil classification system the soil was classified as high plasticity clay (CH). The swelling behavior of Mansfield soil is presented in the following section.

4.2.4.1 1-D Swell strain and Load-back swell pressures

Figure 4-19 shown below presents the 1-D swell strains exhibited by Mansfield soil specimen at two different compaction dry densities, i.e. maximum dry density (MDD) and 95% of maximum dry density (95% MDD).

The specimens exhibited a maximum swell strain of 10.8% at maximum dry density (MDD) condition and 9.5% swell strain at 95% MDD condition.

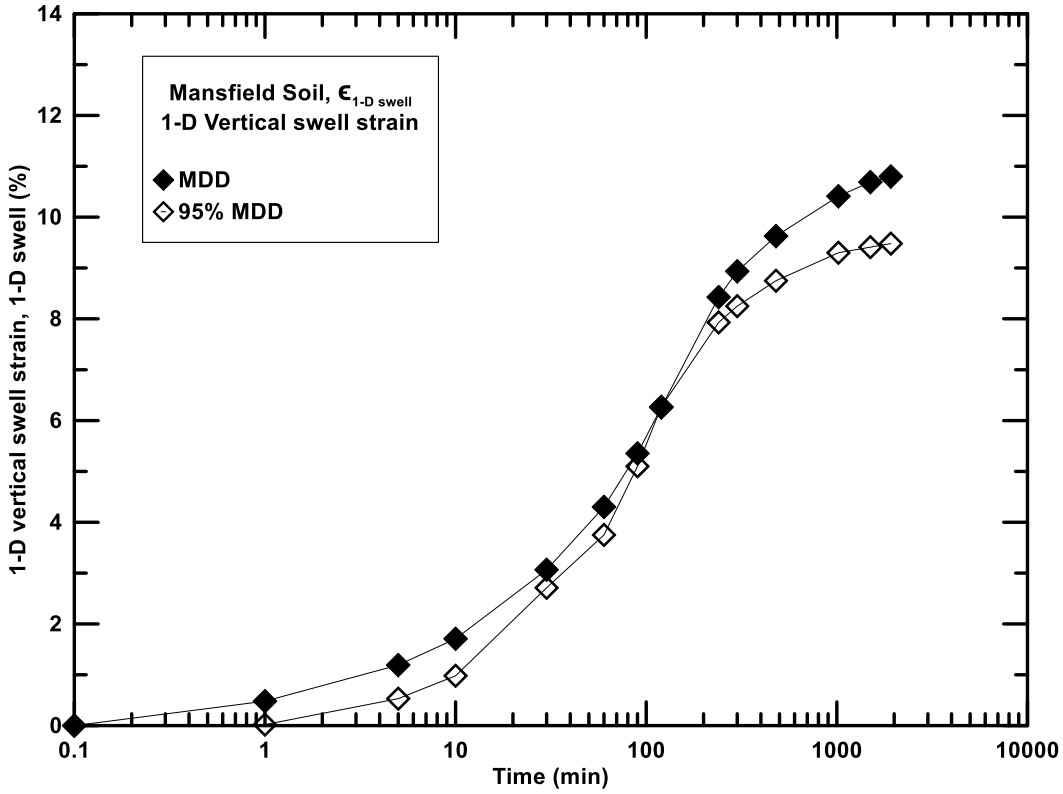

Figure 4-19 One dimensional swell strains for Mansfield soil

Figure 4-20 and Figure 4-21 present the load-back swell pressures exhibited by Mansfield soil at two different densities. Soil specimens compacted at 95% MDD and MDD condition exhibited swell pressures of 138.9 kPa (19.8 psi) and 164.2 kPa (23.5 psi), respectively.

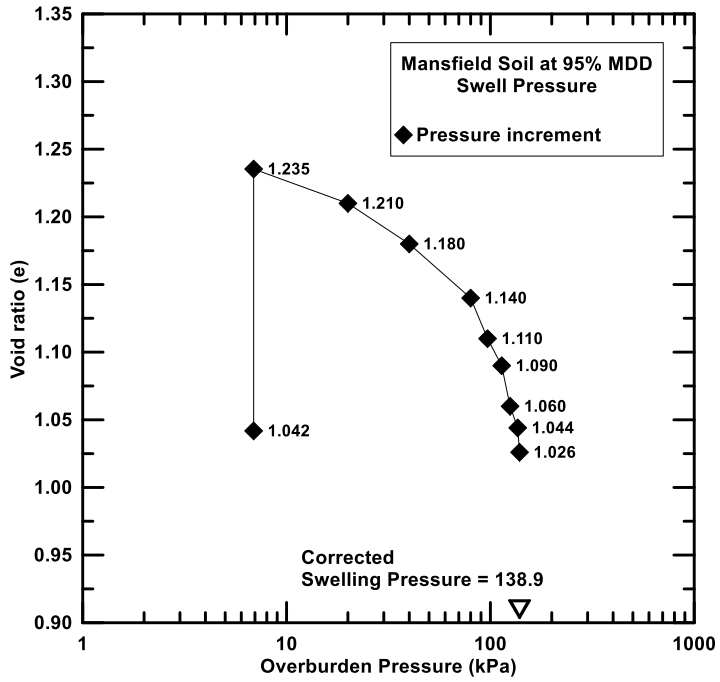

Figure 4-20 Load-back swell pressure test on Mansfield soil at 95% MDD

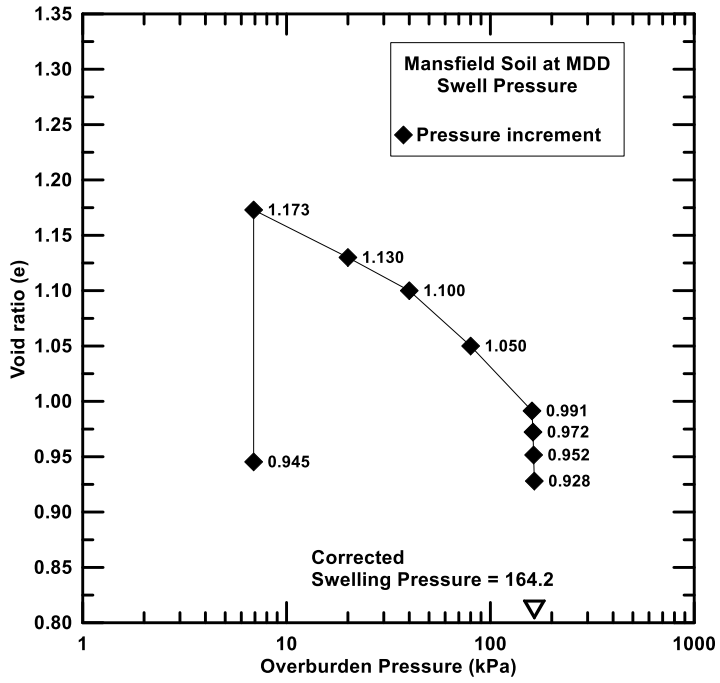

Figure 4-21 Load-back swell pressure test on Mansfield soil at MDD

4.2.4.2 3-D swell strains

Soil specimens of 50.8 mm (2 in.) diameter and 101.6 mm (4 in.) height were compacted at 95% MDD and were tested for 3-D volumetric swell strains. Figure 4-22 presents the 3-D vertical swell strains exhibited by Mansfield soil specimen at three different confinement levels. The specimen showed a maximum vertical swell strain of 4.2% at 7 kPa (1 psi) confinement whereas; it showed 2.7% strain at 100 kPa (14.5 psi) confinement. Similarly, Figure 4-23 shows the radial swell strain exhibited by the same soil specimen at different confinements. The specimen exhibited a maximum radial swell strain of 2.9% at 7 kPa (1 psi) confinement and least radial strain of 2.0% at 100 kPa (14.5 psi) confinement.

The total volumetric strain is calculated from the summation of vertical swell strain and twice of radial swell strain and is presented in Figure 4-24. The specimen showed maximum volumetric swell strains of 10.2% at 7 kPa (1 psi), 7.8% at 50 kPa (7.25 psi) and 6.8% at 100 kPa (14.5 psi) confinement levels.

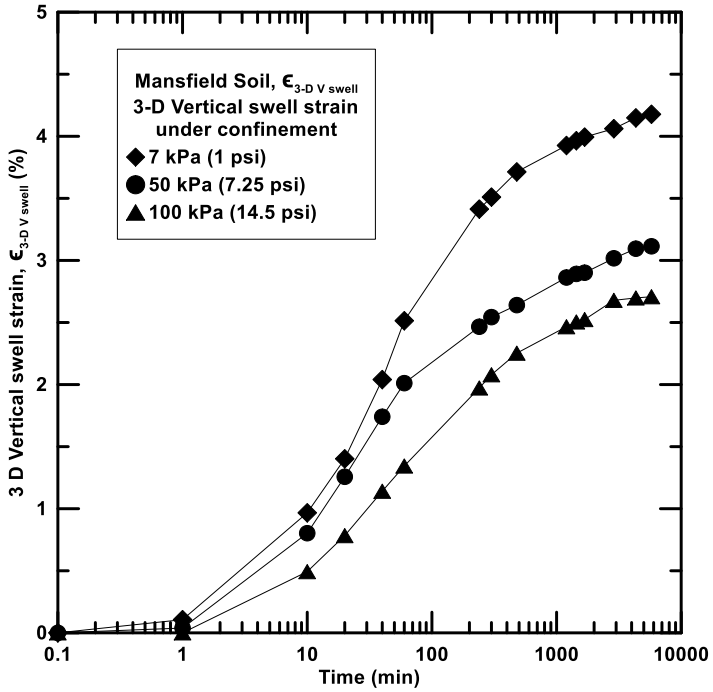

Figure 4-22 Vertical swell strain exhibited by Mansfield soil at different confinements

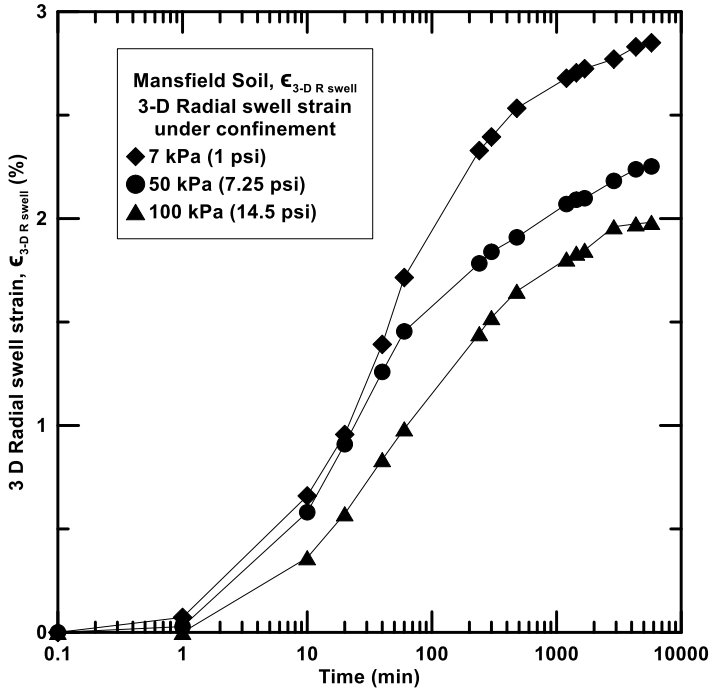

Figure 4-23 Radial swell strain exhibited by Mansfield soil at different confinements

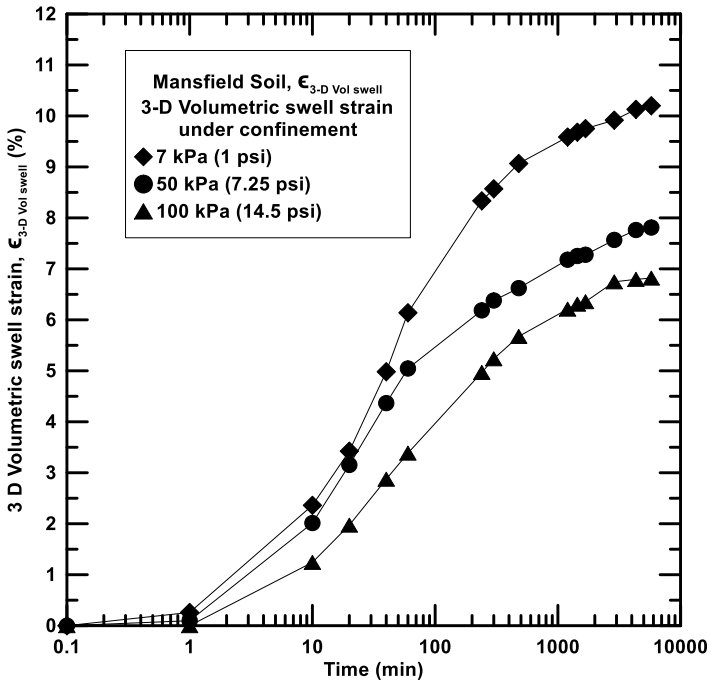

Figure 4-24 Volumetric swell strain exhibited by Mansfield soil at different confinements

4.2.5 Plano Soil

Plano soil was collected from Plano city in Texas. Based on the USCS soil classification system the soil was classified as low plasticity clay (CL). The swelling behavior of Plano soil is presented in the following section.

4.2.5.1 1-D Swell strain and Load-back swell pressures

Figure 4-25 shown below presents the 1-D swell strains exhibited by Plano soil specimen at two different compaction dry densities, i.e. maximum dry density (MDD) and 95% of maximum dry density (95% MDD).

The specimens exhibited a maximum swell strain of 9.1% at maximum dry density (MDD) condition and 7.7% swell strain at 95% MDD condition.

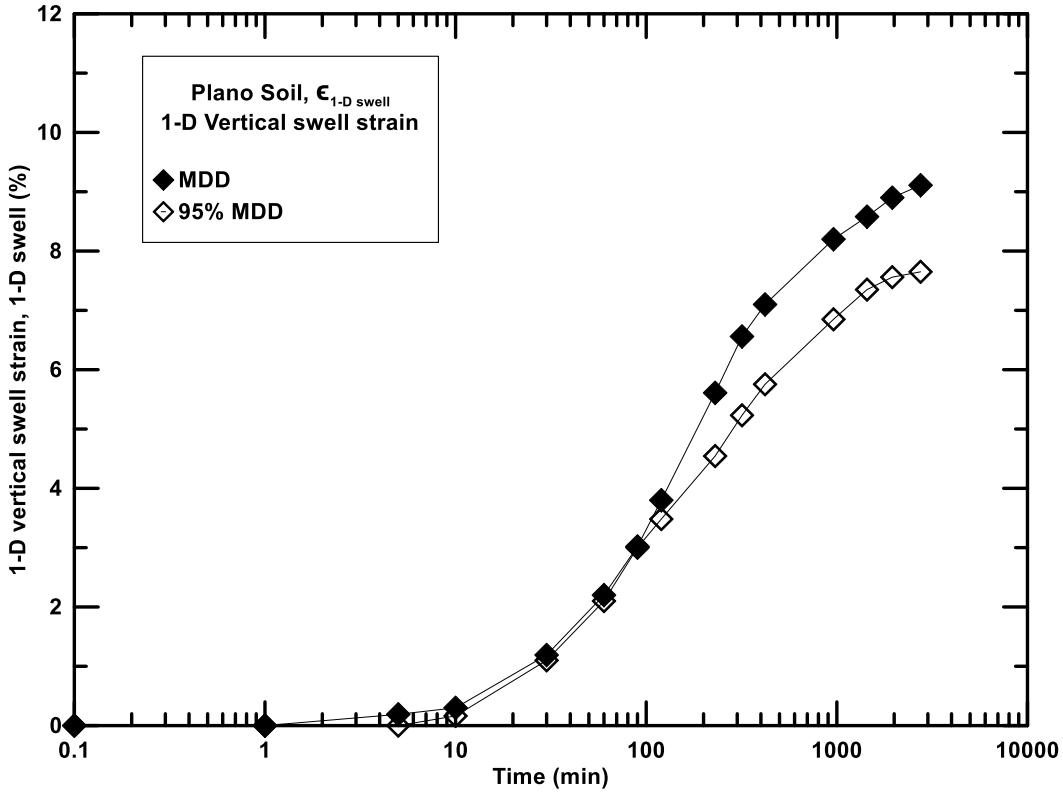

Figure 4-25 One dimensional swell strains for Plano soil

Figure 4-26 and Figure 4-27 present the load-back swell pressures exhibited by Plano soil at two different densities. Soil specimens compacted at 95% MDD and MDD condition exhibited swell pressures of 108.0 kPa (15.4 psi) and 158.0 kPa (22.6 psi), respectively.

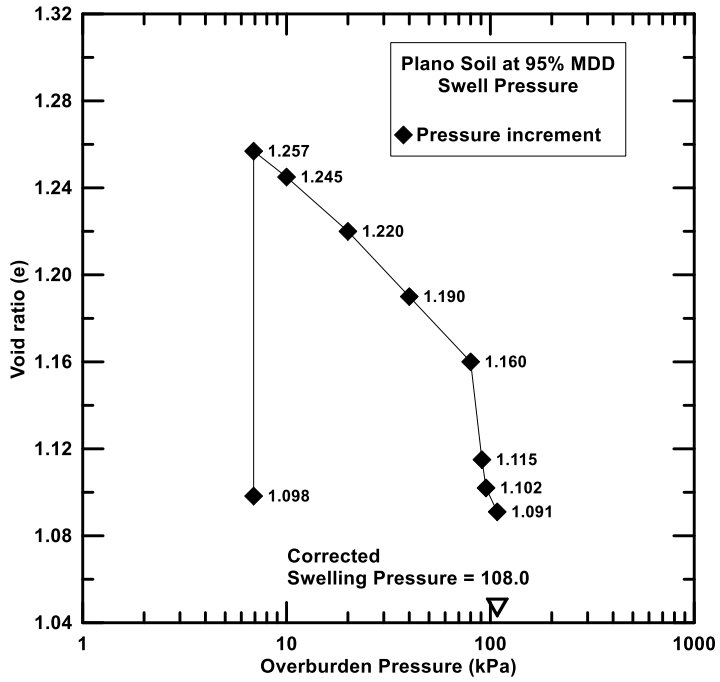

Figure 4-26 Load-back swell pressure test on Plano soil at 95% MDD

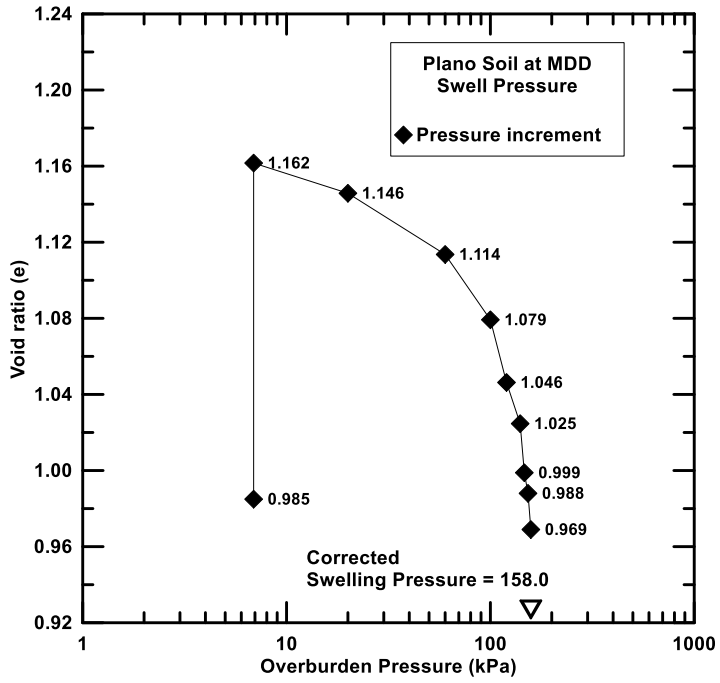

Figure 4-27 Load-back swell pressure test on Plano soil at MDD

4.2.5.2 3-D swell strains

Soil specimens of 50.8 mm (2 in.) diameter and 101.6 mm (4 in.) height were compacted at 95% MDD and were tested for 3-D volumetric swell strains. Figure 4-28 presents the 3-D vertical swell strains exhibited by Plano soil specimen at three different confinement levels. The specimen showed a maximum vertical swell strain of 4.4% at 7 kPa (1 psi) confinement whereas; it showed 1.0% strain at 100 kPa (14.5 psi) confinement. Similarly, Figure 4-29 shows the radial swell strain exhibited by the same soil specimen at different confinements. The specimen exhibited a maximum radial swell strain of 2.4% at 7 kPa (1 psi) confinement and least radial strain of 0.94% at 100 kPa (14.5 psi) confinement.

The total volumetric strain is calculated from the summation of vertical swell strain and twice of radial swell strain and is presented in Figure 4-30. The specimen showed maximum volumetric swell strains of 9.5% at 7 kPa (1 psi), 3.6% at 50 kPa (7.25 psi) and 2.9% at 100 kPa (14.5 psi) confinement levels.

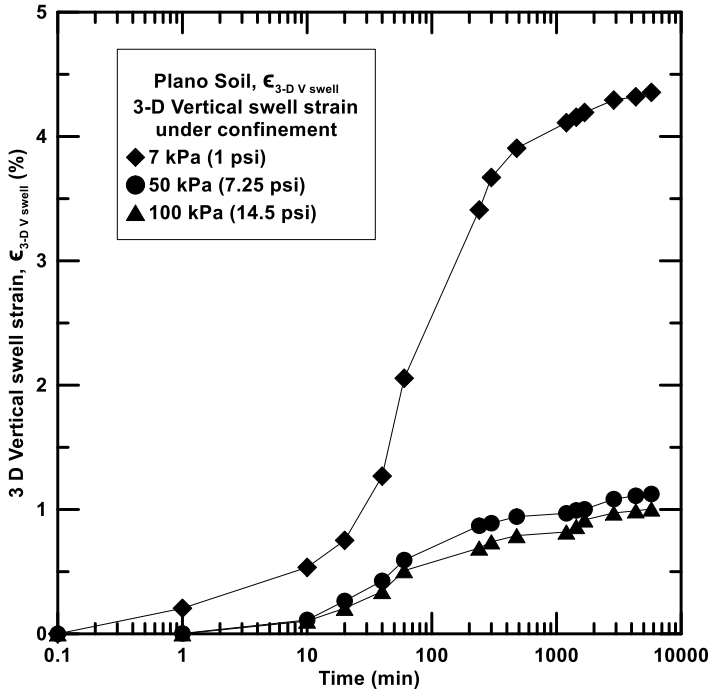

Figure 4-28 Vertical swell strain exhibited by Plano soil at different confinements

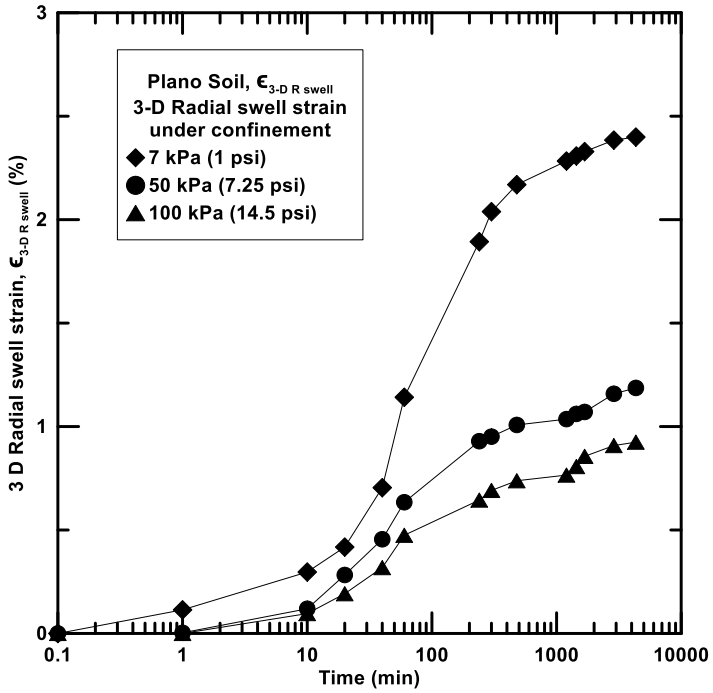

Figure 4-29 Radial swell strain exhibited by Plano soil at different confinements

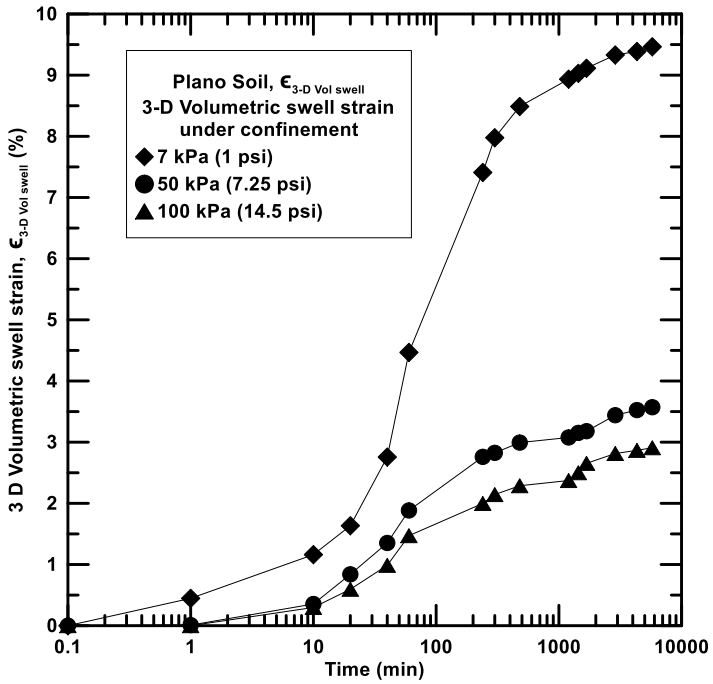

Figure 4-30 Volumetric swell strain exhibited by Plano soil at different confinements

4.2.6 Waco Soil

Waco soil was collected from Waco city in Texas. Based on the USCS soil classification system the soil was classified as high plasticity clay (CH). The swelling behavior of Waco soil is presented in the following section.

4.2.6.1 1-D Swell strain and Load-back swell pressures

Figure 4-31 shown below presents the 1-D swell strains exhibited by Waco soil specimen at two different compaction dry densities, i.e. maximum dry density (MDD) and 95% of maximum dry density (95% MDD).

The specimens exhibited a maximum swell strain of 4.3% at maximum dry density (MDD) condition and 3.6% swell strain at 95% MDD condition.

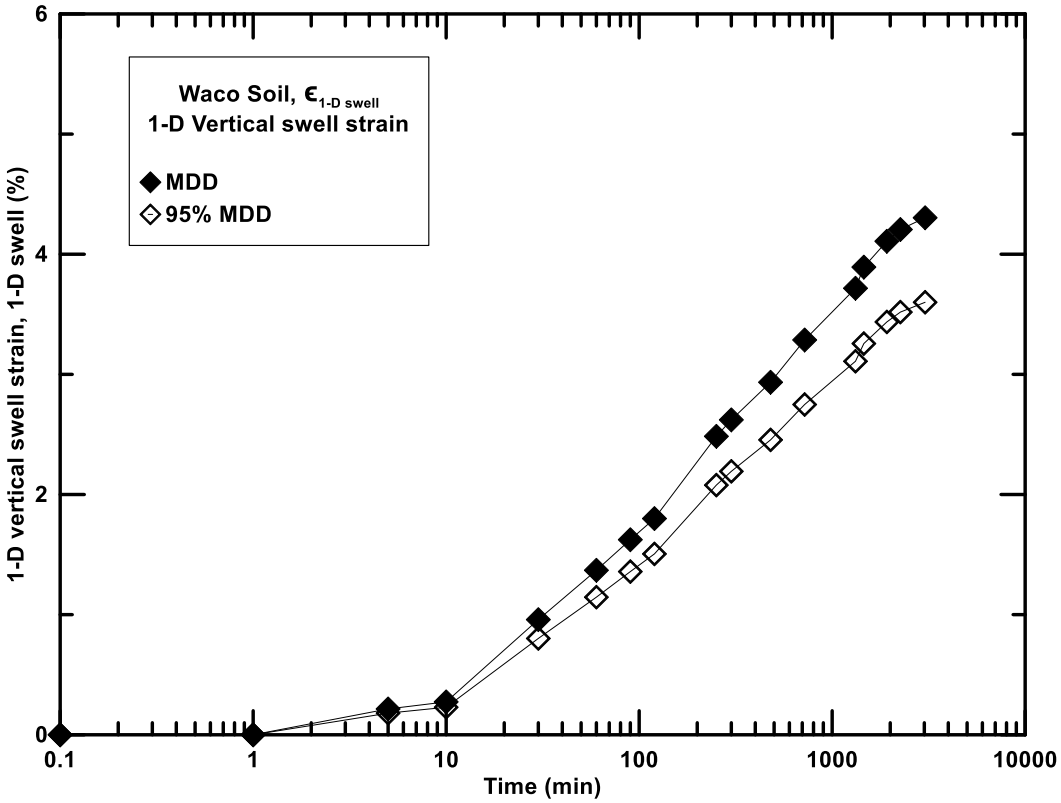

Figure 4-31 One dimensional swell strains for Waco soil

Figure 4-32 and Figure 4-33 present the load-back swell pressures exhibited by Waco soil at two different densities. Soil specimens compacted at 95% MDD and MDD condition exhibited swell pressures of 65.9 kPa (9.4 psi) and 116.5 kPa (16.4 psi), respectively.

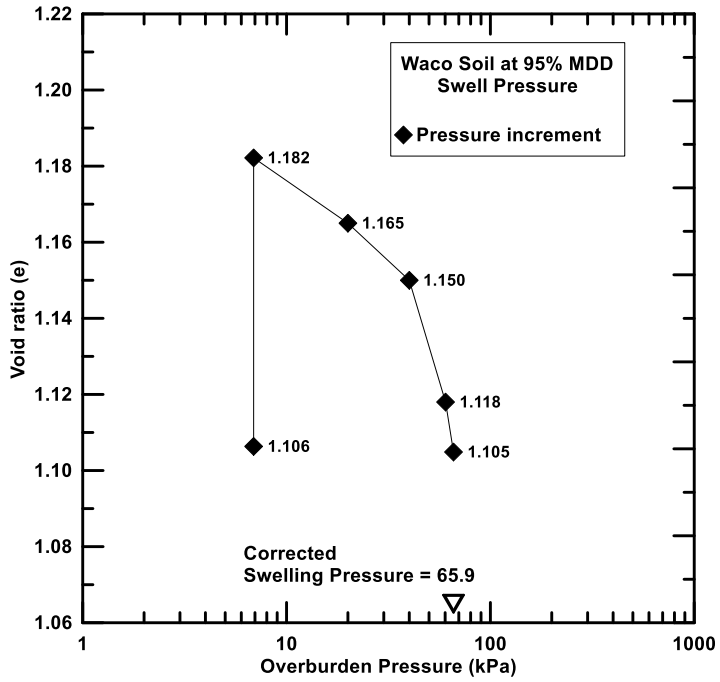

Figure 4-32 Load-back swell pressure test on Waco soil at 95% MDD

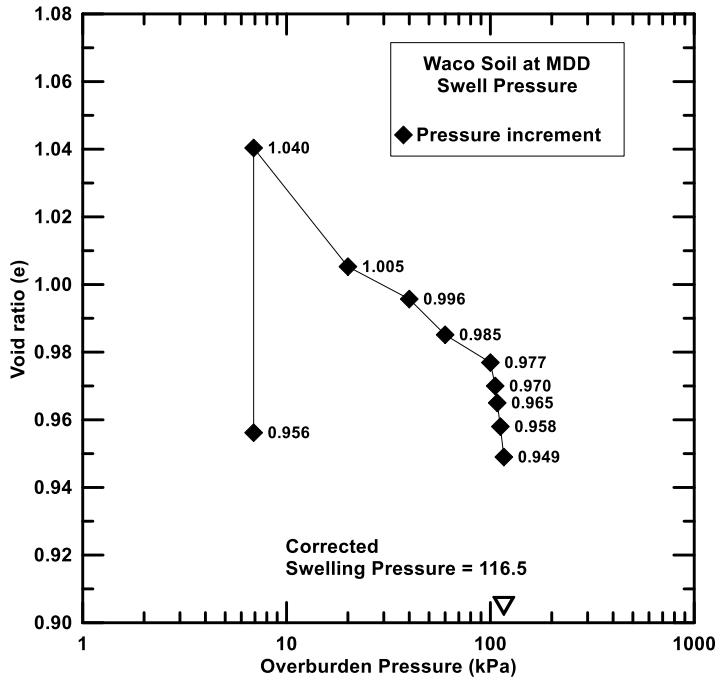

Figure 4-33 Load-back swell pressure test on Waco soil at MDD

4.2.6.2 3-D swell strains

Soil specimens of 50.8 mm (2 in.) diameter and 101.6 mm (4 in.) height were compacted at 95% MDD and were tested for 3-D volumetric swell strains. Figure 4-34 presents the 3-D vertical swell strains exhibited by Waco soil specimen at three different confinement levels. The specimen showed a maximum vertical swell strain of 1.7% at 7 kPa (1 psi) confinement whereas; it showed 0.76% strain at 100 kPa (14.5 psi) confinement. Similarly, Figure 4-35 shows the radial swell strain exhibited by the same soil specimen at different confinements. The specimen exhibited a maximum radial swell strain of 1.7% at 7 kPa (1 psi) confinement and least radial strain of 0.75% at 100 kPa (14.5 psi) confinement.

The total volumetric strain is calculated from the summation of vertical swell strain and twice of radial swell strain and is presented in Figure 4-36. The specimen showed maximum volumetric swell strains of 5.2% at 7 kPa (1 psi), 2.7% at 50 kPa (7.25 psi) and 2.3% at 100 kPa (14.5 psi) confinement levels.

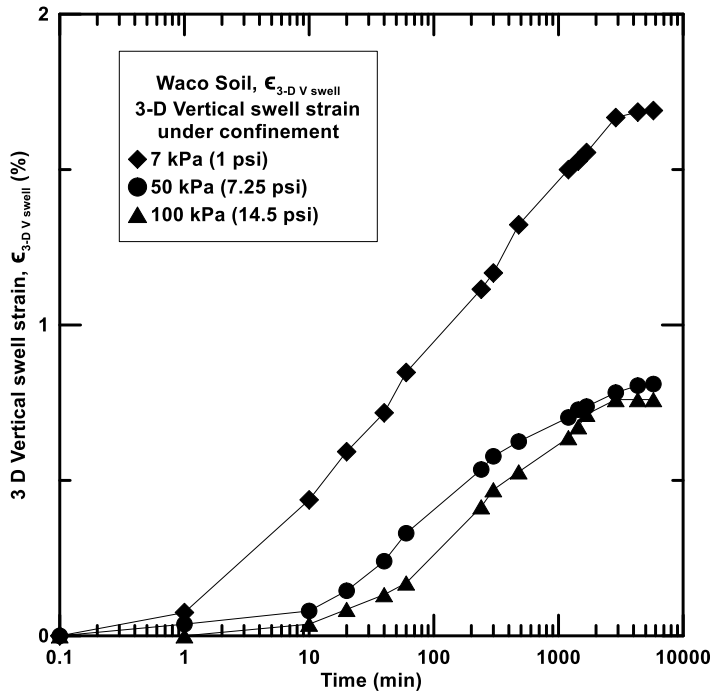

Figure 4-34 Vertical swell strain exhibited by Waco soil at different confinements

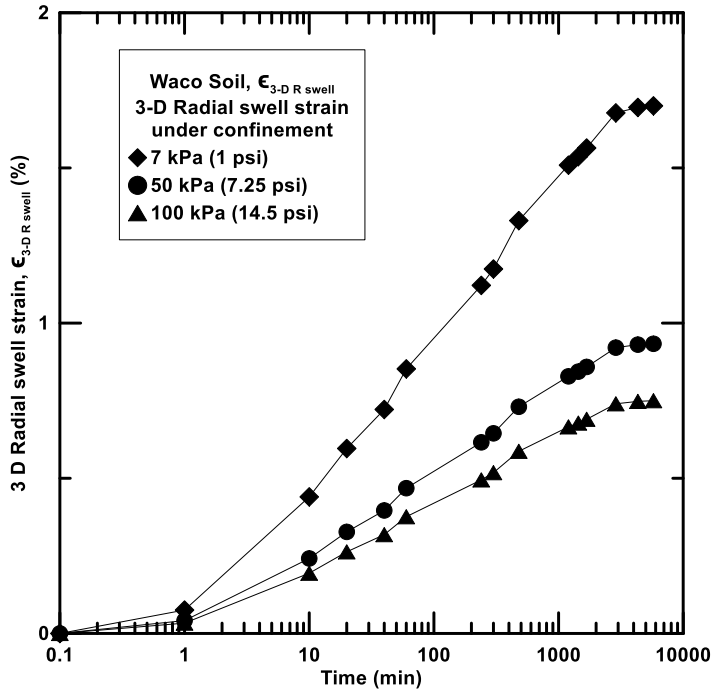

Figure 4-35 Radial swell strain exhibited by Waco soil at different confinements

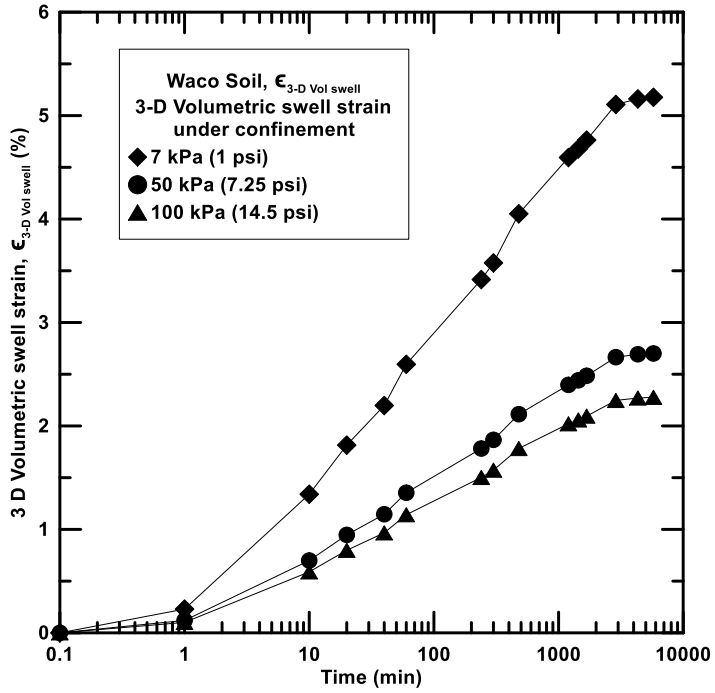

Figure 4-36 Volumetric swell strain exhibited by Waco soil at different confinements

4.3 Influence of Mineral Montmorillonite on swell behavior

Montmorillonite plays an important role in governing the swell behavior. The presence of this mineral in large percentages allows the clay to have higher swelling/shrinking capabilities. Figure 4-37 shown below presents the variation of 1 Dimensional swell with Montmorillonite content. From the test results on six expansive clays it was observed that, with an increase in Montmorillonite content the soils exhibited more 1-D swell strains.

Polynomial fitting models were plotted both for MDD and 95% MDD condition. These fitting models were based on the test soils and show a coefficient of determination (R^2) around 0.8. These models can be used to predict the one dimensional swell strains from the pre-determined mineral Montmorillonite content in a soil.

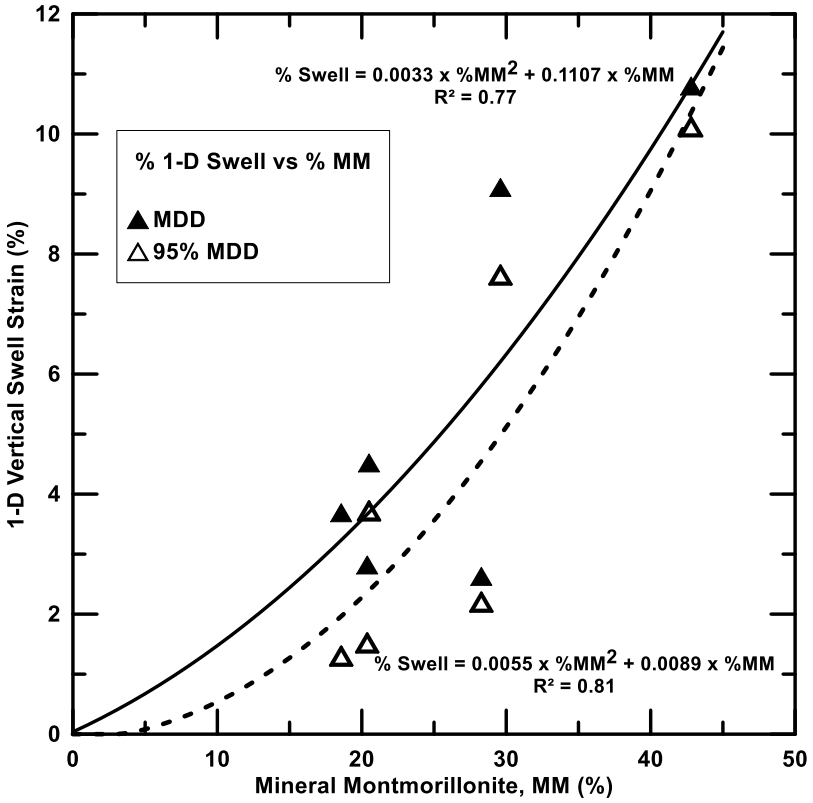

Figure 4-37 Variation of 1-D Vertical Swell with Montmorillonite content

Figure 4-38 shown below presents the variation of swell pressures of expansive clays with percent Montmorillonite content in a soil. The load back swell pressure tests were conducted on soil specimens compacted at MDD and 95% MDD. From the test results it was observed that, with an increase in Montmorillonite content the soils exhibited more swell pressures.

Polynomial fits were plotted both for MDD and 95% MDD conditions. These fitting models were based on 6 soils and are show a coefficient of determination (R^2) around 0.9.

These models are used to predict the one dimensional swell strains from the pre-determined mineral Montmorillonite content in a soil.

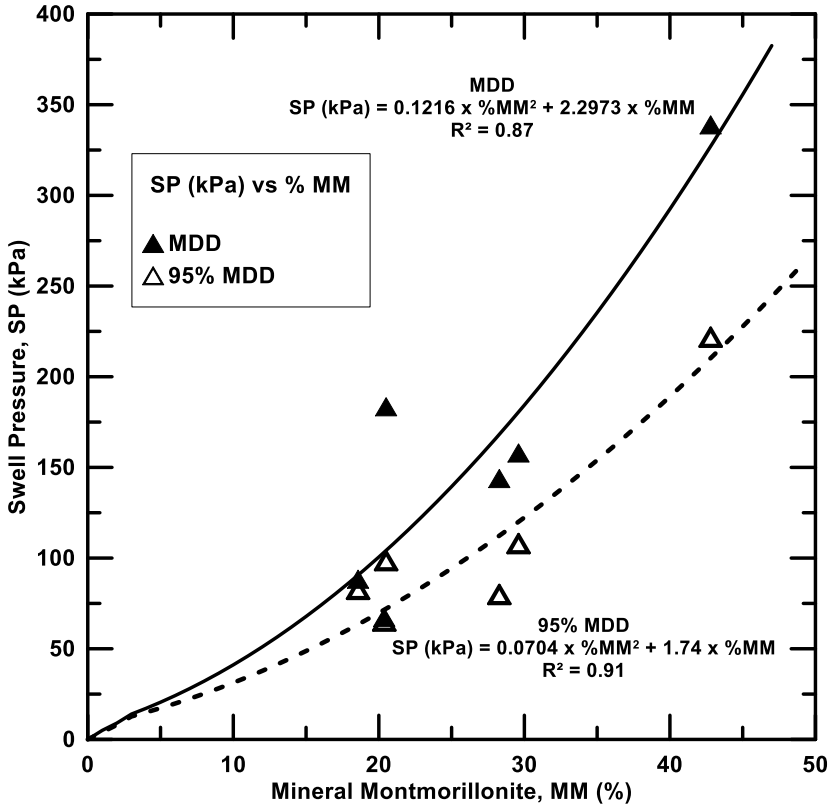

Figure 4-38 Variation of swell pressures with Montmorillonite content for expansive clays

The volumetric swell strains at three confinement pressures (1, 7.25 and 14.5 psi, respectively) are presented and the corresponding fitting models for all the test results of six soils are presented. With an increase in confinement pressure, the volumetric swell strains have decreased. From the test results it was observed that, with an increase in Montmorillonite content the soils exhibited a higher volumetric swell strains. The polynomial models presented here have a coefficient of determination value around 0.9 and hence these models might be considered appropriate for the determination of volumetric swell strains under different confinement pressures and pre-

determined Montmorillonite contents. The variation of volumetric swell strains with Montmorillonite content is shown in Figure 4-39 below.

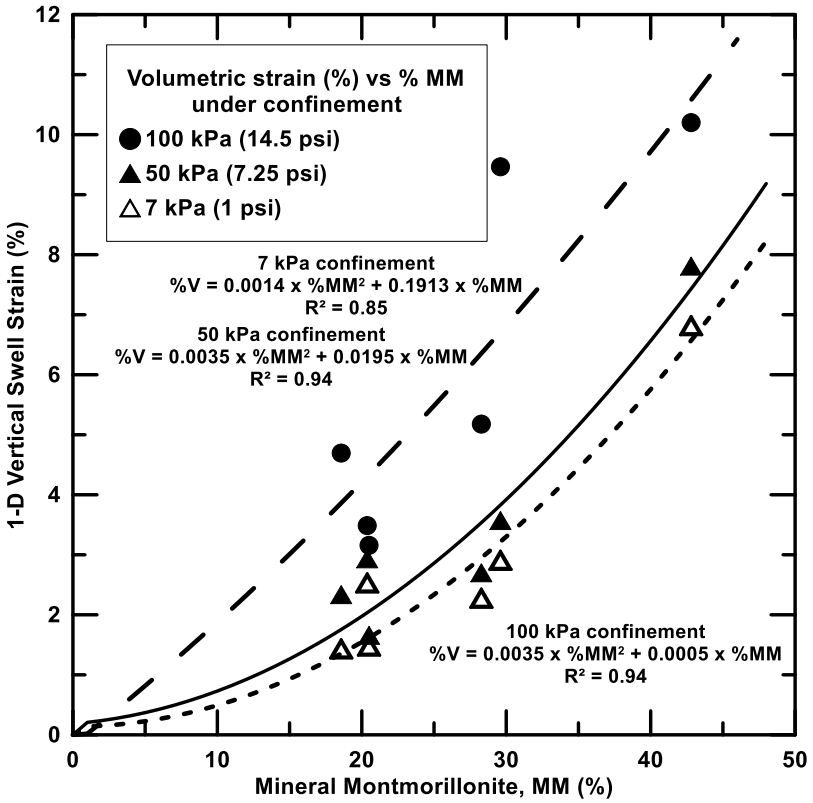

Figure 4-39 Variation of volumetric strains under confinement with Montmorillonite content

The test results of swell strains and swell pressure values exhibited by the soils under different loading and confinement conditions are discussed in this chapter. Also, the variation of swell behavior with clay mineral content was studied and presented. The next chapter deals with the soil composition properties like soil-water relationship and pore distribution.

4.3 Summary

Test results showed that the soil exhibiting the maximum swell strains was Mansfield soil and the one exhibiting the least swell strains was Waco soil. The soils

presented in Table 4-1 are based on the order of their maximum swell strains exhibited in the present swell testing. The soils exhibiting maximum swell strains (Mansfield) also showed a higher swell pressure due to the presence of high amounts of Montmorillonite content present in this soil when compared to the same of the remaining soils.

As expected, soils compacted at maximum dry density (MDD) condition showed higher swell strains and swell pressures due to the presence of more soil and mineral content than at 95% MDD. Table 4-1 below presents the 1-D swell strains and load back swell pressure result summary for all the selected soils.

Table 4-1 Summary of the 1-D swell strains and swell pressure test results

Ranking		1-D Swell strain (%)		Swell Pressure (kPa)	
Soil	PI	MDD	95% MDD	MDD	95% MDD
Mansfield	38	10.8	9.5	164.2	138.9
Plano	12	9.1	7.7	158.0	108.0
Denton	30	6.5	3.5	67.4	65.3
Grapevine 2	26	6.2	4.3	88.4	82.7
Cleburne	21	5.8	3.2	141.7	96.2
Waco	34	4.3	3.6	116.5	65.9

Mansfield clay exhibited the maximum swell strains at both MDD and 95% MDD condition. The soil also exhibited a maximum swell pressure of 23.5 psi at MDD condition and 19.8 psi at 95% MDD condition. Waco soil showed the least swell strain at MDD, however, the smallest swell strain at 95% MDD was exhibited by Cleburne soil. Also, the smallest amount of swell pressures at MDD and 95% MDD conditions was yielded by Denton soil.

All the clays were tested for 3-D swell strains with the help of the novel apparatus designed at UTA and detailed in Chapter 2 and Chapter 3. The remolded clay specimens

of 2” diameter and 4” height are allowed to saturate at confinement levels of 7kPa (1 psi), 50 kPa (7.25) and 100 kPa (14.5 psi). The swell strains exhibited by the soil specimens were measured and the summaries of test results are presented in Table 4-2. Mansfield soil exhibited maximum vertical, radial and volumetric strains under all confinements, while Cleburne soil exhibited the least volumetric strains.

At least confinement levels (7 kPa) all the soils underwent maximum swell strains in both vertical and radial directions. The swell strains reduced considerably as the confinement levels increased for all the clays.

Table 4-2 Summary of the 3-D swell strain test results

Ranking	Vertical strains (%)			Radial Strains (%)			Volumetric Strains (%)		
Soil	σ = 7 kPa	σ = 50 kPa	σ = 100 kPa	σ = 7 kPa	σ = 50 kPa	σ = 100 kPa	σ = 7 kPa	σ = 50 kPa	σ = 100 kPa
Mansfield	4.18	3.11	2.71	2.85	2.25	1.98	10.20	7.81	6.82
Plano	4.36	1.12	1.00	2.42	1.20	0.94	9.46	3.57	2.91
Denton	0.88	0.38	0.07	1.28	1.14	1.04	3.49	2.93	2.53
Grapevine 2	1.67	0.55	0.29	1.48	0.88	0.57	4.69	2.34	1.43
Cleburne	0.73	0.15	0.05	1.20	0.75	0.71	3.16	1.66	1.48
Waco	1.69	0.81	0.76	1.70	0.93	0.75	5.18	2.70	2.28

Where σ = 3-D confinement pressure

Chapter 5

Soil composition test results

5.1 Introduction

The behavior of any expansive soil is dependent on its inherent properties such as clay mineralogy, relationship with moisture content, and pore void distribution. The mineralogy of clay governs the micro parameters like specific surface area and cation exchange capacity which influences the swell shrink behavior of soils as exemplified in Chapter 2.

The next important factor governing the swell behavior is the relationship with moisture content. This is well understood with the help of a soil water characteristic curve (SWCC) which describes the variation of soil suction with volumetric moisture content.

Even though there is a parametric influence on the SWCC which is soil specific and therefore affects the uniqueness of the SWCC as outlined in Chapter 2, in the present research an approach has been made to obtain relationships for the studied soils according to the compaction density and grain distribution.

Thus, in the present chapter, the wetting and drying SWCCs for all the six soils collected were measured with commonly used curve fitting models like Van Genuchten (1980) and Fredlund and Xing (1994).

Pore size distribution plays an important role in the hydraulic conductivity behavior of the clay specimen, which in turn affects the swelling process. This internal distribution of pores in the soil specimen was studied by Mercury Intrusion Porosimetry (MIP) technique. The presence of pores of different sizes are determined and classified to different levels based on the MIP test results. X-ray Tomography technique which was used to scan and reconstruct a solid mass helps in the identification of internal structure of a soil specimen. The pore connectivity and the variation of void ratio with change in

density and moisture content are studied with the help of this laboratory technique. This chapter presents the soil composition test results on all the six soils obtained from different parts of Texas.

5.2 Soil suction studies

The determination of soil water characteristic curve (SWCC) is possible with laboratory measurement techniques like the filter paper and pressure plate method as previously discussed in Chapter 3. The variation of volumetric moisture content of the soil specimens with corresponding changes in soil matric suction is recorded as a SWCC. Soils were subjected to these tests at two compaction dry density conditions, one at MDD condition and other at 95% MDD condition. Also, SWCC were intended to follow drying and wetting path profiles. Van Genuchten (1980) and Fredlund and Xing (1994) fitting models were used to analyze and model the SWCC behavior.

For all the six soils, both models yielded similar SWCCs at each compaction state, therefore only Van Genuchten approach was chosen to be shown in the figures presented in the following sections.

5.2.1 Cleburne Soil SWCCs

Compacted Cleburne soil specimen was subjected to SWCC studies at 95% MDD and OMC condition as well as at MDD and OMC condition. The variation of volumetric moisture content with matric suction for Cleburne soil specimen is shown in Figure 5-1.

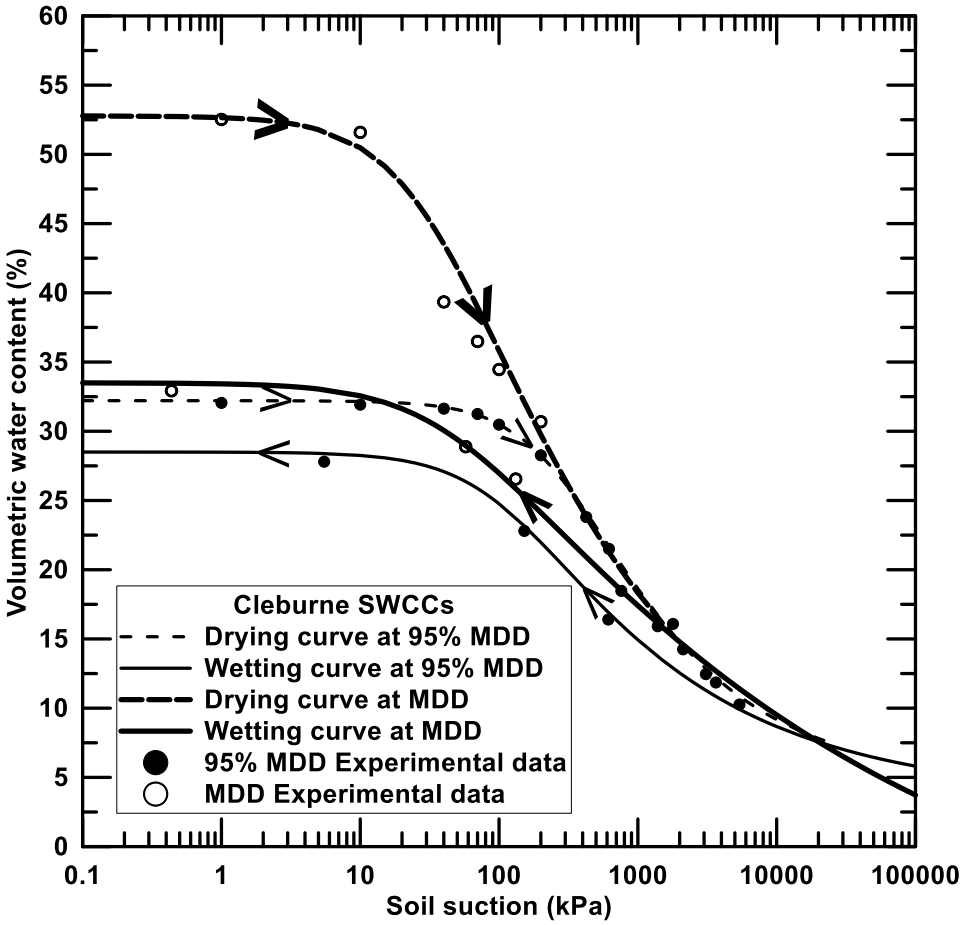

Figure 5-1 Soil water characteristic curves of Cleburne soil (Van Genuchten model)

Cleburne soil being characterized as low plasticity clay exhibited the fundamental features in the SWCCs shown in Table 5-1 (as presented in Chapter 2, Malaya et al., 2011):

Table 5-1 Fundamental features in the SWCCs of Cleburne soil

Fundamental feature	95% MDD	MDD
Volumetric water content at saturation (θs), %	33.2	52.6
Air-entry value, AEV (ψa), kPa	150	23
Residual water content (θr), %	6.0	3.3
Water-entry value (ψw), kPa	5600	6200

Van Genuchten fitting model parameters for the SWCCs of Cleburne soil are presented in Table 5-2.

Table 5-2 Van Genuchten fitting model for SWCCs of Cleburne soil

Parameter	95% MDD		MDD	
	Drying	Wetting	Drying	Wetting
a	0.0035	0.0090	0.0300	0.0230
n	1.50	1.35	1.30	1.14
m	0.333	0.259	0.231	0.123

5.2.2 Denton Soil SWCCs

Compacted Denton soil specimen was subjected to SWCC studies at 95% MDD and OMC condition as well as at MDD and OMC condition. The variation of volumetric moisture content with matric suction for Denton soil specimen is shown in Figure 5-2.

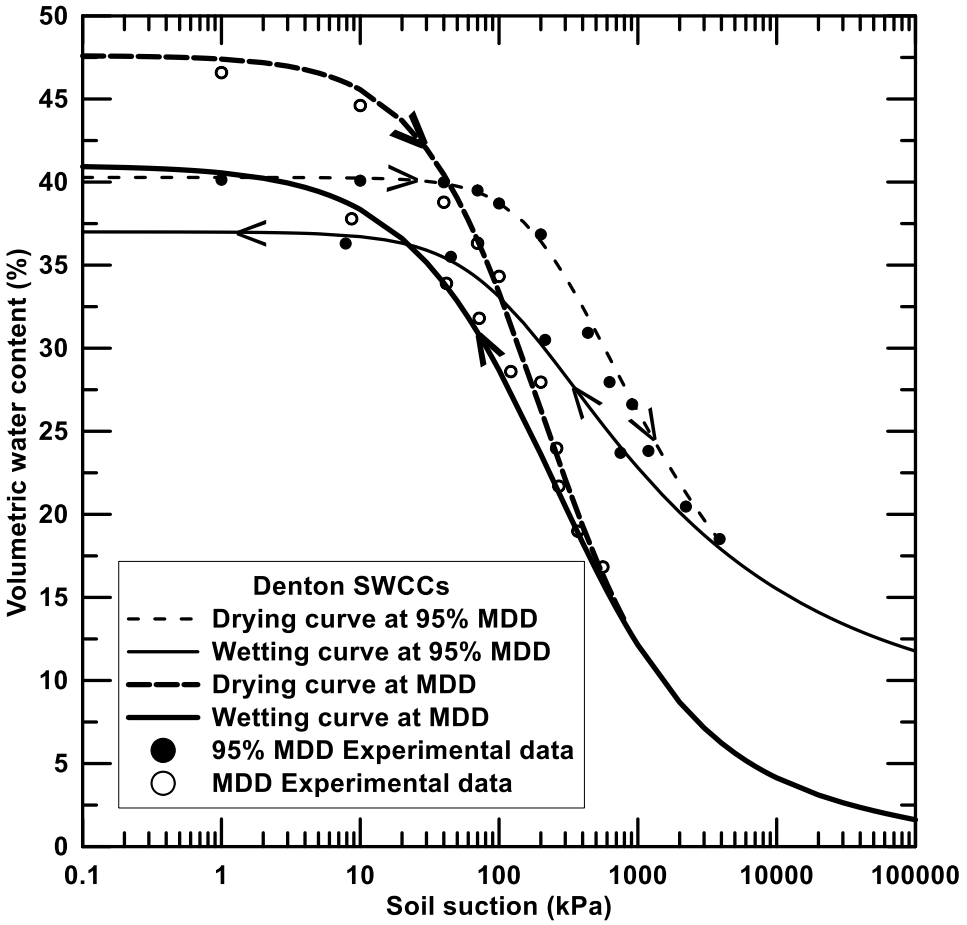

Figure 5-2 Soil water characteristic curves of Denton soil (Van Genuchten model)

Denton soil being characterized as high plasticity clay exhibited the fundamental features in the SWCCs shown in Table 5-3 (as presented in Chapter 2, Malaya et al., 2011):

Table 5-3 Fundamental features in the SWCCs of Denton soil

Fundamental feature	95% MDD	MDD
Volumetric water content at saturation (θs), %	40.3	47.5
Air-entry value, AEV (ψa), kPa	130	28
Residual water content (θr), %	12.1	2.2
Water-entry value (ψw), kPa	860	420

Van Genuchten fitting model parameters for the SWCCs of Denton soil are presented in Table 5-4.

Table 5-4 Van Genuchten fitting model for SWCCs of Denton soil

Parameter	95% MDD		MDD	
	Drying	Wetting	Drying	Wetting
a	0.0042	0.0090	0.0300	0.0200
n	1.65	1.30	1.80	1.40
m	0.200	0.231	0.200	0.286

5.2.3 Grapevine 2 Soil SWCCs

Compacted Grapevine 2 soil specimen was subjected to SWCC studies at 95% MDD and OMC condition as well as at MDD and OMC condition. The variation of volumetric moisture content with matric suction for Grapevine 2 soil specimen is shown in Figure 5-3.

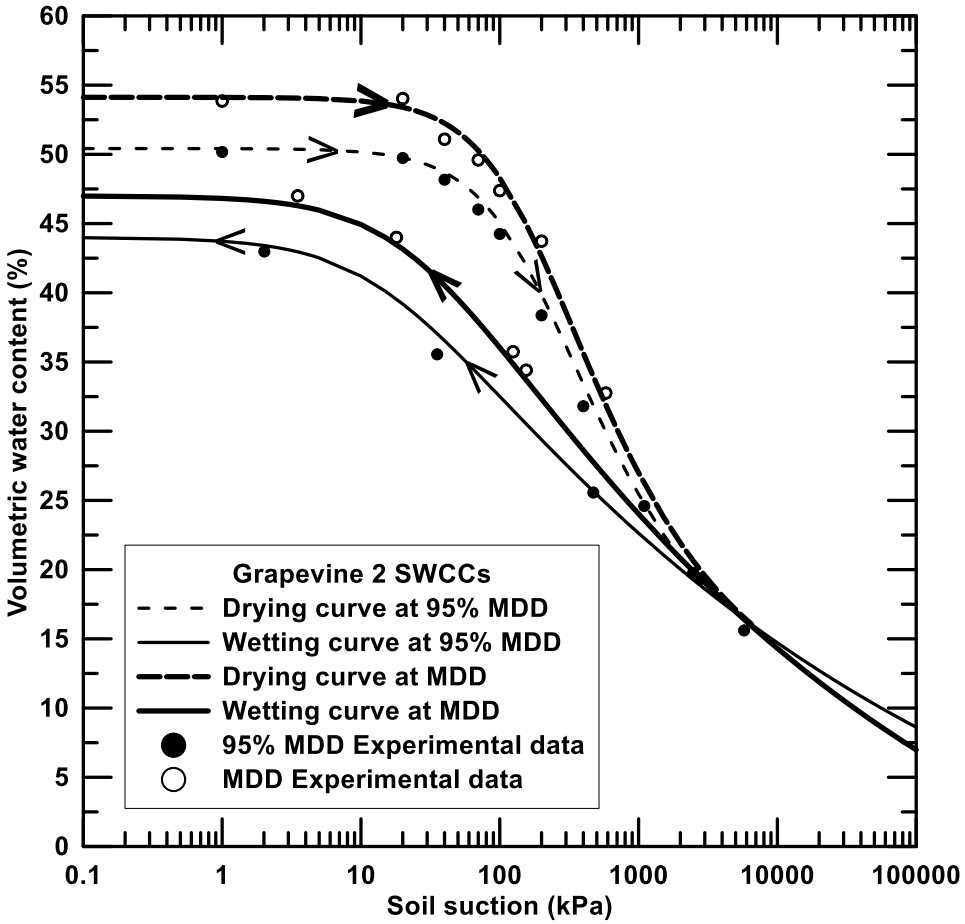

Figure 5-3 Soil water characteristic curves of Grapevine 2 soil (Van Genuchten model)

Grapevine 2 soil being characterized as low plasticity clay exhibited the fundamental features in the SWCCs shown in Table 5-5 (as presented in Chapter 2, Malaya et al., 2011):

Table 5-5 Fundamental features in the SWCCs of Grapevine 2 soil

Fundamental feature	95% MDD	MDD
Volumetric water content at saturation (θs), %	46.8	53.7
Air-entry value, AEV (ψa), kPa	64	56
Residual water content (θr), %	8.8	7.3
Water-entry value (ψw), kPa	480	370

Van Genuchten fitting model parameters for the SWCCs of Grapevine 2 soil are presented in Table 5-6.

Table 5-6 Van Genuchten fitting model for SWCCs of Grapevine 2 soil

Parameter	95% MDD		MDD	
	Drying	Wetting	Drying	Wetting
a	0.0065	0.0680	0.0065	0.0400
n	1.46	1.12	1.46	1.13
m	0.315	0.103	0.315	0.111

5.2.4 Mansfield Soil SWCCs

Compacted Mansfield soil specimen was subjected to SWCC studies at 95% MDD and OMC condition as well as at MDD and OMC condition. The variation of volumetric moisture content with matric suction for Mansfield soil specimen is shown in Figure 5-4.

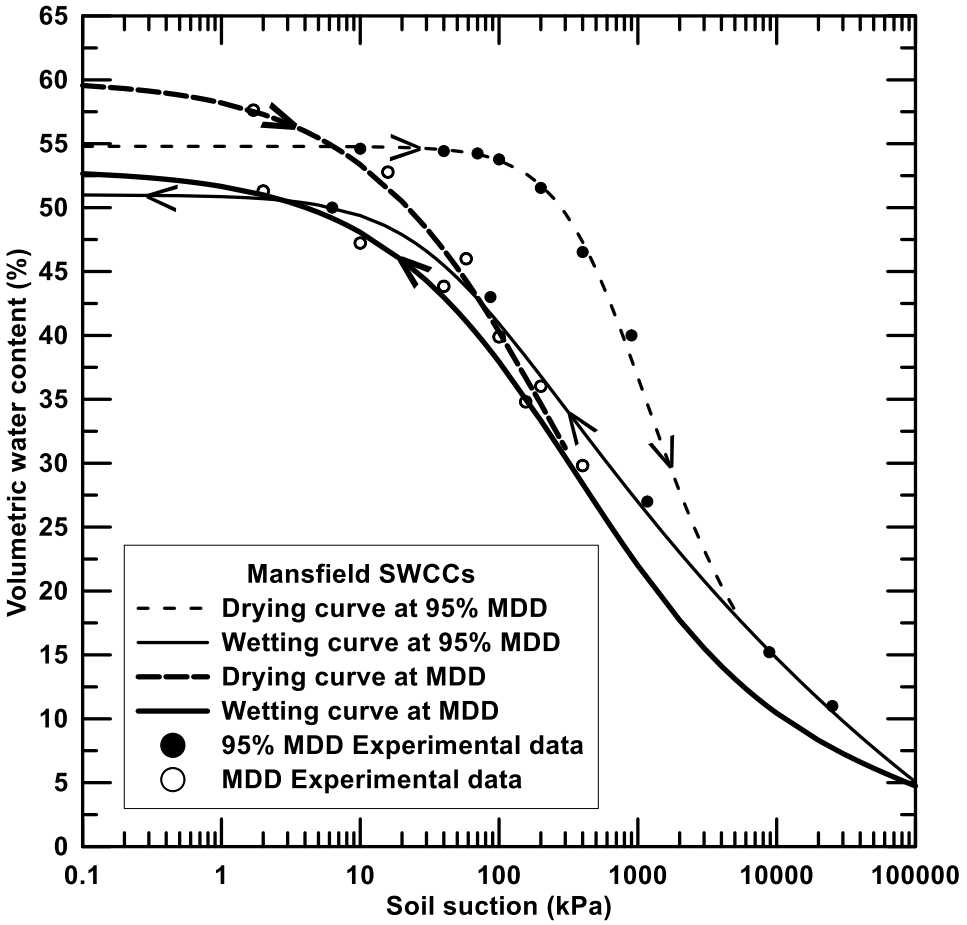

Figure 5-4 Soil water characteristic curves of Mansfield soil (Van Genuchten model)

Mansfield soil being characterized as high plasticity clay exhibited the fundamental features in the SWCCs shown in Table 5-7 (as presented in Chapter 2, Malaya et al., 2011):

Table 5-7 Fundamental features in the SWCCs of Mansfield soil

Fundamental feature	95% MDD	MDD
Volumetric water content at saturation (θs), %	54.9	59.6
Air-entry value, AEV (ψa), kPa	249	18
Residual water content (θr), %	5.0	4.9
Water-entry value (ψw), kPa	10200	8600

Van Genuchten fitting model parameters for the SWCCs of Mansfield soil are presented in Table 5-8.

Table 5-8 Van Genuchten fitting model for SWCCs of Mansfield soil

Parameter	95% MDD		MDD	
	Drying	Wetting	Drying	Wetting
a	0.0017	0.0270	0.0550	0.0250
n	1.58	1.11	1.23	1.30
m	0.367	0.096	0.187	0.231

5.2.5 Plano Soil SWCCs

Compacted Plano soil specimen was subjected to SWCC studies at 95% MDD and OMC condition as well as at MDD and OMC condition. The variation of volumetric moisture content with matric suction for Plano soil specimen is shown in Figure 5-5.

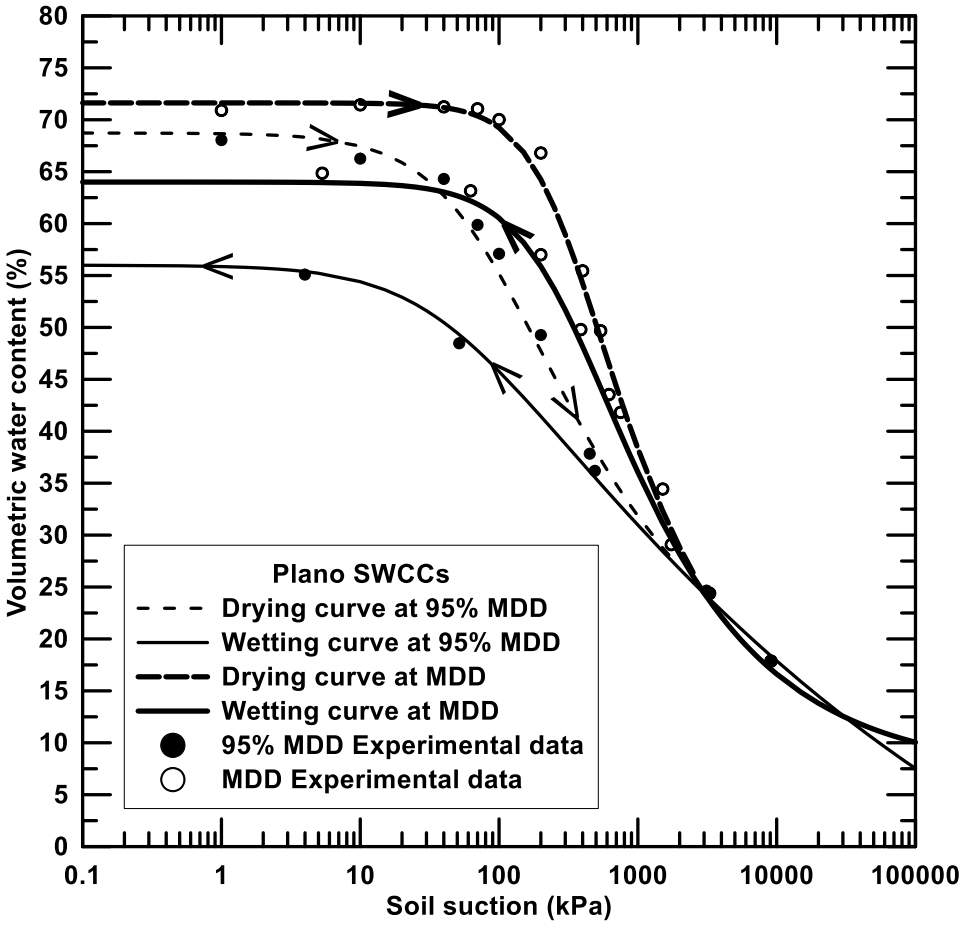

Figure 5-5 Soil water characteristic curves of Plano soil (Van Genuchten model)

Plano soil being characterized as low plasticity clay exhibited the fundamental features in the SWCCs shown in Table 5-9 (as presented in Chapter 2, Malaya et al., 2011):

Table 5-9 Fundamental features in the SWCCs of Plano soil

Fundamental feature	95% MDD	MDD
Volumetric water content at saturation (θs), %	68.7	72.1
Air-entry value, AEV (ψa), kPa	33	165
Residual water content (θr), %	7.4	10.1
Water-entry value (ψw), kPa	8800	870

Van Genuchten fitting model parameters for the SWCCs of Plano soil are presented in Table 5-10.

Table 5-10 Van Genuchten fitting model for SWCCs of Plano soil

Parameter	95% MDD		MDD	
	Drying	Wetting	Drying	Wetting
a	0.0130	0.0250	0.0035	0.0035
n	1.27	1.11	1.90	1.50
m	0.300	0.096	0.300	0.333

5.2.6 Waco Soil SWCCs

Compacted Waco soil specimen was subjected to SWCC studies at 95% MDD and OMC condition as well as at MDD and OMC condition. The variation of volumetric moisture content with matric suction for Waco soil specimen is shown in Figure 5-6.

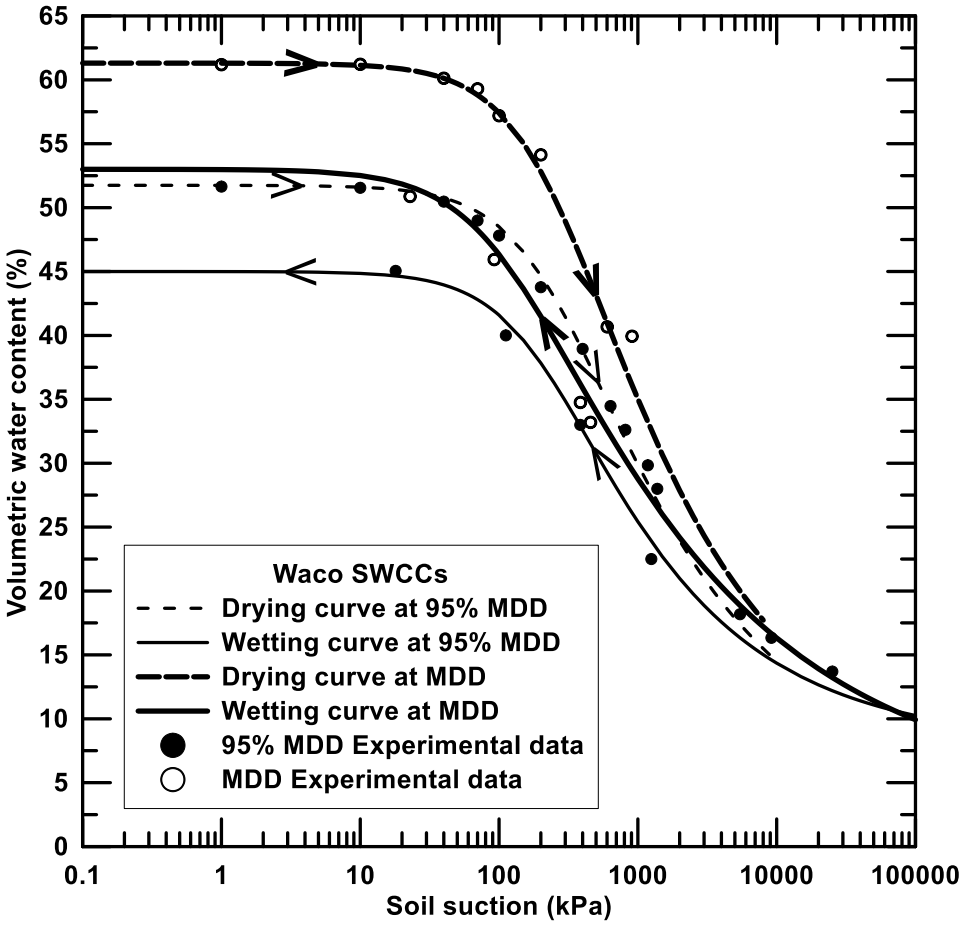

Figure 5-6 Soil water characteristic curves of Waco soil (Van Genuchten model)

Waco soil being characterized as high plasticity clay exhibited the fundamental features in the SWCCs shown in Table 5-11 (as presented in Chapter 2, Malaya et al., 2011):

Table 5-11 Fundamental features in the SWCCs of Waco soil

Fundamental feature	95% MDD	MDD
Volumetric water content at saturation (θs), %	52.1	61.8
Air-entry value, AEV (ψa), kPa	110	102
Residual water content (θr), %	10.3	9.9
Water-entry value (ψw), kPa	510	21000

Van Genuchten fitting model parameters for the SWCCs of Waco soil are presented in Table 5-12.

Table 5-12 Van Genuchten fitting model for SWCCs of Waco soil

Parameter	95% MDD		MDD	
	Drying	Wetting	Drying	Wetting
a	0.0040	0.0050	0.0040	0.0090
n	1.42	1.45	1.42	1.30
m	0.296	0.310	0.296	0.231

5.3 Pore fabric studies using Mercury Intrusion Porosimetry

The measurement of internal pore structure and distribution is essential to study the water conductivity behavior in a soil specimen. The pore size distribution in a soil mass can be evaluated with the help of Mercury Intrusion Porosimetry technique (MIP) as discussed in Chapter 2 and Chapter 3. The variation of dry density of a soil specimen influences the internal pore structure and pore size distribution. Hence, soil specimens were tested at two compaction dry density conditions, i.e. at maximum dry density (MDD) condition and at 95% maximum dry density (95% MDD) condition.

From the previous literature, it was understood that pores ranging below 0.02 micro meters (μm) are classified as micro pores. Pores ranging from 0.02 μm to 12 μm comes under medium pores and pores larger than 12 μm are classified as macro pores. This classification system was used in the current research for proper pore identification. Two soil specimens from the same clay were tested for pore distribution and the test results showed similar behavior. The mercury intrusion porosimetry test yielded good repeatability of test results. The pore size distribution for all the six soils at different dry density conditions are presented in the following sections.

5.3.1 Cleburne soil pore distribution

The mercury intrusion/extrusion curves of Cleburne clay obtained from MIP technique at two compaction densities are shown in Figure 5-7. Cleburne soil which is classified as low plasticity clay showed a cumulative pore volume of 0.134 ml/g at 95% MDD and 0.129 ml/g at MDD, respectively. Figure 5-8 shows the variation of pore diameter with total pore volume. The 95% MDD specimen showed higher macro pore volume of 30% where at MDD it showed 24%.

The specimen exhibited 59% medium pores at 95% MDD and 65% at MDD conditions.

Both the specimens showed equal volume of micro pores (11%). This shows that the micro pore volume is independent of compaction dry density for this particular clay.

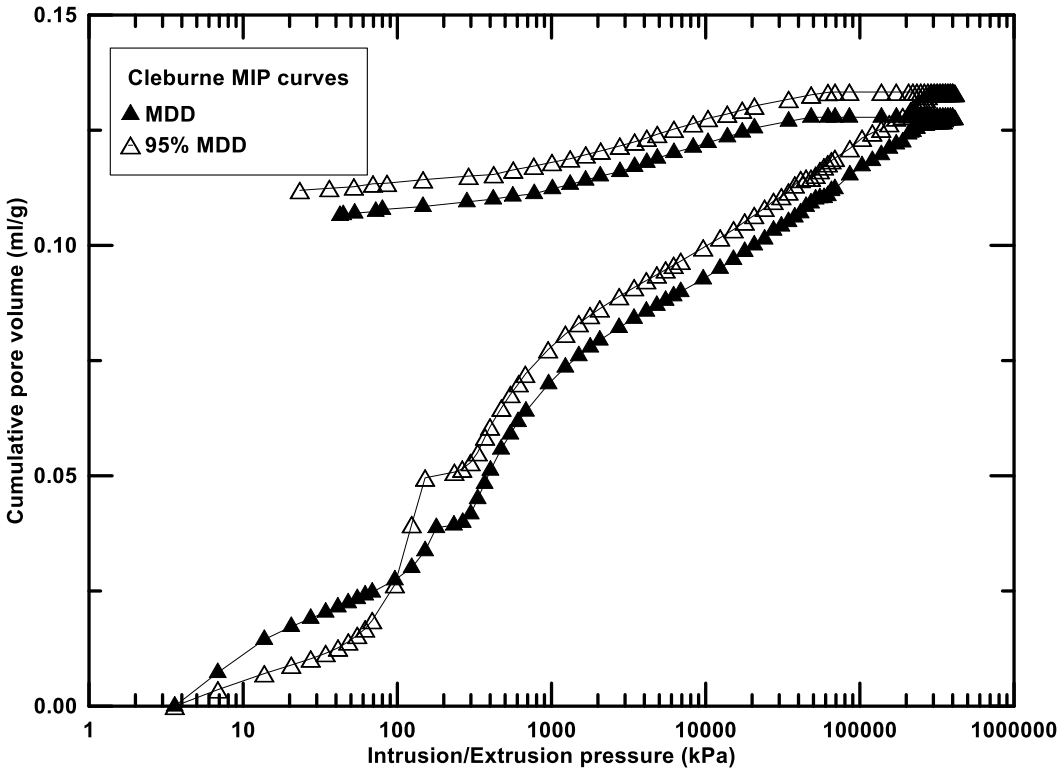

Figure 5-7 Intrusion/Extrusion curves for Cleburne soil at MDD and 95% MDD

It was evident that the soil specimen has more pore volume at 95% MDD condition than at MDD condition. The hysteresis observed between the intrusion and extrusion curves is due to the retention of mercury in the soil pores. This reveals that the specimen retained higher volume of mercury at MDD condition.

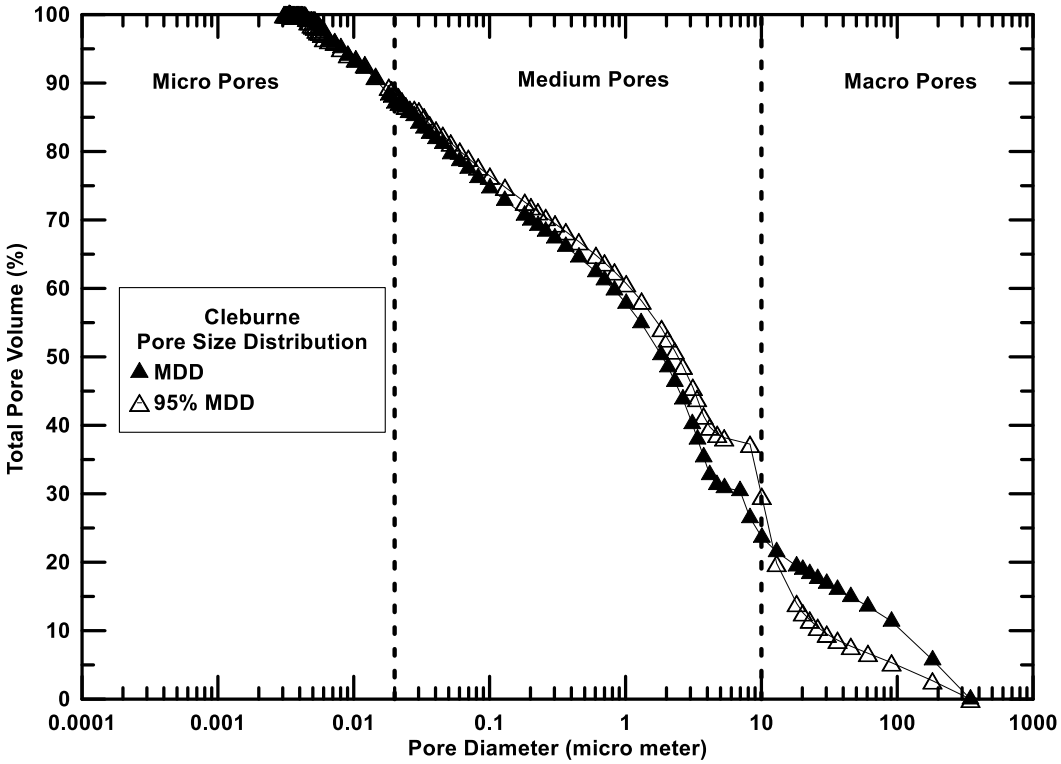

Figure 5-8 Pore size distribution for Cleburne soil at MDD and 95% MDD

5.3.2 Denton soil pore distribution

The mercury intrusion/extrusion curves of Denton clay obtained from MIP technique at two compaction densities are shown in Figure 5-9. Denton soil which is classified as low plasticity clay showed a cumulative pore volume of 0.174 ml/g at 95% MDD and 0.145 ml/g at MDD, respectively. Figure 5-10 shows the variation of pore diameter with total pore volume. The 95% MDD specimen showed higher macro pore volume of 42% where at MDD it showed 27%.

The specimen exhibited 46% medium pores at 95% MDD and 58% at MDD conditions.

Volume of micro pores was 12% at 95% MDD and 15% at MDD conditions.

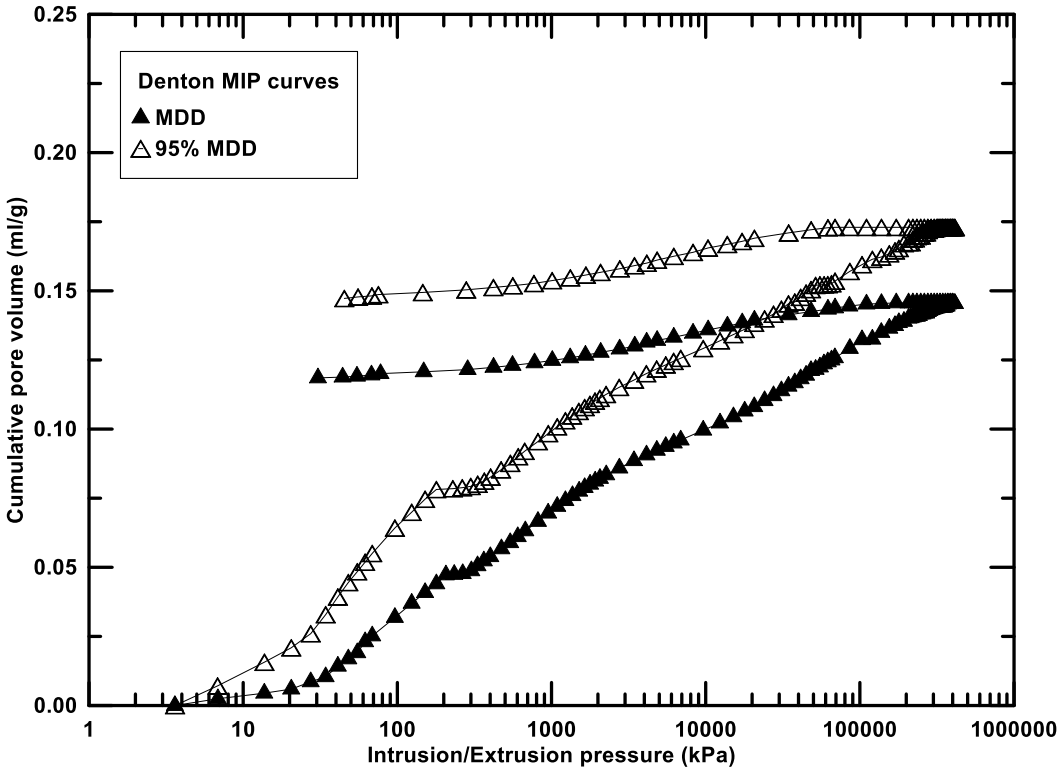

Figure 5-9 Intrusion/Extrusion curves for Denton soil at MDD and 95% MDD

It was evident that the soil specimen carries more pore volume at 95% MDD condition than at MDD condition. The hysteresis observed between the intrusion and extrusion curves is due to the retention of mercury in the soil pores. This reveals that the specimen retained higher volume of mercury at MDD condition.

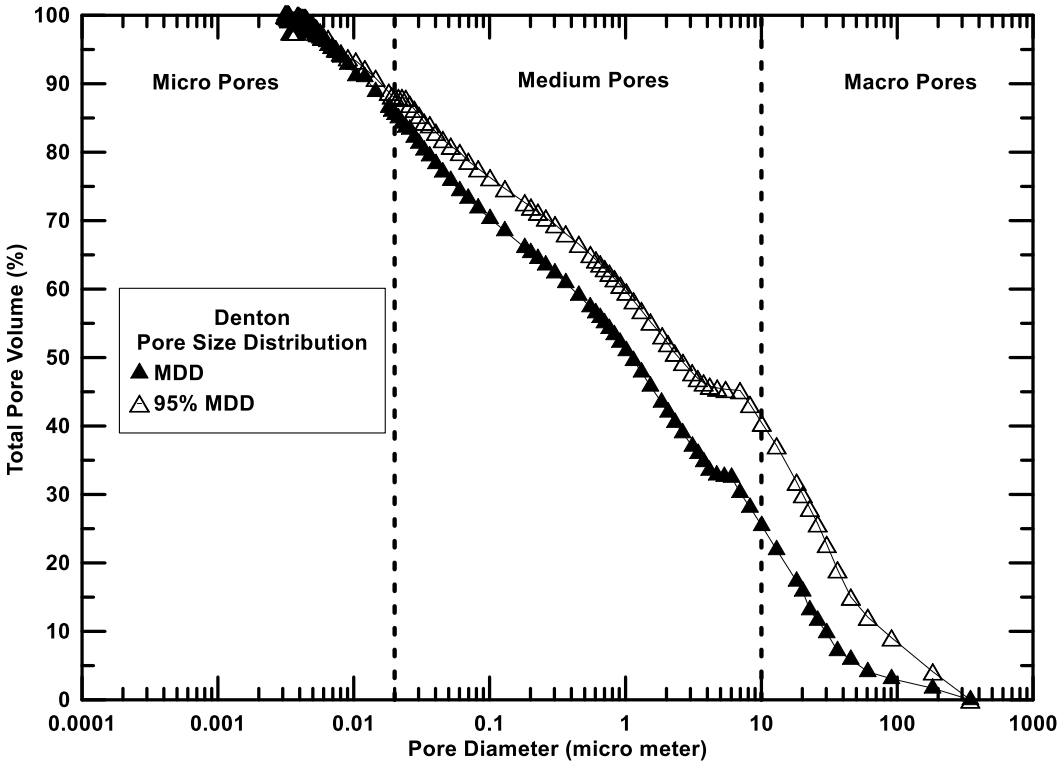

Figure 5-10 Pore size distribution for Denton soil at MDD and 95% MDD

5.3.3 Grapevine 2 soil pore distribution

The mercury intrusion/extrusion curves of Grapevine 2 clay obtained from MIP technique at two compaction densities are shown in Figure 5-11. Grapevine 2 soil which is classified as low plasticity clay showed a cumulative pore volume of 0.176 ml/g at 95% MDD and 0.171 ml/g at MDD, respectively. Figure 5-12 shows the variation of pore diameter with total pore volume. The 95% MDD specimen showed higher macro pore volume of 27% where at MDD it showed 22%.

The specimen exhibited 62% medium pores at 95% MDD and 65% at MDD conditions.

Volume of micro pores was 11% at 95% MDD and 13% at MDD conditions. This shows that the micro pore volume is independent of compaction dry density for this particular clay.

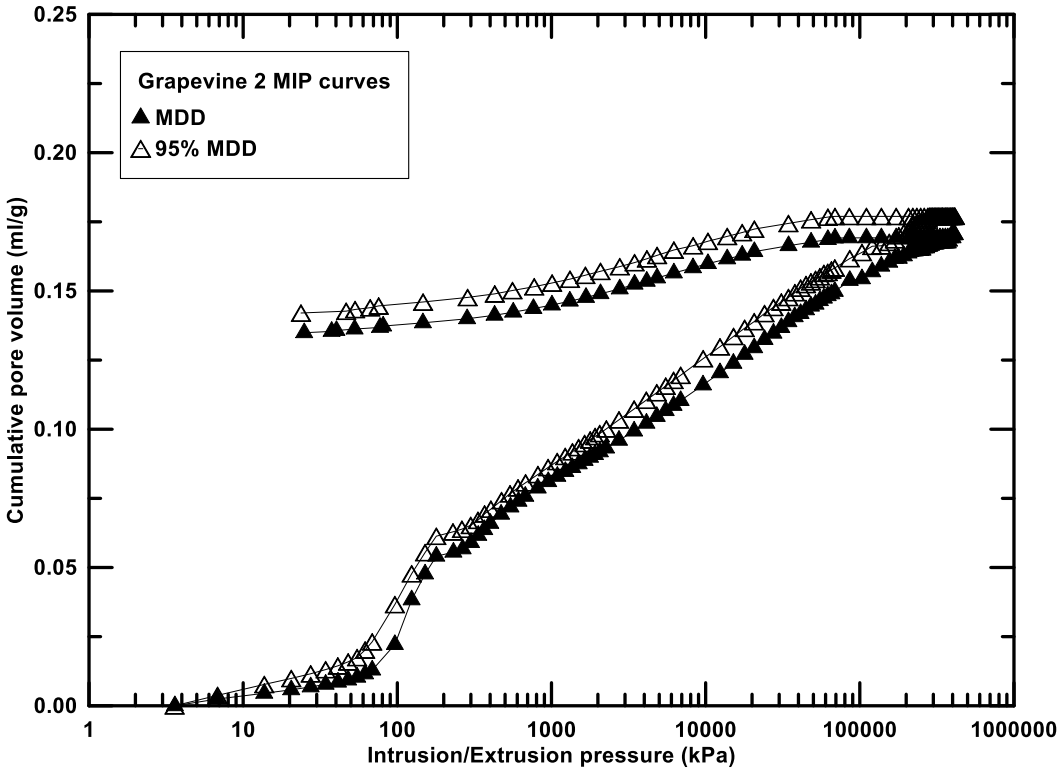

Figure 5-11 Intrusion/Extrusion curves for Grapevine 2 soil at MDD and 95% MDD

It was evident that the soil specimen carries more pore volume at 95% MDD condition than at MDD condition. The hysteresis observed between the intrusion and extrusion curves is due to the retention of mercury in the soil pores. This reveals that the specimen retained higher volume of mercury at MDD condition.

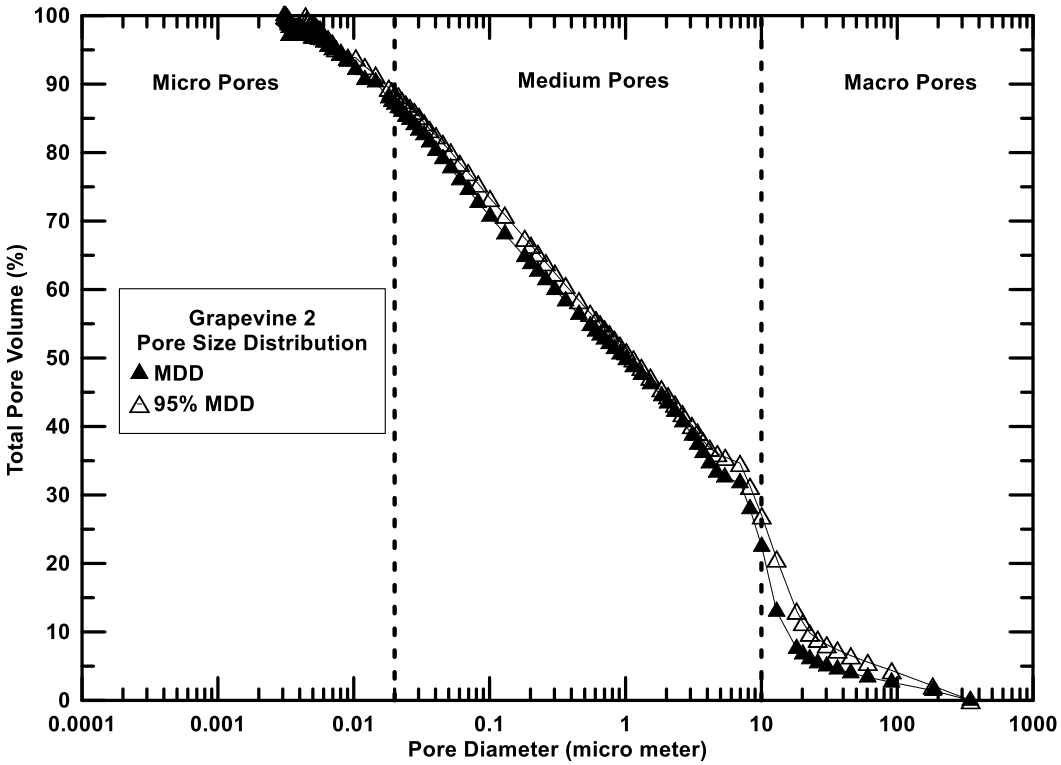

Figure 5-12 Pore size distribution for Grapevine 2 soil at MDD and 95% MDD

5.3.4 Mansfield soil pore distribution

The mercury intrusion/extrusion curves of Mansfield clay obtained from MIP technique at two compaction densities are shown in Figure 5-13. Mansfield soil which is classified as low plasticity clay showed a cumulative pore volume of 0.227 ml/g at 95% MDD and 0.221 ml/g at MDD, respectively. Figure 5-14 shows the variation of pore diameter with total pore volume. The 95% MDD specimen showed higher macro pore volume of 23% where at MDD it showed 14%.

The specimen exhibited 67% medium pores at 95% MDD and 76% at MDD conditions.

Both the specimens showed equal volume of micro pores (10%). This shows that the micro pore volume is independent of compaction dry density for this particular clay.

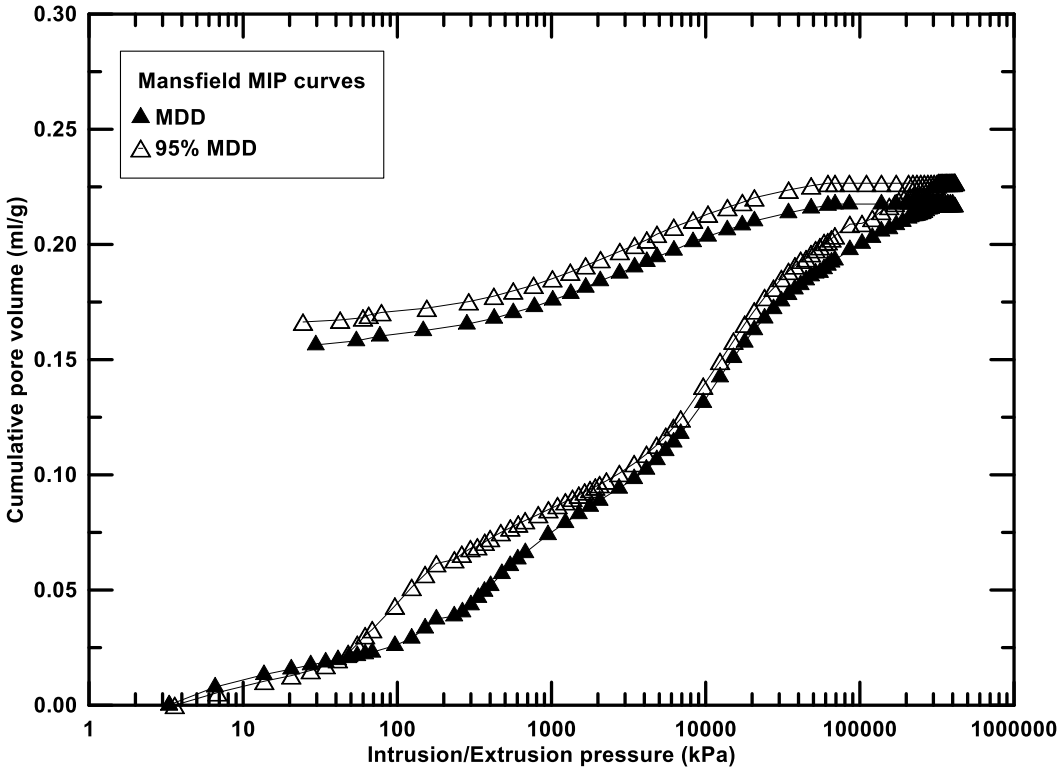

Figure 5-13 Intrusion/Extrusion curves for Mansfield soil at MDD and 95% MDD

It was evident that the soil specimen carries more pore volume at 95% MDD condition than at MDD condition. The hysteresis observed between the intrusion and extrusion curves is due to the retention of mercury in the soil pores. This reveals that the specimen retained higher volume of mercury at MDD condition.

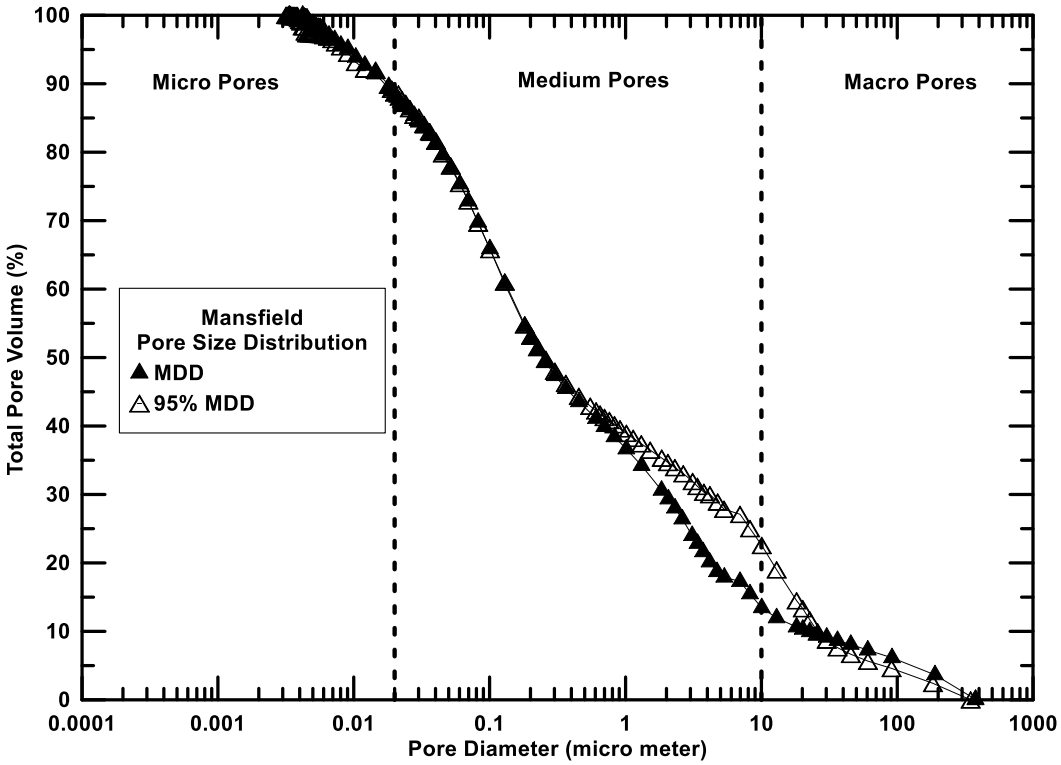

Figure 5-14 Pore size distribution for Mansfield soil at MDD and 95% MDD

5.3.5 Plano soil pore distribution

The mercury intrusion/extrusion curves of Plano clay obtained from MIP technique at two compaction densities are shown in Figure 5-15. Plano soil which is classified as low plasticity clay showed a cumulative pore volume of 0.255 ml/g at 95% MDD and 0.195 ml/g at MDD, respectively. Figure 5-16 shows the variation of pore diameter with total pore volume. The 95% MDD specimen showed higher macro pore volume of 36% where at MDD it showed 50%.

The specimen exhibited 45% medium pores at 95% MDD and 35% at MDD conditions.

Volume of micro pores was 19% 95% MDD and 15% at MDD conditions. This shows that the micro pore volume is independent of compaction dry density for this particular clay.

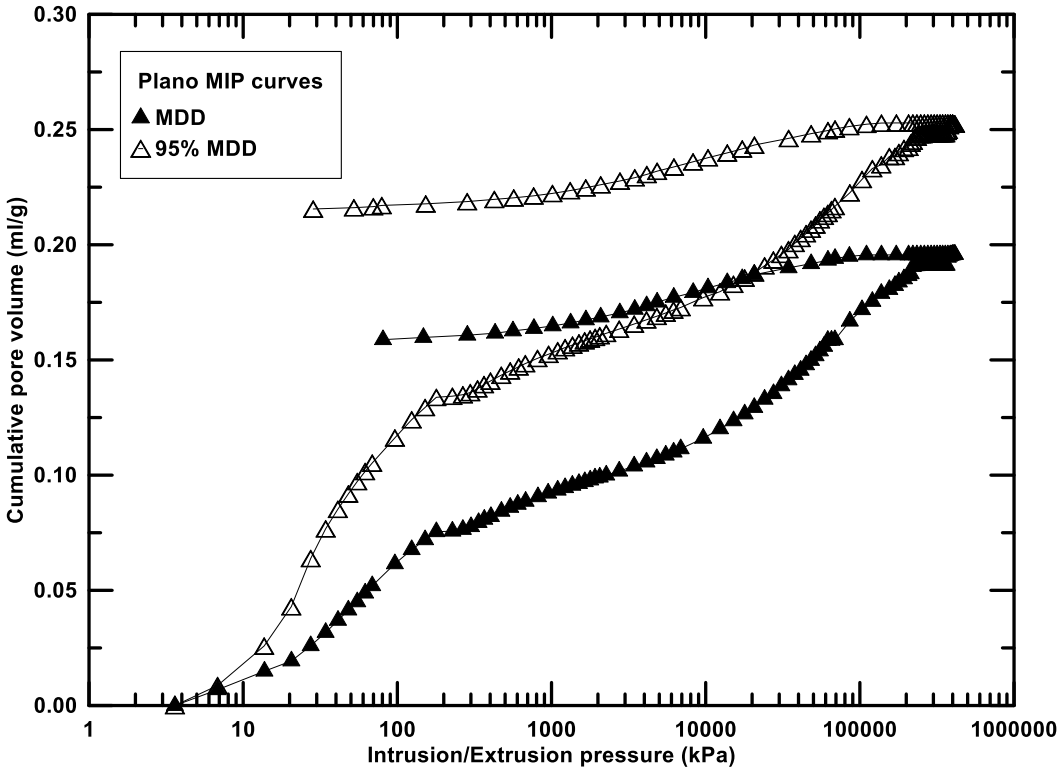

Figure 5-15 Intrusion/Extrusion curves for Plano soil at MDD and 95% MDD

It was evident that the soil specimen carries more pore volume at 95% MDD condition than at MDD condition. The hysteresis observed between the intrusion and extrusion curves is due to the retention of mercury in the soil pores. This reveals that the specimen retained higher volume of mercury at MDD condition.

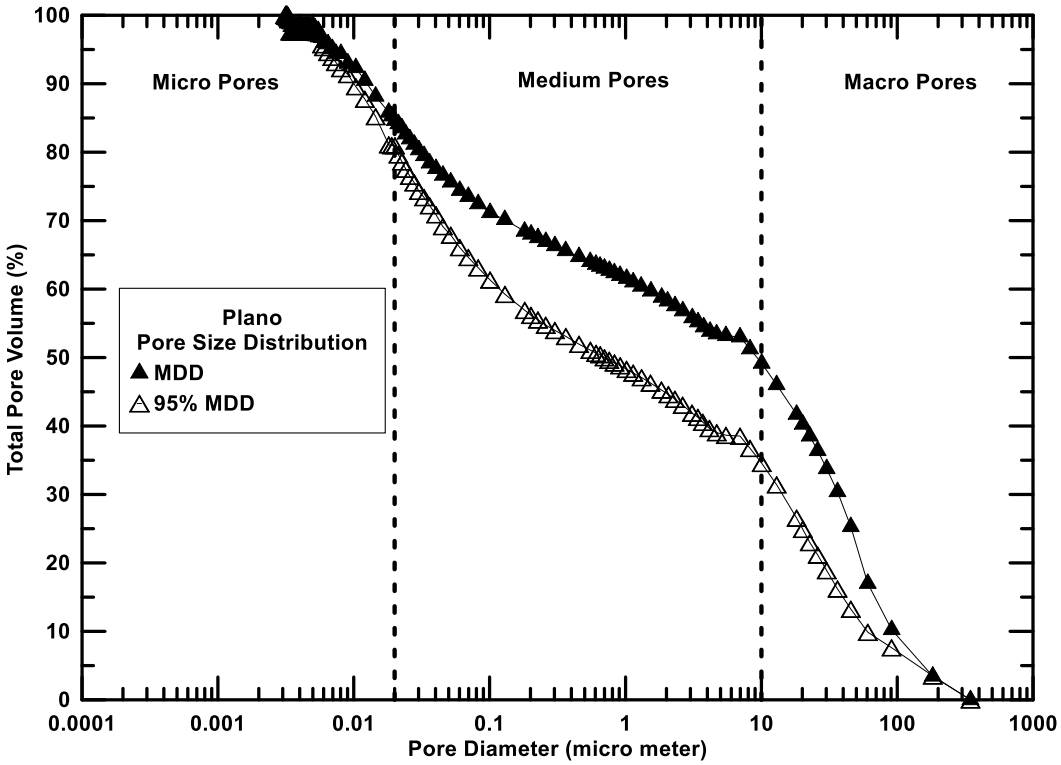

Figure 5-16 Pore size distribution for Plano soil at MDD and 95% MDD

5.3.6 Waco soil pore distribution

The mercury intrusion/extrusion curves of Waco clay obtained from MIP technique at two compaction densities are shown in Figure 5-17. Waco soil which is classified as low plasticity clay showed a cumulative pore volume of 0.207 ml/g at 95% MDD and 0.178 ml/g at MDD, respectively. Figure 5-18 shows the variation of pore diameter with total pore volume. The 95% MDD specimen showed higher macro pore volume of 19% where at MDD it showed 21%. The specimen exhibited 68% of the total volume corresponding to medium pores at 95% MDD and MDD conditions.

Volume of micro pores was 13% at 95% MDD and 11% at MDD conditions. This shows that the micro pore volume is independent of compaction dry density for this particular clay.

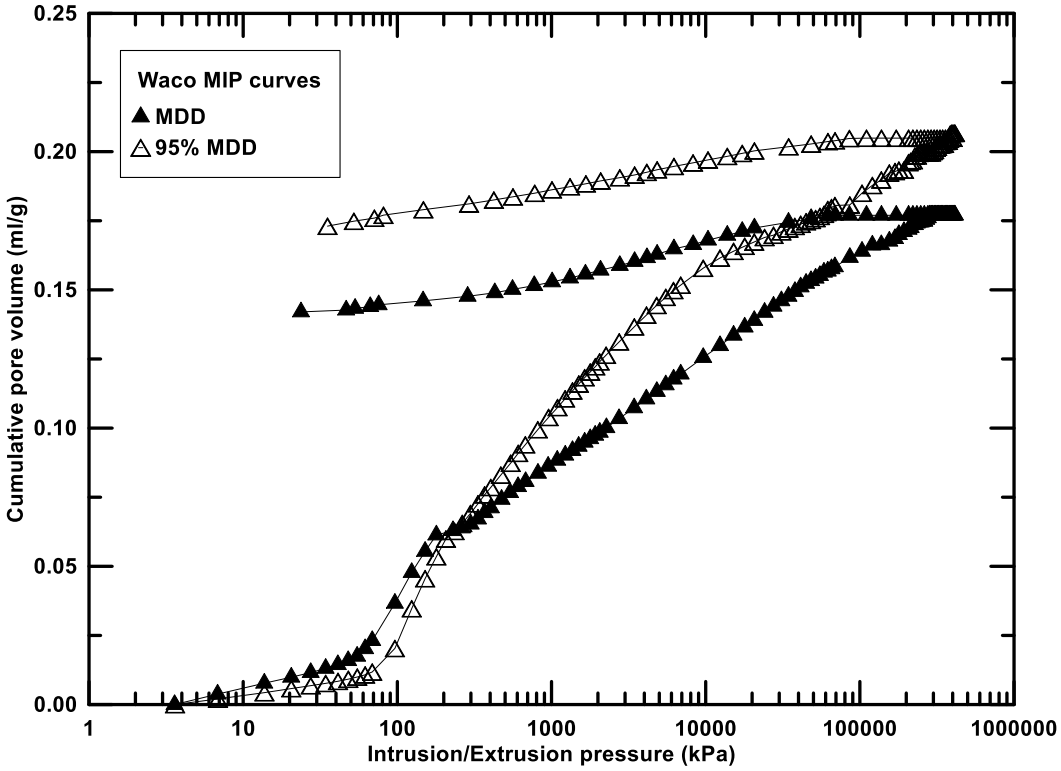

Figure 5-17 Intrusion/Extrusion curves for Waco soil at MDD and 95% MDD

It was evident that the soil specimen carries more pore volume at 95% MDD condition than at MDD condition. The hysteresis observed between the intrusion and extrusion curves is due to the retention of mercury in the soil pores. This reveals that the specimen retained higher volume of mercury at MDD condition.

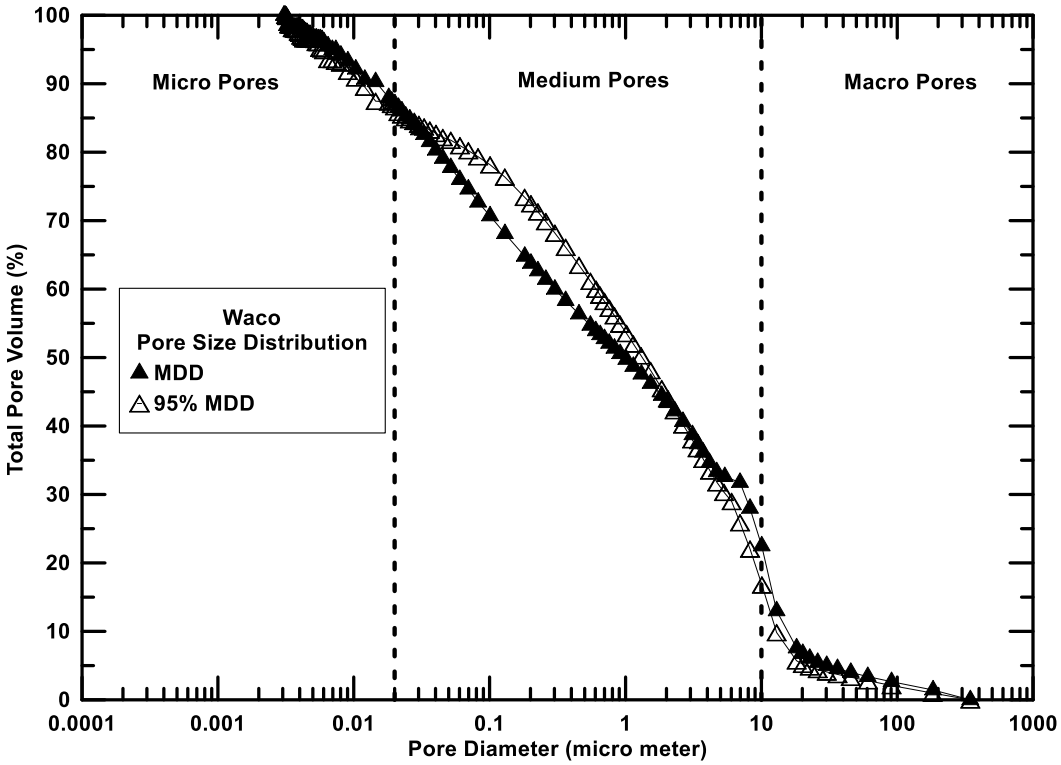

Figure 5-18 Pore size distribution for Waco soil at MDD and 95% MDD

The intrusion extrusion curve from MIP test revealed the volume of mercury intruded in to the pores of the soil specimen and the volume of mercury retained in the specimen after the test. The variation of different pore sizes for all the six soils was identified and presented with the help of MIP technique. The dependency of total volume of mercury induced and pore size variation on the compaction density of the specimen was monitored.

From the above discussions, it was found that the variation of density and moisture content of soils had a major influence on the pore distribution of the soil specimen. The volume of micro pores is found to be more in specimens compacted at MDD than at 95% MDD.

Similarly macro pore volume is found to be in general higher in the case of 95% MDD condition than at MDD condition. The high compaction level at MDD condition packs the soil particles together thereby increasing the micro pore volume and decreasing the macro pore volume when compared to 95% MDD condition. The size and volumes of pores present in the soil specimen as determined by the MIP method are presented in Table 5-13.

Table 5-13 Pore size distribution results obtained from MIP test

Soil	Cumulative volume of MI (ml/g)		Micro pores (%)		Medium pores (%)		Macro pores (%)	
	95% MDD	MDD	95% MDD	MDD	95% MDD	MDD	95% MDD	MDD
Cleburne	0.134	0.129	11	11	59	65	30	24
Denton	0.174	0.145	12	15	46	58	42	27
Grapevine 2	0.176	0.171	11	13	62	65	27	22
Mansfield	0.227	0.221	10	10	67	76	23	14
Plano	0.255	0.195	19	15	45	35	36	50
Waco	0.207	0.178	13	11	68	68	19	21

5.4 X-ray Computed Tomography results

X-ray computed tomography (XCT) is a scanning technique utilized to monitor 3-Dimensional internal pore structure of a solid mass. X-rays are passed through the soil specimen in all directions and the attenuating parameter, which helps in revealing the internal structure of the soil specimen, was monitored. Image reconstruction software helps to create the true 3-D image of the scanned soil specimen from the attenuating parameter.

Procedures followed during this research match the general guidelines developed by Pedarla (2013), thus, the working principles of this computed tomography

were already detailed in Chapter 2 and Chapter 3. Further details may be found in the work documents of the mentioned researcher.

A 1 cm^3 soil specimen was cut from the statically compacted soil. Tomography scanning was performed on soil specimens at different initial conditions and the test results are presented in the coming sections for all the six soils.

5.4.1 Cleburne soil CT scan

The reconstructed Cleburne soil CT scan image at 95% MDD partially sliced to obtain internal sample images is presented in Figure 5-19. The 3-D image shows the packing and arrangement of particles of different sizes. The high density particles are represented by white color and low density particles with darker color.

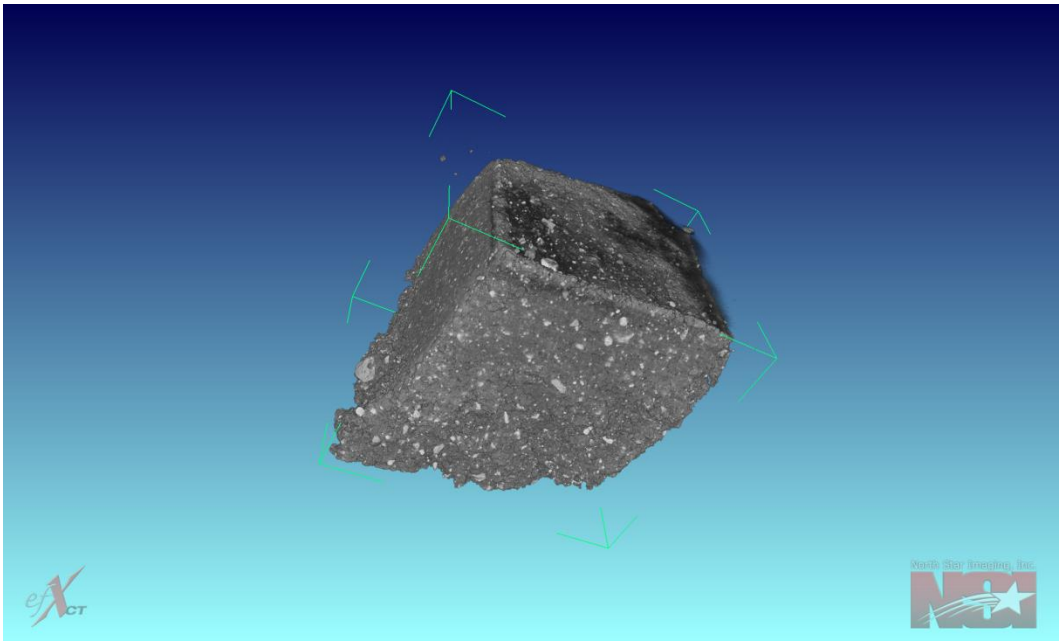

Figure 5-19 Reconstructed Cleburne Soil specimen from XCT technique

Cleburne soil specimen was compacted at two density conditions, 95% MDD and MDD.

The cut samples were oven dried for a period of 24 hours before scanning for X-ray tomography.

Figure 5-20 shows the variation of particle arrangement in the soil mass with change in density from 95% MDD to MDD condition. The void ratio of the mass is calculated using MATLAB image processing program as described in Chapters 2 and Chapter 3. For the Cleburne soil the void ratio varied from 0.558 at 95% MDD to 0.484 at MDD condition. For scaling purposes, both images in the figure have 60 mm side length, despite of their size on paper.

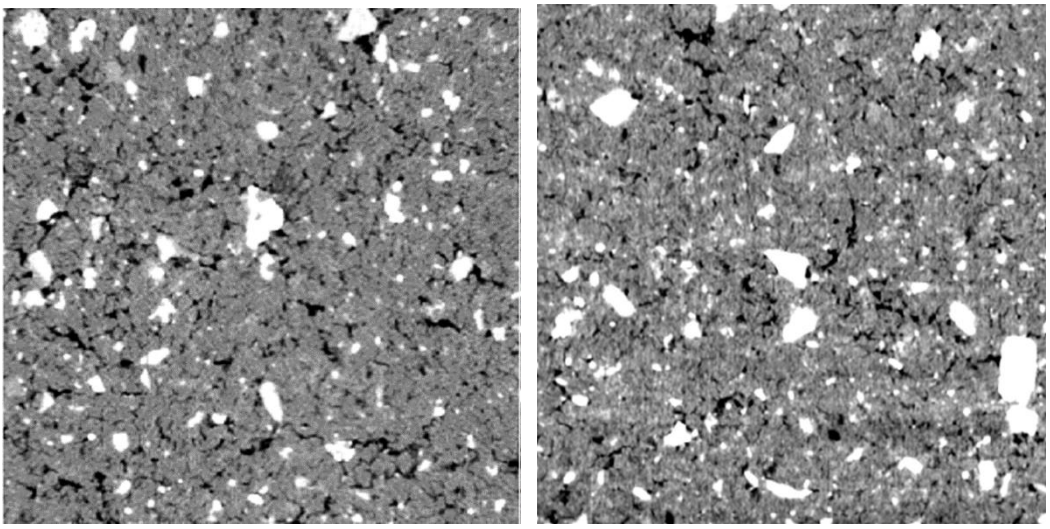

(a) 95% MDD e=0.558 (b) MDD e=0.484

Figure 5-20 (a), (b) XCT images of Cleburne soil at different densities

Figure 5-21 shows the variation of pore structure and void ratio with saturation of the specimen at 95% MDD. For the Cleburne soil, the void ratio decreased from 0.48 at dry side to 0.41 at saturation. For scaling purposes, both images in the figure have 60 mm side length, despite of their size on paper.

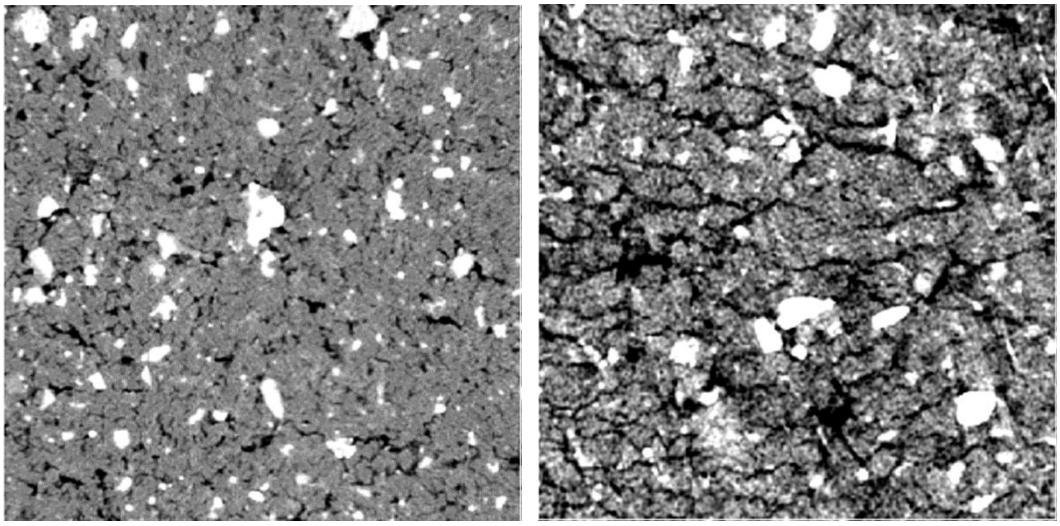

(a) 95% MDD e=0.56 (b) MDD e=0.49

Figure 5-21 XCT images of Cleburne soil, 95% MDD condition; (a) dry, (b) saturated

5.4.2 Denton soil CT scan

The reconstructed Denton soil CT scan image at 95% MDD partially sliced to obtain internal sample images is presented in Figure 5-22. The 3-D image shows the packing and arrangement of particles of different sizes. The high density particles are represented by white color and low density particles with darker color.

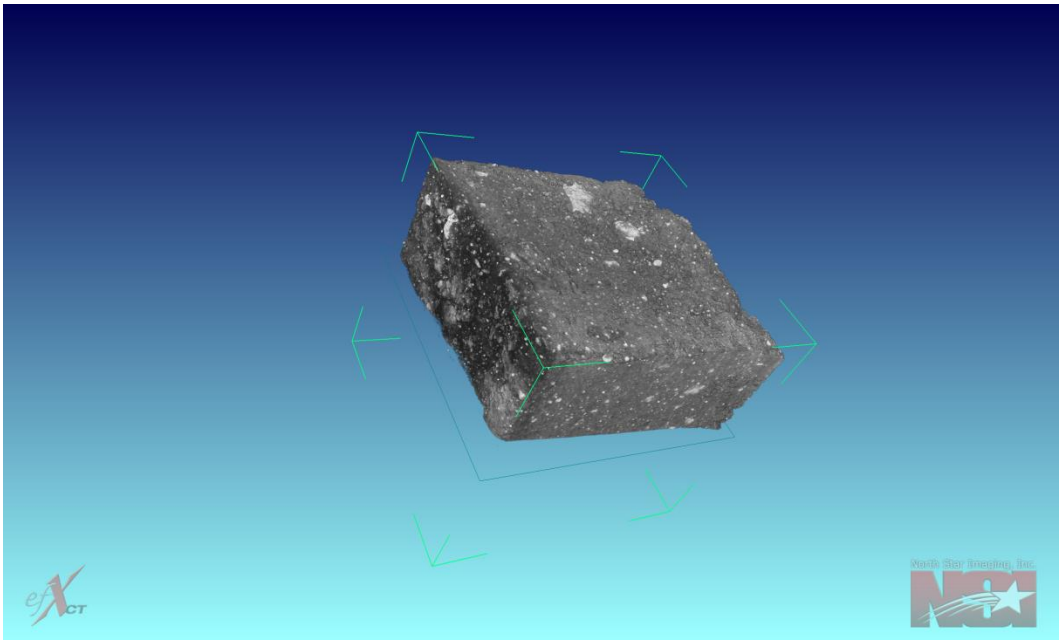

Figure 5-22 Reconstructed Denton Soil specimen from XCT technique

Denton soil specimen was compacted at two density conditions, 95% MDD and MDD.

The cut samples were oven dried for a period of 24 hours before scanning for X-ray tomography.

Figure 5-23 shows the variation of particle arrangement in the soil mass with change in density from 95% MDD to MDD condition. The void ratio of the mass is calculated using MATLAB image processing program as described in Chapters 2 and Chapter 3. For the Denton soil the void ratio varied from 0.763 at 95% MDD to 0.686 at MDD condition. For scaling purposes, both images in the figure have 60 mm side length, despite of their size on paper.

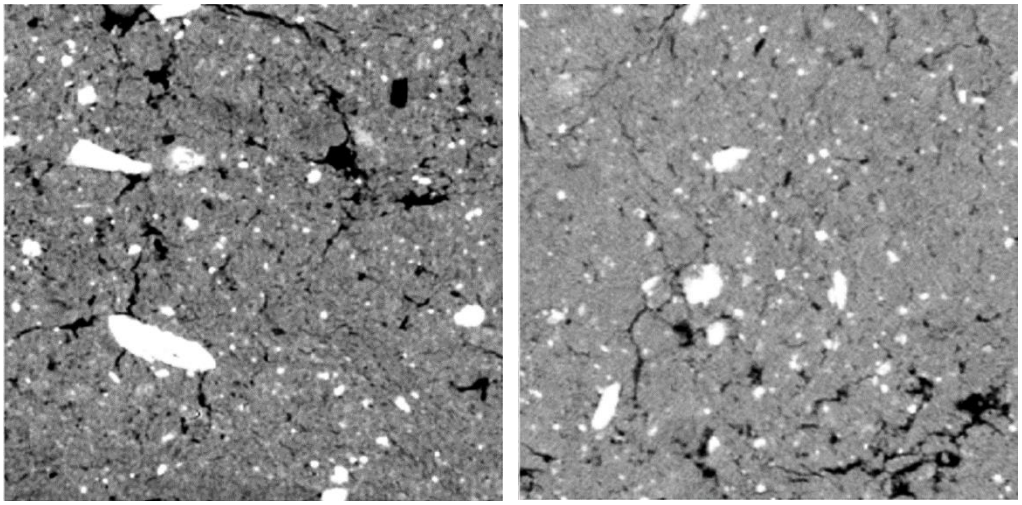

(a) 95% MDD e=0. 763 (b) MDD e=0. 686

Figure 5-23 (a), (b) XCT images of Denton soil at different densities

Figure 5-24 shows the variation of pore structure and void ratio with saturation of the specimen at 95% MDD. For the Denton soil, the void ratio decreased from 0.76 at dry side to 0.33 at saturation. For scaling purposes, both images in the figure have 60 mm side length, despite of their size on paper.

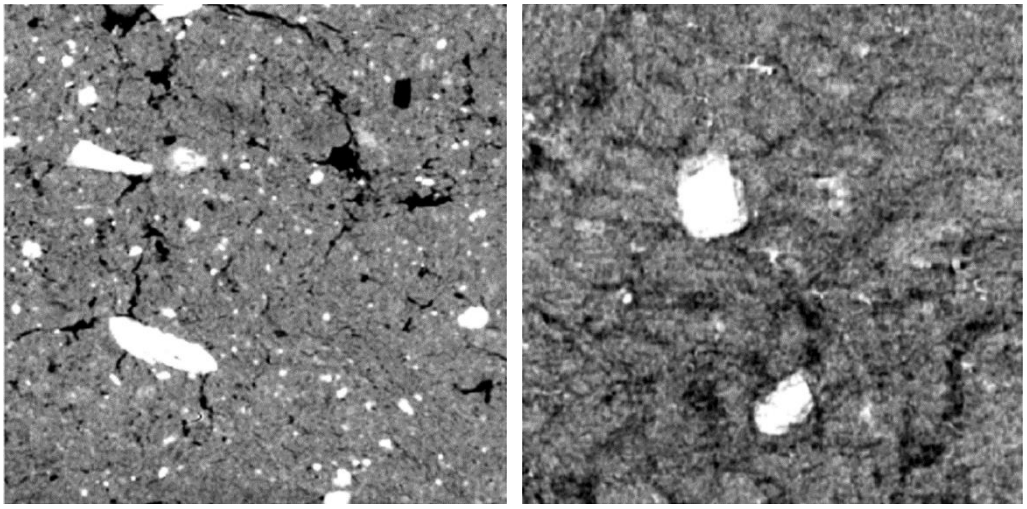

(a) 95% MDD e=0.76 (b) MDD e=0.33

Figure 5-24 XCT images of Denton soil, 95% MDD condition; (a) dry, (b) saturated

5.4.3 Grapevine 2 soil CT scan

The reconstructed Grapevine 2 soil CT scan image at 95% MDD partially sliced to obtain internal sample images is presented in Figure 5-25. The 3-D image shows the packing and arrangement of particles of different sizes. The high density particles are represented by white color and low density particles with darker color.

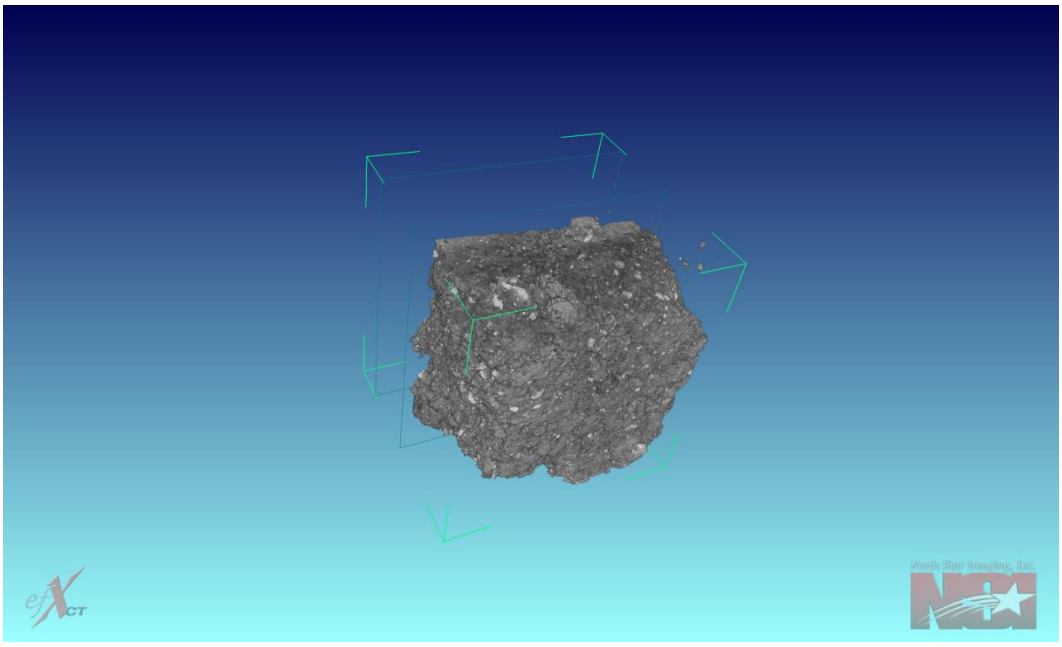

Figure 5-25 Reconstructed Grapevine 2 Soil specimen from XCT technique

Grapevine 2 soil specimen was compacted at two density conditions, 95% MDD and MDD.

The cut samples were oven dried for a period of 24 hours before scanning for X-ray tomography.

Figure 5-26 shows the variation of particle arrangement in the soil mass with change in density from 95% MDD to MDD condition. The void ratio of the mass is calculated using MATLAB image processing program as described in Chapters 2 and Chapter 3. For the Grapevine 2 soil the void ratio varied from 0.701 at 95% MDD to 0.593

at MDD condition. For scaling purposes, both images in the figure have 60 mm side length, despite of their size on paper.

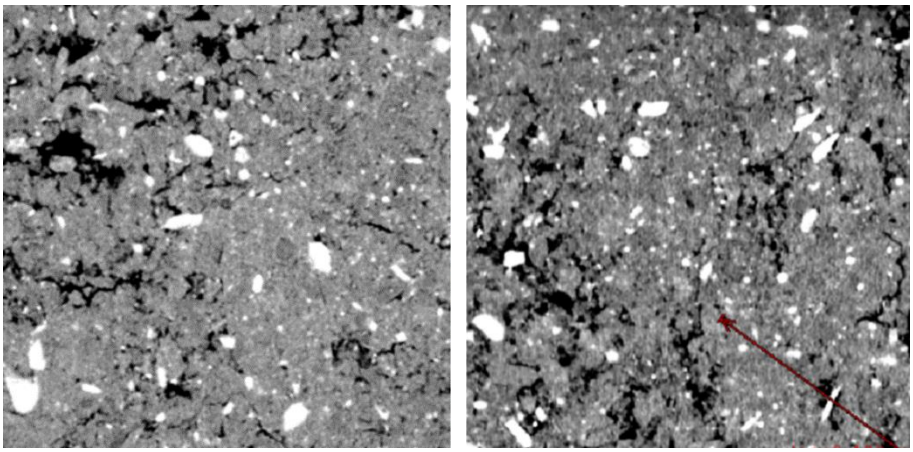

(a) 95% MDD e=0.701 (b) MDD e=0.593

Figure 5-26 (a), (b) XCT images of Grapevine 2 soil at different densities

Figure 5-27 shows the variation of pore structure and void ratio with saturation of the specimen at 95% MDD. For the Grapevine 2 soil, the void ratio decreased from 0.70 at dry side to 0.59 at saturation. For scaling purposes, both images in the figure have 60 mm side length, despite of their size on paper.

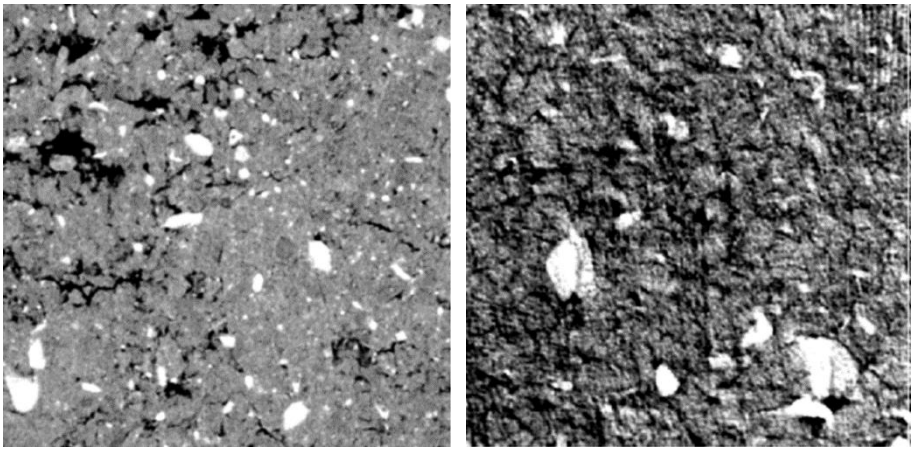

(a) 95% MDD e=0.70 (b) MDD e=0.52

Figure 5-27 XCT images of Grapevine 2 soil, 95% MDD condition; (a) dry, (b) saturated

5.4.4 Mansfield soil CT scan

The reconstructed Mansfield soil CT scan image at 95% MDD partially sliced to obtain internal sample images is presented in Figure 5-28. The 3-D image shows the packing and arrangement of particles of different sizes. The high density particles are represented by white color and low density particles with darker color.

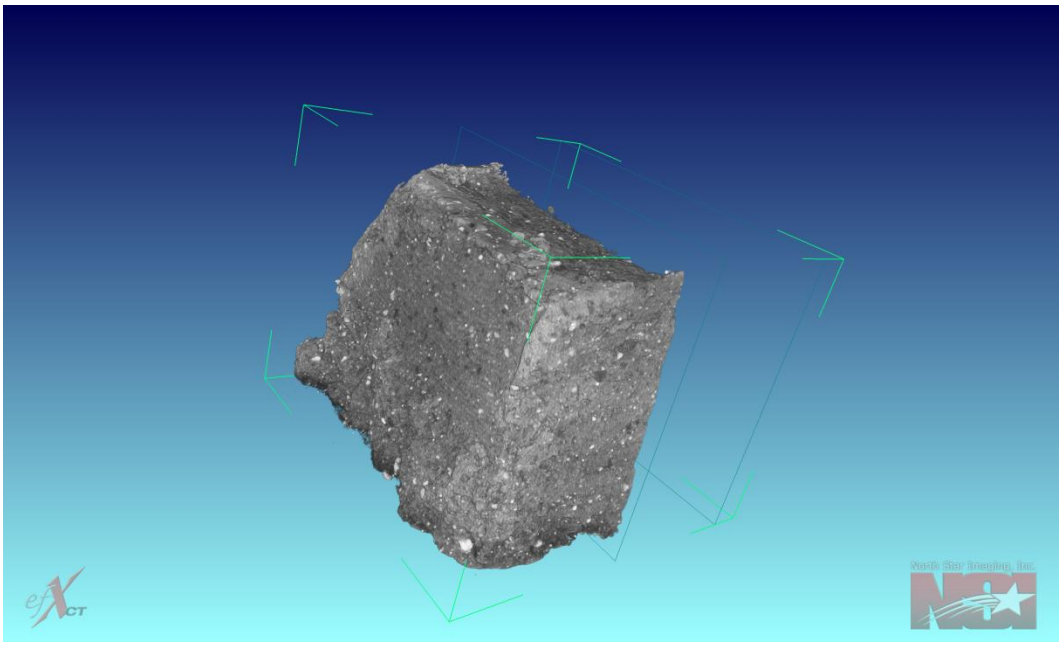

Figure 5-28 Reconstructed Mansfield Soil specimen from XCT technique

Mansfield soil specimen was compacted at two density conditions, 95% MDD and MDD.

The cut samples were oven dried for a period of 24 hours before scanning for X-ray tomography.

Figure 5-29 shows the variation of particle arrangement in the soil mass with change in density from 95% MDD to MDD condition. The void ratio of the mass is calculated using MATLAB image processing program as described in Chapters 2 and Chapter 3. For the Mansfield soil the void ratio varied from 0.965 at 95% MDD to 0.859 at

MDD condition. For scaling purposes, both images in the figure have 60 mm side length, despite of their size on paper.

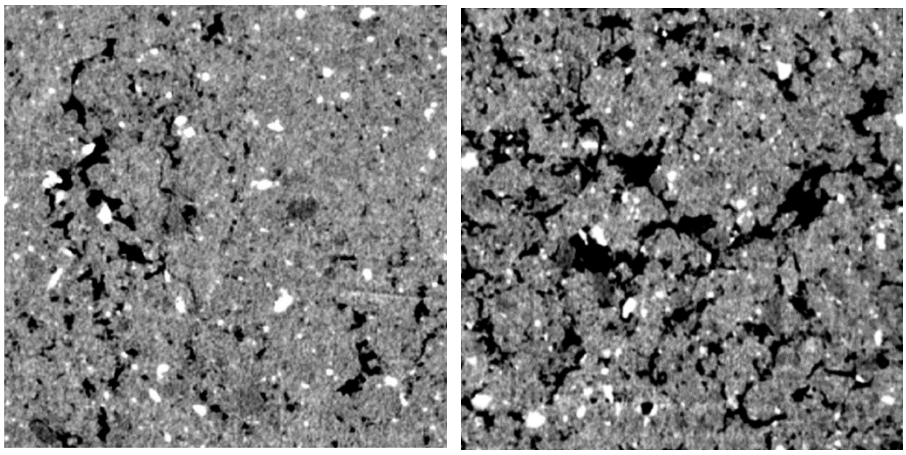

(a) 95% MDD e=0.965 (b) MDD e=0.859

Figure 5-29 (a), (b) XCT images of Mansfield soil at different densities

Figure 5-30 shows the variation of pore structure and void ratio with saturation of the specimen at 95% MDD. For the Mansfield soil, the void ratio decreased from 0.97 at dry side to 0.58 at saturation. For scaling purposes, both images in the figure have 60 mm side length, despite of their size on paper.

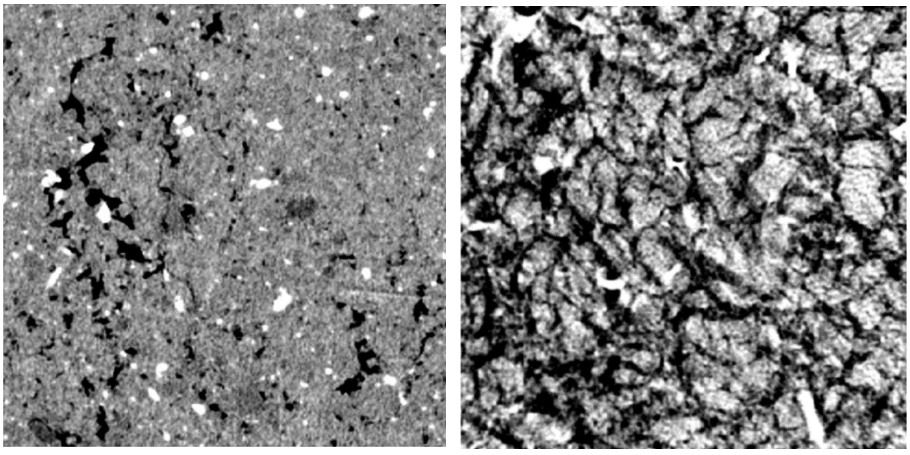

(a) 95% MDD e=0.97 (b) MDD e=0.58

Figure 5-30 XCT images of Mansfield soil, 95% MDD condition; (a) dry, (b) saturated

5.4.5 Plano soil CT scan

The reconstructed Plano soil CT scan image at 95% MDD partially sliced to obtain internal sample images is presented in Figure 5-31. The 3-D image shows the packing and arrangement of particles of different sizes. The high density particles are represented by white color and low density particles with darker color.

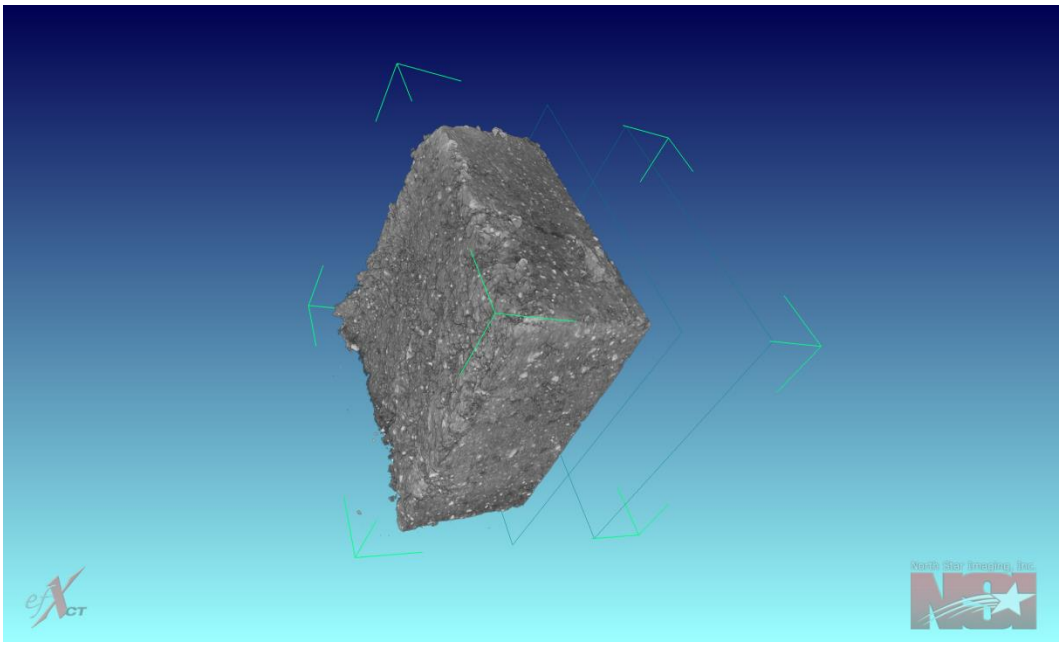

Figure 5-31 Reconstructed Plano Soil specimen from XCT technique

Plano soil specimen was compacted at two density conditions, 95% MDD and MDD.

The cut samples were oven dried for a period of 24 hours before scanning for X-ray tomography.

Figure 5-32 shows the variation of particle arrangement in the soil mass with change in density from 95% MDD to MDD condition. The void ratio of the mass is calculated using MATLAB image processing program as described in Chapters 2 and Chapter 3. For the Plano soil the void ratio varied from 1.013 at 95% MDD to 0.931 at

MDD condition. For scaling purposes, both images in the figure have 60 mm side length, despite of their size on paper.

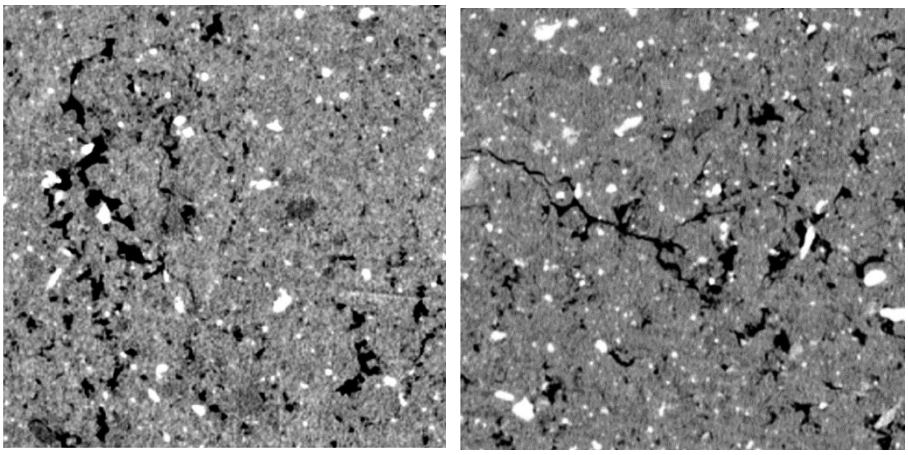

(a) 95% MDD e=1.013 (b) MDD e=0.931

Figure 5-32 (a), (b) XCT images of Plano soil at different densities

Figure 5-33 shows the variation of pore structure and void ratio with saturation of the specimen at 95% MDD. For the Plano soil, the void ratio decreased from 1.01 at dry side to 0.48 at saturation. For scaling purposes, both images in the figure have 60 mm side length, despite of their size on paper.

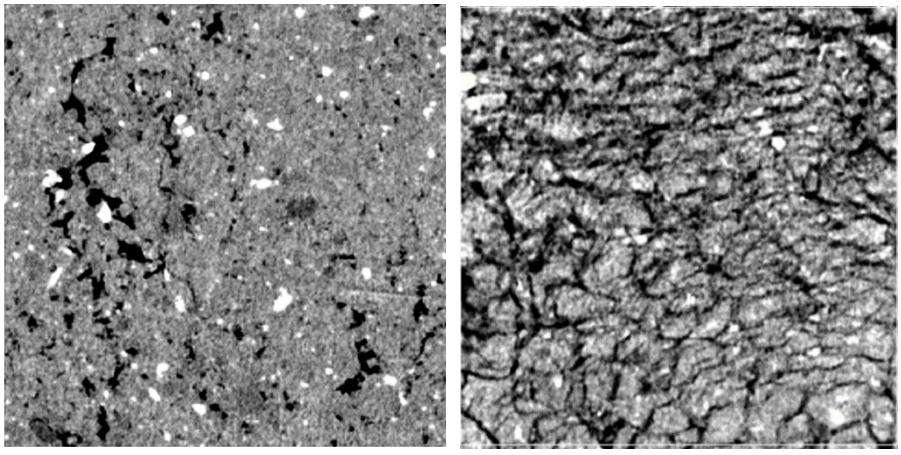

(a) 95% MDD e=1.01 (b) MDD e=0.48

Figure 5-33 XCT images of Plano soil, 95% MDD condition; (a) dry, (b) saturated

5.4.6 Waco soil CT scan

The reconstructed Waco soil CT scan image at 95% MDD partially sliced to obtain internal sample images is presented in Figure 5-34. The 3-D image shows the packing and arrangement of particles of different sizes. The high density particles are represented by white color and low density particles with darker color.

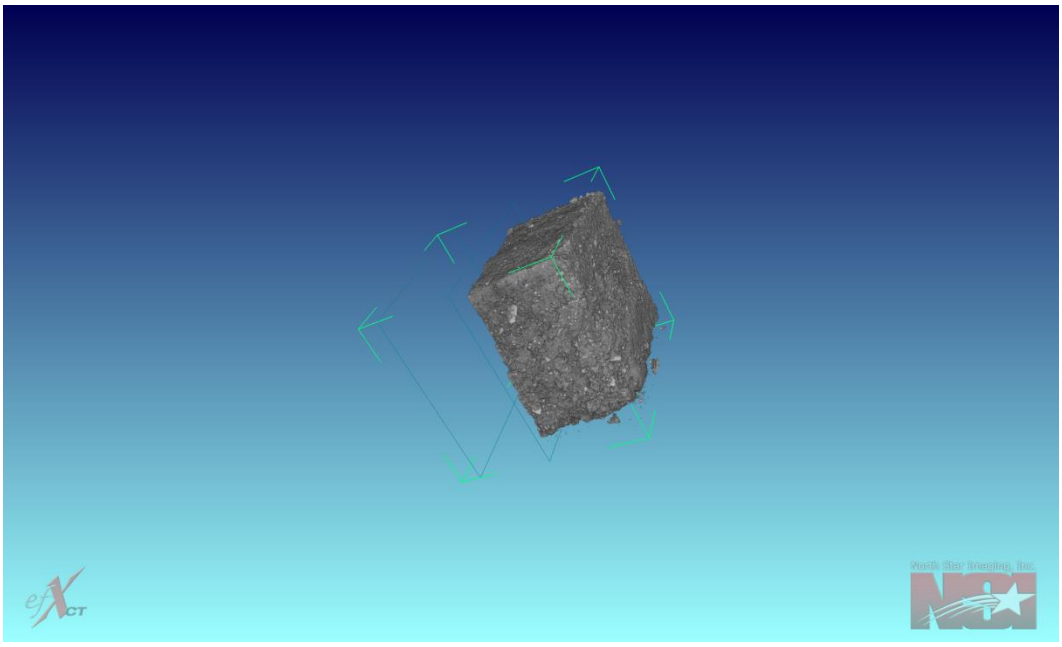

Figure 5-34 Reconstructed Waco Soil specimen from XCT technique

Waco soil specimen was compacted at two density conditions, 95% MDD and MDD.

The cut samples were oven dried for a period of 24 hours before scanning for X-ray tomography.

Figure 5-35 shows the variation of particle arrangement in the soil mass with change in density from 95% MDD to MDD condition. The void ratio of the mass is calculated using MATLAB image processing program as described in Chapters 2 and Chapter 3. For the Waco soil the void ratio varied from 1.037 at 95% MDD to 0.932 at

MDD condition. For scaling purposes, both images in the figure have 60 mm side length, despite of their size on paper.

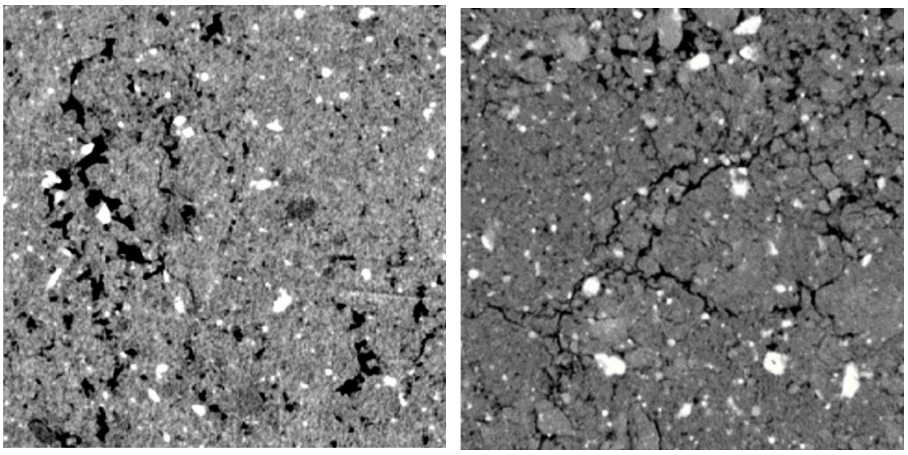

(a) 95% MDD e=1.037 (b) MDD e=0.932

Figure 5-35 (a), (b) XCT images of Waco soil at different densities

Figure 5-36 shows the variation of pore structure and void ratio with saturation of the specimen at 95% MDD. For the Waco soil, the void ratio decreased from 1.04 at dry side to 0.62 at saturation. For scaling purposes, both images in the figure have 60 mm side length, despite of their size on paper.

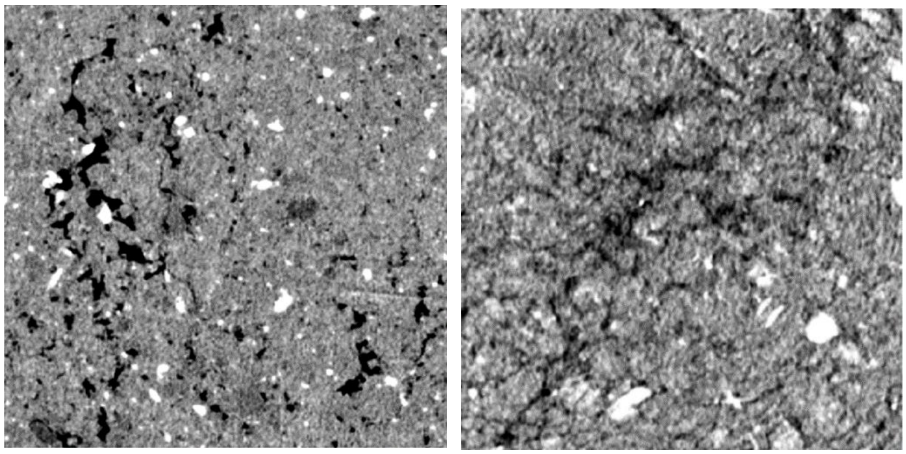

(a) 95% MDD e=1.04 (b) MDD e=0.62

Figure 5-36 XCT images of Waco soil, 95% MDD condition; (a) dry, (b) saturated

It was found that there is a very close match among the void ratio values calculated with the two techniques at dry compaction conditions, only differing by small amounts. The systematic differences can be attributed to sampling technique induced soil disturbance to image analysis related errors. Also, the identification of the sample details might be affected by the resolution threshold values used in order to obtain the void ratio of each sample, since the value provided to the software is usually assumed and may vary from one soil to other.

Nevertheless, and based on the procedures followed, the void ratio calculated from XCT technique has shown a good agreement with weight-volume relationships at both dry density conditions.

5.5 Summary

The present chapter deals with the study of different soil composition parameters on the six soils collected. The mineralogical properties of these test soils are previously measured and presented in Chapter 3.

From mercury intrusion porosimetry testing, it was found that the high particle density at the MDD condition resulted in a lower volume of pore space. It was also found that Macro pores are abundant in specimens with low density (95% MDD), whereas micro and medium pores increase with high dense conditions (i.e. MDD). The inter-connectivity of pores present in the soil specimen was closely observed with the help of X-ray tomography technique. The calculation of void ratio from the sliced sections was achieved using MATLAB image processing program (Pedarla, 2013) and is based on pixel count, defining a threshold value for pixel color intensity.

From the tomography experiment, the variation of pore space and connectivity is clearly noticeable at different densities and moisture levels. The void ratio decreased from 95% MDD to MDD which is due to the more dense packing of particles. The void

ratios determined from the XCT technique are in good agreement with those obtained from weight/volume relationships at dry conditions. The void ratio's generated during saturation condition are very low compared to those obtained from weight/volume relationships. The reason for this shift was that during the saturation process the clay minerals expand and occupy the pore spaces which in turn reduce the overall void ratio and hence were clearly noticed with the help of X-ray tomography. Also a “doubling” effect due to thawing process of the sample may affect the results when scanning saturated specimens.

Both MIP and XCT techniques showed good repeatability of the test results. These tests provided pore size information of the present six expansive soils. All these results are using the modeling analysis attempted in next Chapters.

Chapter 6

Validation of simple swell prediction models

6.1 Introduction

According to the literature review presented in the Chapter 2 of this document as well as from the results obtained in the present research, it is possible to identify and define soil parameters that play a crucial role in swell behavior. These parameters may be used to determine advanced soil variables which may be employed to indirectly evaluate the expansiveness of clays in a stricter mode. Some researchers have recently presented approaches heading towards this purpose.

In a recent effort by Pedarla (2013), three swell prediction models based on the physical attributes of soil as well as the soil pore distribution and mineralogy details are attempted. These models are Diffused Double Layer (DDL) Swell Model, Mechanical Hydro Chemical (MHC) Model and Total Surface Area Ratio Model. A brief summary of the latter is presented next in this chapter.

The Diffused Double Layer (DDL) Swell Model is based on the mineralogy of the studied clays since it is well recognized to be an important factor in swell behavior of expansive soils. The Diffused Double Layer (DDL) theory is considered in this model by incorporation of the diffused double water layer thickness which is known to increase when the clay minerals having high specific surface charged areas attract the moisture content in the soil medium. Thus, the DDL thickness increment contributes to soil heaving.

Mechanical Hydro Chemical (MHC) Model aims to establish a relation among soil matric suction, clay mineral content and the directly measured swell behavior of the studied expansive soils.. The mechanical component of the parameter is assumed to come from the variation of void ratio with soil suction during the swelling of the soil

compacted specimen. The hydro component in the parameter relates the initial moisture content value to its corresponding matric suction at the conditions present in the soil specimen when the swelling begins. Finally, the soil clay mineralogy is considered as the chemical parameter (C) contributing to MHC modeling.

The Total Surface Area Ratio (TSAR) Model intends to assess the swell behavior of a soil specimen with respect to its total surface area. Thus, the model establishes a relation for each soil between its specific surface area as obtained from the specific surface area (SSA) test and the lengths of different pore sizes as encountered by the application of the mercury intrusion porosimetry (MIP) technique. The relationship is a particular variable for each soil and is designated as the 'Total Surface Area Ratio' (TSAR).

Further details about the models may be encountered in Chapter 2, Chapter 3, and the study developed by Pedarla (2013).

Among the objectives of the present research outlined in Chapter 2 there is a need to corroborate the three novel swell prediction models introduced by Pedarla (2013). To develop the validation process of the models, the following steps mentioned below have been accomplished:

1. Swell tests were performed on six soils collected from different places in Texas and expected to behave expansively. The geographical places to collect the soils were chosen expecting to recover soils that had undergone geologic formation processes different to those suffered by the soils used by Pedarla (2013). The swell testing was accomplished according to the methodology presented in Chapter 2 and Chapter 3 which matches the procedures followed by the mentioned author.

2. The formulae presented by Pedarla (2013) for each of the three swell prediction models was followed after completion of the direct swelling behavior assessment for the six soils. Equivalent advanced soil variables as in Pedarla's work were thus found for the six soils used in the present research.
3. The values of advanced soil variables reported by Pedarla (2013) for all the eight expansive soils used in his research as well as those obtained in the present study were plotted following the same graphical approach.
4. The fitting of the three models for all the 14 soils (8 soil for model establishing and 6 soils for model evaluation) was evaluated in accordance to statistical analyses analogous to those employed by Pedarla (2013). Remarks on the fitting of the models are also presented in this document.

In addition to the above outlined, the Diffuse double layer model was intended to be further validated in this chapter, by comparing the values of the strains obtained from the model with respect to those strain values determined by direct DDL theory formulae application considering that it allows for direct and indirect determination of a weighted half the distance between clay layers.

In the following, maximum dry density (MDD) or maximum dry unit weight (MDUW) will be considered equivalent terms and thus used indistinctly.

6.2 Diffused Double Layer (DDL) Swell Model validation

Diffuse double layer (DDL) theory as proposed by Gouy and Chapman (Gouy 1910; Chapman 1913) provides a strong basis for the understanding of swell behavior of a clay specimen (Mitchell and Soga, 2005).

When clay comes in close contact with water, the negative charged clay particles tend to attract the water molecules, which distribute over the surface area of the clay particles thereby increasing the particle size.

The extent to which the clay particles have attraction forces on the water molecules is termed as diffuse double layer thickness. Estimation of double layer thickness can be obtained by the following Equation 6-1.

$$x = \frac{1}{K} = \left(\frac{\in_0 DkT}{2n_0 e^2 v^2}\right)^{\frac{1}{2}} \qquad 6-1$$

Where x is a measure of thickness of double layer, K is the diffuse double layer parameter, $\in_0$ is the permittivity in vacuum, k is Boltzmann constant, T is temperature, D is the dielectric constant of bulk fluid, e is the electronic charge, n_0 is the ionic concentration and v is the valence of exchangeable cations.

This relationship also suggests that there is a direct influence of diffuse double layer on the changes in system composition. Hence, depending on the diffuse double layer, the swelling behavior in expansive clays varies accordingly and is one of the major factors driving this research study.

Gouy–Chapman DDL theory evolved further and developed expressions for interacting particles applied to relate swelling pressure and void ratio for clays (Schanz et al., 2013, Barat et al., 2013), stated as Equations 6-2 to 6-5.

$$P = 2n_0 kT(\cosh u - 1) \qquad 6-2$$

$$-\left(\frac{dy}{d\xi}\right)_{x=0} = \sqrt{(2\cosh z - 2\cosh u)} = \left(\frac{CEC}{SSA}\right)\left(\frac{1}{2 \in_0 Dn_0 kT}\right)^{\frac{1}{2}} \qquad 6-3$$

$$-\left(\frac{dy}{d\xi}\right)_{x=0} = \int_z^u \frac{1}{\sqrt{(2\cosh z - 2\cosh u)}} dy = \int_0^d d\xi = -Kd \qquad 6-4$$

$$e_d = G\rho_w Sd \qquad 6-5$$

Where P is the swelling pressure, u is the nondimensional midplane potential, ξ is the distance function, y is the nondimensional potential at a distance x from the clay surface, z is the nondimensional potential function at the clay particle surface (x = 0), CEC is the cation exchange capacity, SSA is the specific surface area, e_d is the void ratio of the clay specimen according to the DDL theory concept, G is the specific gravity of soil solids, d is half the distance between clay layers, and ρ_w is the unit weight of water.

In present research laboratory works were performed to fulfill the DDL model requirements. Thus, 1-D swell strains and swell pressures were obtained using conventional consolidometer sized specimen of 2.54 cm (1 in) height and 6.3 cm (2.5 in) diameter, compacted at MDD and 95% of the MDD according to AASHTO T-307. The tests observed the Method C (loading-after-wetting test) normalized in the ASTM D4546 – 08 standards.

On the other hand, volumetric swell strains under 3 confinements (7 kPa, 50 kPa and 100 kPa) for all the six soils were measured using the UTA's 3-D swell strain apparatus as discussed in Chapter 2 and Chapter 3. For the volumetric strains, all the specimens were compacted only at 95% MDD. The dimensions of the specimens were 0.1 m (4 in) in height and 0.05 m (2 in) diameter.

Chemical tests were also performed on the soils for mineralogy quantification in accordance with the methodology proposed by Chittoori et al. (2011).

Additional details of the techniques used to characterize the six clayey soils as well as their results may be seen in the work presented by Pedarla (2013) and in Chapter 2 through Chapter 4 of this document as well. Thus, all the 14 soils were first subjected to basic soil classification as well as plasticity and chemical tests. Result details are presented in Table 6-1. Soils worked by Pedarla (2013) are named as follows: Anthem, Burleson, Colorado, Grayson, Keller, Oklahoma, San Antonio, and San Diego.

Table 6-1 Laboratory tests results

Soil	Ref	LL	PI	MDUW (kN/m^3)	OMC (%)	CEC (meq/100g)	SSA (m^2/g)	MM (%)	I (%)	K (%)	USCS Classification
Anthem	1	48	27	1720	18	71.70	118.50	25.20	24.40	50.40	CL
Burleson	1	55	37	1633	19	100.1	132.40	33.70	19.60	46.70	CH
Cleburne	2	38	21	1826	15	57.11	105.79	20.44	6.33	73.23	CL
Colorado	1	63	42	1649	19	91.60	185.00	35.70	35.00	29.30	CH
Denton	2	55	30	1661	19	41.24	156.50	20.37	8.67	70.96	CH
Grapevine 2	2	46	26	1693	19	34.31	156.53	18.57	11.50	69.93	CL
Grayson	1	75	49	1457	24	116.1	223.00	43.30	24.00	32.70	CH
Keller	1	25	11	1890	14	60.00	115.00	21.90	18.40	59.70	CL
Mansfield	2	67	38	1489	26	121.4	176.37	42.82	22.08	35.10	CH
Oklahoma	1	41	21	1593	24	63.30	76.30	19.70	70.00	10.30	CL
Plano	2	24	12	1462	27	54.44	229.31	29.63	37.67	32.70	CL
San Antonio	1	67	43	1608	22	97.40	192.40	37.80	30.90	31.30	CH
San Diego	1	42	28	1736	17	87.20	92.60	26.90	25.30	47.80	CL
Waco	2	58	34	1445	28	126.67	250.10	50.07	18.75	31.18	CH

The conventions in Table 6-1 are: Ref – reference: (1) Padarla 2013, (2) This research, LL – liquid limit, PI – plastic limit, MDUW – maximum dry unit weight, OMC – optimum moisture content, CEC - cation exchange capacity, SSA - specific surface area, %MM - percent mineral Montmorillonite, % K – percent mineral Kaolinite and % I – percent mineral Illite.

Also, a summary of the conventional swelling test results in conjunction with the volumetric or 3-D swell strains measured at confinement pressures of 7 kPa, 50 kPa and

100 kPa on soil specimens compacted at 95% MDUW and MDUW conditions is presented in Table 6-2.

Table 6-2 Summary of the 1-D and 3-D swell strain and swell pressure test results

Ranking			1-D Swell strain (%)		Swell Pressure (kPa)		3-D Swell strain (%) at corresponding confinement pressure (95% MDUW)		
Soil	Ref	PI	MDUW	95% MDUW	MDUW	95% MDUW	7 kPa	50 kPa	100 kPa
Anthem	1	27	5.8	4.5	134.6	94.2	4.8	4.3	2.9
Burleson	1	37	8.8	5.8	183.4	112.8	8.0	6.5	4.7
Cleburne	2	21	5.8	3.2	141.7	96.2	3.2	1.7	1.5
Colorado	1	42	12.0	8.2	194.0	137.7	9.3	7.6	6.3
Denton	2	30	6.5	3.5	67.4	65.3	3.5	2.9	2.5
Grapevine 2	2	26	6.2	4.3	88.4	82.7	4.7	2.3	1.4
Grayson	1	49	14.2	9.8	243.5	168.4	11.7	8.8	7.7
Keller	1	11	7.9	5.6	137.7	98.0	6.8	5.7	3.7
Mansfield	2	38	10.8	9.5	164.2	138.9	10.2	7.8	6.8
Oklahoma	1	21	4.8	3.8	106.6	63.0	5.0	3.7	2.7
Plano	2	12	9.1	7.7	158.0	108.0	9.5	3.6	2.9
San Antonio	1	43	10.2	7.3	231.1	137.7	9.1	7.4	5.8
San Diego	1	28	4.5	3.4	75.5	50.5	4.5	3.4	2.2
Waco	2	34	4.3	3.6	116.5	65.9	5.2	2.7	2.3

Ref – reference: (1) Pedarla 2013, (2) This research

The DDL model involves the formulae given by Pedarla (2013) summarized in the subsequent paragraphs. Further details are presented in the work developed by the mentioned author.

Sample volumetrics have to be applied to determine the fraction of minerals present in the clay portion of expansive soil. Determination of volume of clay fraction (Vc) can be achieved with the following Equations 6-6 through 6-9.

$$V = \gamma_d \times w_s \qquad 6-6$$

$$V_s = \frac{V}{1+e} \qquad 6-7$$

$$V_s = V_{sand} + V_{silt} + V_{clay} \qquad 6-8$$

$$V_{clay} = CF * V_s \qquad 6-9$$

Where V is the total volume of soil solids, ɣd is the unit weight of soil, Ws is the weight of the soil solid particles in the sample, Vs is the volume occupied by solid particles, e is void ratio, Vsand is the volume of sand particles, Vsilt is the volume of silt particles, Vclay is the volume of clay particles, CF is the clay fraction in percentage (obtained from gradation curve of soils).

Table 6-3 below presents the determination of volume of clay fraction present in a compacted clay specimen for 1-D swell strain and swell pressure. The particular 3-D swell test clay fraction volume may be obtained when the volume of clay fraction in the soil specimen used in 1-D swell is multiplied by 4.

Table 6-3 Volume of clay fraction at two dry density conditions

Soil	Ref	Clay %	MM %	I %	K %	95% MDUW condition		MDUW condition	
						Solids (g)	Vol. of clay, Vclay (m^3)	Solids (g)	Vol. of clay, Vclay (m^3)
Anthem	1	32	25.28	24.45	50.27	130	$2.51x10^{-05}$	137	$2.54x10^{-05}$
Burleson	1	52	33.75	19.62	46.63	124	$4.10x10^{-05}$	130	$4.13x10^{-05}$
Cleburne	2	27	20.44	6.33	73.22	138	$1.36x10^{-05}$	176	$1.74x10^{-05}$
Colorado	1	46	35.75	35.00	29.25	125	$3.65x10^{-05}$	132	$3.68x10^{-05}$
Denton	2	46	20.37	8.67	70.96	123	$2.03x10^{-05}$	128	$2.12x10^{-05}$
Grapevine 2	2	49	18.57	11.50	69.93	127	$2.31x10^{-05}$	134	$2.43x10^{-05}$
Grayson	1	55	43.00	23.70	33.30	110	$4.32x10^{-05}$	116	$4.37x10^{-05}$
Keller	1	34	22.00	18.30	59.70	143	$2.70x10^{-05}$	151	$2.71x10^{-05}$
Mansfield	2	62	42.82	22.08	35.10	110	$2.43x10^{-05}$	115	$2.55x10^{-05}$
Oklahoma	1	30	19.70	70.00	10.30	121	$2.36x10^{-05}$	127	$2.39x10^{-05}$
Plano	2	63	29.63	37.67	32.70	107	$2.39x10^{-05}$	113	$2.53x10^{-05}$
San Antonio	1	52	37.87	30.93	31.20	122	$4.12x10^{-05}$	129	$4.17x10^{-05}$
San Diego	1	23	26.90	25.32	47.78	131	$1.80x10^{-05}$	139	$1.83x10^{-05}$
Waco	2	30	50.07	18.75	31.18	106	$1.13x10^{-05}$	115	$1.21x10^{-05}$

Ref – reference: (1) Pedarla 2013, (2) This research

The individual heights of the clay mineral layers could be determined from Equations 6-10 and 6-11:

$$V_{MM} = V_{clay} * MMF \qquad 6-10$$

$$h_{MM} = \frac{V_{MM}}{A} \qquad 6-11$$

Where V_{MM} is the volume of mineral Montmorillonite, MMF is the mineral Montmorillonite fraction in the clay fraction, h_{MM} is the total height of stacked mineral Montmorillonite layers within the soil specimen and A is the total cross-sectional area of

the soil specimen (remains constant during the 1-D swell and swell pressure tests). Since Montmorillonite has the least crystal thickness and high particle compared to Illite and Kaolinite fraction. All the mineral layers are assumed to be stacked perpendicular to the direction of compaction and moisture induced soil swelling.

Table 6-4 below presents the height of individual mineral layers present in the compacted soil specimen.

Table 6-4 Heights of individual crystal layers at different compaction dry densities

Soil	Ref	95% MDUW condition			MDUW condition		
		h_{MM} (m)	h_{ILL} (m)	h_K (m)	h_{MM} (m)	h_{ILL} (m)	h_K (m)
Anthem	1	$1.94x10^{-03}$	$1.88x10^{-03}$	$3.86x10^{-03}$	$2.04x10^{-03}$	$1.97x10^{-03}$	$4.05x10^{-03}$
Burleson	1	$4.21x10^{-03}$	$2.45x10^{-03}$	$5.82x10^{-03}$	$4.42x10^{-03}$	$2.57x10^{-03}$	$6.10x10^{-03}$
Cleburne	2	$8.80x10^{-04}$	$2.73x10^{-04}$	$3.15x10^{-03}$	$1.13x10^{-03}$	$3.49x10^{-03}$	$4.03x10^{-03}$
Colorado	1	$3.94x10^{-03}$	$3.86x10^{-03}$	$3.22x10^{-03}$	$4.16x10^{-03}$	$4.07x10^{-03}$	$3.41x10^{-03}$
Denton	2	$1.31x10^{-03}$	$5.57x10^{-04}$	$4.56x10^{-03}$	$1.37x10^{-03}$	$5.82x10^{-04}$	$4.77x10^{-03}$
Grapevine 2	2	$1.36x10^{-03}$	$8.40x10^{-04}$	$5.11x10^{-03}$	$1.43x10^{-03}$	$8.84x10^{-04}$	$5.37x10^{-03}$
Grayson	1	$5.67x10^{-03}$	$3.13x10^{-03}$	$4.39x10^{-03}$	$5.95x10^{-03}$	$3.28x10^{-03}$	$4.61x10^{-03}$
Keller	1	$1.80x10^{-03}$	$1.49x10^{-03}$	$4.87x10^{-03}$	$1.89x10^{-03}$	$1.57x10^{-03}$	$5.13x10^{-03}$
Mansfield	2	$3.30x10^{-03}$	$1.70x10^{-03}$	$2.70x10^{-03}$	$3.46x10^{-03}$	$1.78x10^{-03}$	$2.84x10^{-03}$
Oklahoma	1	$1.42x10^{-03}$	$5.04x10^{-03}$	$7.42x10^{-03}$	$1.49x10^{-03}$	$5.29x10^{-03}$	$7.79x10^{-03}$
Plano	2	$2.24x10^{-03}$	$2.85x10^{-03}$	$2.48x10^{-03}$	$2.37x10^{-03}$	$3.01x10^{-03}$	$2.62x10^{-03}$
San Antonio	1	$4.73x10^{-03}$	$3.86x10^{-03}$	$3.89x10^{-03}$	$5.00x10^{-03}$	$4.08x10^{-03}$	$4.12x10^{-03}$
San Diego	1	$1.48x10^{-03}$	$1.40x10^{-03}$	$2.64x10^{-03}$	$1.57x10^{-03}$	$1.47x10^{-03}$	$2.78x10^{-03}$
Waco	2	$1.79x10^{-03}$	$6.71x10^{-03}$	$1.12x10^{-03}$	$1.93x10^{-03}$	$7.22x10^{-04}$	$1.20x10^{-03}$

Ref – reference: (1) Pedarla 2013, (2) This research

In Table 6-4, h_{MM} – total height of Montmorillonite layer, h_{ILL} – total height of Illite layer and h_K total height of Kaolinite layer.

Once the layer height is calculated, the number of crystal stacks present in the layer height was calculated using the following Equation 6-12.

$$N = \frac{h_i}{t_i} \qquad 6-12$$

Where N is the number of each mineral layers stacked in the total mineral volume, h_i is the total individual mineral layer height and t_i is the average mineral crystal thickness (Montmorillonite 10 Å, Illite 30 Å, Kaolinte 1000 Å).

Once the number of mineral layer stacks for all three clay minerals are determined, the total diffuse double layer thickness or expansion or swell displacement for a given expansive soil is given by Equation 6-13.

$$TDDLT = \sum_{i=1}^{n} N_i \times DDLT_i \qquad 6-13$$

Where TDDLT is the total diffuse double layer induced swell thickness or displacement, n is the number of clay minerals (i.e. 3) in the soil, Ni is the number of crystal layers pertaining to individual mineral, DDLTi is the diffuse double layer thickness of an individual mineral.

Double layer water thickness and related strains for the soil specimens are then determined using the following Equation 6-14.

$$\epsilon_{DDL}\ (\%) = \frac{TDDLT}{h} \times 100 \qquad 6-14$$

Where ϵ_{DDL} is the strain caused by the formation of diffuse double layer, TDDLT is the total diffuse double layer induced swell displacement calculated for the specimen, h is the initial specimen height. Table 6-5 shows the total double layer induced swell calculated for all the 14 expansive clays at two different density conditions.

Table 6-5 Swell strain estimated from double layer induced swell displacement

Soil	Ref	95% MDUW condition			MDUW condition		
		h (m)	TDDLT (m)	ε_{DDL} (%)	h (m)	TDDLT (m)	ε_{DDL} (%)
Anthem	1	0.0254	0.0427	168.18	0.0254	0.0449	176.60
Burleson	1	0.0254	0.0897	353.00	0.0254	0.0940	370.08
Cleburne	2	0.0254	0.0190	74.96	0.0254	0.0244	95.92
Colorado	1	0.0254	0.0849	334.42	0.0254	0.0897	353.15
Denton	2	0.0254	0.0285	112.06	0.0254	0.0298	117.23
Grapevine 2	2	0.0254	0.0300	118.05	0.0254	0.0315	124.16
Grayson	1	0.0254	0.1191	468.88	0.0254	0.1250	492.22
Keller	1	0.0254	0.0397	156.38	0.0254	0.0418	164.67
Mansfield	2	0.0254	0.0690	271.59	0.0254	0.0724	285.05
Oklahoma	1	0.0254	0.0350	137.75	0.0254	0.0367	144.58
Plano	2	0.0254	0.0493	194.05	0.0254	0.0521	205.12
San Antonio	1	0.0254	0.1009	397.20	0.0254	0.1067	419.99
San Diego	1	0.0254	0.0325	127.86	0.0254	0.0343	134.89
Waco	2	0.0254	0.0370	145.86	0.0254	0.0399	157.06

Ref – reference: (1) Pedarla 2013, (2) This research

Table 6-5 shown above presents the total double layer water induced strain by each of the soil specimens. The specimen strains are calculated based on the initial specimen height and the total double layer formed due to the mineral attraction forces between clay mineral and water molecules.

6.2.1 DDLS Model versus 1-D Swell Strain and Swell Pressure

Cumulative diffusive double layer strains determined for each soil were plotted against measured swell strains for each tested soil. Figure 6-1 and Figure 6-2 present the variation of diffuse double layer strains with the measured swell strains at 95% MDUW and MDUW condition. The fit models had coefficient of determination (R^2) values of 0.96 and 0.97 respectively.

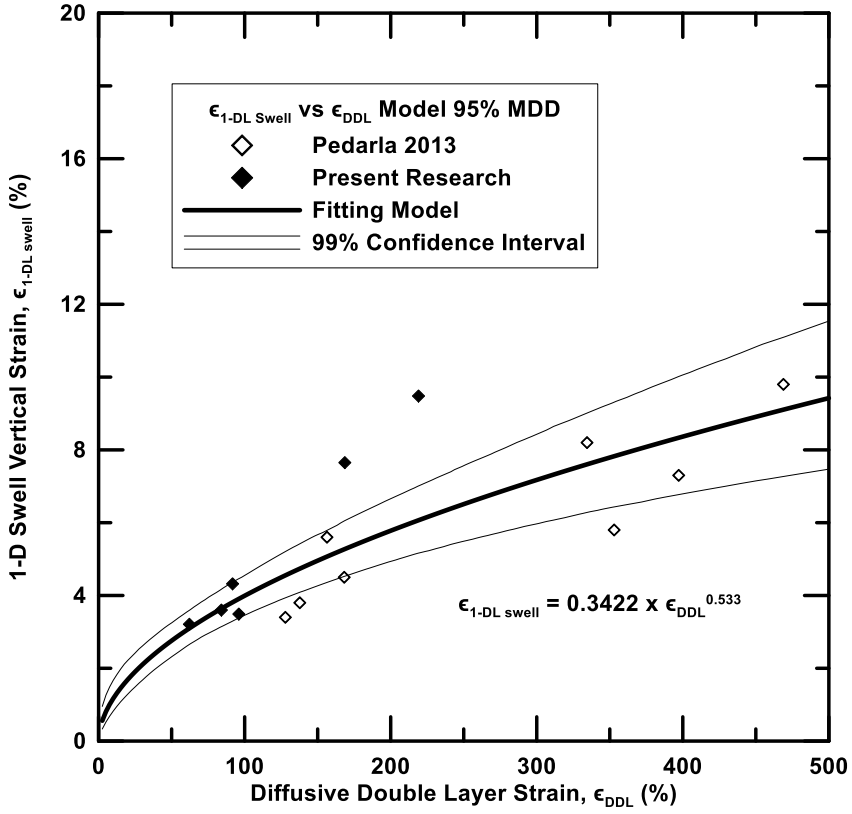

Figure 6-1 DDLS Model for 1 D Swell Strains at 95% MDUW condition

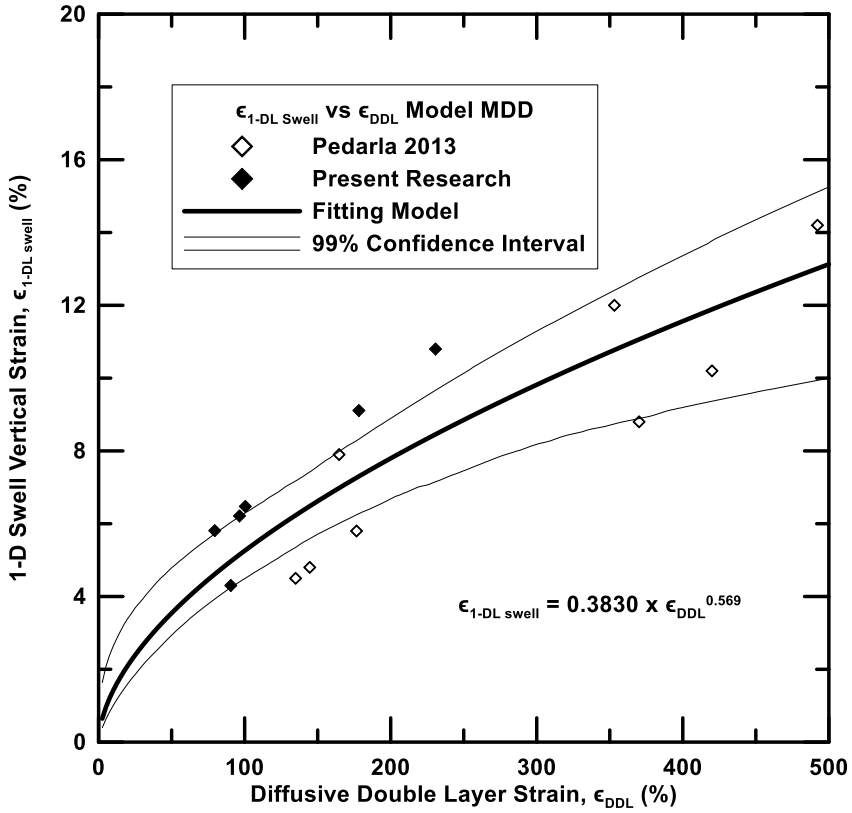

Figure 6-2 DDLS Model for 1 D Swell Strains at MDUW condition

Figure 6-3 and Figure 6-4 present the variation of calculated diffuse double layer swell strains from minerals with measured swell pressure at 95% MDUW and MDUW condition. The fit models had coefficient of determination (R^2) values of 0.90 and 0.93 respectively.

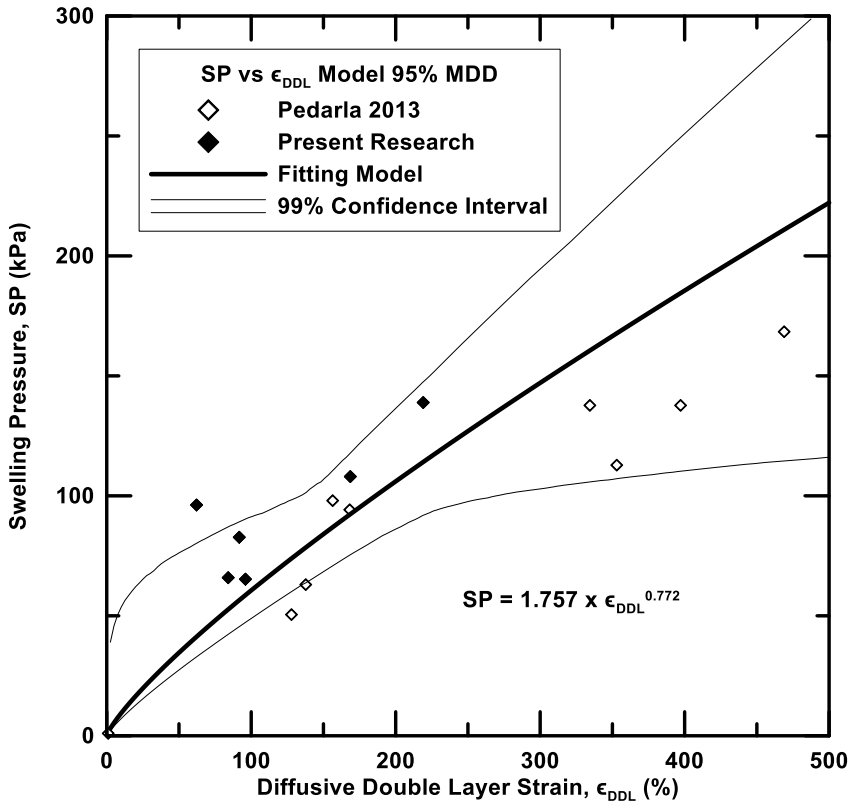

Figure 6-3 DDLS Model for 1 D Swell Pressures at 95% MDUW condition

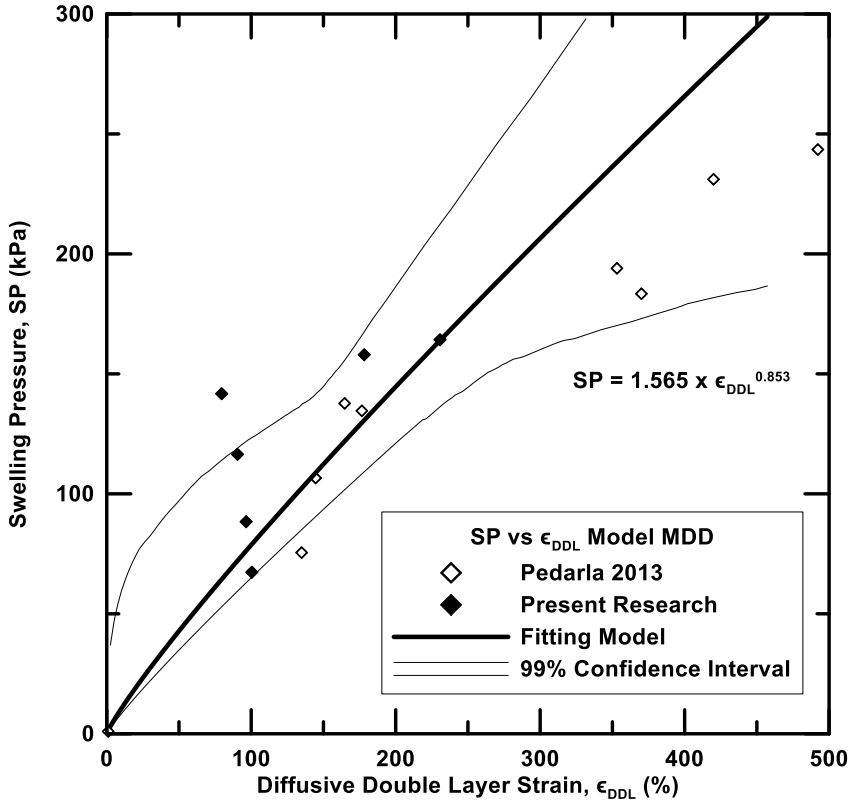

Figure 6-4 DDLS Model for 1 D Swell Pressures at MDUW condition

6.2.2 DDLS Model versus 3-D Swell Strain and Swell Pressure

Volumetric swell strains under three different confinements for all the 14 soils considered were measured using the novel 3-D swell strain apparatus as presented in previous chapters. All the specimens were compacted at 95% MDD for this study. The dimensions of the specimens for this test are 0.1 m (4 in) in height and 0.05 m (2 in) diameter. Figure 6-5, Figure 6-6 and Figure 6-7 show the calculated diffused double layer swell strains and their variation with respect to the measured 3-D swell strain at 7 kPa, 50 kPa and 100 kPa confinement level, respectively. The fit models had coefficient of determination (R^2) values of 0.96, 0.94 and 0.91 respectively.

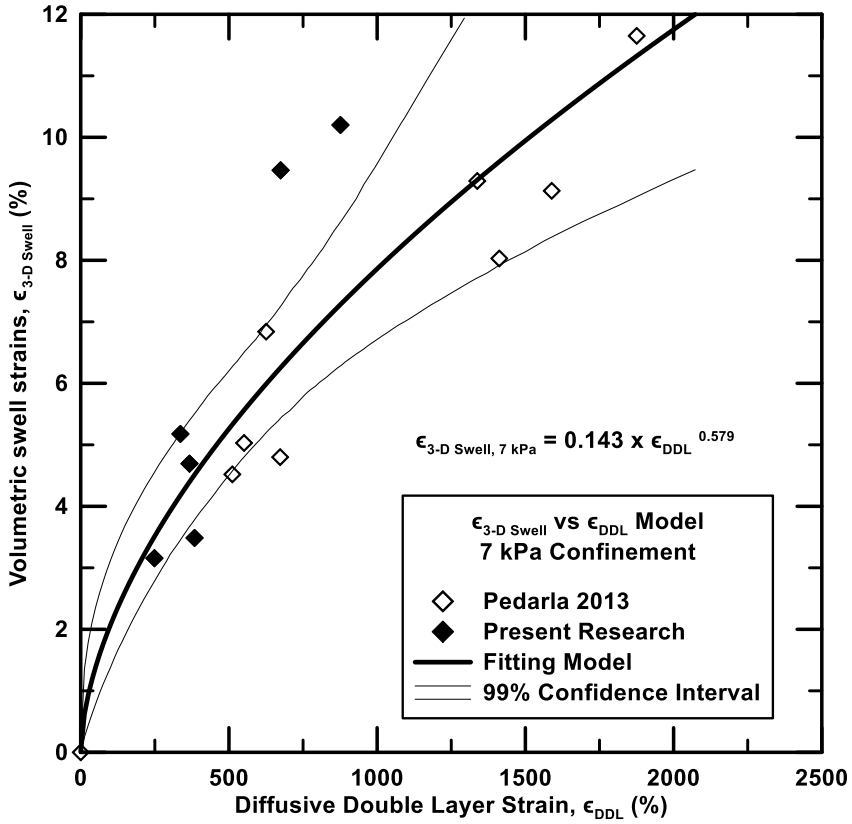

Figure 6-5 DDLS Model for 3 D Swell Strains at 95% MDUW and 7 kPa Confinement

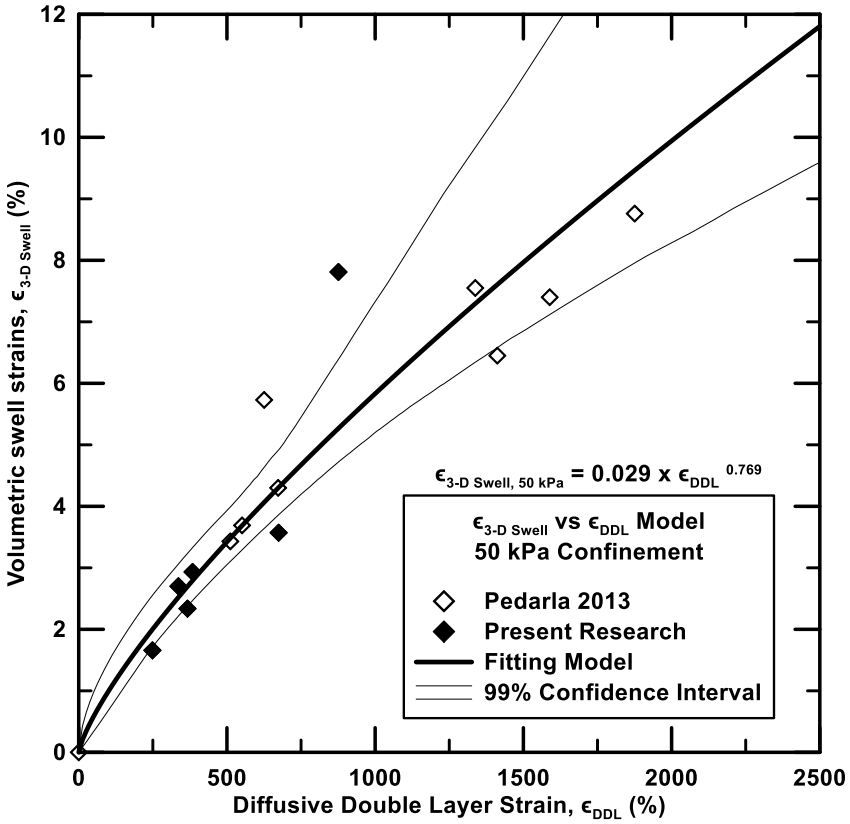

Figure 6-6 DDLS Model for 3 D Swell Strains at 95% MDUW and 50 kPa Confinement

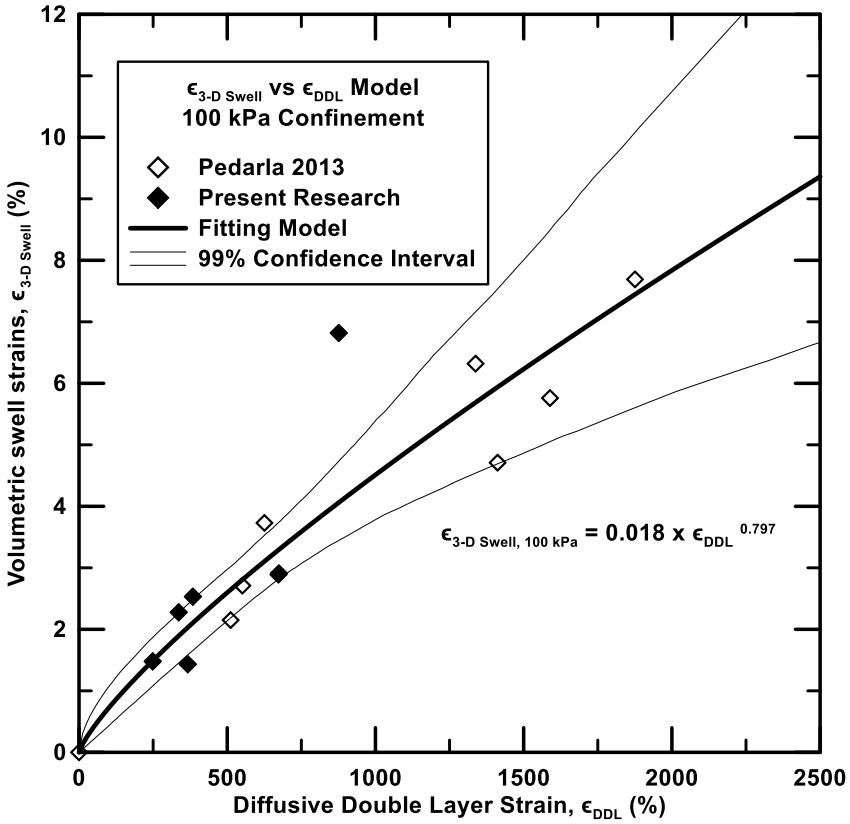

Figure 6-7 DDLS Model for 3 D Swell Strains at 95% MDUW and 100 kPa Confinement

6.2.3 Summary

Overall, DDLS model predictions and comparisons with swell strains and pressures should be treated as an indirect exercise to develop swell strain and pressure predictions.

The following formulation, given by Equation 6-15 was used to determine the correction factors, a and b and these are already depicted in the previous graphs:

$$\epsilon_i, V_i \; or \; SP = a \times {\epsilon_{DDL}}^{b} \qquad 6-15$$

Where ϵ_i is the swell strain measured at different initial compaction conditions, SP is the swell pressure of an expansive clay, ϵ_{DDL} is the diffuse double layer induced swell strain and a, b are the correction factors.

Correction factors ‘a’ and ‘b’ are dependent on several soil features and test procedures like particle arrangement during compaction, moisture access to the clay particles and direction of particle swelling. Therefore, factors ‘a’ and ‘b’ are considered not to be unique and reliant on the swell property that is correlated with ϵ_{DDL}.

For the particular case in which 14 soils were evaluated, including the six soils tested in present research as well as those tested by Pedarla (2013), the values of the factors ‘a’ and ‘b’ are shown in Table 6-6.

Table 6-6 Formulation of correction factors, ‘a’ and ‘b’ DDL Model

Factor	1-D Swell Strain (%)		Swell Pressure (kPa)		3-D Swell Strain at 95% MDD and variable confinements (%)		
	95% MDD	MDD	95% MDD	MDD	7 kPa	50 kPa	100 kPa
a	0.34	0.38	1.76	1.57	0.14	0.03	0.02
b	0.53	0.57	0.77	0.85	0.58	0.77	0.80
R^2	0.96	0.97	0.90	0.93	0.96	0.94	0.91

In general, the DDLS models showed good coefficient of determination values when fitted against the actual experimental swell test properties. From Table 5-13, ‘a’ and ‘b’ parameters represent a composite parameter that accounts for all tested soils. The model parameters show that both ‘a’ and ‘b’ correction parameters increased from 95% MDD to MDD for 1 D swell strain model but not for swell pressure model. These constants represent the variability due to the assumptions used in this modeling analysis.

6.2.4 Validation of Diffuse Double Layer Model

Diffuse double layer model was intended to be additionally validated by comparing the values of the strain obtained from the model (Equation 6-15) with respect to those strain values determined by direct DDL theory formulae application since it

allows for direct and indirect determination of a weighted half the distance between clay layers. Thus, the two different validation procedures adopted for this task were those given by Schanz et al. (2013) and Barat et al. (2013). The first approach was designated herein as swelling pressure based method and follows Equations 6-16, 6-17 and 6-18 (derived from Equations 6-2, 6-3 and 6-4).

$$u = \cosh^{-1}\left(\frac{P}{2n_0 kT} + 1\right) \qquad 6-16$$

$$z = \frac{1}{2}\left\{\left[\left(\frac{CEC}{SSA}\right)^2 \left(\frac{1}{2 \in_0 Dn_0 kT}\right)\right] + 2\cosh u\right\} \qquad 6-17$$

$$d = \frac{1}{K}\int_z^u \frac{1}{\left(\frac{CEC}{SSA}\right)\left(\frac{1}{2 \in_0 Dn_0 kT}\right)^{\frac{1}{2}}} du \qquad 6-18$$

The integral expressed in Equation 6-18 is of elliptic nature; therefore multiple numerical iterations were performed in order to find appropriate values to satisfy the equality among the equations. Simpson quadrature approach given by ‘‘quad’’ MATLAB® routine was used.

Another approach by Barat et al. (2013), here referred to as void ratio based method allows for direct determination of d according to Equation 6-19 (derived from Equation 6-5).

$$d = \frac{e_d}{G\rho_w S} \qquad 6-19$$

Therefore, once the weighted half the distance between clay layers was calculated from both of the mentioned methods, the total diffuse double layer present in each specimen was computed by application of Equation 6-13, however in this case, values of d obtained from both methods were used instead of the diffuse double layer thickness of an individual mineral (DDLTi) values calculated by the model methodology. The total number of crystal layers in the soil sample was kept as the summation of the

number of crystal layers pertaining to individual mineral (Ni) as obtained from Equation 6-12.

Results obtained for the soils used in these studies, considering n_0 value of 10^{-3} M (deionized water) are presented in Table 6-7. Weighted average valence values of 1 and 2 were applied.

Table 6-7 Total number of crystal layers, diffusive double layer strain values, and half the distance between clay layers

Soil	Ref	95% MDUW condition								MDUW condition							
		Model		Void ratio based method		Swelling pressure based method				Model		Void ratio based method		Swelling pressure based method			
		N	ϵ_{DDL} (%)	d (Å)	ϵ_{DDL} (%)	d (Å)	ϵ_{DDL} (%)	d (Å)	ϵ_{DDL} (%)	N	ϵ_{DDL} (%)	d (Å)	ϵ_{DDL} (%)	d (Å)	ϵ_{DDL} (%)	d (Å)	ϵ_{DDL} (%)
						v=1		v=2						v=1		v=2	
Anthem	1	$2.7x10^6$	271.6	19.4	34.0	282.6	477.4	141.3	238.7	$2.6x10^6$	285.1	22.2	29.4	299.9	435.5	150.0	217.7
Burleson	1	$5.3x10^6$	194.1	19.7	23.2	277.9	304.7	138.9	152.4	$5.1x10^6$	205.1	21.9	19.4	301.5	269.8	150.8	134.9
Cleburne	2	$1.3x10^6$	118.1	17.2	11.9	284.8	166.0	142.4	83.0	$1.0x10^6$	124.2	20.3	9.9	301.2	155.8	150.6	77.9
Colorado	1	$5.6x10^6$	112.1	13.6	12.3	254.0	167.2	127.0	83.6	$5.3x10^6$	117.2	15.6	10.3	270.7	158.9	135.3	79.4
Denton	2	$1.6x10^6$	145.9	17.0	13.6	262.1	256.2	131.0	128.1	$1.5x10^6$	157.1	19.4	10.9	263.6	220.7	131.8	110.3
Grapevine 2	2	$1.8x10^6$	75.0	14.8	10.3	234.3	152.1	117.1	76.0	$1.7x10^6$	95.9	17.0	6.8	237.4	112.4	118.7	56.2
Grayson	1	$7.1x10^6$	168.2	15.7	24.0	245.8	323.1	122.9	161.6	$6.8x10^6$	176.6	17.0	19.9	263.7	289.9	131.9	145.0
Keller	1	$2.5x10^6$	353.0	15.2	46.1	273.6	633.3	136.8	316.6	$2.3x10^6$	370.1	18.7	39.5	290.1	556.6	145.0	278.3
Mansfield	2	$4.1x10^6$	334.4	19.2	34.0	284.4	591.9	142.2	296.0	$3.9x10^6$	353.2	21.2	28.1	297.0	526.0	148.5	263.0
Oklahoma	1	$3.3x10^6$	468.9	39.9	47.4	308.1	736.6	154.0	368.3	$3.1x10^6$	492.2	43.9	41.7	333.6	653.8	166.8	326.9
Plano	2	$3.4x10^6$	156.4	15.3	18.2	212.9	281.7	106.5	140.8	$3.2x10^6$	164.7	17.3	14.0	227.5	252.3	113.8	126.1

Table 6-7—Continued

San Antonio	1	$6.4x10^6$	137.8	16.1	56.3	246.7	428.4	123.4	214.2	$6.1x10^6$	144.6	16.9	48.9	271.9	377.0	136.0	188.5
San Diego	1	$2.1x10^6$	397.2	23.8	42.6	329.5	685.0	164.8	342.5	$2.0x10^6$	420.0	27.4	38.3	349.0	587.8	174.5	293.9
Waco	2	$2.2x10^6$	127.9	13.7	22.5	276.7	286.4	138.4	143.2	$2.0x10^6$	134.9	15.9	18.5	298.3	256.3	149.2	128.2

Ref – reference: (1) Pedarla 2013, (2) This research

Figure 6-8 and Figure 6-9 present the correlation among the diffusive double layer strain calculated values, in the soils compacted at 95% MDUW and MDUW conditions, respectively, considering 10^{-3} M as the ionic concentration of the pore fluid.

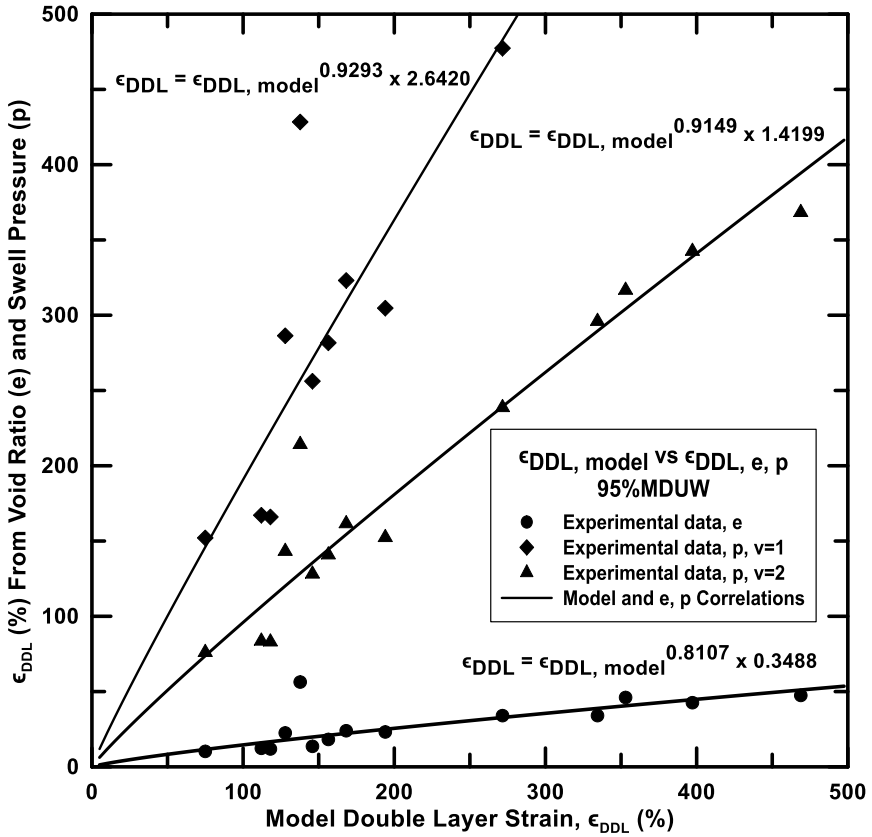

Figure 6-8 Diffusive double layer strain correlation, 95% MDUW, $n_0 = 10^{-3}$ M

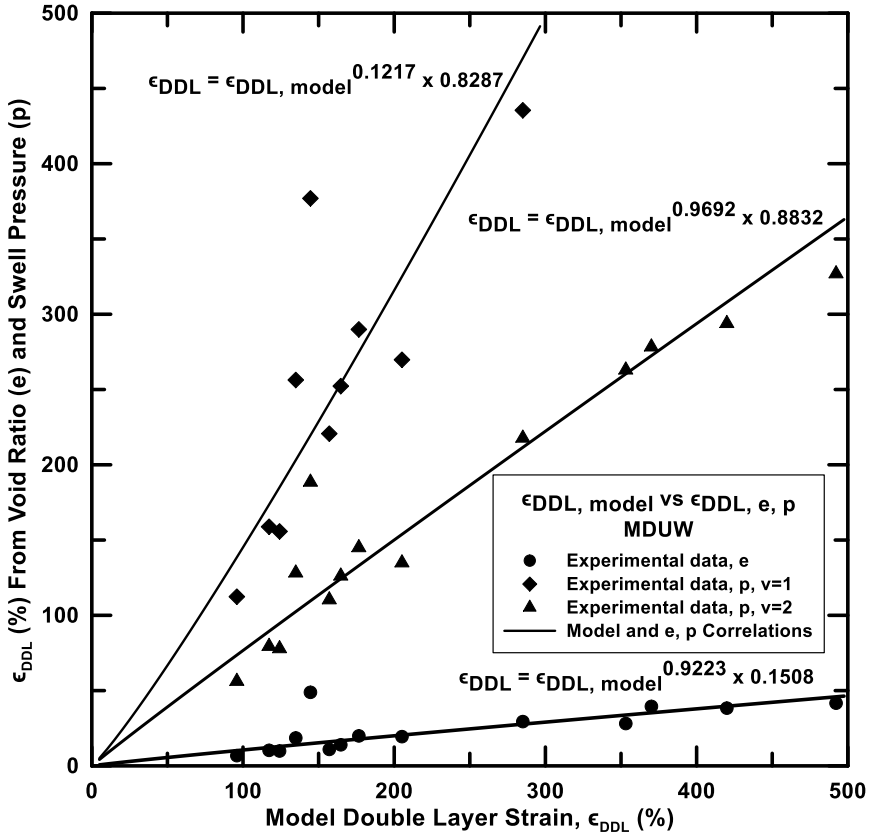

Figure 6-9 Diffusive double layer strain correlation, MDUW, $n_0 = 10^{-3}$ M

Thus, according to the described DDL model validation procedure, based on the two previously mentioned approaches, the diffusive double layer strain results may be closer to those yielded by the proposed model when the swelling pressure based method was used considering an ionic concentration of the pore fluid, $n_0 = 10^{-3}$ M and a value of the exchangeable cations valence of the soil ranging from 1 to 2. Weighted average valence values had been found to be comprehended between 1.14 and 1.95 for almost pure bentonite minerals (Schanz et al., 2013). Hence, it seems to be reasonable to assume weighted valence ranging between the mentioned values for fine soils with relatively high percentages of clay fraction and minerals.

Strain and d values calculated from the void ratio based method did not generate good correlation with the values computed from the proposed model. Further refinement on this approach may be necessary.

6.3 Mechanical Hydro Chemical (MHC) Model validation

As presented in Chapter 2, several researchers have proposed prediction models for expansive soils behavior based on soil suction measurements (McKeen, 1992; Likos et al., 2003; Cocka, 2000, 2002) since it is known that soil matric suction highly influences the swelling behavior of a soil. However, soil mineralogy is not considered in most of the models for swelling prediction. The Mechanical Hydro Chemical (MHC) Model (Pedarla, 2013) incorporates a herein called mechanical hydro-chemical parameter which considers the effect of initial matric suction, air-entry suction, slope of soil suction-void ratio plot and the content and percentages of clay minerals in the soil.

The first important factor affecting swelling behavior observed in the MHC model is designated as the Chemical factor (C). It is weighted from the summation of the individual products between a swell factor (SF) assigned to each clay mineral (Montmorillonite, Illite and Kaolinite) and the corresponding content of the minerals in the swelling soil tested sample. The model makes the assumption that only the three above outlined clay minerals exist in the soil.

SF values assigned to minerals are: 90 for Montmorillonite, 9 for Illite and 1 for Kaolinite. The total contribution for swell factor from these three minerals sums 100.

The total chemical factor (C) which represents the chemical activity of a particular soil is given by Equation 6-20.

$$C = CF \times \sum_{i=1}^{n} SF \times f_i \qquad 6-20$$

Where, C is the chemical factor for particular clay, CF is the clay fraction, SF is the swell factor, and fi is the fraction of each particular mineral assumed to exist in the clay.

The second factor affecting swelling behavior of soils is designated as the Physico-Mechanical factor. This factor accounts for important physical attributes of soil like grain size and pore distribution. Also, it intends to represent the variation in matric suction and void ratio undergone by a soil specimen as the swelling process occurs. The coupled effect of the latter in

the Physico-Mechanical factor is determined from the slope of the void ratio – matric suction plot which is known as specific moisture capacity. The plot has to be constructed using data from the free swell test (loading-after-wetting test) to get void ratio information and from the pressure plate test and filter paper technique to get matric suction information. For model completion, the drying and the wetting curves of the SWCC have been assumed to be the same, thus, no hysteresis effects on the SWCC are considered.

Pedarla (2013) noticed that it is possible to make the soil specimen to follow an idealized path during hydration (Figure 2-20) and then designated it as modified specific moisture capacity (α) or simply equivalent mechanical hydro parameter.

Once α has been found for each soil, the combined effect of the total Mechanical Hydro Chemical Parameter (MHCP) is determined from the following Equation 6-21.

$$MHCP = \pi(\alpha, C) \qquad 6-21$$

Where MHCP is the Mechanical Hydro Chemical Parameter, α is the mechanical hydro parameter, i.e. the idealized slope of logarithmic value of matric suction - void ratio plot, and C is the chemical parameter that accounts for soil swelling.

The modified slope of the void ratio – matric suction plot has negative value due to obvious geometric correspondence in graphical data (Figure 2-20); however this effect is neglected in the determination of MHCP value.

6.3.1 Mechanical Hydro Chemical (MHC) Model using 14 soils

The present model results are studied on soil specimens of the 14 soils analyzed (8 soils from Pedarla, 2013, and 6 soils from the present research) compacted at 95% MDD condition. MHC model is formulated on the basis of the MHCP value for each soil. The MHCP value is dependent on sensitive parameters like slope of void ratio, matric suction from drying SWCCs and clay mineral content. MHCP values measured for each soil are correlated against the measured 1-D and 3-D swell strains and swell pressures.

Table 6-8 presents the determination of the mechanical hydro-chemical parameters (MHCP) for soil specimens of the 14 soils compacted at 95% MDD. MHCP is calculated based on values of clay minerals (chemical component), percent of clay particles in the soil specimen, the soil matric suction obtained from drying SWCCs and void ratio properties from free swell tests (Mechanical component).

Table 6-8 Calculation of MHCP from soil properties at 95% MDD condition

Soil	Ref	CF (%)	MM (%)	I (%)	K (%)	C	e_o	e_f	Ψ_o (kPa)	Ψ_o (kPa)	α	MHCP
Anthem	1	48	25.20	24.40	50.40	8.5	0.717	0.786	466	10	0.041	0.351
Burleson	1	55	33.70	19.60	46.70	16.8	0.790	0.930	700	11	0.078	1.310
Cleburne	2	38	20.44	6.33	73.23	4.4	0.572	0.623	115	10	0.048	0.207
Colorado	1	63	35.70	35.00	29.30	16.5	0.777	0.906	1000	20	0.075	1.238
Denton	2	55	20.37	8.67	70.96	7.8	0.821	0.884	277	10	0.044	0.344
Grapevine 2	2	46	18.57	11.50	69.93	7.1	0.714	0.788	346	10	0.048	0.340
Grayson	1	75	43.30	24.00	32.70	22.7	1.034	1.231	200	10	0.151	3.433
Keller	1	25	21.90	18.40	59.70	7.5	0.582	0.646	100	10	0.07	0.524
Mansfield	2	67	42.82	22.08	35.10	20.4	1.042	1.235	572	176	0.379	7.721
Oklahoma	1	41	19.70	70.00	10.30	7.4	0.937	1.017	207	30	0.095	0.702
Plano	2	24	29.63	37.67	32.70	16.5	1.098	1.257	275	32	0.169	2.789
San Antonio	1	67	37.80	30.90	31.30	19.5	0.908	1.067	500	20	0.113	2.206
San Diego	1	42	26.90	25.30	47.80	6.4	0.691	0.710	600	20	0.011	0.072
Waco	2	58	50.07	18.75	31.18	8.0	1.106	1.182	294	46	0.095	0.762

Ref – reference: (1) Pedarla 2013, (2) This research

Figure 6-10 presents the variation of calculated MHCP values with measured 1-D swell strains. The fit model had coefficient of determination (R^2) value of 0.91.

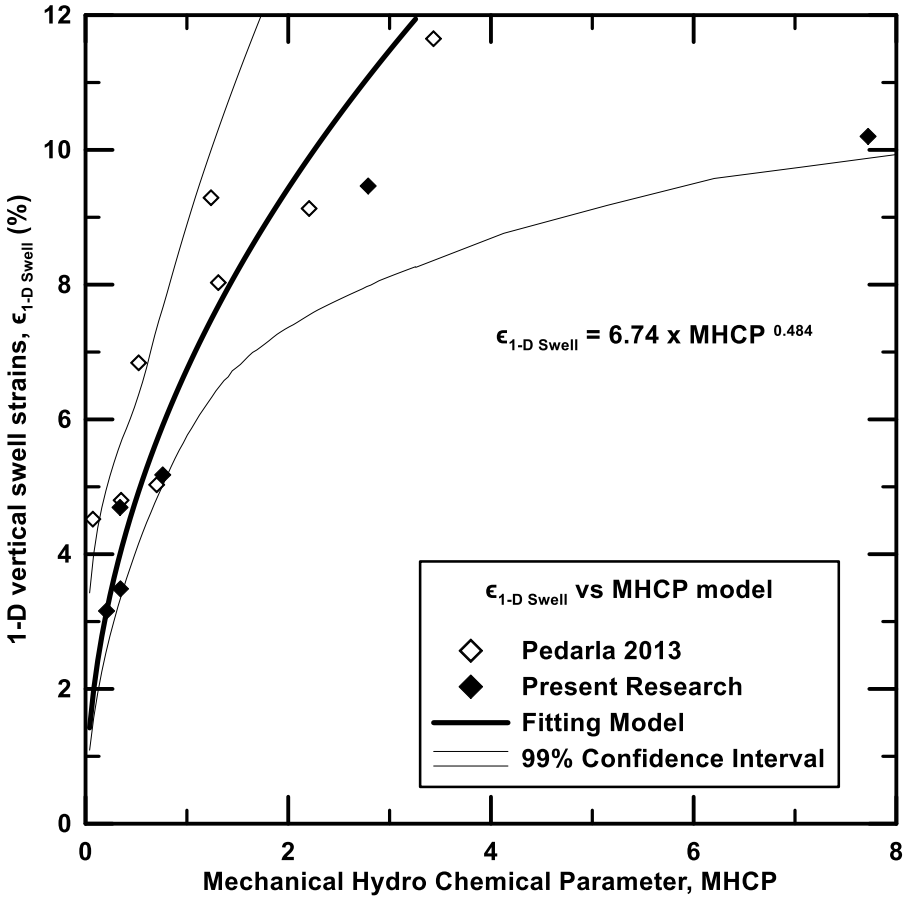

Figure 6-10 1-D Swell Strain MHC Model at 95% MDD condition

Figure 6-11 presents the variation of calculated MHCP values with measured swell pressure. The fit model had coefficient of determination (R^2) value of 0.79.

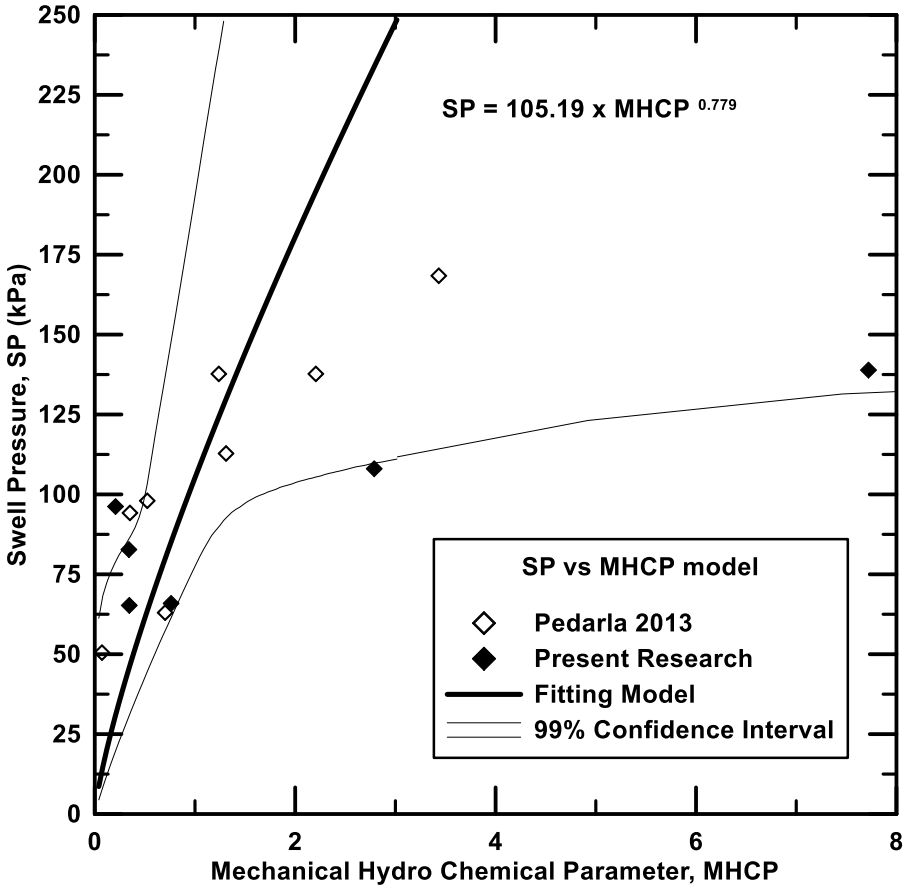

Figure 6-11 1-D Swell Pressure MHC Model at 95% MDD condition

Figure 6-12, Figure 6-13 and Figure 6-14 present the variation of calculated MHCP values with measured 3-D swell strains at confinements of 7 kPa, 50 kPa and 100 kPa, respectively. The fit models for each confinement had coefficient of determination (R^2) value of 0.77, 0.49, and 0.62, respectively.

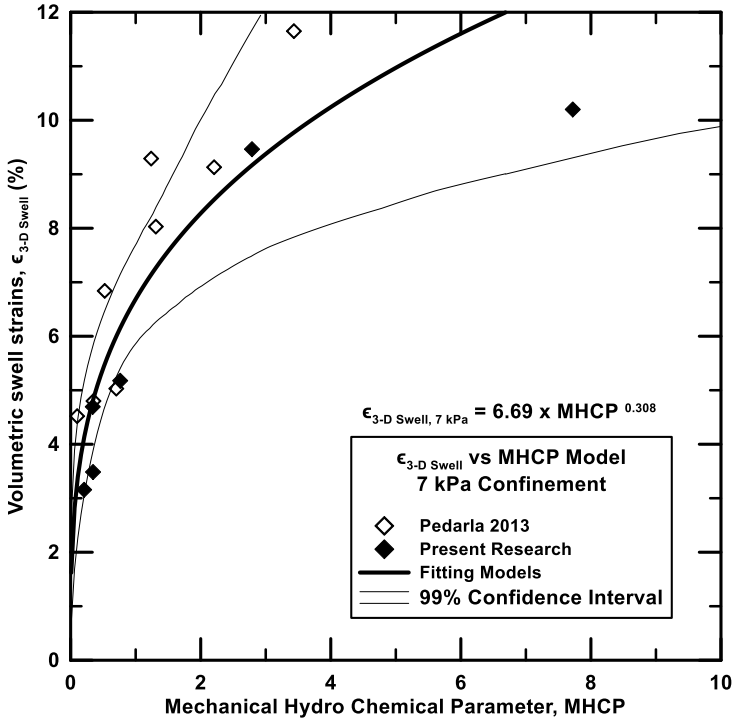

Figure 6-12 3-D Swell Strain MHC Model at 95% MDD condition and 7 kPa confinement

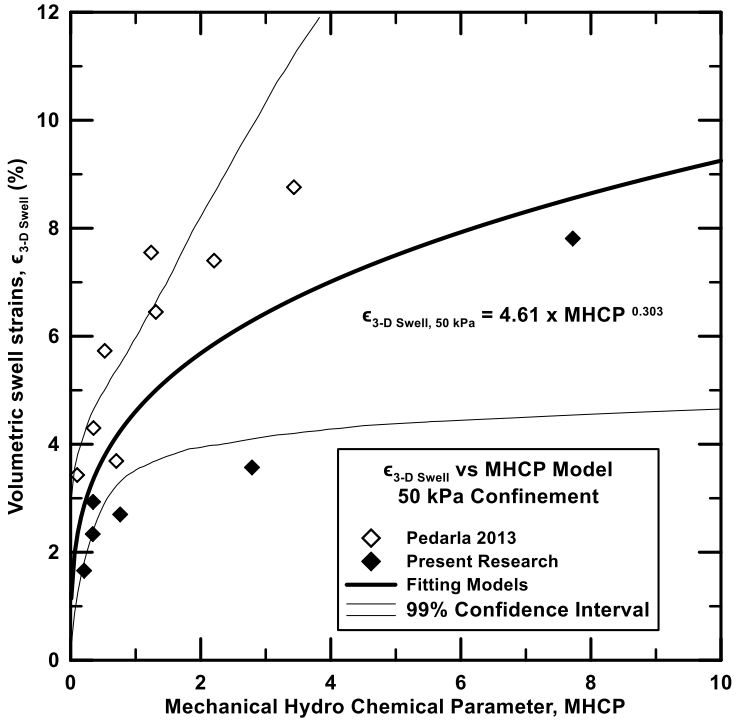

Figure 6-13 3-D Swell Strain MHC Model at 95% MDD condition and 50 kPa confinement

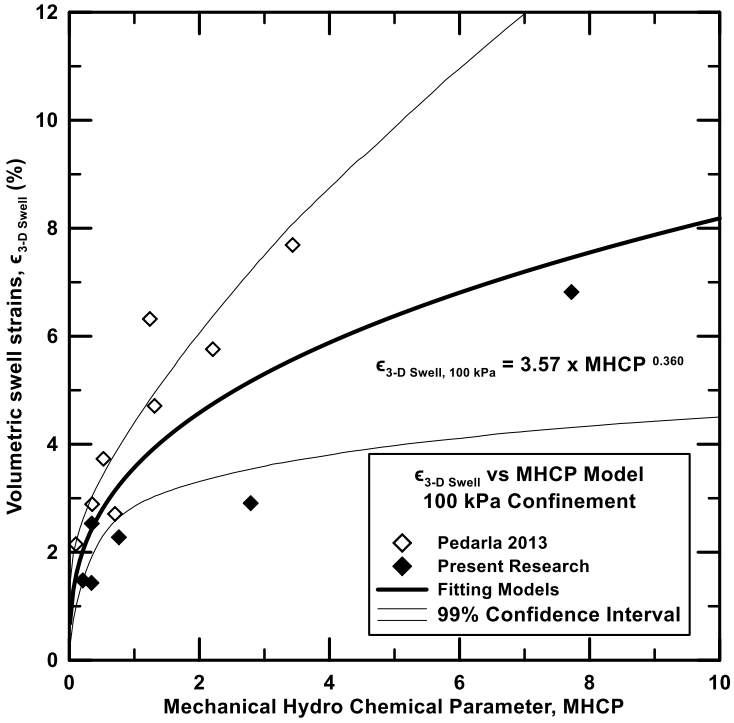

Figure 6-14 3-D Swell Strain MHC Model at 95% MDD condition and 100 kPa confinement

6.3.2 Summary

The present model was defined based on swell tests performed on soil specimens compacted at 95% MDD. In this case, it is reasonable to determine correction factors, a and b, as for the DDL model. These factors are already shown in the previous graphs. Thus, the correlations among swell strains and swell pressure with the MHCP may be assumed to be defined by a formulation similar to that presented in Equation 6-15.

The values of the factors ‘a’ and ‘b’ are shown in Table 6-9 in which 14 soils have been evaluated, including the six soils tested in present research as well as those tested by Pedarla (2013),

Table 6-9 Formulation of correction factors, ‘a’ and ‘b’ MHC model

Factor	1-D Swell Strain (%)	Swell Pressure (kPa)	3-D Swell Strain at variable confinements (%)		
			7 kPa	50 kPa	100 kPa
a	6.74	105.19	6.96	4.61	3.57
b	0.48	0.78	0.31	0.30	0.36
R^2	0.91	0.79	0.77	0.49	0.62

Overall, the MHC models did not reveal good coefficient of determination values after fitting the MHCP to the experimental swell test properties, except by the 1-D swell strain correlation. However, it is considered that a multiple regression analysis may generate better fitting, when considering the MHCP in conjunction with other variables presented in this document.

6.4 Total Surface Area Ratio (TSAR) Model validation

The surface area of Montmorillonite mineral is very high when compared to that of other minerals (Mitchell and Soga, 2005). Thus, the reaction to hydration is more drastic in clay specimens having higher percentages of Montmorillonite mineral than in soils having preeminence of other mineral components. An elevated value of the weighted surface area of these types of soils makes them to attract larger amounts of moisture. TSAR model developed by Pedarla (2013) attempts to represent the variation of surface area parameter with the soil swelling behavior of expansive clay.

The model is based on the so called Total Surface Area Ratio (TSAR) which is defined as the ratio between the total surface areas calculated from the clay mineralogy in a soil specimen and from Mercury Intrusion Porosimetry (MIP) tests of the same soil specimen. TSAR value for a soil specimen is determined from the following Equation 6-22.

$$TSAR = \frac{TSA_{CM}}{TSA_{MIP}} \qquad 6-22$$

Where TSAR is the total surface area ratio, TSA_{CM} is total surface area from clay minerals quantification and TSA_{MIP} is total pore area form mercury intrusion porosimetry studies.

The total surface area of the compacted specimen from clay mineralogy is determined from the product between the weight of soil solids present in the clay fraction of the specimen and the specific surface area (SSA) for the clayey soil tested found according to the procedure summarized in Chapter 3. The latter is presented in formulation fashion by Equation 6-23.

$$W_C = W_S \times CF \qquad 6-23$$

Where Wc is the weight of clay fraction in a soil, Ws is the weight of solids and CF is the clay fraction of soil. After the weight of clay solids is known the clay fraction total surface area of the soil specimen is given by the Equation 6-24.

$$TSA_{Clay\ Minerals} = W_C \times SSA \qquad 6-24$$

Where $TSA_{clay\ minerals}$ is the total surface area calculated from clay minerals, SSA is the specific surface area for the soil, Wc is the weight of clay fraction in a soil.

The total pore surface area from MIP data is found from the volume of mercury intruded into the soil specimen at different intrusion pressures during MIP tests. The equation given by Washburn's (1921) allows for direct correlation of pore volume to pore diameters in the soil sample. For calculation purposes, the assumption of cylindrical shaped pores existing in the soil specimen is made in the model. Thus, the volume occupied by the pores of the specimen at each pore diameter could be determined.

Since the volume occupied by the pores at each diameter is known from MIP test results, the total length of each pore could be calculated by the following Equation 6-25.

$$L_P = \frac{V_P}{A_P} \qquad 6-25$$

Where Lp is the length of individual pore, Vp is the volume of individual pore and Ap is the area of the pore.

Since the entire pore lengths are known, the total pore surface area from individual pores is calculated using the following Equation 6-26.

$$TPAL_{MIP} = \pi d_1 L_1 + \pi d_2 L_2 + \cdots + \pi d_n L_n = \sum_{i=1}^{n} \pi d_n L_n \qquad 6-26$$

Where TPA_{MIP} is the total pore area of a particular diameter pore from MIP test, di is the average diameter of the pore and L_n is the particular pore length. The total surface area ratio (TSAR) model was determined for the 14 soils at MDD and 95% MDD compaction conditions. Also, the total surface area from clay mineralogy and MIP test are based on the compacted specimen having a volume of 8.02 x 10^{-5} m^3. The determination of total surface area from clay mineralogy and MIP tests as well as the total surface area ratio (TSAR) for the 14 soils at the studied density conditions is presented in Table 6-10.

Table 6-10 Total surface area and TSAR at two dry density conditions

Soil	Ref	SSA (m^2/g)	Wc (g/8.02 x 10^{-5} m^3)		$TSA_{clay\ minerals}$ (m^2/8.02 x 10^{-5} m^3)		TSA_{MIP} (m^2/8.02 x 10^{-5} m^3)		TSAR	
			95%MDD	MDD	95%MDD	MDD	95%MDD	MDD	95%MDD	MDD
Anthem	1	118.5	41.9	44.1	4944.7	5230.8	2387.3	2620.1	2.1	2.0
Burleson	1	132.4	64.7	68.1	7613.0	9016.8	2107.9	2609.3	3.6	3.3
Cleburne	2	105.8	30.7	32.4	3251.4	3422.6	1381.1	1386.3	2.4	2.5
Colorado	1	185.0	57.8	60.8	9871.6	11254.5	1750.9	2057.4	5.6	5.1
Denton	2	156.5	49.9	52.5	7810.8	8221.9	1683.1	2009.0	4.6	4.1
Grapevine 2	2	156.5	49.4	52.0	7737.9	8145.1	1755.2	2222.2	4.4	3.7
Grayson	1	223.0	61.1	64.3	14784.9	14331.8	2541.6	3785.8	5.8	4.2
Keller	1	115.0	49.0	51.5	5606.9	5926.7	2425.9	2447.0	2.3	2.4
Mansfield	2	176.4	56.6	59.6	9985.7	10511.3	2072.4	2197.5	4.8	4.8
Oklahoma	1	76.3	36.4	38.3	2769.6	2924.4	3572.9	4220.4	0.8	0.7
Plano	2	229.3	60.5	63.7	13873.2	14603.4	2863.3	3124.7	4.8	4.7
San Antonio	1	192.4	63.7	67.1	12205.8	12902.4	2969.0	2883.3	4.1	4.5
San Diego	1	92.6	30.4	32.0	2807.0	2965.3	1577.5	1352.0	1.8	2.2
Waco	2	250.1	18.8	19.8	4706.7	4954.4	2538.3	1458.4	1.9	3.4

Ref – reference: (1) Pedarla 2013, (2) This research

Figure 6-15 and Figure 6-16present the variation of calculated TSAR values with measured 1-D swell strains at 95% MDD and MDD, respectively. The fit model had coefficient of determination (R^2) value of 0.84 and 0.85, respectively.

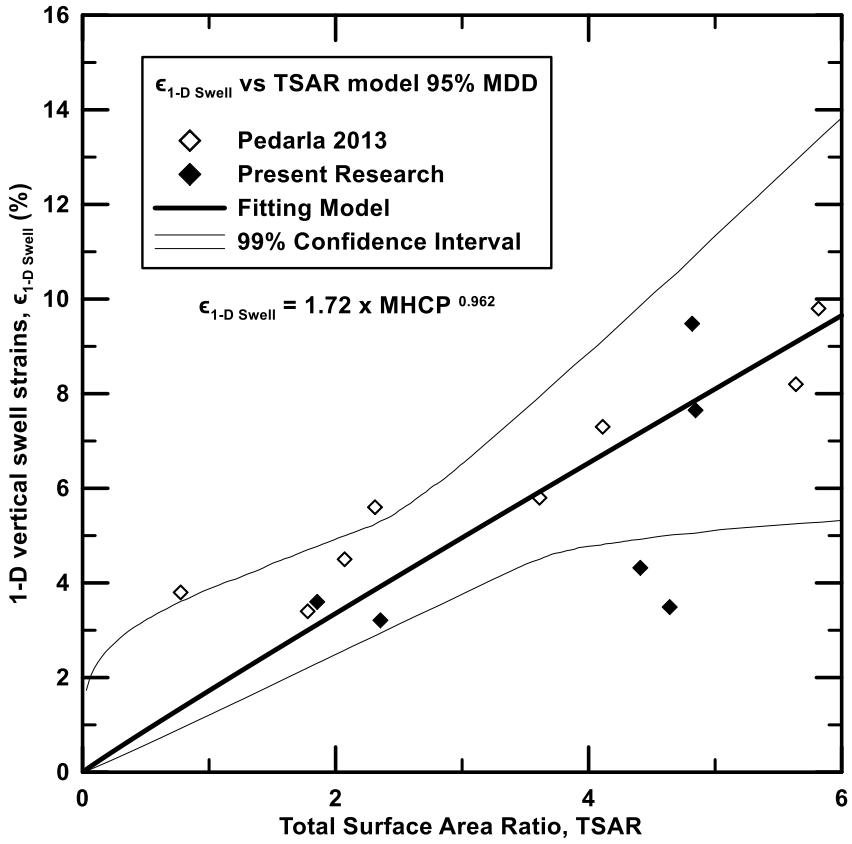

Figure 6-15 1-D Swell Strain TSAR Model at 95% MDD condition

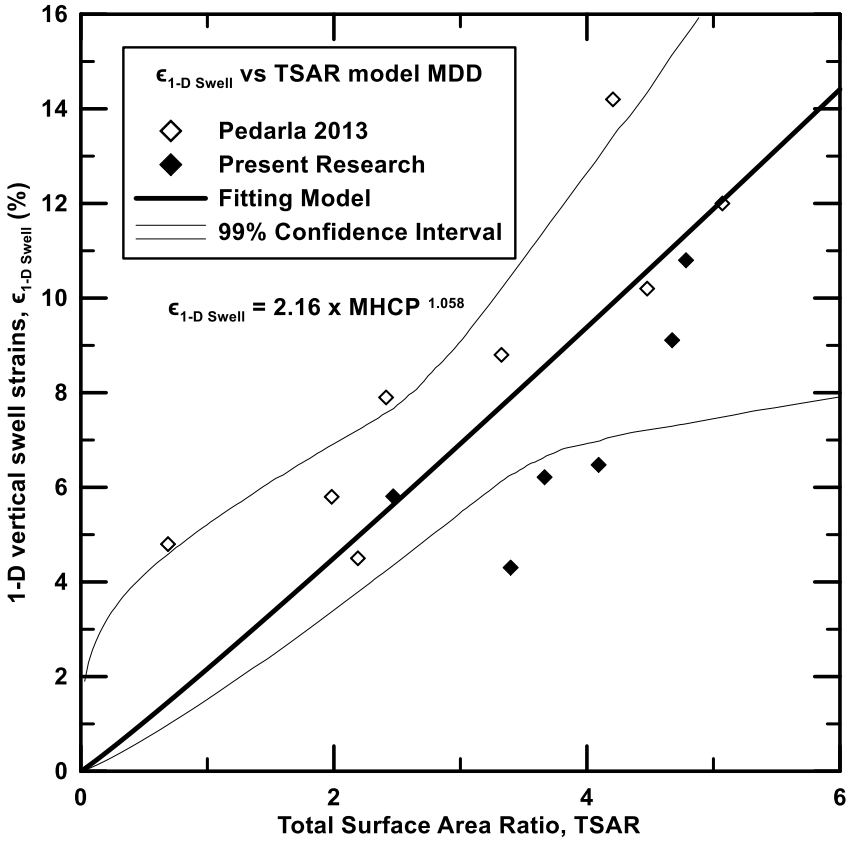

Figure 6-16 1-D Swell Strain TSAR Model at MDD condition

Figure 6-17, Figure 6-18, and Figure 6-19present the variation of calculated TSAR values with measured swell pressure at 95% MDD and MDD, respectively. The fit model had coefficient of determination (R^2) value of 0.81 and 0.78, respectively.

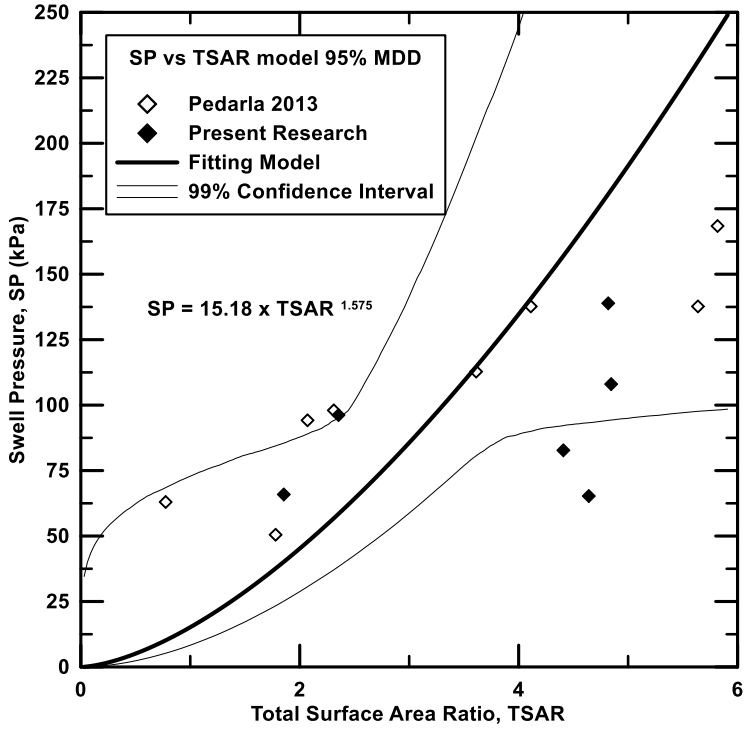

Figure 6-17 1-D Swell Pressure TSAR Model at 95% MDD condition

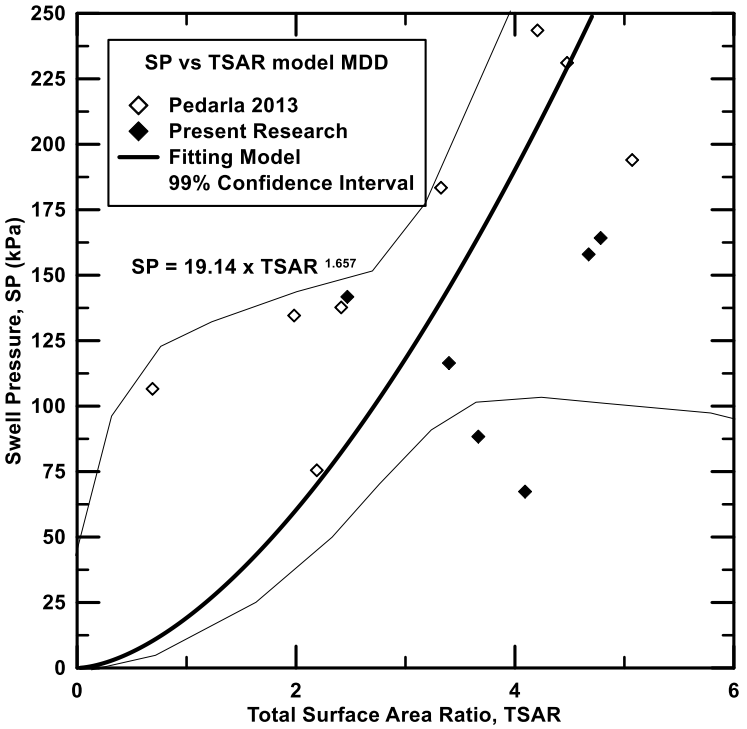

Figure 6-18 1-D Swell Pressure TSAR Model at MDD condition

Figure 6-19, Figure 6-20 and Figure 6-21present the variation of calculated TSAR values with measured 3-D swell strains at confinements of 7 kPa, 50 kPa and 100 kPa, respectively. The fit models for each confinement had coefficient of determination (R^2) value of 0.79, 0.72, and 0.73, respectively.

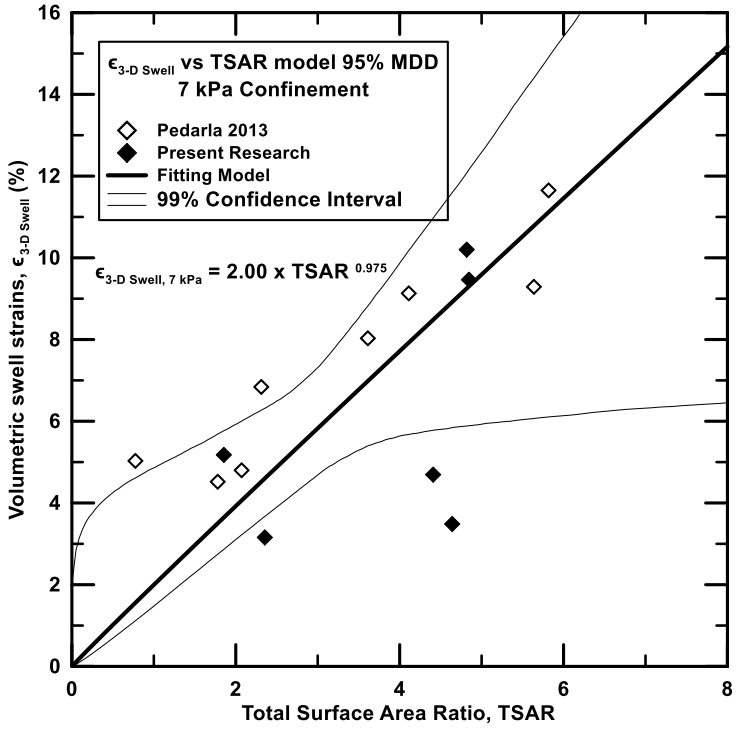

Figure 6-19 3-D Swell Strain TSAR Model at 95% MDD condition and 7 kPa confinement

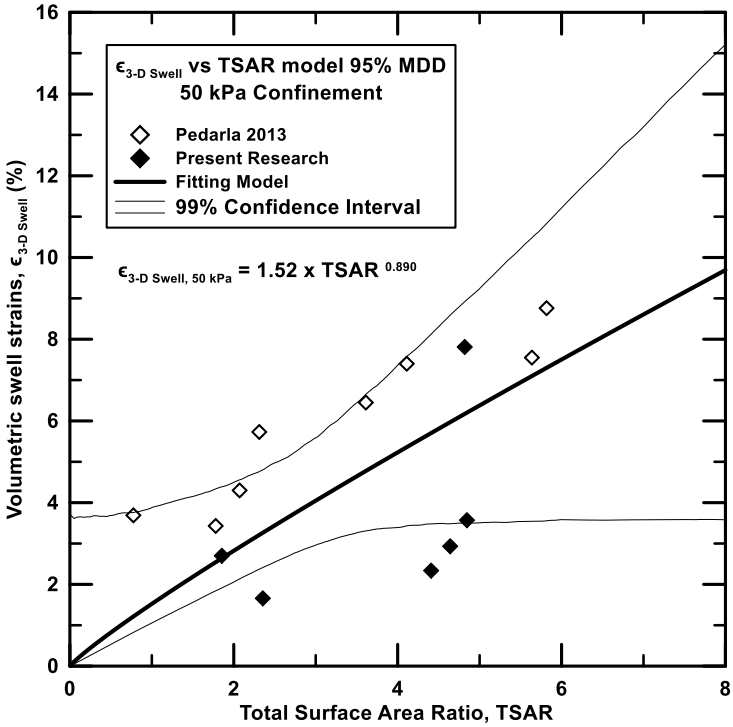

Figure 6-20 3-D Swell Strain TSAR Model at 95% MDD condition and 50 kPa confinement

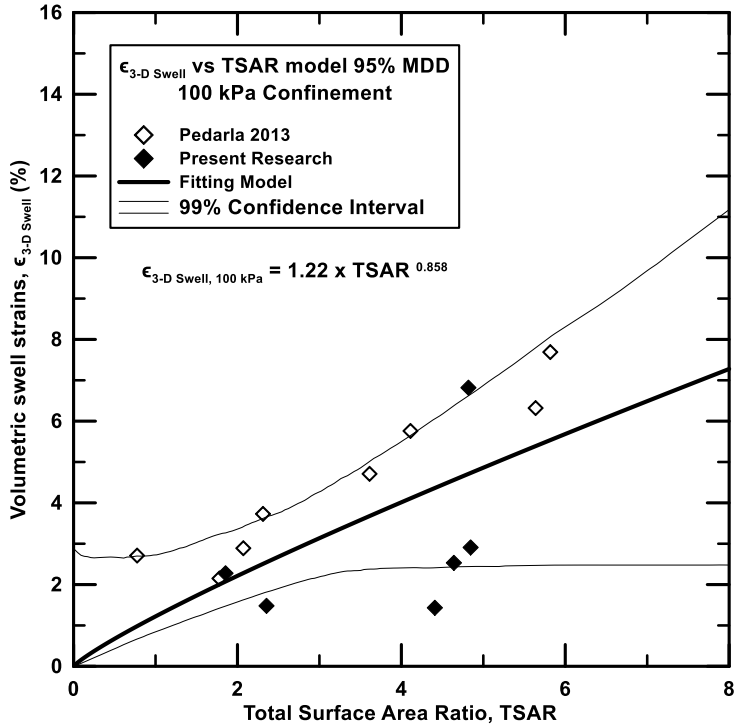

Figure 6-21 3-D Swell Strain TSAR Model at 95% MDD condition and 100 kPa confinement

6.3.2 Summary

The present model was defined based on swell tests performed on soil specimens compacted at 95% MDD and MDD. The correction factors, a and b, determined in this model follow same methodology as for the DDL model. The factors are presented in the previous graphs. Thus, the correlations among swell strains and swell pressure with the TSAR may be assumed to be defined by a formulation similar to that presented in Equation 6-15.

The values of the factors 'a' and 'b' are shown in Table 6-11 in which 14 soils have been evaluated, including the six soils tested in present research as well as those tested by Pedarla (2013),

Table 6-11 Formulation of correction factors, 'a' and 'b' TSAR model

Factor	1-D Swell Strain (%)		Swell Pressure (kPa)		3-D Swell Strain at variable confinements at 95% MDD (%)		
	95% MDD	MDD	95% MDD	MDD	7 kPa	50 kPa	100 kPa
a	1.72	2.16	15.18	19.14	2.00	1.52	1.22
b	0.96	1.06	1.58	1.66	0.98	0.89	0.86
R^2	0.84	0.85	0.81	0.78	0.79	0.72	0.73

Overall, the TSAR models revealed mediocre coefficient of determination values after fitting the TSAR to the experimental swell test properties, except by the 1-D swell strain correlation. However, it is considered that a multiple regression analysis may generate better fitting, when considering the MHCP in conjunction with other variables here in presented.

In this chapter, an approach to validate the formulation of the three swell prediction models based on soil composition and unsaturated soil properties proposed by Pedarla (2013) has been attempted. The validation process was performed by conducting tests on a set of six soils different to that used by Pedarla (2013) and then compared with three swell prediction models. The models exhibited variable degrees of prediction with of a good, acceptable or even mediocre level of agreement, based on their coefficient of determination. Some of the variability

may be explained in the lightly differences arisen at the laboratory testing performance, procedural performance or device bankruptcies.

However, it is considered that the development of a multiple regression analysis to generate a unified model formulation may yield better results by increasing the model prediction capability, if the conjunct effect of the parameters found through the three models is considered.

The next chapter details the multiple regression analysis generated to define a unified model formulation as well as the level of prediction developed by the latter.

Chapter 7

Statistical Regression and Artificial Neural Network models for swell prediction

7.1 Introduction

For several years, researchers have remarked the vital importance of swell potential in the classification of swelling soils to ensure a safe design of structures to be built either upon or inside a clayey soil. There are several design approaches to estimate heave of surface and the consequent pressure exerted by the soil to the structures laying on it. These approaches are mainly based on numerical and analytical methods developed from previously established relationships among soil physical, chemical or mineralogical properties and the real physical soil swelling characteristics assessed using laboratory devices.

Since the very beginning of the soil mechanics, the application of correlations has been found to be a very useful tool to determine several soil properties as swell potential, despite of their semi-empirical or purely empirical support. The usefulness of correlations relies on their simplicity that makes to avoid the time consuming and expensive testing which is usually also of destructive character.

Validation procedures for simple regression swell prediction models proposed by Pedarla (2013) have been presented in Chapter 6. It was found that the models exhibited variable degrees of prediction with of good, acceptable or even mediocre level of agreement, according to their coefficient of determination.

Due to the outlined above, especially to the relatively low prediction performance of some of the simple regression models given by the mentioned author and in an attempt to improve the valuable data, the main objective accomplished in this research is to obtain more reliable multiple linear regression predictive models to correlate soil swell behavior to advanced soil features already presented in previous chapters that play an important role in swelling of soils. These soil swelling variables are the diffusive double layer strain (ϵ_{DDL}), the mechanical hydro chemical parameter (MHCP), and the total surface area ratio (TSAR). Another multiple

linear regression approach for swell prediction is presented by using data obtained in this research and validating it with data obtained from literature. For doing so, a new parameter designated as weighted Montmorillonite percentage (M_w) has been introduced.

It is considered that the multiple linear regression models presented herein are an important advance in soil swelling behavior prediction since they consider more elaborated variables of soil. Up to the date there is no knowledge of models including such type of advanced parameters in the same analysis. Therefore, the models are considered to be very valuable for at least the preliminary stage of designing a structure, when the data joined with interpretation is based on engineering experiences.

Moreover, in recent years, new soft computing techniques such as artificial neural networks have been successfully utilized for establishing predictive models to estimate swelling or other soil related parameters. These techniques are attractive to researchers in several fields because of the wide range of uncertainty tolerated by them. Thus software based techniques are nowadays being increasingly used as alternate statistical tool and are applied in this chapter as an alternative to conventional multiple linear regression for analyzing the soil swell prediction capability of the data.

This chapter aims to determine the empirical relationships for estimation of soil swell behavior by using conventional multiple linear regression (MLR) and artificial neural network (ANN) models, as well as to compare the prediction capabilities of the models and to analyze the prediction performances.

7.2 Multiple linear regression models

The multiple linear regression (MLR) has been considered a valuable technique to predict the variance in an interval dependent since its first use conferred to Pearson in 1908. MR is based on linear combinations of intervals, dichotomous, or dummy independent variables an its general purpose consist in getting further knowledge about the relationship among

several independent or predictor variables and a dependent or criterion variable. The MR is usually presented in the form shown in Equation 7-1.

$$y = b_1 x_1 + b_2 x_2 + \cdots + b_n x_n + c \qquad 7-1$$

Where, b_n are the regression coefficients which represent how the dependent variable y changes when there is a 1 unit variation in the corresponding independent variable x_n; c is a constant and may be described simply as the point where the regression line intercepts the y axis at the point when all the independent variables are cero.

In order to allow for the regression performance there are coefficients designated beta weights which are the standardized versions of the b_n coefficients. Also, the ratio of the relative predictive power of the independent variables is represented by the ratio of the beta coefficients. At this point it is important to mention the key conceptual limitation of any regression technique which is that it is only possible ascertain relationships through these kind of techniques, but never to be sure about underlying causal mechanism.

Despite of the possible drawbacks the multiple linear regression technique may present, an analysis using it was performed to correlate the measured 1-D and 3-D swell strains, as well as the 1-D swell pressure to the three soil swelling parameters presented in Chapter 6 (i.e. ϵ_{DDL}, MHCP, TSAR).

The adjusted coefficient of determination (R_a^2) among the measured and predicted values has been considered in the present work as a good indicator to check the prediction performance of the model. The R_a^2 was calculated according to Equation 7-2.

$$R_a{}^2 = 1 - \frac{\frac{(y_i - y_i')^2}{n-k-1}}{\frac{(y_i - \bar{y})^2}{n-1}} \qquad 7-2$$

Where yi and yi' are the measured and predicted values, respectively. Also, the number of data points per k number of independent variables is designated as n. If the R_a^2 is 100 the model will reach maximum fitting agreement.

Similarly, in this study, the performance of the prediction capacity of predictive models developed was additionally controlled by calculating the variance accounted for index (VAF) which is equivalent to the unadjusted coefficient of determination (R^2) but in percentage; and the root mean square error (RMSE) index, as presented in Equation 7-3 and Equation 7-4, respectively (Alvarez et al., 1999; Finol et al., 2001; Gokceoglu, 2002; Yilmaz et al., 2011).

$$VAF = \left[1 - \frac{var(y_i - y_i')}{var(y_i)}\right] \times 100 \qquad 7-3$$

$$RSME = \sqrt{\frac{1}{N}\sum_{i=1}^{n}(y_i - y_i')^2} \qquad 7-4$$

Where yi and yi' are the measured and predicted values, respectively. If the VAF is 100 and RMSE is 0, then the model will be excellent.

Another accuracy index on the fitted values in statistics known as the Mean absolute percentage error (MAPE) was also calculated using Equation 7-5. MAPE is useful for comparison of the prediction performances of the MR models and usually expresses accuracy as a percentage.

$$MAPE = \frac{1}{N}\sum_{i=1}^{n}\left|\frac{y_i - y_i'}{y_i}\right| \times 100 \qquad 7-5$$

In this case, yi is the actual o measured value and yi' is the predicted value.

The obtained values of R_a^2, VAF, RMSE and MAPE are presented in the following for each model considered. The prediction performances are also commented.

7.2.1 1-D Swell Strain and Swell Pressure MLR models

Multiple linear regression models applied on data were performed to predict the 1-D swell strain ($\epsilon_{1\text{-D Swell}}$) and swell pressure (SP) dependent variables for all the 14 worked soils at MDD compaction condition. The independent variables used to fit the models were the diffusive double layer strain (ϵ_{DDL}) and the total surface area ratio (TSAR).

The 1-D swell strain and swell pressure MLR models are given below by Equation 7-6 and Equation 7-7, respectively. Values of R_a^2, VAF, RMSE and MAPE exhibited by the models as well as the ranges of the independent variables for which the models are valid are presented in Table 7-1.

$$\epsilon_{1-D\ Swell}\ (\%) = 1.45 + 0.01 \times \epsilon_{DDL} + 1.04 \times TSAR \qquad 7-6$$

$$SP\ (kPa) = 61.86 + 0.35 \times \epsilon_{DDL} + 2.81 \times TSAR \qquad 7-7$$

Table 7-1 ϵ_{DDL} and SP MLR models: performance indices and independent variables ranges

Index		R_a^2	VAF	RMSE	MAPE	ϵ_{DDL} (%)		TSAR	
						Max	Min	Max	Min
MLR Model	$\epsilon_{1\text{-D Swell}}$	0.86	87.8	1.02	11.99	492.2	5.1	79.5	0.7
	SP	0.78	81.6	22.37	16.64				

Figure 7-1 and Figure 7-2 show the relationships among the measured and the predicted 1-D swell strain and swell pressure values obtained from the MLR models.

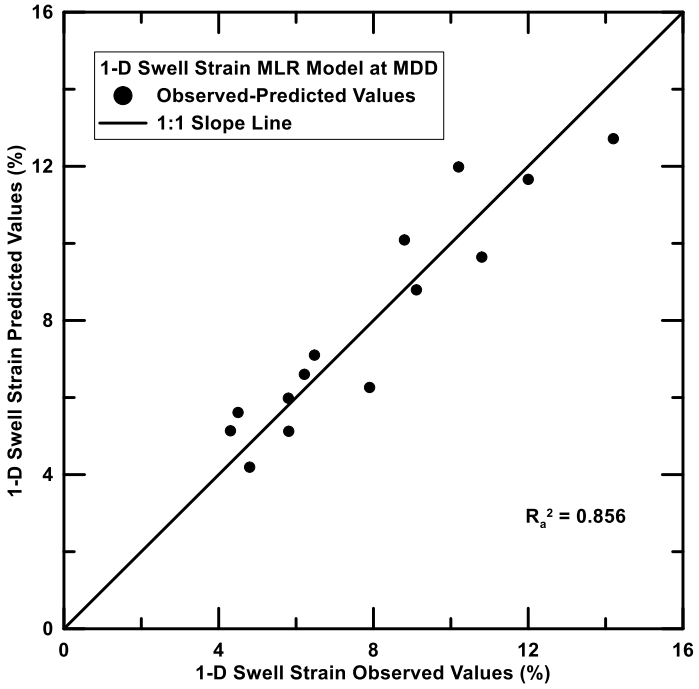

Figure 7-1 Observed and predicted values for 1-D Swell Strain MLR Model at MDD

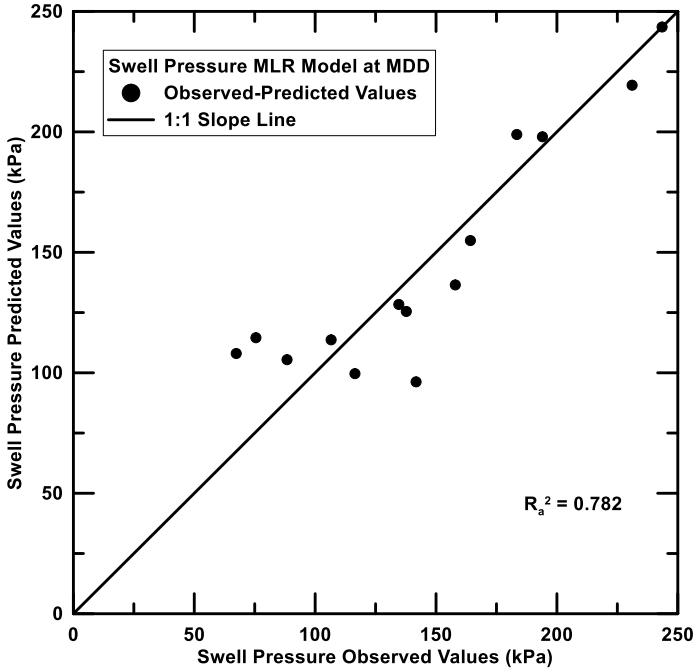

Figure 7-2 Observed and predicted values for Swell Pressure MLR Model at MDD

7.2.2 1-D and 3-D Swell Strain and Swell Pressure MLR models

Multiple linear regression models applied on data were performed to predict the 1-D swell strain ($\epsilon_{1\text{-D Swell}}$), swell pressure (SP) and 3-D swell strain ($\epsilon_{3\text{-D Swell}}$) dependent variables for all the 14 worked soils at 95% MDD compaction condition. The independent variables used to fit the models were the diffusive double layer strain (ϵ_{DDL}), the mechanical hydro chemical parameter (MHCP); and the total surface area ratio (TSAR).

The MLR models for the dependent variables: 1-D swell strain, swell pressure and 3-D swell strain under three different confinements (7 kPa, 50 kPa and 100 kPa) are given below by Equation 7-8 through Equation 7-12. Values of R_a^2, VAF, RMSE and MAPE exhibited by the models as well as the ranges of the independent variables for which the models are valid are presented in Table 7-2.

$$\epsilon_{1-D\ Swell}\ (\%) = 2.02 + 0.01 \times \epsilon_{DDL} + 0.56 \times MHCP + 0.36 \times TSAR \qquad 7-8$$

$$SP\ (kPa) = 44.07 + 0.15 \times \epsilon_{DDL} + 4.79 \times MHCP + 5.26 \times TSAR \qquad 7-9$$

$$\epsilon_{3-D\ Swell,7\ kPa}\ (\%) = 2.74 + 0.01 \times \epsilon_{DDL} + 0.59 \times MHCP + 0.17 \times TSAR \qquad 7-10$$

$$\epsilon_{3-D\ Swell,50\ kPa}\ (\%) = 1.69 + 0.01 \times \epsilon_{DDL} + 0.38 \times MHCP - 0.12 \times TSAR \qquad 7-11$$

$$\epsilon_{3-D\ Swell,100\ kPa}\ (\%) = 0.80 + 0.01 \times \epsilon_{DDL} + 0.40 \times MHCP + 0.02 \times TSAR \qquad 7-12$$

Table 7-2 $\epsilon_{1\text{-D Swell}}$, SP and $\epsilon_{3\text{-D Swell}}$ MLR models: performance indices and independent variables ranges

Index		R_a^2	VAF	RMSE	MAPE	ϵ_{DDL} (%)		MHCP		TSAR	
						Max	Min	Max	Min	Max	Min
MLR Model	$\epsilon_{1\text{-D Swell}}$	0.89	91.31	0.67	9.72	468.88	62.15	7.72	0.07	5.82	0.78
	SP	0.80	84.67	13.14	12.22						
	$\epsilon_{3\text{-D Swell, 7 kPa}}$	0.84	87.90	0.92	12.44						
	$\epsilon_{3\text{-D Swell, 50 kPa}}$	0.86	89.22	0.74	13.98						
	$\epsilon_{3\text{-D Swell, 100 kPa}}$	0.89	91.71	0.57	13.91						

The relationships among the measured and the predicted values for the dependent variables: 1-D swell strain, swell pressure and 3-D swell strain under three different confinements (7 kPa, 50 kPa and 100 kPa) obtained from the MLR models are depicted in Figure 7-3 through Figure 7-7.

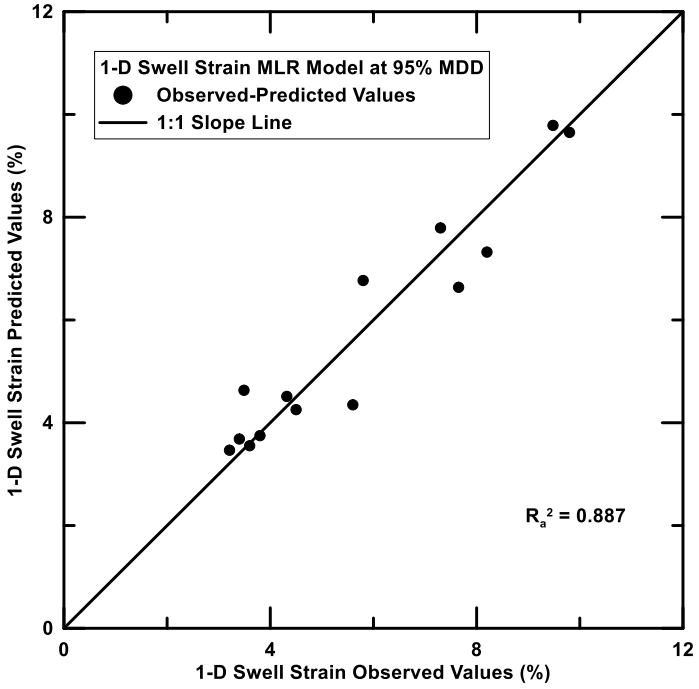

Figure 7-3 Observed and predicted values for 1-D Swell Strain MLR Model at 95% MDD

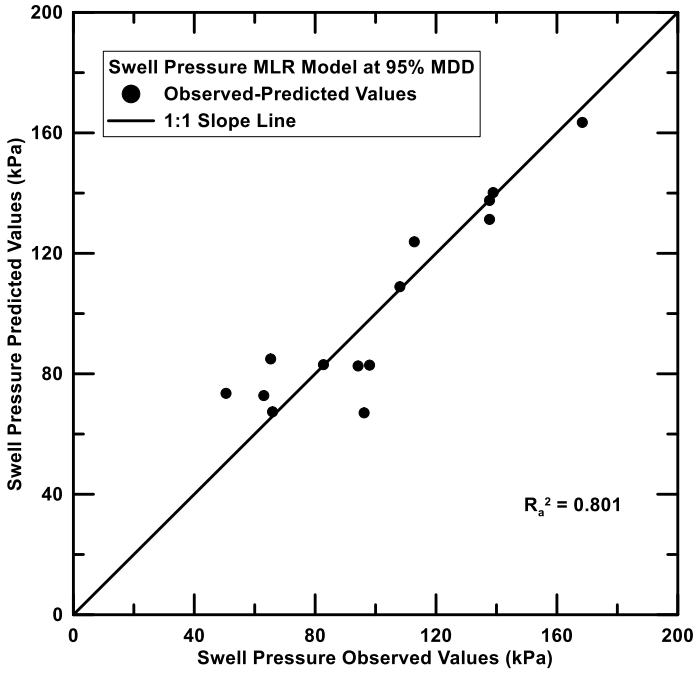

Figure 7-4 Observed and predicted values for Swell Pressure MLR Model at 95% MDD

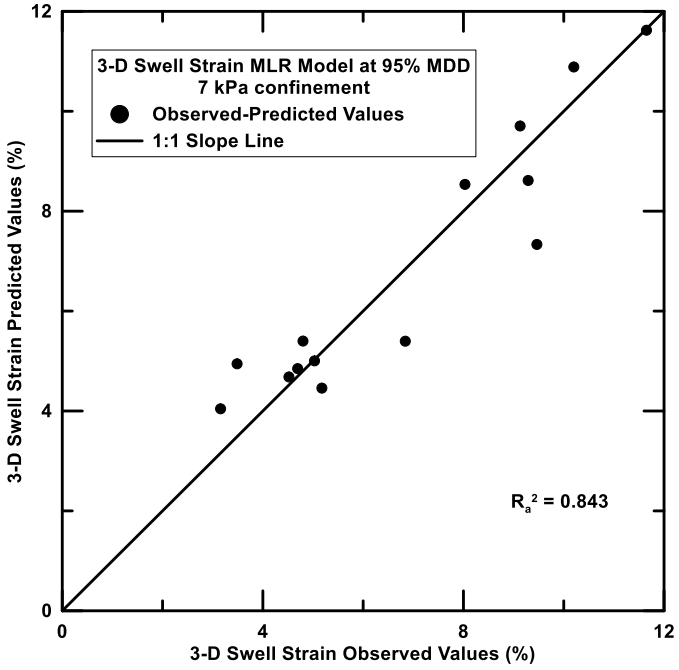

Figure 7-5 Observed and predicted values for 3-D Swell Strain (7 kPa confinement) MLR Model at 95% MDD

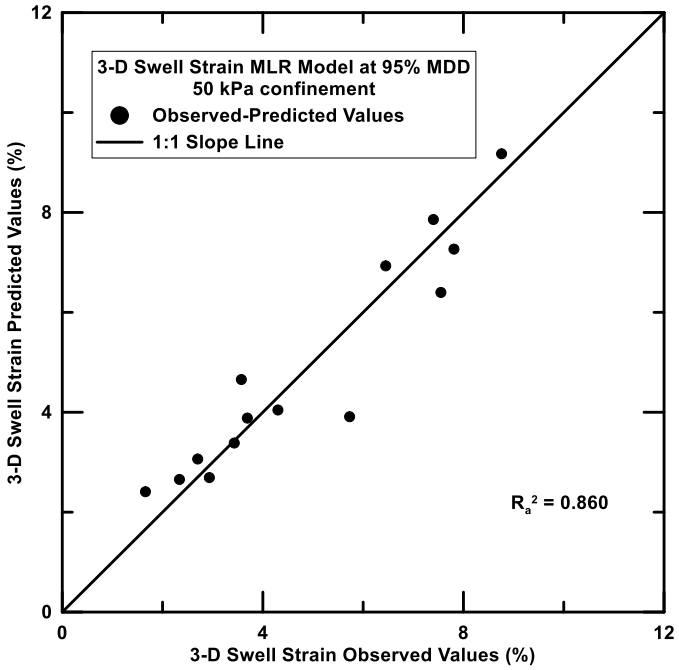

Figure 7-6 Observed and predicted values for 3-D Swell Strain (50 kPa confinement) MLR Model at 95% MDD

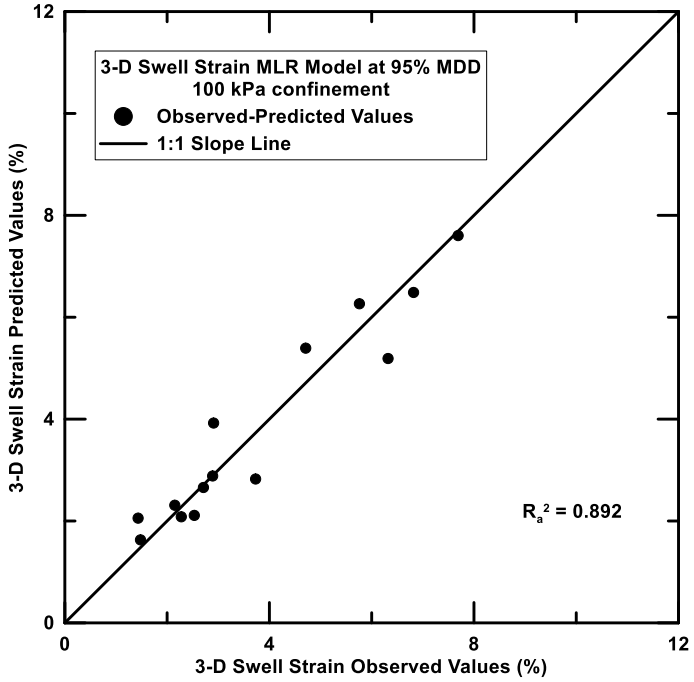

Figure 7-7 Observed and predicted values for 3-D Swell Strain (100 kPa confinement) MLR Model at 95% MDD

7.2.3 Summary

According to the previously presented results, it may be observed that the higher prediction performances were found in the 1-D swell strain MLR models, at both MDD and 95% MDD compaction conditions. The adjusted coefficient of determination (R_a^2) for the 1-D swell strain case is not lower than 0.856. The swell pressure MLR models for both compaction cases exhibited the worst correlation agreement, considering that the R_a^2 ranged between 0.78 and 0.80. Intermediate prediction behavior was found in the 3-D swell strain MLR models, with R_a^2 ranging between 0.84 and 0.89.

7.2.4 Alternative Mechanical Hydro Chemical (MHC) Model

The MHC model presented and validated in Chapter 6 was set based on swell and suction tests results performed on soil specimens compacted at 95% MDD condition, due to the lack of SWCCs at MDD in the work accomplished by Pedarla (2013).

In the present section an attempt is made to evaluate testing results for soil specimens compacted at MDD condition. Thus, for this analysis only 8 soils have been utilized. Six soils correspond to the soils tested during the present work and two soils were found from literature after an exhaustive review.

It is not straight forward to find a literature reference containing the same testing procedures as those followed in the present research. However, the search yielded that Lin (2012) observed equivalent compaction, swell, suction and chemical testing methods as those used in this work, thus, his research may be somehow useful to independently validate results between both researches.

Lin collected clayey soils from one place in Oklahoma and one clayey soil from a Texas location. The soils were designated as Hollywood and Eagle Ford, respectively. He developed a laboratory program on remolded compacted samples that included determination of the compaction features of soil based on the Harvard miniature test instead of standard compaction proctor test in order to save soil. Lin relied on this compaction process as designed and calibrated by Khoury et al. (2005) which results closely matched the compaction characteristics of a standard proctor test.

Mineralogy tests were accomplished to determine the soil specific surface area (SSA) through ethylene glycol monoethyl ether (EGME) method (Cerato et al., 2002) and the cation exchange capacity (CEC) of soils by the 1 N ammonium acetate extraction method (Rhoades, 1982).

Drying SWCCs based on matric suction were obtained performing pressure plate tests and filter paper technique. Fredlund and Xing (1994) formulation was used to fit the experimental data. Swell strains and pressures were determined applying ASTM D4546 Method C (loading-after-wetting test).

Most of the soils variables needed to determine the mechanical hydro-chemical parameter (MHCP) as presented by Pedarla (2013) in his Mechanical Hydro Chemical (MHC) Model were found from the above outlined tests performed by Lin.

However, mineralogy characterization was partially incomplete since total potassium test was not performed and the results from this test are required to a complete quantitative estimation of the clay mineralogy of any fine grained soil according to the procedure proposed by Chittoori et al. (2011) and followed in both, Pedarlas's and the present work. Consequently, MHCP estimation may not be completed in concordance to the procedure proposed by Pedarla (2013).

Thus, bearing in mind that the clay mineral montmorillonite which has a swelling factor (SF) of 90 as assigned by Pedarla (2013) plays a more important role in soil swelling behavior than clay minerals illite (SF=9) and kaolinite (SF=1), it is considered that the error in soil swelling behavior characterization might be neglected if only montmorillonite is considered to obtain a modified chemical parameter herein named as weighted montmorillonite percentage (M_w). The procedure followed to find M_w is presented in the next paragraphs.

Based on to the procedure proposed by Chittoori et al. (2011) for clay minerals quantification, it is possible to determine the percentage of montmorillonite in the clay fraction of any soil (M) from SSA and CEC test results.

The percentage of montmorillonite in a soil (M_s) may be found when the montmorillonite percentage in the clay fraction of the soil obtained from the mineralogy quantification procedure (M) is multiplied by the soil clay fraction (CF).

Then, another multiplication of the percentage of montmorillonite in the soil (M_s), this time by the swelling factor of montmorillonite (SF=90) will yield the weighted montmorillonite percentage (M_w). The mathematical procedure is summarized in Equation 7-13.

$$M_W = M_S \times SF = M \times \frac{1}{100} \times CF \times SF \qquad 7-13$$

The weighted montmorillonite percentage (M_w) representing the chemically related swell activity of clays may be utilized as one of the independent variables to establish the herein proposed MLR model.

The second independent variable corresponds to the idealized slope of the void ratio – matric suction plot as proposed by Pedarla (2013) and designated by him as the modified specific moisture capacity (α) or simply equivalent mechanical hydro parameter (Figure 2-20). The procedure to find α is the same as presented in Chapter 6.

A review of the test results obtained in Lin's research development is presented below in Table 7-3.

Table 7-3 Laboratory tests results (Lin, 2012)

Soil	LL	PI	MDUW (kN/m^3)	OMC (%)	CEC (meq/100g)	SSA (m^2/g)	USCS Classification
Hollywood	54	34	16.7	20.6	26.4	145.5	CH
Eagle Ford	92	57	14.2	27.1	49.6	213.5	CH

The calculated values for the weighted montmorillonite percentage (M_w) and the modified specific moisture capacity (α) obtained in the research developed by Lin as well as during the present work are presented in Table 7-4 and Table 7-5 shown below.

Table 7-4 Independent variables calculation for MLR model at MDD condition (Lin, 2012)

Soil	$\epsilon_{1\text{-D Swell}}$ (%)	SP (kPa)	M (%)	CF (%)	M_W (%)	e_o	e_f	Ψ_o (kPa)	Ψ_f (kPa)	α
Hollywood	5.6	141	15.6	62	8.7	1.243	2.196	771	1	0.330
Eagle Ford	12.7	263	27.1	66	16.1	2.002	7.247	1122	1	1.720

Where: $\epsilon_{1\text{-D Swell}}$: 1-D Swell strain; SP: Swell pressure

Table 7-5 Independent variables calculation for MLR model at MDD condition

Soil	$\epsilon_{1\text{-D Swell}}$ (%)	SP (kPa)	M (%)	CF (%)	M_W (%)	e_o	e_f	Ψ_o (kPa)	Ψ_f (kPa)	α
Cleburne	5.8	141.7	20.4	22	4.5	0.229	0.300	245	1	0.030
Denton	6.5	67.4	20.4	39	8.0	0.740	0.853	115	1	0.055
Grapevine 2	6.2	88.4	18.6	38	7.1	0.630	0.730	600	265	0.282
Mansfield	10.8	164.2	42.8	50	21.4	0.939	1.148	40	10	0.345
Plano	9.1	158.0	29.6	54	16.1	0.985	1.162	1000	3000	0.339
Waco	4.3	116.5	50.1	17	8.6	0.956	1.040	645	1	0.030

Where: $\epsilon_{1\text{-D Swell}}$: 1-D Swell strain; SP: Swell pressure

Multiple linear regression models were applied on data to predict the 1-D swell strain ($\epsilon_{1\text{-D Swell}}$) and swell pressure (SP) dependent variables for all the 10 worked soils at MDD compaction condition.

The independent variables used to fit the models were the weighted montmorillonite percentage (M_w) and the modified specific moisture capacity (α).

The 1-D swell strain and swell pressure MLR models are given below by Equation 7-13 and Equation 7-14, respectively.

Values of R_a^2, VAF, RMSE and MAPE exhibited by the models as well as the ranges of the independent variables for which the models are valid are presented in Table 7-6.

$$\epsilon_{1-D\ Swell}\ (\%) = 3.18 + 0.34 \times M_W + 2.34 \times \alpha \qquad 7-13$$

$$SP\ (kPa) = 83.33 + 2.77 \times M_W + 77.12 \times \alpha \qquad 7-14$$

Table 7-6 ϵ_{DDL} and SP MLR models: performance indices and independent variables ranges

Index		R_a^2	VAF	RMSE	MAPE	M_w (%)		α	
						Max	Min	Max	Min
MLR Model	$\epsilon_{1\text{-D Swell}}$	0.85	89.6	0.67	7.20	19.23	4.06	1.720	0.030
	SP	0.71	79.4	18.99	10.80				

Figure 7-8 and Figure 7-9 show the relationships among the measured and the predicted 1-D swell strain and swell pressure values obtained from the MLR models.

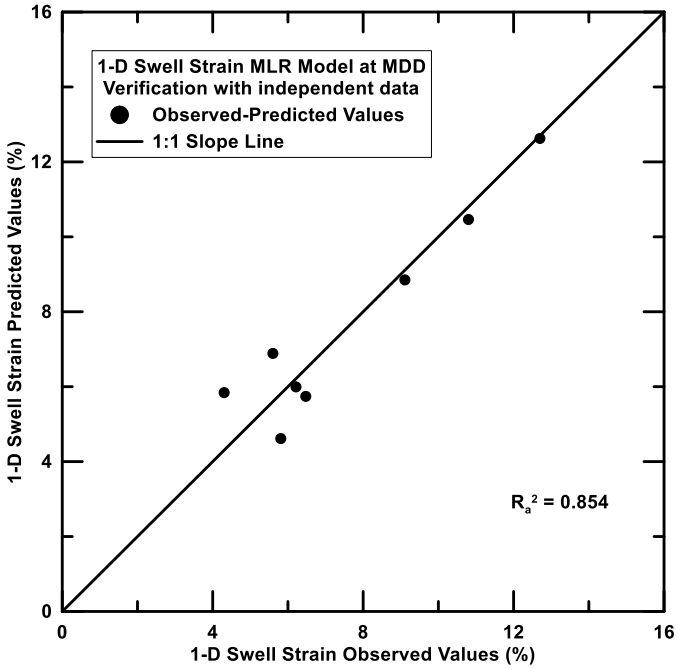

Figure 7-8 Observed and predicted values for 1-D Swell Strain MLR Model at MDD

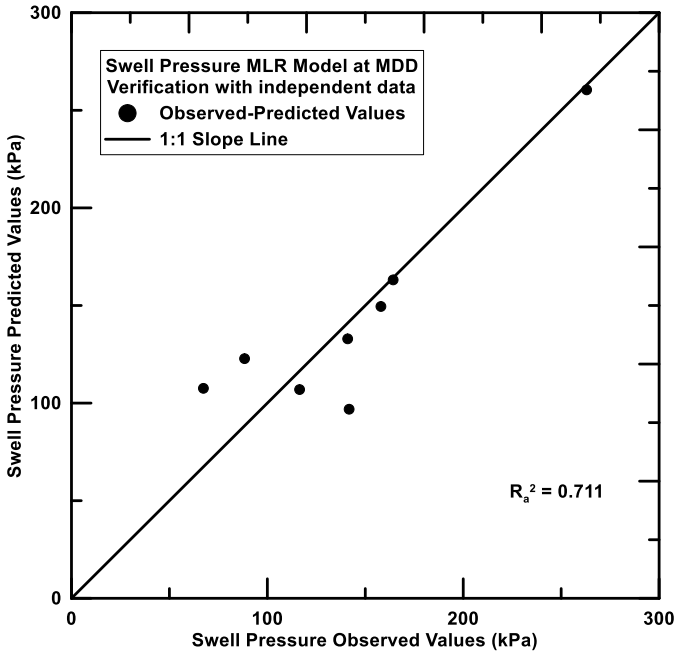

Figure 7-9 Observed and predicted values for Swell Pressure MLR Model at MDD

It is observed that the higher prediction performance is once again generated by the 1-D swell strain MLR model. The adjusted coefficient of determination (R_a^2) for the 1-D swell strain case is 0.854. The swell pressure MLR model exhibited relatively middling correlation agreement, considering that the R_a^2 was found to be 0.71.

7.3 Artificial Neural Network models

Artificial neural networks (ANN) are a soft computer approach suitable to substitute statistical analysis and techniques like simple and multiple linear regressions, trigonometric, among other (Singh et al., 2003). ANN present a significant capability to derive a general solution from complex and inaccurate data and therefore are a valuable tool for inferring patterns and identifying trends complex enough to be detected by human reasoning or even other computer based techniques. In recent years, the ANN technique has been increasingly applied in geotechnical engineering when complex soil behavior features are difficult to be simulated by theoretical models.

High levels of analysis expertise in any category of information may be achieved by a trained neural network. The network mimics the human brain learning process detecting important patterns that will help to predict future behavior and enhance the degree of knowledge the network may achieve once the learning or training process is repeated. Thus, at the end of the training process the neural network is assumed to act as an expert.

Three fundamental components define an ANN: the transfer function, the network architecture and the learning law (Simpson, 1990). In order to solve a problem satisfactorily these three components need to be clearly stated.

There are different classes of architectures to support the ANN functioning. However, it has been noticed that a single hidden layer network arranged with several connection weights is suitable to approximate any continuous function (Hornik et al., 1989). Consequently, for the analyses to be performed in the present research, the network with a single hidden layer has

been trained varying the number of nodes from 1 to 15. In all the cases, a network with a sole hidden layer containing twelve nodes is accepted as the best network architecture.

Also, the Levenberg-Marquardt algorithm has been adopted to train the ANN in this study since it has proven to be effective when the number of weights in a network is less than 300. This algorithm performs faster and finds better targets than other algorithms (Roweis, 2006).

Overall, ANN models with 2, 3 and 2 input parameters have been developed. The models were designated as ANN-2 MDD, ANN-3 95% MDD and ANN-2 MDD ALT. Details of the networks and results obtained by the application of the ANN technique are described next.

7.3.1 ANN-2 MDD

A two-parameter ANN model was developed to compare and validate the multiple linear regression models performed to predict the 1-D swell strain ($\epsilon_{1\text{-D Swell}}$) and swell pressure (SP) for all the 14 worked soils at MDD compaction condition.

Hence, the ANN model adopted the same two parameters used as the MLR independent variables (ϵ_{DDL} and TSAR), which in turn interpret the 1-D swell strain ($\epsilon_{1\text{-D Swell}}$) and swell pressure (SP) as an output of the model. The model was developed by training with 8 soils of the 14 used in this research. Three soils were used in each validation and testing steps.

Figure 7-10 and Figure 7-11 present the correlation between each of the predicted and measured soil swell behavior features. The R^2 values of the selected ANN model are found to be 0.95 and 0.99 for 1-D swell strain and swell pressure, respectively. Comparisons indicate good capability of the model for predicting these two variables in soils according to the procedures follower in the present research.

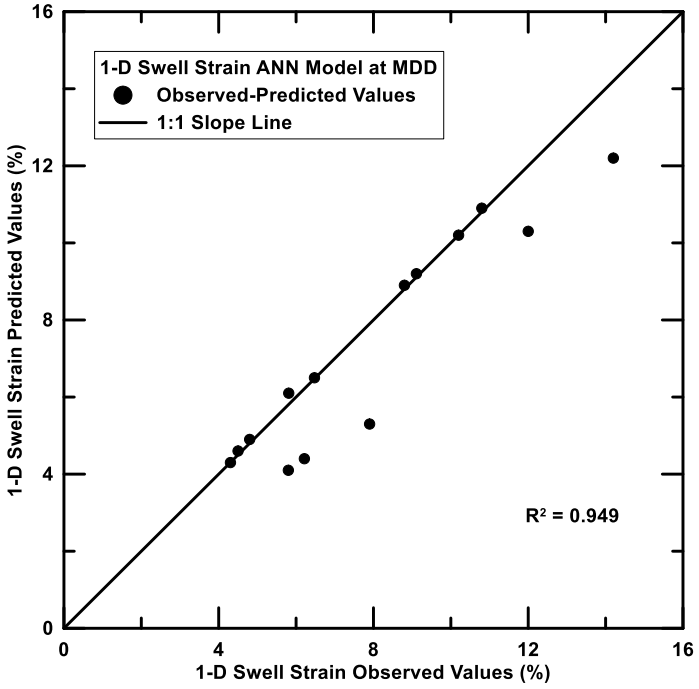

Figure 7-10 Observed and predicted values for 1-D Swell Strain ANN Model at MDD

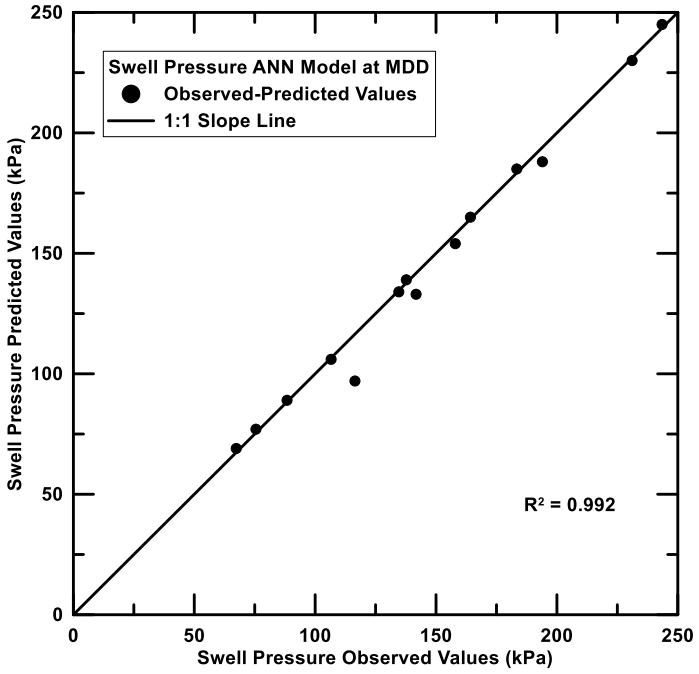

Figure 7-11 Observed and predicted values for Swell Pressure ANN Model at MDD

7.3.2 ANN-3 95% MDD

A three-parameter ANN model was developed to compare and validate the multiple linear regression models performed to predict the 1-D swell strain ($\epsilon_{1\text{-D Swell}}$) and swell pressure (SP) dependent variables for all the 14 worked soils at 95% MDD compaction condition. The ANN model adopted the same two parameters used as the MLR independent variables (ϵ_{DDL}, MHCP, TSAR). These parameters were used to interpret the 1-D swell strain ($\epsilon_{1\text{-D Swell}}$) and swell pressure (SP) as an output of the model. The model was developed by training with 8 soils of the 14 used in this research. Three soils were used in each validation and testing steps.

Figure 7-12 and Figure 7-13 present the correlation between each of the predicted and measured soil swell behavior features. The R^2 values of the selected ANN model are found to be 0.97 and 0.91 for 1-D swell strain and swell pressure, respectively. Comparisons indicate excellent capability of the model for predicting these two variables in soils according to the procedures follower in the present research.

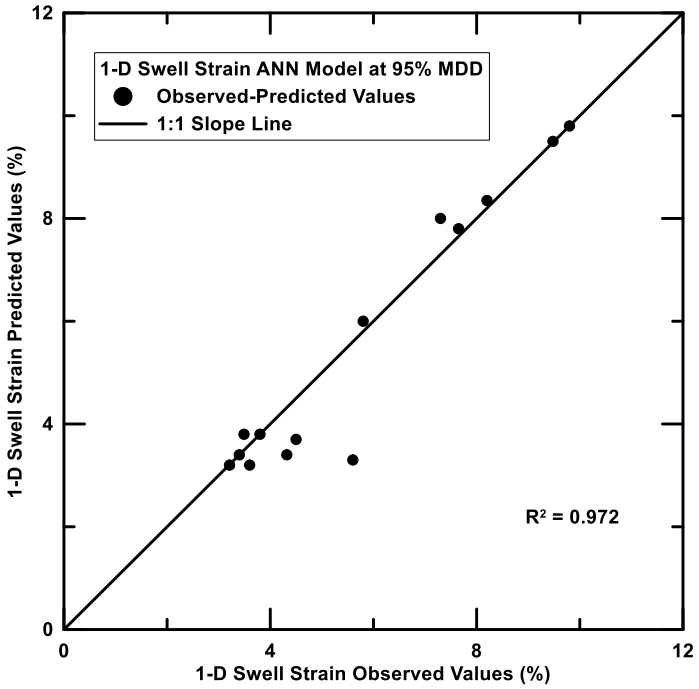

Figure 7-12 Observed and predicted values for 1-D Swell Strain ANN Model at 95% MDD

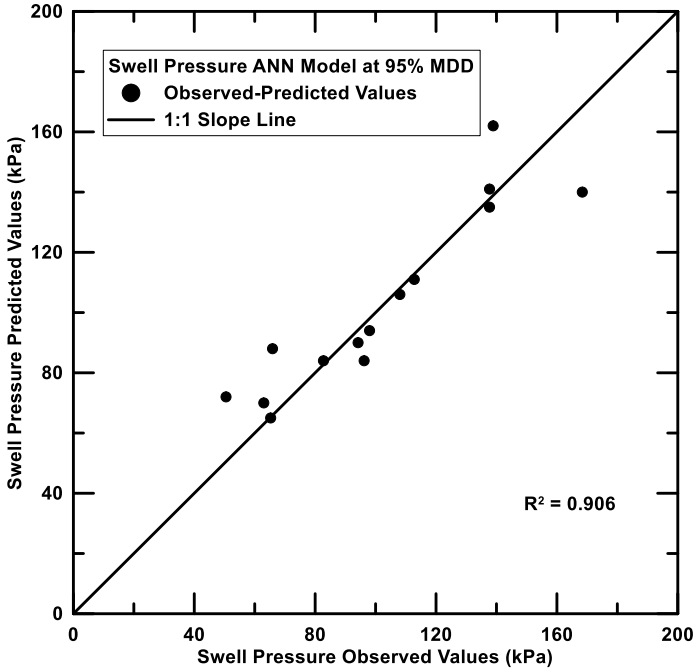

Figure 7-13 Observed and predicted values for Swell Pressure ANN Model at 95% MDD

7.3.3 ANN-2 MDD ALT

A alternative two-parameter ANN model was developed to compare and validate the multiple linear regression models performed to predict the 1-D swell strain ($\epsilon_{1\text{-D Swell}}$) and swell pressure (SP) for the 10 worked soils at MDD compaction condition (2 additional soils reported by Lin, 2012, were included in the analysis).

Hence, the ANN model adopted the same two parameters used as the MLR independent variables (M_w and α), which in turn interpret the 1-D swell strain ($\epsilon_{1\text{-D Swell}}$) and swell pressure (SP) as an output of the model. The model was developed by training with 5 soils of the 10 used in this research. Two soils were used in validation stage and 2 soils were applied in the testing step.

Figure 7-14 and Figure 7-15 present the correlation between each of the predicted and measured soil swell behavior features. The R^2 values of the selected ANN model are found to be 0.91 and 0.88 for 1-D swell strain and swell pressure, respectively. Comparisons indicate

good capability of the model for predicting these two variables in soils according to the procedures follower in the present research.

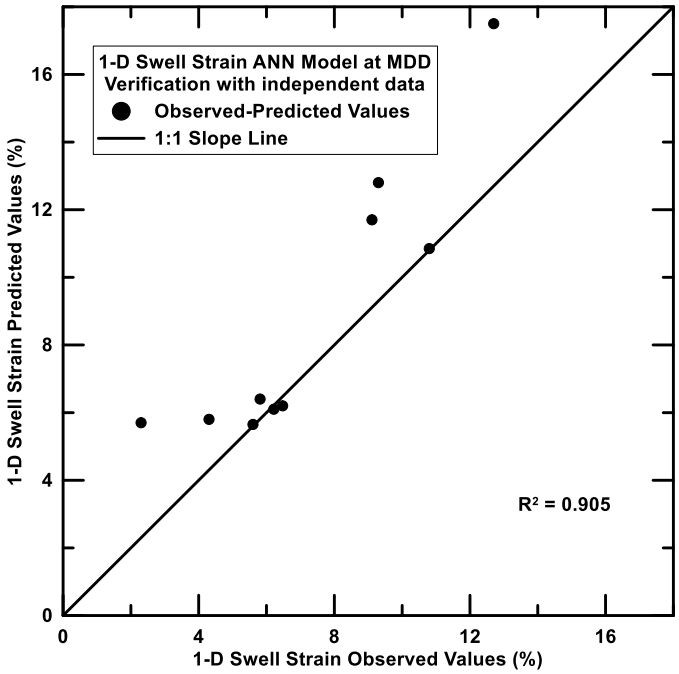

Figure 7-14 Observed and predicted values for 1-D Swell Strain ANN Model at MDD

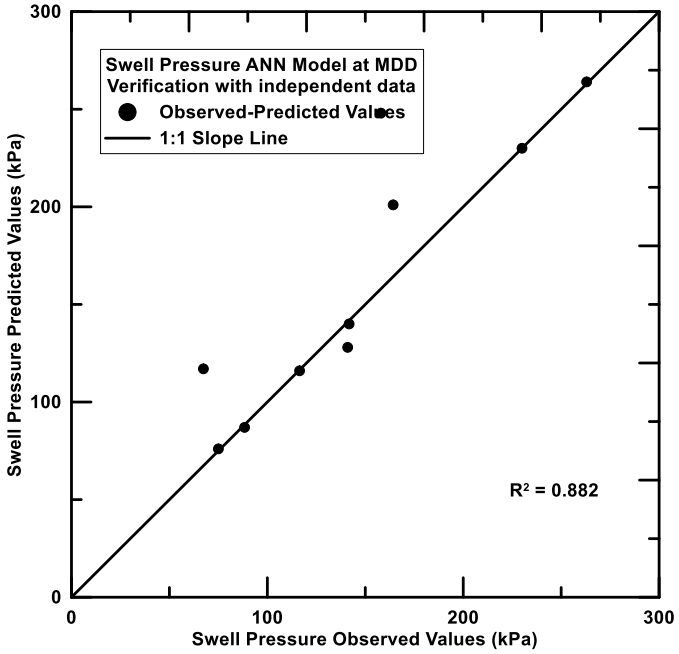

Figure 7-15 Observed and predicted values for Swell Pressure ANN Model at MDD

7.4 Summary

Multiple linear regression (MLR) analyses as well as artificial neural network (ANN) approach have been utilized in this chapter for evaluating the soil swell behavior and consequently establishing soil swell predicting models desired to behave with acceptable prediction performance level.

Overall, the MRL models present acceptable prediction capacity, but their prediction capability is lower than that exhibited by the ANN models. It may be related to the existence of underlying causal mechanism inferring the swell behavior prediction which might be not easily foreseen by the MLR models.

The prediction ability of the ANN models is proomising and reiterates the usefulness of the technique for inferring patterns and identifying trends complex enough to be detected by human reasoning or even other computer based techniques including MLR.

The Alternative Mechanical Hydro Chemical (MHC) Model might be used to determine the swell behavior of clayey soils when not all the tests needed to perform the mineralogical quantification have been completed.

The model presents acceptable level of soil swell behavior prediction especially when worked with the ANN approach.

Next chapter summarizes the finding and recommendations for future works to be developed when related to swell behavior of soils.

Chapter 8

Summary of Findings and Future Recommendations

Geotechnical engineers may choose to characterize the soil swelling behavior either using direct or indirect methods. Direct methods include the development of laboratory testing programs to identify the swelling potential of soils. On the other hand, indirect methods have been extendedly developed based on correlations that link soil swelling behavior to basic soil indexes like plastic index or activity, instead of using more advanced variables of soil as initial moisture content, mineralogy, suction and pore structure. The main focus of the present research is to acquire a better understanding of the swelling soil behavior and the development of a general and unified approach that includes both analytical and numerical formulation for the prediction of the volume change properties and responses of expansive soils by considering clay mineralogy, pore distribution and unsaturated soil mechanics principles.

A total of six natural expansive soils collected from different geographical origin in Texas have been studied in this research. Basic soil classification testing was conducted and then a comprehensive soil swell behavior characterization was accomplished using different types of swell tests as well as variable compaction and confining conditions.

Key soil composition parameters influencing the swell behavior of intact or compacted specimens of expansive clays have been identified and studied using techniques like clay mineralogy, soil-water characteristic, mercury intrusion porosimetry and X-ray Tomography.

Three swell prediction models proposed in a previous study (Pedarla 2013) which followed the same laboratory procedures applied in this work have been evaluated and validated according to the swell test results obtained in the present research.

The models rely on soil composition parameters like mineralogy, total surface area and matric suction properties and were developed applying simple linear regression technique to correlate these parameters to the swell features of the eight soils in the research of reference.

After evaluation and validation of the simple linear regression models, statistical multiple linear regression and artificial neural networks techniques were applied to find the most suitable correlations among the basic variables of the three simple linear regression models and the swell test results of the fourteen soils gathered between the reference (Pedarla 2013) and the present research. Hence, a unified formulae to assess the pooled effect of the same soil composition parameters (mineralogy, total surface area and matric suction properties) in the prediction and characterization of swelling soil behavior has been introduced in the current research.

8.1 Summary of Findings

The findings from the soil swell and composition studies conducted are presented in the following sections. The subsequent summarizes the most important findings obtained from the present research.

8.2.1 Findings from Soil composition, swell behavior and pore distribution studies

1. Basic soil classification studies on all the six expansive clays were performed and results from the plasticity indices show that Mansfield soil exhibited a high PI value while Plano soil attained the least value. Grain size distribution analysis on these soils revealed that the same soils have consequent higher and lover clay fraction values respectively.

2. The mineral contents of the expansive clays are determined using standard chemical analyses methods. From the results, Waco soil exhibited the highest Montmorillontie mineral content in its clay fraction. Similarly, Plano soil had the highest Illite mineral content and Cleburne soil has the highest Kaolinite content in the respective clay fraction.

3. From the swell test results, it was found out that the soil exhibiting the maximum swell strains was Mansfield soil and the one exhibiting the least swell strains was Cleburne soil. The soils exhibiting maximum swell strains (Mansfield) also showed a higher swell pressure due to the presence of high Montmorillonite content (second place). Soils compacted at maximum dry density (MDD) condition showed higher swell strains and swell pressures due to the

presence of more soil particles and mineral content than the soil samples compacted at 95% MDD condition.

4. 3-D swell strain tests conducted with a novel test apparatus produced results that are comparable with the 1-D vertical swell strain test results. The measured radial strains are low when compared to the measured vertical strains of the same soil specimen. This reduction in radial swell strains is attributed due to the large height/diameter ratio of the specimen and also the direction of compaction of the soil specimen. Mansfield soil showed the highest volumetric swell strains and Cleburne soil exhibited the lowest swell strains almost at all confining pressures. As the confining pressure applied to the soil specimen has decreased swell strains in soils increased.

5. Drying soil water characteristic curves were obtained for all the soils using standard laboratory techniques. Mansfield and Grapevine 2 soils exhibited large air entry suction value among other soils whereas Plano soil exhibited low air entry value. An approach was made to develop wetting SWCCs according to a new methodology herein followed.

6. Mercury intrusion porosimetry studies revealed the internal pore size distribution in a soil specimen. It was found that the variation of dry density and moisture content of soils had a major influence on the pore distribution of the soil specimen. The volume of micro pores is found to be more in specimens compacted at MDD than specimens compacted at 95% MDD. Similarly, macro pore volume is found to be higher in the case of 95% MDD compaction condition than at MDD condition. The high compaction level at MDD condition packs the soil particles together thereby increasing the micro pore volume and decreasing the macro pore volume when compared to 95% MDD condition.

7. All the soil specimens compacted at various dry density conditions were studied using X-ray Tomography test. The output images from tomography are analyzed using pixel count code in MATLAB software. The void ratio calculated from XCT technique is in good agreement with weight-volume relationships at both dry density conditions. At the saturation

level, all the soils showed a decrease in void ratio when measured with X-ray computed tomography test. This is due the fact that the free expansion of soil particles was neglected during the measurement of void ratio from weight/volume relationships; the predicted void ratio was high. The XCT technique assisted researchers in identifying the actual void space available after the swelling of the soil specimen.

8.2.2 Findings on validation process of the analytical models based on soil composition parameters

The validation process was performed by conducting tests on a set of six soils completely different to those used by Pedarla (2013) and then compared with the three swell prediction models. The models were refined on their formulations and this enhancement procedure made the models to exhibit best performance when statistical power functions were employed to fit the data. Variable degrees of prediction with a good, acceptable or even mediocre level of agreement in some cases were found from the coefficient of determination obtained in the power functions. The development of a multiple regression analysis to generate a unified model formulation was considered may yield better results by increasing the model prediction capability, if the conjunct effect of the parameters found through the three models is considered. The use of artificial neural networks was considered to be a valid alternative to analyze the data as well.

8.2.3 Findings on the multiple linear regression and artificial neural network models for swell prediction

Multiple linear regression technique was employed to develop unified models to predict the soil swelling behavior. The models present acceptable prediction capacity, but their prediction capability is lower than that exhibited by the models found through artificial neural network. It may be related to the existence of underlying causal mechanism inferring the swell behavior prediction which might be not easily foreseen by the multiple linear regression models.

The prediction ability of the artificial neural network models is superior and reiterates the usefulness of the technique for inferring patterns and identifying trends complex enough to be detected by human reasoning or even other computer based techniques including multiple linear regression.

An Alternative Mechanical Hydro Chemical (MHC) Model introduced in the present research may be used to determine the swell behavior of clayey soils when not all the tests needed to perform the mineralogical quantification have been completed. The model was independently validated based on data found in the literature and presents acceptable level of soil swell behavior prediction especially when worked with the artificial neural network approach.

8.3 Future Recommendations

A unified formulae to assess the pooled effect of the soil composition parameters (mineralogy, total surface area and matric suction properties) in the prediction and characterization of swelling soil behavior has been introduced in the current research. The unified model is based on the results and the validation process completed on three swell prediction models proposed in a previous research.

The unified model showed a good validity with the measured swell data especially when alternative analysis techniques like artificial neural networks were used to infer the correlation among the data. However, considering the own limitations related to the assumed boundary conditions of all the three models used to develop the unified model, the following future recommendations are suggested.

1. According to the results obtained in the present research, the methodology followed to define the wetting SWCCs worked and yielded reasonable results, however, further refinement with systematic verification testing is necessary to establish the procedure consistency and usefulness. A wetting SWCC undoubtedly may provide better insights into the swell prediction model analysis.

2. Correction factors ‘a’ and ‘b’ to be applied in the power functions defined to correlate the data in the three basic regression models should be studied with additional detail varying soil conditions affecting them like particle arrangement during compaction, moisture access to the clay particles, and direction of particle swelling, among others.

3. Additional testing including other direct methodologies and devices to assess soil swell behavior should be applied following the same procedures needed to define the three basic validated models in order to define their particular power function. This process may broaden the characterization of expansive soils since it is recognized that the soils swell potential characterization may vary depending on the type of test performed for the latter.

4. A systematic analysis of any possible new soil swell behavior data obtained from other direct methodologies and devices that conforms the procedures required to obtain the basic parameters from the three validated models must be subjected to multilinear regression and artificial neural network techniques in order to allow for direct comparison of the results with those presented in the current research.

5. Further refinement may be performed on the manner of finding the basic parameters from the three validated models, for instance, in the case of the swelling factor of the Mechanical hydro chemical model. This factor may be analyzed on the sight of the diffusive double layer theory according to the mathematical validation analysis performed in the present research to the diffusive double layer model.

References

1. Abu-Kiefa, M.A. (1998) "General regression neural networks for driven piles in cohesionless soils" Journal of Geotechnical and Geoenviromental Engineering, ASCE, 124(12), 1177-1185.
2. Adeli, H. (2001) "Neural networks in civil engineering: 1989-2000" Computer-Aided Civil and Infrastructure Engineering, 16(2), 126-142.
3. Agrawal, G., Chameau, J.A., and Bourdeau, P.L. (1997) "Assessing the liquefaction susceptibility at a site based on information from penetration testing" Artificial neural networks for civil engineers: Fundamentals and applications, N. Kartam, I. Flood, and J. H. Garrett, eds., New York, 185-214.
4. Agrawal, G., Weeraratne, S., and Khilnani, K. (1994) "Estimating clay liner and cover permeability using computational neural networks" Proceedings of the 1st Congress on Computing in Civil Engineering, Washington.
5. Agus, S.S., Leong, E.C., and Rahardjo, H. (2001) "Soil-water characteristic curves of Singapore residual soils" Geotechnical and Geology Engineering, 19(3-4), 285–309.
6. Ahmad, I., El Naggar, H., and Kahn, A.N. (2007) "Artificial neural network application to estimate kinematic soil pile interaction response parameters" Soil Dynamics and Earthquake Engineering, 27(9), 892-905.
7. Ahmed, S., Lovell, C.W. and Diamond, S. (1974) "Pore sizes and strength of compacted clay" Journal of the Geotechnical Engineering Division, ASCE, 100(4):407–425.
8. Aı¨t-Mokhtar, A., Amiri, O., Dumargue, P. and Bouguerra, A. (2004) "On the applicability of Washburn law: study of mercury and water flow properties in cement-based materials" Material Structures, 37:107–113.

9. Alonso, E.E., and Gens J.V. (1999) "Modeling the mechanical behavior of expansive clays" Engineering Geology, vol. 54, pp. 173-183.
10. Al-Raoush, R.I. and Willson, C.S. (2005) "Extraction of physically realistic pore network properties from three-dimensional synchrotron X-ray microtomography images of unconsolidated porous media systems. Journal of Hydrology, 300, 44–64.
11. Alvarez, G.M., and Babuska, R. (1999) "Fuzzy model for the prediction of unconfined compressive strength of rock samples" International Journal of Rock Mechanics and Mining Sciences, 36, 339–349.
12. Anderson, S.H., Peyton, R.L., Wigger, J.W. and Gantzer, C.J. (1992) "Influence of aggregate size on solute transport as measured using computed tomography" Geoderma, 53, 387–398.
13. Aravena, J.E., Berli, M., Ghezzehei, T.A. and Tyler, S.W. (2011) "Effects of root-induced compaction on rhizosphere hydraulic properties - X-ray microtomography imaging and numerical simulations" Environmental Science and Technology, 45, 425–431.
14. Ashayeri, I., and Yasrebi, S. (2009) "Free-swell and swelling pressure of unsaturated compacted clays; experiments and neural networks modeling" Geotechnical and Geological Engineering, 27(1), 137-153.
15. Bache, B. W. (1976) "The measurement of cation exchange capacity of soils" Journal of the Science of Food and Agriculture, 27(3), 273-280.
16. Barat T.V., Sivapullaiah, P.V. and Allam M.M. (2013) "Novel procedure for the estimation of swelling pressures of compacted bentonites based on diffuse double layer theory" Environmental Earth Sciences, V 70, pp. 303-314.

17. Barbour, S.L. (1998) “Nineteenth Canadian geotechnical colloquium: The soil-water characteristic curve: A historical perspective” Canadian Geotechnical Journal, 35(5), 873–894.
18. Basheer, I.A. (1998) "Neuromechanistic-based modeling and simulation of constitutive behavior of fine-grained soils" PhD Thesis, Kansas State University, Manhattan, KS.
19. Basheer, I.A. (2000) "Selection of methodology for neural network modeling of constitutive hysteresis behavior of soils" Computer-Aided Civil and Infrastructure Engineering,15(6), 445-463.
20. Basheer, I.A. (2002) "Stress-strain behavior of geomaterials in loading reversal simulated by time-delay neural networks" Journal of Materials in Civil Engineering, 14(3), 270-273.
21. Basheer, I.A., and Najjar, Y.M. (1998) "Modeling cyclic constitutive behavior by neural networks: Theoretical and real data" Proceedings of the 12th Engineering Mechanics Conference, La Jolla, California, 952-955.
22. Basheer, I.A., Reddi, L.N., and Najjar, Y.M. (1996) "Site characterization by neuronets: An application to the landfill sitting problem” Ground Water, 34, 610-617
23. Baveye, P., Rogasik, H., Wendroth, O., Onasch, I. and Crawford, J.W. (2002) “Effect of sampling volume on the measurement of soil physical properties: simulation with X-ray tomography data” Measurement Science and Technology, 13, 775–784.
24. Baziar, M.H., and Ghorbani, A. (2005) "Evaluation of lateral spreading using artificial neural networks" Soil Dynamics and Earthquake Engineering, 25(1), 1-9.

25. Bekhor, S., and Livneh, M. (2013) “Limitation of the artificial neural networks methodology for predicting the vertical swelling percentage of expansive clays”. Journal of Materials in Civil Engineering.
26. Bekhor, S., and Livneh, M. (2014) “Using the Artificial Neural Networks Methodology to Predict the Vertical Swelling Percentage of Expansive Clays” Journal of Materials in Civil Engineering, 26(6), 06014007.
27. Benardos, A.G., and Kaliampakos, D.C. (2004) "Modeling TBM performance with artificial neural networks” Tunneling and Underground Space Technology, 19(6), 597-605.
28. Birle, E., Heyer, D., and Vogt, N. (2008) “Influence of the initial water content and dry density on the soil-water retention curve and the shrinkage behavior of a compacted clay” Acta Geotechnica, Springer, 3(3), 191–200.
29. Bowels, J.E. (1988) “Foundation analysis and design” McGraw-Hills Inc., U.S.A.
30. Brooks, R.H., and Corey, A.T. (1964) “Hydraulic properties of porous medium hydrology” Hydrology Paper, 3, Department of Civil Engineering, Colorado State University, Fort Collins, CO.
31. Brunauer, S., Emmett, P.H., and Teller, E. (1938) “Adsorption of gases in multimolecular layers” Journal of the American Chemical Society, 60(2), 309-319.
32. Burckhard, S.R., Pirkl, D., Schaefer, V.R., Kulakow, P., and Leven, B. (2000) “A study of soil water-holding properties as affected by TPH contamination” Proceeding Conference on Hazardous Waste Research, Great Plains/Rocky Mountain Hazardous Substance Research Center, Manhattan, KS, 356–359.
33. Cal, Y. (1995) "Soil classification by neural-network” Advances in Engineering Software, 22(2), 95-97.

34. Camberato, J.J. (2001) “Cation exchange capacity—Everything you want to know and so much more”: http://www.scstma.org/upkeep/resources/files/Clemson%20Cation%20Exchange%20Capacity%20Article.pdf.

35. Carroll, D. (1970) “Clay minerals: a guide to their X-ray identification” Geological Society of America, Special Paper 126: 1-80.

36. Carter, D.L., Mortland, M.M., and Kemper, W.D. (1986) “Specific surface” Methods of soils analysis. Part 1: Physical and mineralogical methods, 2nd Ed., A. Klute, ed., Soil Science Society of America (SSSA), Madison, WI.

37. Celik, S., and Tan, O. (2005) "Determination of pre-consolidation pressure with artificial neural network” Civil Engineering and Environmental Systems, 22(4), 217-231.

38. Cerato, A.B., and Luteneggerl, A.J. (2002) “Determination of surface area of fine-grained soils by the ethylene glycol monoethyl ether” Geotechnical Testing Journal, 25, 315-321.

39. Chan, W.T., Chow, Y.K., and Liu, L.F. (1995) "Neural network: An alternative to pile driving formulas" Computers and Geotechnics, 17, 135-156.

40. Chapman, H.D. (1965) “Cation-exchange capacity” Methods of soil analysis—Chemical and microbiological properties, C.A. Black, ed., SSSA, Madison, WI, 891–901.

41. Chapman, L.A. (1913) “Contribution to the theory of electrocapillarity” Philosophical Magazine 25 (6), 475–481.

42. Chen, Y.L., Azzam, R., and Zhang, F. (2006) "The displacement computation and construction pre-control of a foundation pit in Shanghai utilizing FEM and intelligent methods” Geotechnical and Geological Engineering, 24(6), 1781-1801.

43. Chen, Y.L. (1988) “Foundations on Expansive Soils” Elsevier Science Publishing Company Inc., NewYork, pp. 714-728.

44. Chittoori, B.C.S. (2008) “Clay mineralogy effects on long-term performance of chemically treated expansive clays” Ph.D. dissertation, University of Texas at Arlington, TX, 326 pp.

45. Chittoori, B.C.S., and Puppala, A.J. (2011) "Quantitative estimation of clay mineralogy in fine-grained soils" Journal of Geotechnical and Geoenvironmental Engineering, vol. 137(11), pp. 997-1008.

46. Chittoori, B.S., Puppala, A.J., Saride, S., Nazarian, S., and Hoyos, L.R. (2009) “Durability studies of lime stabilized clayey soils” Proceedings 17th International Conference on Soil Mechanics and Geotechnical Engineering, M. Hamza et al., eds., Millpress, Rotterdam, Netherlands, 2208–2211.

47. Cho, S., and Lee, S. (2002) "Evaluation of Surficial Stability for Homogeneous Slopes Considering Rainfall Characteristics" Journal of Geotechnical Geoenvironment Engineering, vol. 128(9), pp. 756-763.

48. Clausnitzer, V. and Hopmans, J.W. (2000) “Pore-scale measurements of solute breakthrough using microfocus X-ray computed tomography” Water Resource Research, 36, 2067–2079.

49. Cokca, E. (2000) “Comparison of suction and oedometer methods for the measurement of swelling pressure” Engineering Geology, 33(2): 141–147.

50. Cokca, E., (2002) “Relationship between methylene blue value, initial soil suction and swell percent of expansive soils” Turkish Journal of Engineering and Environmental Sciences, 26, p. 521.

51. Croney, D., and Coleman, J.D. (1961) “Pore pressure and suction in soils” Proceedings, Conf. on Pore Pressure and Suction in Soils, Butterworths, London, 31–37.

52. Dakshanamurthy, V. and Raman, V. (1973) “A simple method of identifying an expansive soil” Soils and foundations, Japanese Society of Soil Mechanics and Foundation Engineering 13 (1), 97–104.

53. Das, S.K., and Basudhar, P.K. (2006) "Undrained lateral load capacity of piles in clay using artificial neural network" Computers and Geotechnics, 33(8), 454-459.

54. Das, S.K., Samui, P., Sabat, A.K., and Sitharam, T.G. (2010) “Prediction of swelling pressure of soil using artificial intelligence techniques” Environmental Earth Science, 61(2):393–403.

55. De Bruyn, C.M.A., Collins, L.F., and Williams, A.A.B. (1957) “The specific surface, water affinity, and potential expansiveness of clays” Clay Minerals Bulletin, 3, 120-128.

56. Delage, P., and Graham, J. (1996) “Mechanical behavior of unsaturated soils: understanding the behavior of unsaturated soils requires reliable conceptual models”, In: Alonso EE, Delage P (eds) Proceedings of 1st International Conference on Unsaturated Soils, Paris vol 3. Balkema, Presses des Ponts et Chausse´es, pp. 1223–1256.

57. Delage, P., and Lefebvre, G. (1984) “Study of the structure of a sensitive Champlain clay and of its evolution during consolidation” Canadian Geotechnical Journal, 21:21–35.

58. Delage, P., and Pellerin, M. (1984) “Influence de la lyophilisation sur la structure d’une argile sensible du Quebec” Clay Mineralogy, 19:151–160.

59. Delage, P., Tessier, D., and Audiguier, M.M. (1982) “Use of the cryoscan apparatus for observation of freeze-fractured planes of a sensitive Quebec clay in scanning electron microscopy” Canadian Geotechnical Journal, 19:111–114.

60. Delerue, J.F., Perrier, E., Timmerman, A. and Swennen, R. (2003) “3D Soil image characterization applied to hydraulic properties computation” In: Applications of X-ray Computed Tomography in the Geosciences (eds. F. Mees, R. Swennen, M. Van Geet and P. Jacobs), pp. 167–176. Geological Society Special Publication, London.

61. Diamond, S. (1970) “Pore size distribution in clays” Clays Mineralogy 18:7–23.

62. Ellis, G.W., Yao, C., and Zhao, R. (1992) "Neural network modeling of the mechanical behavior of sand" Proceedings of the Engineering Mechanics, 421-424.

63. Erzin, Y., and Erol, O. (2007) “Swell pressure prediction by suction methods” Engineering Geology, Science Direct, 92(3-4), 133–145.

64. Erzin, Y., and Gunes, N. (2013) “The unique relationship between swell percent and swell pressure of compacted clays” Bulletin of Engineering Geology and the Environment, 72(1), 71-80.

65. Erzin, Y., Gumaste, S.D., Gupta, A.K. and Singh, D.N. (2009) “ANN models for determining hydraulic conductivity of compacted fine grained soils” Canadian Geotechnical Journal, 46, 955-968.

66. Ferentinou, M.D., and Sakellariou, M.G. (2007) "Computational intelligence tools for the prediction of slope performance” Computers and Geotechnics, 34(5), 362-384.

67. Fies, J.C., and Bruand, A. (1998) “Particle packing and organization of the textural porosity in clay-silt-sand mixtures” European Journal of Soil Science, 49:557–567.

68. Finol, J., Guo, Y.K., and Jing, X.D. (2001) “A rule based fuzzy model for the prediction of petrophysical rock parameters” Journal of Petroleum Science and Engineering, 29, 97–113.

69. Flavel, R.J., Guppy, C.N., Tighe, M., Watt, M., McNeill, A. and Young, I.M. (2012) Non-destructive quantification of cereal roots in soil using high-resolution X-ray tomography" Journal of Experimental Botany, 63, 2503–2511.

70. Fredlund, D. G. (1969) "Consolidometer test procedural factors affecting swell properties", Proceedings of the Second International Conference on Expansive Soils, Texas A and M University, College Station, TX, pp. 435–456.

71. Fredlund, D.G. and Xing, A. (1994) "Equations for the soil water characteristic curve" Canadian Geotechnical Journal, vol. 31, pp. 521-532.

72. Fredlund, D.G., and Rahardjo, H. (1993) "Soil Mechanics for Unsaturated Soils" Wiley, New York.

73. Fu, Q., Hashash, Y.M.A., Hung, S., and Ghaboussi, J. (2007) "Integration of laboratory testing and constitutive modeling of soils" Computers and Geotechnics, 34(5), 330- 345.

74. Gantzer, C.J. and Anderson, S.H. (2002) "Computed tomographic measurement of macroporosity in chisel-disk and no-tillage seedbeds" Soil and Tillage Research, 64, 101–111.

75. Ghaboussi, J., and Sidarta, D.E. (1998) "New nested adaptive neural networks (NANN) for constitutive modeling" Computers and Geotechnics, 22(1), 29-52.

76. Goh, A.T.C. (1994a) "Nonlinear modeling in geotechnical engineering using neural networks" Australian Civil Engineering Transactions, CE36(4), 293-297.

77. Goh, A.T.C. (1994b) "Seismic liquefaction potential assessed by neural network" Journal of Geotechnical and Geoenvironmental Engineering, ASCE, 120(9), 1467-1480.

78. Goh, A.T.C. (1995a) "Empirical design in geotechnics using neural networks" Geotechnique, 45(4), 709-714.

79. Goh, A.T.C. (1995b) "Modeling soil correlations using neural networks" Journal of Computing in Civil Engineering, ASCE, 9(4), 275-278.

80. Goh, A.T.C. (1996a) "Neural-network modeling of CPT seismic liquefaction data" Journal of Geotechnical Engineering, ASCE, 122(1), 70-73.

81. Goh, A.T.C. (1996b) "Pile driving records reanalyzed using neural networks" Journal of Geotechnical Engineering, ASCE, 122(6), 492-495.

82. Goh, A.T.C. (2002) "Probabilistic neural network for evaluating seismic liquefaction potential" Canadian Geotechnical Journal, 39(1), 219-232.

83. Goh, A.T.C., and Kulhawy, F.H. (2003) "Neural network approach to model the limit state surface for reliability analysis" Canadian Geotechnical Journal, 40(1235-1244), 6.

84. Goh, A.T.C., Kulhawy, F.H., and Chua, C.G. (2005) "Bayesian neural network analysis of undrained side resistance of drilled shafts" Journal of Geotechnical and Geoenvironmental Engineering, 131(1), 84-93.

85. Goh, A.T.C., Wong, K.S., and Broms, B.B. (1995) "Estimation of lateral wall movements in braced excavation using neural networks" Canadian Geotechnical Journal, 32, 1059-1064.

86. Gokceoglu, C. (2002) "A fuzzy triangular chart to predict the uniaxial compressive strength of Ankara agglomerates from their petrographic composition" Engineering Geology, 66, 39–51.

87. Gokceoglu, C., Yesilnacar, E., Sonmez, H., and Kayabasi, A. (2004) "A neuro-fuzzy model for modulus of deformation of jointed rock masses" Computers and Geotechncis, 31(5), 375-383.

88. Gouy, G. (1910) "Sur la constitution de la charge electrique a la surface d'un electrolyte" Anniue Physique (Paris) 4 (9), 457–468.

89. Grevers, M.C.J., Jong, E.D. and St. Arnaud, R.J. (1989) “The characterization of soil macroporosity with CT scanning” Canadian Journal of Soil Science, 69, 629–637.

90. Gribb, M.M., and Gribb, G.W. (1994) "Use of neural networks for hydraulic conductivity determination in unsaturated soil” Proceedings of the 2nd International Conference on Ground Water Ecology, Bethesda, 155-163.

91. Grim, R.E. (1968) “Clay Mineralogy” 2nd Edition. McGraw-Hill, New York, 596 pp.

92. Habibagahi, G., and Bamdad, A. (2003) "A neural network framework for mechanical behavior of unsaturated soils" Canadian Geotechnical Journal, 40(3), 684-693.

93. Haj-Ali, R., Pecknold, D.A., Ghaboussi, J., and Voyiadjis, G.Z. (2001) "Simulated micromechanical models using artificial neural networks" Journal of Engineering Mechanics, 127(7), 730-738.

94. Hajnos, M., Lipiec, J., Świeboda, R., Sokołowska, Z., and Witkowska-Walczak, B. (2006) “Complete characterization of pore size distribution of tilled and orchard soil using water retention curve, mercury porosimetry, nitrogen adsorption, and water desorption methods” Geoderma, 135: 307–314.

95. Hanna, A.M., Morcous, G., and Helmy, M. (2004) "Efficiency of pile groups installed in cohesionless soil using artificial neural networks" Canadian Geotechnical Journal, 41(6), 1241-1249.

96. Hanna, A.M., Ural, D., and Saygili, G. (2007) "Neural network model for liquefaction potential in soil deposits using Turkey and Taiwan earthquake data" Soil Dynamics and Earthquake Engineering, 27(6), 521-540.

97. Hashash, Y.M.A., Jung, S., and Ghaboussi, J. (2004) "Numerical implementation of a neural network based material model in finite element analysis" International Journal for Numerical Methods in Engineering, 59(7), 989-1005.

98. Heeraman, D.A., Hopmans, J.W. and Clausnitzer, V. (1997) “Three dimensional imaging of plant roots in situ with X-ray computed tomography” Plant and Soil, 189, 167–179.

99. Helliwell, J.R., Sturrock, C.J., Grayling, K.M., Tracy, S.R., Flavel, R.J., Young, I.M., and Mooney, S.J. (2013) “Applications of X- ray computed tomography for examining biophysical interactions and structural development in soil systems: a review” European Journal of Soil Science, 64(3), 279-297.

100. Hoffman, R. (1975) “A study of the advancing interface. Interface shape in liquid–gas systems” Journal of Colloid Interface Science, 50:228–241.

101. Holtz, W.G., and Gibbs, H.J. (1956)"Engineering properties of expansive clays" Transactions of the American Society of Civil Engineers, vol. 121, pp. 641–663.

102. Hornik, K.M., Stinchcombe, M., and White, H. (1989) “Multilayer feed forward networks are universal approximators” Neural Networks, 2(5), 359–366.

103. Ikizler, S.B., Aytekin, M., Kocabas¸ F., and Vekli, M. (2010) “Prediction of swelling pressures of expansive soils using artificial neural networks” Advanced Engineering Software 41(4):647–65.

104. Javadi, A., Rezania, M., and Mousavi, N.M. (2006) "Evaluation of liquefaction induced lateral displacements using genetic programming" Computers and Geotechnics, 33(4-5), 222-233.

105. Jones, D. E., and Holtz, W. J. (1973) “Expansive soils: The hidden disaster” Civil Engineering, New York, vol. 430(8), pp. 49-51.

106. Jotisankasa, A. (2005) “Collapse behavior of compacted silty clay” Ph.D. thesis, Imperial College, London.
107. Juang, C.H., and Chen, C.J. (1999) "CPT-based liquefaction evaluation using artificial neural networks" Computer-Aided Civil and Infrastructure Engineering, 14(3), 221-229.
108. Juang, C.H., Holtz R.D. (1986b) “A probabilistic permeability model and the pore size density function” International Journal of Numerical Analysis, 10:543–553
109. Kaestner, A., Schneebeli, M. and Graf, F. (2006) “Visualizing three dimensional root networks using computed tomography” Geoderma, 136, 459–469.
110. Kalantari, B. (1991) “Construction of foundations on expansive soils” M.Sc. Thesis, Department of Civil Engineering University of Missouri Columbia, Missouri, pp. 35-44.
111. Kalantari, B. (2012) “Foundations on Expansive Soils; A Review” Research journal of applied sciences, engineering and technology, 4(18):3231.
112. Kayabali, K., and Demir, S., (2011) “Measurement of swelling pressure: direct method versus indirect methods” Canadian Geotechnical Journal, 48 (3), 354-364.
113. Ketcham, R.A. and Carlson, W.D. (2001) “Acquisition, optimization and interpretation of X-ray computed tomographic imagery: applications to the geosciences” Computers and Geosciences, 27, 381–400.
114. Khoury, N., and Khoury, C. (2005) “New laboratory methods for characterization of compaction in fine-grained soils” Internal report (revised in 2008) School of Civil Engineering and Environmental Science, the University of Oklahoma.
115. Kim, Y., and Kim, B. (2006) "Use of artificial neural networks in the prediction of liquefaction resistance of sands” Journal of Geotechnical and Geoenvironmental Engineering, 132(11), 1502-1504.

116. Kim, Y., and Kim, B. (2008) "Prediction of relative crest settlement of concrete-faced rockfill dams analyzed using an artificial neural network model" Computers and Geotechnics, 35(3), 313-322.
117. Knudsen, D., Peterson, G.A., and Pratt, P.F. (1982) "Lithium, sodium and potassium" Methods of soil analysis, Part 2, A. L. Page, ed., American Society of Agronomy, Madison, WI, 229–231.
118. Krahn, J., and Fredlund, D.G. (1972) "On total, matric and osmotic suction" Soil Science, 114(5), 339–348.
119. Kung, G.T., Hsiao, E.C., Schuster, M., and Juang, C.H. (2007) "A neural network approach to estimating deflection of diaphram walls caused by excavation in clays" Computers and Geotechnics, 34(5), 385-396.
120. Kurup, P.U., and Dudani, N.K. (2002) "Neural network for profiling stress history of clays from PCPT data" 2002, 128(7), 569-579.
121. Lee, C., and Sterling, R. (1992) "Identifying probable failure modes for underground openings using a neural network" International Journal of Rock Mechanics and Mining Science and Geomechanics Abstracts, 29(1), 49-67.
122. Lee, I.M., and Lee, J.H. (1996) "Prediction of pile bearing capacity using artificial neural networks" Computers and Geotechnics, 18(3), 189-200.
123. Lee, S.J., Lee, S.R., and Kim, Y.S. (2003) "An approach to estimate unsaturated shear strength using artificial neural network and hyperbolic formulation" Computers and Geotechnics, 30(6), 489-503.
124. Lefik, M., and Schrefler, B.A. (2003) "Artificial neural network as an incremental nonlinear constitutive model for a finite element code" Computer Methods in Applied Mechanics and Engineering, 192(31-32), 3265-3283.

125. Likos, W.J., Olsen, H.W., Krosley, L., and Lu, N. (2003) “Measured and estimated suction indices for swelling potential classification” Journal of Geotechnical and Geoenvironmental Engineering, 129(7), 665-668.
126. Lin B., Cerato A.B. (2012a) “Prediction of expansive soil swelling based on four micro-scale properties” Bulletin of Engineering Geology and Environment, 71:71–78.
127. Lin B., Cerato A.B. (2012b) “Investigation on soil water characteristic curves of untreated and stabilized highly clayey expansive soils”.
128. Lipiec, J., Walczak, R., Witkowska-Walczak, B., Nosalewicz, A., Slowinska-Jurkiewicz, A., and Slawinski, C. (2007) “The effect of aggregate size onwater retention and pore structure of two silt loam soils of different genesis” Soil Tillage Residual, 97:239–246
129. Lu, N., and Likos, W.J. (2004) “Unsaturated soil mechanics”, Wiley, New York.
130. Lu, Y. (2005) "Underground blast induced ground shock and its modeling using artificial neural network” Computers and Geotechnics, 32(3), 164-178.
131. Malaya, C. and Sreedeep, S. (2012) “Critical Review on the Parameters Influencing Soil-Water Characteristic Curve” Journal of Irrigation and Drain Engineering, 138(1), 55–62.
132. Mayoraz, F., and Vulliet, L. (2002) "Neural networks for slope movement prediction" The International Journal of Geomechanics, 2(2), 153-173.
133. McKeen, R.G. (1992) “A model for predicting expansive soil behavior” Proceedings, 7th International. Conference on Expansive Soils, Vol. 1, Dallas, 1– 6.
134. Millot, G. (1970) “Geology of Clays” Springer, New York, 425 pp.
135. Mitchell, J.K., and Soga, K. (2005) “Fundamentals of Soil Behavior” 3rd Edition, John Wiley and Sons Inc., Hoboken, New Jersey.

136. Moon, H.K., Na, S.M., and Lee, C.W. (1995) "Artificial neural-network integrated with expert-system for preliminary design of tunnels and slopes" Proceedings of the 8th International Congress on Rock Mechanics, Rotterdam: Balkema, 901-905.
137. Mooney, S.J. (2002) "Three-dimensional visualization and quantification of soil macroporosity and water flow patterns using computed tomography" Soil Use and Management, 18, 142–151.
138. Moser, A. P. (2001) "Buried Pipe Design" 2nd Edition, McGraw-Hill.
139. Murphy, V.N.S. (2010) «Soil Mechanics and Foundation engineering" CBS Publishers and Distributors Pvt.Ltd., New Delhi, pp. 924-940
140. Najjar, Y. M., and Huang, C. (2007) "Simulating the stress-strain behavior of Georgia kaolin via recurrent neuronet approach" Computers and Geotechnics, 34(5), 346-362.
141. Najjar, Y.M., Ali, H.E., and Basheer, I.A. (1999) "On the use of neuronets for simulating the stress-strain behavior of soils" Proceedings of the 7th International Symposium on Numerical Models in Geomechanics, Graz, Austria, 657-662.
142. Najjar, Y.M., and Ali, H E. (1998) "CPT-based liquefaction potential assessment: A neuronet approach" ASCE Geotechnical Special Publication, 1, 542-553.
143. Najjar, Y.M., and Basheer, I.A. (1996) "Neural network approach for site characterization and uncertainty prediction" ASCE Geotechnical Special Publication, 58(1), 134-148.
144. Najjar, Y.M., Basheer, I.A., and Naouss, W.A. (1996b) "On the identification of compaction characteristics by neuronets" Computers and Geotechnics, 18(3), 167-187.

145. Nawari, N.O., Liang, R., and Nusairat, J. (1999) "Artificial intelligence techniques for the design and analysis of deep foundations" Electronic Journal of Geotechnical Engineering, http://geotech.civeng.okstate.edu/ejge/ppr9909.

146. Neaupane, K., and Achet, S. (2004) "Some applications of a back-propagation neural network in geo-engineering" Environmental Geology, 45(4), 567-575.

147. Nelson, D., and Miller, D. J. (1992) "Expansive Soils Problems and practice in Foundation and Pavement Engineering" John Wiley and Sons, New York, pp. 40-80.

148. Ni, S.H., Lu, P.C., and Juang, C.H. (1996) "A fuzzy neural network approach to evaluation of slope failure potential" Journal of Microcomputers in Civil Engineering, 11, 59-66.

149. Nunan, N., Ritz, K., Rivers, M., Feeney, D.S. and Young, I.M. (2006) "Investigating microbial micro-habitat structure using X-ray computed tomography" Geoderma, 133, 398–407.

150. Nuth, M., and Laloui, L. (2008) "Advances in modeling hysteresis water retention curve in deformable soils" Computational Geotechnic, 35(6), 835–844.

151. Padmini, D., Ilamparuthi, K., and Sudheer, K.P. (2008) "Ultimate bearing capacity prediction of shallow foundations on cohesionless soils using neurofuzzy models" Computers and Geotechnics, 35(1), 33-46.

152. Pedarla, A. (2013) "SWCC and clay mineralogy based models for realistic simulation of swell behavior of expansive soils", Ph.D. dissertation, University of Texas at Arlington, TX, 338 pp.

153. Penumadu, D., and Chameau, J.L. (1997) "Geomaterial modeling using artificial neural networks" Artificial neural networks for civil engineers: fundamentals and applications, N. Kartam, I. Flood, and J. Garrett, eds., ASCE, New York, 160-184

154. Penumadu, D., and Zhao, R. (1999) "Triaxial compression behavior of sand and gravel using artificial neural networks (ANN)" Computers and Geotechnics, 24(3), 207-230.

155. Penumadu, D., Dean, J. (2000) “Compressibility effect in evaluating the pore-size distribution of kaolin clay using mercury intrusion porosimetry” Canadian Geotechnical Journal, 37:393–405.

156. Penumadu, D., Jin-Nan, L., Chameau, J.L., and Arumugam, S. (1994) "Rate dependent behavior of clays using neural networks” Proceedings of the 13th Conference of the International Society of Soil Mechanics and Foundation Engineering, New Delhi, 1445-1448.

157. Perret, J., Prasher, S.O., Kantzas, A. and Langford, C. (1999) “Three dimensional quantification of macropore networks in undisturbed soil cores” Soil Science Society of America Journal, 63, 1530–1543.

158. Peth, S., Nellesen, J., Fischer, G. and Horn, R. (2010) “Non-invasive 3D analysis of local soil deformation under mechanical and hydraulic stresses by mu CT and digital image correlation” Soil and Tillage Research, 111, 3–18.

159. Pires, L.F., Bacchi, O.O.S. and Reichardt, K. (2007) “Assessment of soil structure repair due to wetting and drying cycles through 2D tomographic image analysis”. Soil and Tillage Research, 94, 537–545.

160. Provenzano, P., Ferlisi, S., and Musso, A. (2004) "Interpretation of a model footing response through an adaptive neural fuzzy inference system” Computers and Geotechnics, 31(3), 251-266.

161. Pulat, H.F., Yukselen-Aksoy, Y., and Egeli, İ. (2014) “The effect of soil mineralogy and pore fluid chemistry on the suction and swelling behavior of soils” Bulletin of Engineering Geology and the Environment, 73(1), 37-42.

162. Punthutaecha, K., Puppala, A.J., Vanapalli, S.K., and Inyang, H. (2006) “Volume change behaviors of expansive soils stabilized with recycled ashes and fibers” Journal of Materials in Civil Engineering, vol. 18(2), pp. 295-306.

163. Puppala, A.J., Thammanoon, M., Soheil, N., and Hoyos, L.R. (2011) "Threshold moisture content and matric suction potentials in expansive clays prior to initiation of cracking in pavements" Canadian Geotechnical Journal, v 48, n 4, p 519-531.

164. Rahardjo, H., Li, X.W., Toll, D. G., and Leong, E.C. (2001) “The effect of antecedent rainfall on slope stability” Geotechnical and Geological Engineering, vol.19 (3-4), pp. 371-399.

165. Rahman, M.S., Wang, J., Deng, W., and Carter, J.P. (2001) "A neural network model for the uplift capacity of suction cassions" Computers and Geotechnics, 28(4), 269-287.

166. Rankine, R., and Sivakugan, N. (2005) "Prediction of paste backfill performance using artificial neural networks” Proceedings of the 16th International Society for Soil Mechanics and Foundation Engineering Osaka, Japan, 1107-1110.

167. Rao, B. H., Venkataramana, K., and Singh, D. N. (2011) “Studies on the determination of swelling properties of soils from suction measurements” Canadian Geotechnical Journal, 48(3), 375-387.

168. Rawas, A.A., Hago, A.W., and Al-Sarmi, H. (2005) “Effect of lime, cement and Sarooj (artificial pozzolan) on the swelling potential of an expansive soil from Oman” Journal of Building and Environment, vol. 40(5), pp. 681–687.

169. Rhoades, J.D. (1982) “Cation exchange capacity” Methods of soil analysis, Part 2: Chemical and microbiological properties, A. L. Page et al.

170. Rizzo, D.M., and Dougherty, D.E. (1994) "Application of artificial neural networks for site characterization using hard and soft information” Proceedings of the 10th

International Conference on Computational Methods in Water Resources, Dordrecht: Kluwer Academic, 793-799.

171. Rizzo, D.M., Lillys, T.P., and Dougherty, D.E. (1996) "Comparisons of site characterization methods using mixed data" ASCE Geotechnical Special Publication, 58(1), 157-179.
172. Rogasik, H., Onasch, I., Brunotte, J., Jegou, D. and Wendroth, O. (2003) "Assessment of soil structure using X-ray computed tomography" In: Applications of X-ray Computed Tomography in the Geosciences (eds. F. Mees, R. Swennen, M. Van Geet and P. Jacobs), pp. 151–165. Geological Society Special Publication, London.
173. Romo, M., Garcia, S.R., Mendoza, M.J., and Taboada-Urtuzuastegui, V. (2001) "Recurrent and Constructive-Algorithm Networks for Sand Behavior Modeling" The International Journal of Geomechanics, 1(4), 371-387.
174. Roweis, S. (2006) "Levenberg-Maquardart optimization": ⟨ http://www.cs.nyu.edu/~roweis/notes/lm.pdf⟩ (Jul. 16, 2015).
175. Santamarina, J.C., Klein, K.A., Wang, Y.H., and Prencke, E. (2002) "Specific surface: determination and relevance" Canadian Geotechnical Journal, 39(1), 233-241.
176. Sasanian, S., and Newson, T.A. (2013) "Use of mercury intrusion porosimetry for microstructural investigation of reconstituted clays at high water contents" Engineering Geology, 158, 15-22.
177. Schanz, T. and Tripathy, S. (2009) "Swelling pressure of a divalent-rich bentonite: Diffuse double-layer theory revisited" Water resources research, V 45.

178. Schanz, T., Khan M.I. and Al-Badran, Y. (2013) “An Alternative Approach for the Use of DDL Theory to Estimate the Swelling Pressure of Bentonites” Applied Clay Science, Vol. 83-84, October, pp. 383-390.

179. Seed, H.B., Woodward, R.J., and Lundgren, R. (1962) “Prediction of swelling potential for compacted clays” Proceeding ASCE Journal of Soil Mechanics and Foundations, Div. 88 (SM3), 53–87.

180. Shahin, M.A., and Indraratna, B. (2006) "Modeling the mechanical behavior of railway ballast using artificial neural networks" Canadian Geotechnical Journal, 43(1), 1144- 1152.

181. Shahin, M.A., and Jaksa, M.B. (2004) "Probabilistic assessment of the uncertainty associated with the pullout capacity of marquee ground anchors" Proceedings of the 9th Australia New Zealand Conference on Geomechanics, Auckland, In Press.

182. Shahin, M.A., and Jaksa, M.B. (2005a) "Modeling the pullout capacity of marquee ground anchors using neurofuzzy technique" Proceedings of the International Journal of Modeling and Simulation, MODSIM 2005, Melbourne, Australia, 66-72.

183. Shahin, M.A., and Jaksa, M.B. (2005b) "Neural network prediction of pullout capacity of marquee ground anchors" Computers and Geotechnics, 32(3), 153-163.

184. Shahin, M.A., and Jaksa, M.B. (2006) "Pullout capacity of small ground anchors by direct cone penetration test methods and neural methods" Canadian Geotechnical Journal, 43(6), 626-637.

185. Shahin, M.A., Jaksa, M.B., and Maier, H.R. (2001) "Artificial neural network applications in geotechnical engineering" Australian Geomechanics, 36(1), 49-62.

186. Shahin, M.A., Jaksa, M.B., and Maier, H.R. (2002a) "Artificial neural network based settlement prediction formula for shallow foundations on granular soils” Australian Geomechanics, 37(4), 45-52.

187. Shahin, M.A., Maier, H.R., and Jaksa, M.B. (2002b) "Predicting settlement of shallow foundations using neural networks" Journal of Geotechnical and Geoenvironmental Engineering, ASCE, 128(9), 785-793.

188. Shahin, M.A., Jaksa, M.B., and Maier, H.R. (2003a) "Neurofuzzy networks applied to settlement of shallow foundations on granular soils" Proceedings of the 9th International Conference on Applications of Statistics and Probability in Civil Engineering, ICASP9, San Francisco, Millpress, Rotterdam, 1379-1383.

189. Shahin, M.A., Maier, H.R., and Jaksa, M.B. (2003b) "Closure to: Predicting settlement of shallow foundations on cohesionless soils using neural networks" Journal of Geotechnical and Geoenvironmental Engineering, ASCE, 128(9), 785-793. of the International Congress on Modeling and Simulation, MODSIM 2003, Townsville, Queensland, 1886-1891.

190. Shahin, M.A., Maier, H.R., and Jaksa, M.B. (2003c) "Neural and neurofuzzy techniques applied to modeling settlement of shallow foundations on granular soils" Proceedings.

191. Shahin, M.A., Maier, H.R., and Jaksa, M.B. (2003d) "Settlement prediction of shallow foundations on granular soils using B-spline neurofuzzy models" Computers and Geotechnics, 30(8), 637-647.

192. Shahin, M.A., Jaksa, M.B., and Maier, H.R. (2004a) "Application of neural networks in foundation engineering" International e-Conference on Modern Trends in Foundation Engineering: Geotechnical Challenges and Solutions, http://www.civil.iitm.ac.in.

193. Shahin, M.A., Jaksa, M.B., and Maier, H.R. (2005a) "Neural network basedstochastic design charts for settlement prediction" Canadian Geotechnical Journal, 42(1), 110-120.

194. Shahin, M.A., Jaksa, M.B., and Maier, H.R. (2005b) "Stochastic simulation of settlement of shallow foundations based on a deterministic neural network model" Proceedings of the International Congress on Modeling and Simulation, MODSIM 2005, Melbourne (Australia), 73-78.

195. Shahin, M.A., Jaksa, M.B., and Maier, H.R. (2008) "State of the art of artificial neural networks in geotechnical engineering" Electronic Journal of Geotechnical Engineering, 8, 1-26.

196. Shang, J.Q., Ding, W., Rowe, R.K., and Josic, L. (2004) "Detecting heavy metal contamination in soil using complex permittivity and artificial neural networks" Canadian Geotechnical Journal, 41(6), 1054-1067.

197. Shi, J., Ortigao, J.A.R., and Bai, J. (1998) "Modular neural networks for predicting settlement during tunneling" Journal of Geotechnical and Geoenvironmental Engineering, ASCE, 124(5), 389-395.

198. Shi, J.J. (2000) "Reducing prediction error by transforming input data for neural networks" Journal of Computing in Civil Engineering, ASCE, 14(2), 109-116.

199. Sidarta, D.E., and Ghaboussi, J. (1998) "Constitutive modeling of geomaterials from non-uniform material tests" Computers and Geomechanics, 22(10), 53-71.

200. Sillers, W.C., Fredlund, D.G., and Zakerzadeh, N. (2001) "Mathematical attributes of some soil-water characteristic curve models" Geotechnical and Geology Engineering, 19(3–4), 243–283.

201. Simms, P.H., Yanful, E.K. (2004) "A discussion of the application of mercury intrusion porosimetry for the investigation of soils, including an evaluation of its use to estimate volume change in compacted clayey soils". Geotechnique 54(6):421–426.

202. Simpson, P.K. (1990) “Artificial neural system-foundation, paradigm, application and implementation” New York, Pergamon Press.
203. Singh, T.N., and Singh, V. (2005) "An intelligent approach to prediction and control ground vibration in mines” Geotechnical and Geological Engineering, 23(3), 249-262.
204. Singh, T.N., Kanchan, R., Verma, A.K., and Singh, S. (2003) “An intelligent approach for prediction of triaxial properties using unconfined uniaxial strength” Mining Engineering Journal, 5, 12–16.
205. Sinha, S.K., and Wang, M.C. (2008) "Artificial neural network prediction models for soil compaction and permeability” Geotechnical Engineering Journal, 26(1), 47-64.
206. Sivakugan, N., Eckersley, J.D., and Li, H. (1998) "Settlement predictions using neural networks” Australian Civil Engineering Transactions, CE40, 49-52.
207. Sivapullaiah, P.V., Sitharam, T.G. and Rao, K.S.S. (1987) “Modified free swell index for clays” Geotechnical Testing Journal, 10(2):80–85.
208. Snethen, D.R., Townsend, F.C., Johnson, L.D., Patrick, D.M. and Vedros, S.P.J. (1975) “Review of engineering experiences with expansive soils in highway subgrades”, US Army Engineer Water Ways Experiment Station, FHWA, USA.
209. Sreedeep, S., and Singh, D.N. (2011) “A critical review of the methodologies employed for soil suction measurement” International Journal of Geomechanics, 11(2), 99–104.
210. Sridharan, A., and Prakash, K. (2000) “Classification procedures for expansive soils” Proceedings of the ICE-Geotechnical Engineering, 143(4), 235-240.
211. State of California Department of Transportation (2008) “Maintenance Technical Advisory Guide Volume II - Rigid Pavement Preservation”, Second Edition.

212. Teh, C.I., Wong, K.S., Goh, A.T.C., and Jaritngam, S. (1997) "Prediction of pile capacity using neural networks" Journal of Computing in Civil Engineering, ASCE, 11(2), 129-138.

213. Thakur, V.K.S., and Singh, D.N. (2005) "Swelling and suction in clay minerals" Advanced Experimental Unsaturated Soil Mechanics. In: Tarantino A, Romero E, Cui YJ (eds.)" Proceedings International Symposium (Experus 2005), Trento, Italy. A.A. Balkema, Rotterdam, pp. 27–31.

214. Tutumluer, E., and Seyhan, U. (1998) "Neural network modeling of anisotropic aggregate behavior from repeated load triaxial tests" Transportation Research Record 1615, National Research Council, Washington, DC.

215. Ural, D.N., and Saka, H. (1998) "Liquefaction assessment by neural networks" Electronic Journal of Geotechnical Engineering, http://www.ejge.com/Ppr9803/ Ppr9803.htm.

216. Uzundurukan, S.; Keskin, S. N.; Yıldırım, H., and Göksan, T. S. (2013) "Suction and Swell Characteristics of Compacted Clayey Soils" Arabian Journal for Science and Engineering, Section B, Engineering 39 (2), 747-752.

217. Van Der Merwe, D.H. (1964) "The prediction of heave from the plasticity index and percentage clay fraction of soils" Civil Engineering in South Africa 6 (6), 103–106.

218. Van Genuchten, M.T. (1980) "A closed-form equation for predicting the hydraulic conductivity of unsaturated soils" Journal of Soil Science Society of America, Vol. 44, pp. 892–898.

219. Vanapalli, S.K., Fredlund, D.G., and Pufahl, D.E. (1999) "The influence of soil structure and stress history on the soil-water characteristic of a compacted till" Geotechnique, vol.49(2),pp.143-159.

220. Viola, R., Tuller, M., Or, D., and Drasdis, J. (2005) “Microstructure of clay-sand mixtures at different hydration states” Proceedings of International Symposium on Advanced Experimental Unsaturated Soil Mechanics, Trento, Italy, In: Tarantino A, Romero E, Cui YJ (eds) Advanced experimental unsaturated soil mechanics. Taylor, Francis Group, London, pp. 437–442, 27–29.
221. Washburn, E.W., (1921) “Note on a method of determining the distribution of pore sizes in a porous material”, Proceedings of the National Academy of Sciences 4, pp. 115– 116.
222. Webb, P.A., Orr, C. (1997) “Analytical methods in fine particle technology” Micromeritics Instrument Corp, Norcross.
223. Wildenschild, D., Hopmans, J.W., Vaz, C.M.P., Rivers, M.L., Rikard, D. and Christensen, B.S.B. (2002) “Using X-ray computed tomography in hydrology: systems, resolutions, and limitations” Journal of Hydrology, 267, 285–297.
224. Williams, H.F.L. (2003) "Urbanization pressure increases potential for soils-related hazards Denton County, Texas" Environmental Geology, vol. 44(8), pp. 933-938.
225. Yang, H., Rahardjo, H., and Fredlund, D.G. (2004) “Factors affecting drying and wetting soil-water characteristic curves of sandy soils” Canadian Geotechnical Journal, 41(5), 908–920.
226. Yang, Y., and Rosenbaum, M.S. (2002) "The artificial neural network as a tool for assessing geotechnical properties” Geotechnical Engineering Journal, 20(2), 149-168.
227. Yilmaz, I. (2006) “Indirect estimation of the swelling percent and a new classification of soils depending on liquid limit and cation exchange capacity” Engineering Geology, 85(3), 295-301.

228. Yilmaz, I., and Kaynar, O. (2011) “Multiple regression, ANN (RBF, MLP) and ANFIS models for prediction of swell potential of clayey soils” Expert Systems with Applications, 38(5), 5958-5966.

229. Yoo, C., and Kim, J. (2007) "Tunneling performance prediction using an integrated GIS and neural network” Computers and Geotechnics, 34(1), 19-30.

230. Young-Su, K., and Byung-Tak, K. (2006) "Use of artificial neural networks in the prediction of liquefaction resistance of sands” Journal of Geotechnical and Geoenvironmental Engineering, 132(11), 1502-1504.

231. Yukselen, Y., and Kaya, A. (2006) “Prediction of cation exchange capacity from soil index properties” Clay Miner., 41(4), 827–833.

232. Yukselen-Aksoy, Y., and Kaya, A. (2010) “Predicting soil swelling behavior from specific surface area” Proceedings of the ICE-Geotechnical Engineering,163(4), 229-238.

233. Zeng, Y., Gantzer, C.J., Payton, R.L. and Anderson, S.H. (1996) “Fractal dimension and lacunarity of bulk density determined with X-ray computed tomography” Soil Science Society of America Journal, 60, 1718–1724.

234. Zhao, H. (2008) "Slope reliability analysis using a support vector machine" Computers and Geotechnics, 35(3), 459-467.

235. Zhou, Y., and Wu, X. (1994) "Use of neural networks in the analysis and interpretation of site investigation data” Computer and Geotechnics, 16, 105-122.

236. Zhu, J.H., Zaman, M.M., and Anderson, S.A. (1998a) "Modeling of soil behavior with a recurrent neural network" Canadian Geotechnical Journal, 35(5), 858-872.

237. Zhu, J.H., Zaman, M.M., and Anderson, S.A. (1998b) "Modeling of shearing behavior of a residual soil with recurrent neural network" International Journal of Numerical and Analytical Methods in Geomechanics, 22(8), 671-687.

238. Zhu, J.H., Zaman, M.M., and Trafalis, T.B. (1996) "Prediction of shear stress-strain behavior of soil with recurrent neural network" Intelligent Engineering Systems Through Artificial Neural Networks, 6, 809-814.

239. Zong, Y., Yu, X., Zhu, M., and Lu, S. (2015) “Characterizing soil pore structure using nitrogen adsorption, mercury intrusion porosimetry, and synchrotron-radiation-based X-ray computed microtomography techniques” Journal of Soils and Sediments, 15(2), 302-312.

Biographical Information

Alejandro H. Pino Bravo was born in Popayan, Cauca, Colombia, on January 14th, 1978. He graduated from Universidad del Cauca, Colombia, with a Bachelor of Sciences Degree in Civil Engineering in 2001. After graduating, he worked as a staff civil engineer for several consulting companies in Colombia, and obtained the degree of specialist in geotechnical engineering from the Universidad Nacional de Colombia in 2007. He joined University of Texas at Arlington (UTA) to pursue his Masters of Science degree in Civil Engineering under Professor Laureano Hoyos advising. He defended his thesis successfully in July 2013 which topic was “EFFECT OF SUCTION ON DYNAMIC PROPERTIES OF UNSATURATED SOILS AT SMALL- TO MID-SHEAR STRAIN AMPLITUDES”.

In 2015, he completed his doctoral program with Geotechnical Engineering as the concentration area of research in the Department of Civil Engineering at the University of Texas at Arlington (UTA), Arlington, Texas. He focused his graduate work on expansive soils behavior and soil composition properties for prediction of soil swelling under the guidance of Professor Anand J. Puppala. He successfully defended his dissertation in October 2015.

At UTA, he worked in various research areas related to soil-suction testing, expansive soils behavior and advanced internal structure of solid study techniques like Mercury Intrusion Porosimetry and X-ray Computed Tomography.